Symmetry and variational analyses of fluid interface equations in the thin film limit

Thesis by
Zachary George Nicolaou

In Partial Fulfillment of the Requirements for the
degree of
Doctor of Philosophy

CALIFORNIA INSTITUTE OF TECHNOLOGY
Pasadena, California

2017
Defended September 7, 2016

Zachary George Nicolaou
ORCID: 0000-0003-4542-4256

ACKNOWLEDGEMENTS

Thanks to my advisor Sandra Troian and the LIS^{2}T group at Caltech for introducing me to this fascinating field of study and giving guidance and constructive critcism. Thanks to my physics and mathetmatics teachers at Caltech, the Univeristy of Cambridge, and Northwestern for thorough training and attention. Thanks to my family and friends for support and for a stimulating social environment. Thanks to Jessica Kunke for her loving support and for motivation to improve myself. Thanks for the financial support from the NSF Graduate Research Fellowship and from Caltech as a teaching assistant, and thanks to the dedicated students I've had the opportunity to teach.

ABSTRACT

This thesis concerns a class of nonlinear partial differential equations up to fourth order in spatial derivatives that models thin viscous films. In Chapter 1, we review the derivations of thin film equations from the fundamental transport equations. Section 1.1 contains the derivation for a thermocapillary driven film to familiarize the reader with the key long-wavelength approximation that has been successful in modeling a myriad of thin viscous films. In Section 1.2, we consider the coupling between a thin viscous layer and a much thicker fluid layer with much larger viscosity and conductivity and show how a novel, non-local thermocapillary thin film equation can be derived to model such a system. We then review the wider class of thin film equations in Section 1.3, note the important Cahn-Hilliard variational form of these equations, and demonstrate that classic mathematical results concerning the inverse problem of the calculus of variations permit an algorithmic procedure for discovering Lyapunov functionals. In Chapter 2, we review applications of symmetry methods to partial differential equations. Section 2.1 contains an original geometrical motivation for the study of self-similar reductions which draws an analogy with the fixed points of dynamical systems. In Section 2.2, we derive for the first time the full set of symmetries of the fully two-dimensional thin film equations. We then enumerate the possible symmetry reductions of the thin film equations, and discover several which have not been previously recognized. In Chapter 3, we consider rotationally invariant, steady droplet solutions and their stability. In Section 3.1, we derive stability criteria for thermocapillary-driven droplets, and show a novel correspondence between droplet stability, droplet volume, and droplet Lyapunov energy. We consider thin films under other forces in Section 3.2 and make new predictions about conditions under which such films develop into droplets, columns, or jets of fluid. In Chapter 4, we consider the scale invariant symmetry reductions of thin film equations. In Section 4.1 we describe the extraordinarily rich variety of such solutions in the spreading of a insoluble surfactant on a thin viscous film, identify previously unrecognized scale invariant solutions which are well-behaved at the origin, and demonstrate their relevance with finite element simulations. Lastly, in Section 4.2, we illustrate for capillary driven films some numerical solutions to the novel reductions we uncovered in Chapter 2. Each chapter concludes with a Notes section which summarizes the new results contained therein and relates them to the wider literature.

PUBLISHED CONTENT AND CONTRIBUTIONS

[1] Z. G. Nicolaou. “Stability and instability of axisymmetric droplets in thermocapillary-driven thin films”. In: *Nonlinearity* (under review 2016).

[2] Z. G. Nicolaou and S. M. Troian. “Scale Invariant Draining of the Inner Droplet in the Spreading of an Insoluble Surfactant on a Thin Viscous Film”. In: *Phys. Rev. E* (preparing for submission 2016).

[3] Z. G. Nicolaou and S. M. Troian. “Reynolds’ transport theorem without external advection assumptions”. In: *Phys. Fluids* (preparing for submission 2016).

[4] Z. G. Nicolaou and S. M. Troian. “Embedded symmetries and classes of self-similar solutions of the thin film equations”. In: *Phys. Rev. Fluids* (preparing for submission 2016).

The contents of Section 3.1 are currently under review at Nonlinearity [1]. The research and manuscript writing was done by Z. G. Nicolaou. S. M. Troian offered advice and received acknowledgement in the paper.

The contents of Section 4.1 have been drafted in a manuscript being prepared for submission to Physical Review E [2]. The research and manuscript writing was done by Z. G. Nicolaou under advice and revisions from S. M. Troian.

The contents of Appendix B have been drafted in a manuscript being prepared for submission to Physics of Fluids [3]. The research and writing preparation was done by Z. G. Nicolaou under advice and revisions from S. M. Troian.

The contents of Section 2.2 are currently being drafted in a manuscript to be submitted to Physical Review Fluids [4]. The research and manuscript writing was done by Z. G. Nicolaou under advice and revisions from S. M. Troian.

LIST OF ILLUSTRATIONS

LIST OF TABLES

LIST OF SYMBOLS

A Discretized matrix operator of the Lyapunov energy change. 93, 94

A_{VdW} Non-dimensional Hamaker constant. 27

B Thin film momentum integration constant. 7, 16, 17

C Thin film heat integration constant. 8, 18, 19

C_1 Lagrange multiplier enforcing volume conservation. 76, 77, 81, 84–86, 91, 101–103, 105, 106, 111

C_c Contact line slope. 76, 77, 80, 84, 85, 88, 89, 92, 100, 101, 103–107, 111, 112, 117

D Dimension of the Cartesian space. 154–163

D_0 Gap-film thickness ratio. 3, 8, 9, 27, 73, 74, 114, 115, 120

E Change in the Lyapunov energy from the base state. 92–94, 100

F Lyapunov energy. 10, 11, 26–31, 73, 75–85, 88, 90–92, 100–108, 118, 161, 162

G Lie group of symmetries. 39

H Dimensionless film thickness. 6–11, 16–22, 24–28, 30, 31, 33, 42–60, 64–67, 71–81, 84–86, 89–106, 108, 110–117, 122–128, 130, 131, 134, 136, 138–146

H_{LSD} Height of the largest stable droplet. 112, 113

$H_{\max}$ Height of a steady state droplet. 78, 86–89, 97–100, 107, 109, 112, 114, 118

H_ε A one-parameter family of film height functions parameterized by ε. 77, 78, 80, 81, 84, 85, 88–92, 99–102, 106

I Integral expression. 155, 156, 160

J Jacobian of the map from Cartesian coordinates to Lagrangian coordinates. 160, 161

L Lateral length scale. 5–9, 14, 16–18, 28, 122, 123

M Number of discretized elements in the finite element approximation. 93, 97, 98

Y Dimensionless interface-lateral Cartesian Y coordinate. 6, 44–53, 56–58, 64–66, 116, 117, 122, 123, 143

Z Dimensionless interface-lateral Cartesian Z coordinate. 5–8, 14–19, 26, 27

Δ Differential functions which determine a partial differential equation. 35–43, 58, 60–62, 68, 70

ΔV Dimensionful electric voltage applied between top and bottom substrates. 27, 111, 120

Γ Dimensionless insoluble surfactant concentration. 28, 30, 31, 42, 57–60, 64–67, 122–125, 127, 128, 130, 131, 134, 136, 138–140

Λ Multiplier of a conservation law. 41, 42

Ω An arbitrary domain, usually in $\mathbb{R}^2$. 74–80, 82–85, 154–164

Ω_s Domain of the surface coordinate variables. 155–159, 162, 163

Φ Body force potential. 25–27, 72

Π External interfacial normal force density. 25–27, 72

Σ Dimensionless thin film surface tension. 6–8, 17, 19–22, 24–28, 72, 73

Θ Dimensionless thin film temperature. 6, 8, 17–19

α Scaling exponent. 49–62, 65–67, 123–142, 144–147

$\bar{D}_0$ Thick-thin gap with ratio. 13, 15–25

$\bar{G}$ Non-dimensional thin film gravitational number. 27, 110, 111

$\bar{T}_0$ Flat interface temperature for thick-thin coupled films. 13, 17–19

$\bar{\text{Ca}}$ Thin film Capillary number. 6, 7, 9, 17, 19–28, 31, 42, 50, 51, 53–58, 72, 73, 76, 77, 79, 80, 84, 85, 110, 111, 117, 122, 123, 135, 141

$\bar{\text{E}}$ Thin film non-dimensional electrohydrodynamic driving force number. 27, 110, 111

$\bar{\text{Ma}}$ Thin film Marangoni number. 6, 7, 9, 17, 19–28, 30, 31, 57, 58, 72, 73, 110, 111, 122, 123

$\bar{\mathrm{Pe}}$ Thin film Peclet number. 8, 28, 30, 57, 58, 122, 123, 135

$\bar{\mu}$ Thick-thin viscosity ratio. 13, 16, 17, 19–25

$\bar{\nabla}_L$ Dimensionful lateral gradient. 3–5, 8, 14, 17

$\bar{\nabla}_S$ Dimensionful surface gradient. 4, 5

$\bar{k}$ Thick-thin conductivity ratio. 13, 19–23, 25

$\bar{t}$ Dimensionful time. 3–5, 8, 14, 17, 122

β Fluid slip length. 25–27, 72, 73

$\boldsymbol{\tau}_{\text{ext}}$ External interfacial shear force density. 25, 26, 73

$\boldsymbol{\xi}$ Lagrangian coordinates for a moving domain in $\mathbb{R}^D$. 154–156, 160, 161, 163

χ Conductive heat transfer number. 9–11, 27, 74, 109–111, 113, 114

χ_{EHD} Dielectric and gap width ratio number. 27, 110, 111, 113, 114, 119

δ Jensen's scaling exponent. 124, 126, 140

ϵ Thin film parameter. 5–9, 13, 16–19, 23, 26–28

η Invariants of a symmetry. 39, 58–61, 125, 126, 128

$\frac{\partial \tau_{\text{ext}}}{\partial H}$ External interfacial shear force density surface tension function. 26, 72

$\frac{\mathrm{d}^2 q}{(2\pi)^2}$ Non-dimensional 2D momentum space integration measure. 14, 15, 17–21, 24, 25

γ Insoluble surfactant concentration. 28, 122, 123

γ_{m} Insoluble surfactant concentration scale. 28, 122, 123

$\hat{\mathbf{n}}$ Interface or boundary normal unit vector. 4, 5, 8, 16, 18

$\hat{\mathbf{n}}_c$ Two-dimensional outward poining normal to the contact line. 79, 80, 82–85

$\hat{\mathbf{n}}_s$ The outward pointing normal vector to the boundary of a D-dimensional domain. 154, 157–159, 161–163

$\hat{\mathbf{t}}$ Interface or boundary tangent vectors. 5

$\hat{\mathbf{x}}$ Unit vector in x direction. 3, 5, 6, 15, 17, 29, 30

$\hat{\mathbf{y}}$ Unit vector in y direction. 3, 5, 6, 15

$\hat{\mathbf{z}}$ Unit vector in z direction. 3–5, 8, 18

κ Thermal conductivity ratio. 3, 8, 9, 27, 73, 74, 85, 86, 108, 109, 111, 114

$\lambda_{\max}$ Wavelength of the fastest growing unstable mode. 9, 22, 23, 113–115

$\mathbb{D}$ Frechet derivative operator. 30, 40–42

$\mathbf{A}$ Thin film momentum integration constant. 7, 16

$\mathbf{E}$ Dimensionful symmetric rate of strain tensor. 4, 16

$\mathbf{M}_{\boldsymbol{\xi}\to\mathbf{x}}$ Map taking Lagrangian coordinates to Cartesian coordinates. 156, 160, 161

$\mathbf{M}_{\mathbf{x}\to\boldsymbol{\xi}}$ Map taking Cartesian coordinates to Lagrangian coordinates. 156, 160, 161, 163

$\mathbf{Q}_L$ Lateral volumetric fluid flux. 10, 26, 29, 30, 73, 76, 81

$\mathbf{S}_{\mathbf{w}_s\to\mathbf{x}}$ Parameterization of surface in $\mathbb{R}^D$ from the surface coordinates. 156–159, 162, 163

$\mathbf{T}$ Dimensionful stress tensor. 4, 16

$\mathbf{U}$ Propagator for the flow of the velocity field for the Lagrangian coordinates. 160, 163

$\mathbf{U}_L$ Dimensionless two-dimensional lateral velocity vector. 5–7, 14–17, 19

$\mathbf{V}_c$ Velocity of the contact line. 79–81

$\mathbf{X}_L$ Dimensionless interface-lateral Cartesian two-dimensional vector. 5–8, 10, 14–22, 24–31, 50, 51, 73–78, 80, 81, 110, 111, 113, 122, 123

$\mathbf{X}_c$ A point on the contact line of a droplet. 76, 77, 79, 80, 82–85

$\mathbf{a}$ Momentum space integration constant. 15, 16

$\mathbf{b}$ Thick film momentum space integration constant. 15, 16

$\mathbf{n}_s$ Non-normalized normal vector to the boundary of a D-dimensional domain. 157, 159

$\mathbf{p}$ Two-dimensional wave vector. 21, 22, 113

$\mathbf{q}$ Momentum space integration variables. 14–21, 24, 25

$\mathbf{t}$ Non-normalized tangent vector to the boundary of a D-dimensional domain. 157, 162, 163

$\mathbf{u}_L$ Dimensionful two-dimensional lateral velocity vector. 3–5, 8, 12, 14, 17

$\mathbf{v}$ A velocity flow field in D-dimensional space. 154, 155, 158–161, 163, 164

$\mathbf{v}_s$ Velocity of a surface point on the boundary of a in a moving domain. 158, 159, 161–163

$\mathbf{w}_s$ Surface coordinates used to parameterize the boundary of a domain. 155–159, 162, 163

$\mathbf{x}$ Cartesian coordinates for D-dimensional Cartesian space. 154–164

$\mathbf{x}_L$ Dimensionful interface-lateral Cartesian two-dimensional vector. 3, 5

$\mathcal{D}$ Insoluble surfactant surface diffusion constant. 28, 123

$\mathcal{E}$ Density of the change in the Lyapunov energy from the base state. 92, 93

$\mathcal{F}$ Lyapunov energy density. 11, 27, 28, 31, 73, 74, 76–78, 82–84, 161, 162

$\mathcal{L}_\Gamma$ Integral operator in the Fredholm equation for thick-thin film Γ. 20, 21

$\mathcal{L}_{\tilde{\mathbf{A}}}$ Integral operator in the Fredholm equation for thick-thin film $\tilde{A}$. 20, 21

$\mathcal{M}$ State space manifold whose coordinates are the dependent and independent variables. 36–39

$\mathcal{S}$ Manifold of the graph of a solution in the state space. 36, 37, 39

$\mathcal{U}$ Manifold whose coordinates are the dependent variables. 36

$\mathcal{V}$ Non-dimensional voltage constant. 27

$\mathcal{V}$ Volume density. 82–84

$\mathcal{X}$ Manifold whose coordinates are the independent variables. 36

$\mathrm{Pe}^{(2)}$ Thick layer Peclet number. 18

$\mathrm{Re}^{(2)}$ Thick film Reynolds' number. 14

Re_H Thin film Reynolds' number. 6

$\mathscr{P}$ Projection operator enforcing volume conservation constraint. 96, 97

$\mathscr{S}$ Extended phase space subvariety. 36–40, 42, 60–62, 68

$\mathscr{V}$ Volume of fluid. 10, 26, 73, 77–85, 88, 108, 109, 112, 118

$\mathscr{W}$ First integral of the planar system. 130, 140

μ Thin film fluid viscosity. 2, 4–7, 9, 12–14, 16, 17, 23, 26, 27, 119, 122, 123

∇ Three or D-dimensional gradient operator. 3, 158–162

∇_L Dimensionless lateral gradient. 6, 7, 9–11, 14–22, 24–31, 42, 50, 51, 57, 58, 72–76, 78–81, 84, 90, 91, 110, 111, 122, 123, 141

ν Multiindex used to denote arbitrary partial derivatives. 35–37, 40–43

ϕ Independent variable in Jensen's planar system. 124–127

ϕ_{sym} Symmetry generator coefficient in the dependent variable direction. 38–40, 42, 43, 45

ϕ_ε Eigenfunction of the Laplacian on the domain Ω. 158, 159

ψ Intermediate function in Lyapunov construction. 29, 30

ψ_ε Solution of the Laplace equation with Neumann boundary conditions. 159

ρ Thin film fluid density, or more general density field variable in a thermodynamic setting. 4, 6, 8, 12, 14, 17, 18, 27, 111, 119, 161, 162

σ Interface surface tension. 2, 4–6, 12, 13, 17, 26, 28, 72, 73, 122, 123

σ_0 Surface tension scale. 2, 6, 9, 10, 13, 17, 26, 28, 119, 122, 123

σ_T Surface tension temperature coefficient. 2, 6, 9, 10, 13, 17, 23, 111

σ_γ Surface tension surfactant coefficient. 28, 123

$\star$ Two-dimensional (Hodge) dual vector. 14–17, 19, 20, 24, 25, 29, 50, 51, 81

τ Independent variable for planar system for scale invariant solutions in the surfactant spreading problem. 59, 60, 126–130

θ Non-dimensional azimuthal angle. 52, 55–57, 65–67, 89–93, 95, 99–106, 117, 137, 141, 142, 144

$\tilde{A}$ Discretized matrix operator of the Lyapunov energy change with metric rescaling. 94–97

$\tilde{H}$ Symmetry invariant used as dependent variable in thin film equation reductions. 50–58, 60, 64–67, 123–125, 130, 131, 134–137, 141–144

$\tilde{K}$ Discretized matrixed enforcing Golub's constraint. 97

$\tilde{P}$ Pressure Fourier transform. 14, 15

$\tilde{R}$ Symmetry invariant used as independent variable in thin film equation reductions. 51, 53, 54, 58–61, 64, 65

$\tilde{U}_1$ Lateral velocity Fourier transform component. 14, 15

$\tilde{U}_2$ Lateral velocity Fourier transform component. 14, 15

$\tilde{U}_Z$ Normal velocity Fourier transform. 14, 15

$\tilde{X}$ Symmetry invariant used as independent variable in thin film equation reductions. 50, 51, 53, 54, 64, 65

$\tilde{Y}$ Symmetry invariant used as independent variable in thin film equation reductions. 50, 51

$\tilde{\Gamma}$ Symmetry invariant used as dependent variable in thin film equation reductions. 58, 60, 61, 64–67, 123–125, 130, 131, 134–137

$\tilde{\mathbf{A}}$ Thick-thin bilayer Fredholm integral equation variable. 16, 17, 19–22, 24

$\tilde{\theta}$ Symmetry invariant used as independent variable in thin film equation reductions. 52, 55–58, 60, 65–67, 141–144

$\tilde{t}$ Symmetry invariant used as independent variable in thin film equation reductions. 51–54, 64

$\tilde{v}$ Discretized vector corresponding to a perturbation with metric rescaling. 94–97

ε Parameter describing a continuous family of perturbations or solutions. 77, 78, 80–85, 88–92, 99–102, 104, 106, 122, 123, 154–164

$\vec{v}$ Vector generator of a symmetry in state space. 38–40, 50, 51, 53–58, 64–67, 123, 125

ξ Similarity variable for rotationally or translationally invariant solutions to the surfactant spreading problem. 123–125, 127–131, 134–140

ξ_{sym} Symmetry generator coefficient in the independent variable direction. 38–40, 42–49

ζ Planar variables for scale invariant solutions in the surfactant spreading problem. 59, 125–132, 134, 138–140, 146

a Vector constraint corresponding to volume conservation with metric rescaling. 95–97

a_Z Momentum space integration constant. 15, 16

b Linear stability growth rate. 21, 22, 113

b_Z Thick film momentum space integration constant. 15, 16

b_{max} Growth rate of the fastest growing unstable mode. 22, 23, 113, 115

c Thin film specific heat capacity. 8, 17, 18

d_0 Gap thickness scale for confined films. 2, 3, 8, 12–14, 18, 23, 73, 111, 119, 120

e Thick film heat integration constant. 18

g Gravitational constant. 27, 111, 119

g_{EHD} Non-dimensional gravitation and electrohydrodynamic number. 111–115, 119, 120

g_{TC} Non-dimensional gravitation and thermocapillary number. 110–114

h Dimensionful film thickness. 3–6, 8, 122

h_0 Film thickness scale. 2, 3, 5, 6, 9, 12, 13, 27, 73, 111, 113, 119, 122, 123

k Thin film fluid heat conductivity. 2, 3, 8, 12, 13, 17, 18, 73

m Total mass in a thermodynamic setting. 161, 162

n Dimensionality constant, zero for translationally invariant solutions and one for rotationally invariant solutions. 124–131, 138–140

p Dimensionful pressure in thin film fluid. 4, 5, 12, 14, 16

q Momentum space integration variable magnitude. 14–21, 24

s Order of prolongation. 36, 37, 39

t Dimensionless time. 5–7, 9–11, 14, 19, 21, 22, 25–31, 44–48, 50–59, 64–67, 73–75, 78–81, 108, 110, 111, 113, 116, 117, 122–125, 129, 131, 134–145, 154, 155

u A dependent variable. 29, 30, 34–41, 82–84

u_c Characteristic lateral velocity scale. 5–9, 14, 16–18, 23, 26–28, 122, 123

u_z Dimensionful fluid velocity in z direction. 3–5, 8, 12, 14, 17

v Discretized vector corresponding to a perturbation. 93–95

x Dimensionful interface-lateral Cartesian x coordinate. 3, 122

x An independent variable. 34–41

y Dimensionful interface-lateral Cartesian y coordinate. 3, 122

z Dimensionful interface-normal Cartesian z coordinate. 2–5, 8, 14, 17, 18

d^2X Non-dimensional 2D integration measure. 10, 11, 16–21, 24–31, 73, 75, 79, 80

ε Dielectric constant of thin film. 27, 111, 119

$\varepsilon_{\mathrm{EHD}}$ Dielectric constant ratio. 27, 111, 114, 115, 120

$|\mathbf{p}|$ Two-dimensional wave vector magnitude. 21–23, 25, 113

TABLE OF CONTENTS

Chapter 1

DERIVATIONS OF THIN FILM EQUATIONS

In this introductory chapter, we discuss various derivations of thin film equations from the governing transport equations of fluid mechanics. These derivations rely on a long wavelength approximation, sometimes called the lubrication approximation or the thin film approximation, in which the surface-normal length scale is assumed to be significantly smaller than the surface-lateral length scale. In Section 1.1, the derivation of a specific and historically important case of a thermocapillary-driven thin film is carried out from first principles. This derivation is well known, and the purpose of including it in its entirety here is to familiarize the reader with the approach and collect intermediate results that are used in the following section. In Section 1.2, a new non-local thermocapillary thin film equation is derived under the assumption that a thick fluid layer with large conductivity and viscosity lies on top of the thin film. A linear stability analysis is carried out for this new equation, and a limiting case is matched with another model with two thin coupled layers. In Section 1.3, a general form of the thin film equation including various other driving forces and slip effects is noted. There we also discuss the Cahn Hilliard form of these equations and present an algorithmic procedure for finding Lyapunov functionals. Finally, Section 1.4 contains a discussion of the history and literature in the field, with an attempt to place the new research contained in this chapter in a wider context. Readers with little background in thin film literature may prefer to read Section 1.4 first to get an orientation of the history of the field.

1.1 Thermocapillary driven thin films

The spatiotemporal evolution of thin viscous films has been studied for well over a century. The modern formulation to model a wide class of such films utilizes a long wavelength (or lubrication or thin film) approximation of the Navier-Stokes equations that encapsulates this evolution in a small number of nonlinear partial differential equations. In this section, a detailed derivation of one such thermocapillary driven film will be carried out in order to illustrate this thin film limit.

Recent experimental studies have generated interest in the spontaneous generation of nanopillars in heated polymer films, with the promise of technological applications [5–13]. In such experiments, a thin polymer film a few hundreds of nanometers in

thickness is subjected to a temperature gradient, as depicted in Fig. 1.1. The film undergoes an instability which results in the growth of nanopillar structures. Such spontaneously generated, nanoscale patterns are expected to find application in the manufacture of optical and electrical components.

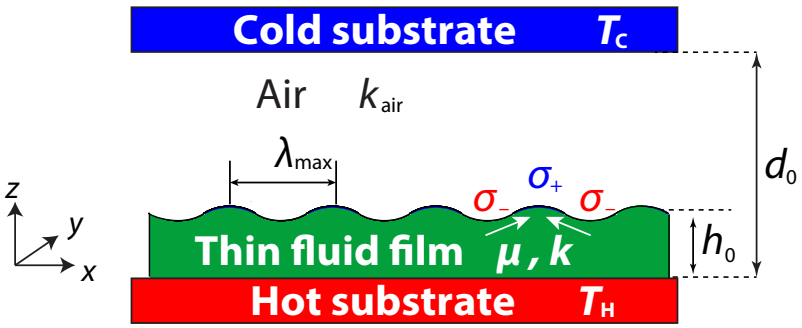

Figure 1.1: A thin fluid film with thickness h_0, viscosity μ, and conductivity k is confined between a hot substrate below at temperature T_H and a cold substrate a distance d_0 above at temperature T_C with a layer of air above it with conductivity k_{air}. Cooler portions of the film have larger surface tension σ which pulls more fluid towards the cold substrate, driving the growth of protrusions.

Protrusions in the fluid film are observed to spontaneously grow at a wavelength $\lambda_{\max} \gg h_0$. It has been proposed [12, 13] that the cause of this instability is variations in the surface tension σ due to changes in temperature in the film – colder portions tend to have higher surface tension which pulls more fluid closer towards the cool substrate. This mechanism of instability has been historically termed the Bénard-Maragoni instability. To model this phenomenon, surface tension is assumed to decrease linearly with the temperature of the interface

$$\sigma(T) = \sigma_0 - \sigma_T(T - T_0), \tag{1.1}$$

where $\sigma_0 = \sigma(T_0)$ is the surface tension at some reference temperature T_0 and $\sigma_T \equiv -\frac{\partial \sigma}{\partial T}$ is positive for most fluids. This description is adequate for many fluids over sufficiently small ranges of temperature, and in particular is a good description of fluids in recent experiments. For the reference temperature, an appropriate choice is the temperature of the flat film of height h_0. In the flat film geometry, the temperature decreases linearly in the thin film from T_H at the hot substrate at $z = 0$ and again linearly in the air gap above the film to T_C at the cold substrate at $z = d_0$. There is a jump in the derivative $\frac{\partial T}{\partial z}$ such that the heat flux is continuous across the film $k \frac{\partial T}{\partial z}\Big|_{z=h_0^-} = k_{\text{air}} \frac{\partial T}{\partial z}\Big|_{z=h_0^+}$. Ensuring continuity of the temperature at the interface

as well, the flat film interface temperature is

$$T_0 = T_C + \frac{(D_0 - 1)(T_H - T_C)}{D_0 + \kappa - 1}, \tag{1.2}$$

where

$$D_0 \equiv \frac{d_0}{h_0} > 1, \quad \kappa \equiv \frac{k_{\text{air}}}{k},$$

are, respectively, the gap width aspect ratio and the ratio of the thermal conductivity of the air to the fluid [13, 14].

To model the film, the fluid is assumed to be incompressible and Newtonian and the viscosity is taken as constant. For nano-scale systems of interest, the Mach numbers are generally quite small so that the incompressible assumption is well justified. On the other hand, the viscosity of polymer melts like those used in experiments is known to be strongly temperature dependent [15]. The constant viscosity assumption is justifiable when the relative changes in the viscosity are small compared to the average value of the viscosity, and this follows when the absolute temperatures are high and when the scale of temperature variations are relatively small. This approximation is better justified for smaller molecular weight polymers, which have smaller viscosity variations with temperature. Furthermore, quantitative inclusions of viscosity variations have not shown major qualitative differences, as dynamical features like growth rates are altered slightly, but geometric features such as the prominent length scale are not significantly changed. Thus for the sake of simplicity, we will assume the fluid's viscosity is constant.

For this derivation, lower case symbols will denote dimensionful quantities while upper case symbols will denote non-dimensional ones where possible. Since the vertical (or surface-normal) scale is significantly smaller than any lateral scale, the vertical Cartesian coordinate z will be treated differently from the lateral Cartesian coordinates $\mathbf{x}_L = (x, y)$. A long wavelength approximation will be developed below to derive a partial differential equation which describes the spatio-temporal evolution of the film height profile, defined by the surface $z = h(\mathbf{x}_L, \bar{t})$, where $\bar{t}$ denotes time. The three-dimensional velocity field of the fluid, $\mathbf{u}_L + u_z\hat{\mathbf{z}}$ is separated into a lateral component, $\mathbf{u}_L$, and a vertical component, $u_z\hat{\mathbf{z}}$, where $\hat{\mathbf{z}}$ is the unit vector normal to the flat film and $\mathbf{u}_L \cdot \hat{\mathbf{z}} = 0$. Similarly, the three-dimensional dimensionful gradient operator ∇ is split into lateral and vertical parts, $\nabla = \bar{\nabla}_L + \frac{\partial}{\partial z}\hat{\mathbf{z}}$, where $\bar{\nabla}_L \equiv \frac{\partial}{\partial x}\hat{\mathbf{x}} + \frac{\partial}{\partial y}\hat{\mathbf{y}}$. The Navier-Stokes equations are likewise divided into lateral and

vertical components

$$\rho\left(\frac{\partial u_z}{\partial \bar{t}} + \left(\mathbf{u}_L \cdot \bar{\nabla}_L\right) u_z + u_z \frac{\partial u_z}{\partial z}\right) = -\frac{\partial p}{\partial z} + \mu\left(\left(\bar{\nabla}_L\right)^2 u_z + \frac{\partial^2 u_z}{\partial z^2}\right), \tag{1.3}$$

$$\rho\left(\frac{\partial \mathbf{u}_L}{\partial \bar{t}} + \left(\mathbf{u}_L \cdot \bar{\nabla}_L\right) \mathbf{u}_L + u_z \frac{\partial \mathbf{u}_L}{\partial z}\right) = -\bar{\nabla}_L p + \mu\left(\left(\bar{\nabla}_L\right)^2 \mathbf{u}_L + \frac{\partial^2 \mathbf{u}_L}{\partial z^2}\right), \tag{1.4}$$

where ρ is the fluid's density, μ the fluid's viscosity, and p the fluid pressure, subject to the continuity equation for an incompressible fluid

$$\bar{\nabla}_L \cdot \mathbf{u}_L + \frac{\partial u_z}{\partial z} = 0. \tag{1.5}$$

For the nano-scale films of interest here, the Bond number is generally very small, and so gravitational body forces have been neglected. On the other hand, the effect of disjoining pressures like van der Waals interactions can be relevant for very small film thicknesses, but will be excluded here for simplicity. Elaborations accounting for such forces are certainly possible, however, and will be discussed later. To solve Eqns. 1.3-1.5, no-slip boundary and impenetrability conditions are taken along the supporting hot substrate

$$u_z|_{z=0} = 0, \quad \mathbf{u}_L|_{z=0} = \mathbf{0}. \tag{1.6}$$

Along the fluid-gas interface, the boundary conditions are the kinematic boundary condition for a free interface,

$$\left(u_z - \mathbf{u}_L \cdot \bar{\nabla}_L h - \frac{\partial h}{\partial \bar{t}}\right)\Big|_{z=h} = 0, \tag{1.7}$$

along with the stress balance condition at the free interface,

$$\left(\mathbf{T}_{\text{air}} - \mathbf{T}\right) \cdot \hat{\mathbf{n}} + \bar{\nabla}_S \sigma - \sigma \hat{\mathbf{n}} \left(\bar{\nabla}_S \cdot \hat{\mathbf{n}}\right)\Big|_{z=h} = 0, \tag{1.8}$$

where $\mathbf{T}$ is the stress tensor in the thin fluid film, $\mathbf{T}_{\text{air}}$ the stress tensor in the air, $\hat{\mathbf{n}}$ is the unit normal vector at the free interface pointing outward from the fluid, and $\bar{\nabla}_S \equiv \left(\bar{\nabla}_L + \hat{\mathbf{z}}\frac{\partial}{\partial z}\right) - \hat{\mathbf{n}}\left(\hat{\mathbf{n}} \cdot \left(\bar{\nabla}_L + \hat{\mathbf{z}}\frac{\partial}{\partial z}\right)\right)$ is the surface gradient operator. The stress tensor in a Newtonian viscous fluid is $\mathbf{T} = 2\mu\mathbf{E} - p\mathbb{I}$, where $\mathbb{I}$ is the identity and $\mathbf{E}$ is the symmetric rate of strain tensor which decomposes into lateral and vertical components as

$$\begin{aligned}\mathbf{E} = \frac{1}{2}\Big(&\bar{\nabla}_L \mathbf{u}_L + \left(\bar{\nabla}_L \mathbf{u}_L\right)^{\mathrm{T}} + 2\frac{\partial u_z}{\partial z}\hat{\mathbf{z}} \otimes \hat{\mathbf{z}} \\ &+ \left(\bar{\nabla}_L u_z + \frac{\partial \mathbf{u}_L}{\partial z}\right) \otimes \hat{\mathbf{z}} + \hat{\mathbf{z}} \otimes \left(\bar{\nabla}_L u_z + \frac{\partial \mathbf{u}_L}{\partial z}\right)\Big),\end{aligned} \tag{1.9}$$

where $\otimes$ is the outer product and the superscript T is the transpose. Equations 1.3-1.9 are simply statements of momentum conservation and some physical assumptions about the fluid properties – standard derivations can be found in fluid mechanics references [16, 17]. The unit normal vector to the surface defined by the level surface $z - h(\mathbf{x}_L) = 0$ is known from basic geometry,

$$\hat{\mathbf{n}} = \frac{\hat{\mathbf{z}} - \bar{\nabla}_L h}{\sqrt{1 + |\bar{\nabla}_L h|^2}}. \tag{1.10}$$

The free interface is considered as a two-dimensional manifold embedded in $\mathbb{R}^3$ and parameterized with coordinates $\mathbf{x}_L$ via $z = h(\mathbf{x}_L, \bar{t})$. The surface quantities σ and $\hat{\mathbf{n}}$ are then regarded as functions of the surface coordinates $\mathbf{x}_L$ and time $\bar{t}$ only. The stress balance conditions on the free interface Eq. 1.8 decompose into a surface normal component and tangential component

$$\left(p - p_0 - 2\mu\hat{\mathbf{n}} \cdot \mathbf{E} \cdot \hat{\mathbf{n}} - \sigma\bar{\nabla}_S \cdot \hat{\mathbf{n}}\right)\Big|_{z=h} = 0, \tag{1.11}$$

$$\left(2\mu\hat{\mathbf{n}} \cdot \mathbf{E} \cdot \hat{\mathbf{t}}_i - \bar{\nabla}_S\sigma \cdot \hat{\mathbf{t}}_i\right)\Big|_{z=h} = 0, \quad i = 1, 2, \tag{1.12}$$

where $\hat{\mathbf{t}}_i$ are tangent vectors to the surface with $\hat{\mathbf{t}}_i \cdot \hat{\mathbf{n}} = 0$ and we have assumed that, aside from a constant pressure p_0 component, the stresses in the air are negligible since the viscosity of the air is relatively small. Tangent vectors are chosen primarily in the $\hat{\mathbf{x}}_1 = \hat{\mathbf{x}}$ and $\hat{\mathbf{x}}_2 = \hat{\mathbf{y}}$ directions,

$$\hat{\mathbf{t}}_i \equiv \frac{\hat{\mathbf{x}}_i + \hat{\mathbf{z}}\bar{\nabla}_L h \cdot \hat{\mathbf{x}}_i}{\sqrt{1 + \left|\bar{\nabla}_L h \cdot \hat{\mathbf{x}}_i\right|^2}}. \tag{1.13}$$

To non-dimensionalize these equations, suitable scales must be specified. The appropriate vertical length scale is the thickness of the the initially flat film h_0, but there is not yet any obvious lateral length scale L. An appropriate scale for L will be determined below. The long wavelength approximation is possible assuming that

$$\epsilon^2 \equiv \frac{h_0^2}{L^2} \ll 1.$$

The appropriate scale for the lateral components of the velocity will be denoted u_c, and will also be specified below, while the appropriate vertical velocity scale is ϵu_c (as determined by requiring the balance of Eq. 1.5). The scale of the variations in pressure is determined by the balance of Eq. 1.4 to be $\mu u_c/\epsilon^2 L$. Lastly, the advective time scale L/u_c is used. Using these scales, the non-dimensionalized variables are

$$\mathbf{X}_L \equiv \frac{\mathbf{x}_L}{L}, \quad Z \equiv \frac{z}{\epsilon L}, \quad \mathbf{U}_L \equiv \frac{\mathbf{u}_L}{u_c}, \quad U_Z \equiv \frac{u_z}{\epsilon u_c}, \quad t \equiv \frac{\bar{t}}{L/u_c}, \quad P \equiv \frac{p - p_0}{(\mu u_c/\epsilon^2 L)}.$$

The components of $\mathbf{X}_L$ will be called either (X, Y) or $\left(X^1, X^2\right)$ depending on the context, and lateral gradient will be denoted $\nabla_L = \hat{\mathbf{x}}\frac{\partial}{\partial X} + \hat{\mathbf{y}}\frac{\partial}{\partial Y}$. Defining the Reynolds' number $\mathrm{Re}_h = \epsilon\rho u_c L/\mu = \rho u_c h_0/\mu$, the non-dimensionalized Navier-Stokes and continuity equations Eqns. 1.3-1.5 are

$$\frac{\partial P}{\partial Z} = -\epsilon^3 \mathrm{Re}_h \left(\frac{\partial U_Z}{\partial t} + (\mathbf{U}_L \cdot \nabla_L)U_Z + U_Z\frac{\partial U_Z}{\partial Z}\right) + \epsilon^4\nabla_L^2 U_Z + \epsilon^2\frac{\partial^2 U_Z}{\partial Z^2},$$
$$\frac{\partial^2 \mathbf{U}_L}{\partial Z^2} - \nabla_L P = \epsilon\mathrm{Re}_h \left(\frac{\partial \mathbf{U}_L}{\partial t} + (\mathbf{U}_L \cdot \nabla_L)\mathbf{U}_L + U_Z\frac{\partial \mathbf{U}_L}{\partial Z}\right) - \epsilon^2\nabla_L^2\mathbf{U}_L,$$
$$\nabla_L \cdot \mathbf{U}_L + \frac{\partial U_Z}{\partial Z} = 0.$$

Assuming $\epsilon^2 \ll 1$ and $\epsilon\mathrm{Re}_h \ll 1$, we neglect the remainders on the right hand side and the thin film (or lubrication or long-wavelength) approximation results

$$\frac{\partial P}{\partial Z} = 0, \tag{1.14}$$
$$\frac{\partial^2 \mathbf{U}_L}{\partial Z^2} - \nabla_L P = 0, \tag{1.15}$$
$$\nabla_L \cdot \mathbf{U}_L + \frac{\partial U_Z}{\partial Z} = 0. \tag{1.16}$$

To solve Eqns. 1.14-1.16, the boundary conditions Eq. 1.6, Eq. 1.11, and Eq. 1.12 must also be non-dimensionalized. There are two natural scales for the surface tension: σ_0, the surface tension of the initially flat film with height $h = h_0$, and $\sigma_T(T_H - T_0)$, a characteristic scale for changes in the surface tension due to changes in temperature in the fluid, where T_0 is the reference flat film temperature in Eq. 1.2. The film height, temperature, and surface tension are then non-dimensionalized as

$$H \equiv \frac{h}{h_0}, \quad \Theta \equiv \frac{T - T_0}{T_H - T_0}, \quad \Sigma \equiv \frac{\sigma - \sigma_0}{\sigma_T(T_H - T_0)}. \tag{1.17}$$

Define the non-dimensional thin film capillary and Marangoni numbers

$$\bar{\mathrm{Ca}} \equiv \frac{\mu u_c}{\epsilon^3\sigma_0}, \quad \bar{\mathrm{Ma}} \equiv \frac{\epsilon\sigma_T(T_H - T_0)}{\mu u_c}.$$

Multiplying Eq. 1.11 by $\epsilon^2 L/\mu u_c$, the non-dimensional normal stress balance is

$$\begin{aligned} P + \bar{\mathrm{Ca}}^{-1}\nabla_L^2 H = {} & \frac{\epsilon^2}{1 + \epsilon^2|\nabla_L H|^2}\Big(- 2\frac{\partial \mathbf{U}_L}{\partial Z} \cdot \nabla_L H - 2\epsilon^2 \nabla_L U_Z \cdot \nabla_L H + 2\frac{\partial U_Z}{\partial Z} \\ & + \epsilon^2 \nabla_L H \cdot ((\nabla_L \mathbf{U}_L) + (\nabla_L \mathbf{U}_L)^{\mathrm{T}}) \cdot \nabla_L H\Big) \\ & + \bar{\mathrm{Ca}}^{-1}\left(\left(1 - \frac{1}{\sqrt{1 + \epsilon^2|\nabla_L H|^2}}\right)\nabla_L^2 H + \epsilon^2\frac{\nabla_L H \cdot \nabla_L |\nabla_L H|^2}{2(1 + \epsilon^2|\nabla_L H|^2)^{(3/2)}}\right) \\ & - \epsilon^2\bar{\mathrm{Ma}}\left(\frac{\nabla_L^2 H}{\sqrt{1 + \epsilon^2|\nabla_L H|^2}} - \epsilon^2\frac{\nabla_L H \cdot \nabla_L |\nabla_L H|^2}{2(1 + \epsilon^2|\nabla_L H|^2)^{(3/2)}}\right)\Sigma. \end{aligned} \tag{1.18}$$

In a similar fashion, multiplying Eq. 1.12 by $\epsilon L/\mu u_c$ non-dimensionalizes to

$$\frac{\partial \mathbf{U}_L}{\partial Z} - \bar{\mathrm{Ma}}\nabla_L\Sigma = -\epsilon^2 \cdot \left(\nabla_L U_Z + 2\frac{\partial U_Z}{\partial Z}\nabla_L H - \left(\frac{\partial \mathbf{U}_L}{\partial Z}\cdot\nabla_L H\right)\nabla_L H \right.$$
$$\left. - \left(\nabla_L \mathbf{U}_L + (\nabla_L \mathbf{U}_L)^{\mathrm{T}}\right)\cdot\nabla_L H - \epsilon^2\left(\nabla_L U_Z \cdot \nabla_L H\right)\nabla_L H\right)$$
$$+ \bar{\mathrm{Ma}}\left(\sqrt{1+\epsilon^2|\nabla_L H|^2} - 1\right)\nabla_L\Sigma. \tag{1.19}$$

Keeping only the leading order capillary and Marangoni terms, Eqns. 1.6-1.7 and Eqns. 1.11-1.12 non-dimensionalize to

$$U_Z|_{Z=0} = 0, \quad \mathbf{U}_L|_{Z=0} = \mathbf{0}, \tag{1.20}$$
$$\left(P + \bar{\mathrm{Ca}}^{-1}\nabla_L^2 H\right)\Big|_{Z=H} = 0, \tag{1.21}$$
$$\left(\frac{\partial \mathbf{U}_L}{\partial Z} - \bar{\mathrm{Ma}}\nabla_L\Sigma\right)\Big|_{Z=H} = 0, \tag{1.22}$$
$$\left(U_Z - \mathbf{U}_L\cdot\nabla_L H - \frac{\partial H}{\partial t}\right)\Big|_{Z=H} = 0. \tag{1.23}$$

Now Eqns. 1.14-1.16 are integrated with respect to Z, applying Eq. 1.20 to find

$$\mathbf{U}_L = \frac{Z^2}{2}\nabla_L P + Z\mathbf{A}, \tag{1.24}$$
$$U_Z = -\frac{Z^3}{6}\nabla_L^2 P - \frac{Z^2}{2}\nabla_L\cdot\mathbf{A}, \tag{1.25}$$
$$P = B, \tag{1.26}$$

where $\mathbf{A}$ and B are integration constants depending only on $\mathbf{X}_L$ and not Z. The integration constant B is eliminated using Eq. 1.21

$$B = -\bar{\mathrm{Ca}}\nabla_L^2 H,$$

while the integration constant $\mathbf{A}$ is eliminated using Eq. 1.22

$$\mathbf{A} = \left(\bar{\mathrm{Ca}}^{-1} H\nabla_L\nabla_L^2 H + \bar{\mathrm{Ma}}\nabla_L\Sigma\right). \tag{1.27}$$

Substituting Eqns. 1.24-1.27 into the final, kinematic boundary condition Eq. 1.23 and simplifying a bit yields the partial differential equation

$$\frac{\partial H}{\partial t} + \nabla_L\cdot\left(\bar{\mathrm{Ma}}\frac{H^2}{2}\nabla_L\Sigma + \bar{\mathrm{Ca}}^{-1}\frac{H^3}{3}\nabla_L\nabla_L^2 H\right) = 0. \tag{1.28}$$

The heat transport in the thin film is governed by

$$\rho c\left(\frac{\partial T}{\partial \bar{t}}+\mathbf{u}_L\cdot\bar{\nabla}_L T+u_z\frac{\partial T}{\partial z}\right)=k\left(\bar{\nabla}_L^2 T+\frac{\partial^2 T}{\partial z^2}\right), \tag{1.29}$$

with $T|_{z=0}=T_H$, where c is the heat capacity in the thin fluid film. On non-dimensionalization, the thin film temperature Péclet number $\bar{\mathrm{Pe}}_T=\epsilon^2 L u_c\rho c/k$ arises, and we assume that $\bar{\mathrm{Pe}}_T\ll 1$. Under this approximation, heat is transferred through the film strictly conductively with other convective and radiative effects negligible. Under the assumption that the Péclet number in the air layer is also small, the heat transport in the air layer is identical to that in the fluid layer with the appropriate modifications of the boundary condition $T|_{z=d_0}=T_C$, density, heat capacity, and conductivity, and the final leading order non-dimensional equations are

$$\begin{aligned}&\frac{\partial^2\Theta}{\partial Z^2}=0,\quad \Theta|_{Z=0}=1 \text{ for } Z<H,\\ &\frac{\partial^2\Theta}{\partial Z^2}=0,\quad \Theta|_{Z=D_0}=-\frac{D_0-1}{\kappa} \text{ for } Z>H.\end{aligned}$$

This is easily integrated with respect to Z to give the temperature in terms of two integration constants C and C_{air} which depend only on $\mathbf{X}_L$,

$$\begin{aligned}&\Theta=1+CZ \text{ for } Z<H,\\ &\Theta=-\frac{D_0-1}{\kappa}+C_{\text{air}}\left(Z-D_0\right) \text{ for } Z>H,\end{aligned} \tag{1.30}$$

These two layers are coupled together with boundary conditions that ensure continuity of temperature and the normal component of the heat flux across the interface,

$$T|_{z\to h^-}=T|_{z\to h^+},\quad k\left(\bar{\nabla}_L T+\hat{\mathbf{z}}\frac{\partial T}{\partial z}\right)\cdot\hat{\mathbf{n}}\bigg|_{z\to h^-}=k_{\text{air}}\left(\bar{\nabla}_L T+\hat{\mathbf{z}}\frac{\partial T}{\partial z}\right)\cdot\hat{\mathbf{n}}\bigg|_{z\to h^+},$$

which non-dimensionalize to leading order to

$$\Theta|_{Z\to H^-}=\Theta|_{Z\to H^+},\quad \left.\frac{\partial\Theta}{\partial Z}\right|_{Z\to H^-}=\kappa\left.\frac{\partial\Theta}{\partial Z}\right|_{Z\to H^+}. \tag{1.31}$$

Inserting Eq. 1.30 into Eq. 1.31 and solving for C and C_{air} yields

$$C=-\frac{D_0+\kappa-1}{\kappa(D_0+(\kappa-1)H)},\qquad C_{\text{air}}=-\frac{D_0+\kappa-1}{D_0+(\kappa-1)H}. \tag{1.32}$$

In order to relate Σ to H, Eq. 1.1 non-dimensionalizes to $\Sigma=-\Theta|_{Z=H}$. Using Eq. 1.30 and Eq. 1.32, the surface tension is

$$\Sigma=-\Theta|_{Z=H}=-1+\frac{\left(D_0+\kappa-1\right)H}{D_0+(\kappa-1)H}. \tag{1.33}$$

Substituting Eq. 1.33 into Eq. 1.28 results in

$$\frac{\partial H}{\partial t} + \nabla_L \cdot \left(\bar{\mathrm{Ma}} \frac{D_0(D_0+\kappa-1)}{(D_0+(\kappa-1)H)^2} \frac{H^2}{2} \nabla_L H + \bar{\mathrm{Ca}}^{-1} \frac{H^3}{3} \nabla_L \nabla_L^2 H \right) = 0. \tag{1.34}$$

Note at this point that two non-dimensional groups $\bar{\mathrm{Ma}}$ and $\bar{\mathrm{Ca}}$ appear in Eq. 1.34, while the two scales L and u_c on which these non-dimensional groups depend have not yet been specified. In order for the scales to be appropriate, each contribution in Eq. 1.34 and in Eqns. 1.24-1.25 must be $O(1)$. The remaining scales can be specified by the following choices for the non-dimensional groups

$$\bar{\mathrm{Ma}} = \frac{D_0+\kappa-1}{D_0}, \quad \bar{\mathrm{Ca}} = \frac{3}{(4\pi)^2}. \tag{1.35}$$

These particular choices follow [13], and they ensure that the non-dimensional wavelength of the fastest growing unstable mode $\lambda_{\max}/L$ is 1 and that the growth rate of the fastest growing unstable mode is π^2. This is appropriate because these length and time scales are the most relevant one during the development of the instability. This length scale is a thermocapillary one determined by a balance between the Marangoni and capillary contributions. Note also that the factors of D_0 and κ in Eqns. 1.34-1.35 collapse into a single non-dimensional number

$$\chi \equiv \frac{\kappa-1}{D_0}.$$

This number is closely related to the two layer Biot number $F = -\chi/(1+\chi)$ defined by Van Hook [14], and encodes information about how heat is transported through the air layer above the film. While $\chi < 0$ usually holds for confined films, $\chi > 0$ gives an appropriate description for unconfined fluid films with convective rather than conductive boundary conditions. Furthermore, there is yet another inequality $\chi > -1$ which always holds. When expressed in terms of u_c and L, Eq. 1.35 can be written

$$u_c \equiv \left(\frac{3}{(4\pi)^2}\right)^{1/2} (1+\chi)^{-3/2} \left(\frac{\sigma_0}{\mu}\right)^{-1/2} \left(\frac{\sigma_T(T_H-T_0)}{\mu}\right)^{3/2},$$
$$L \equiv \left(\frac{3}{(4\pi)^2}\right)^{-1/2} (1+\chi)^{1/2} \left(\frac{\sigma_T(T_H-T_0)}{\sigma_0}\right)^{-1/2} h_0.$$

Given typical values of σ_T, σ_0, μ, $T_H - T_0$, and χ used in previous experiments, it is easy to verify that all the remainders that were neglected above are indeed much smaller than one, so that we can have some confidence in our approximations. Note, however, that the key assumption $\epsilon^2 = h_0^2/L^2 \ll 1$ depends crucially on the ratio

$\sigma_T(T_H - T_0)/\sigma_0$. The thin film approximation will not be possible unless the applied temperature gradient is sufficiently small. Fortunately, this restriction is usually not severe, because the variations in surface tension are typically small compared to the mean surface tension over relevant temperature ranges. Using Eq. 1.35 the thin film equation Eq. 1.34 in terms of χ is

$$\frac{\partial H}{\partial t} + \nabla_L \cdot \left(\left(\frac{1+\chi}{1+\chi H} \right)^2 \frac{H^2}{2} \nabla_L H + \frac{H^3}{(4\pi)^2} \nabla_L \nabla_L^2 H \right) = 0. \tag{1.36}$$

Qualitative features and Lyapunov energy

Note that Eq. 1.36 is a local conservation equation - changes in the film height H are directly related to the divergence of a volumetric flux

$$\mathbf{Q}_L \equiv \left(\frac{1+\chi}{1+\chi H} \right)^2 \frac{H^2}{2} \nabla_L H + \frac{H^3}{(4\pi)^2} \nabla_L \nabla_L^2 H.$$

This is simply a reflection of the mass conservation equation for an incompressible fluid, so that the total volume

$$\mathscr{V}[H] \equiv \int \mathrm{d}^2 X \; H(\mathbf{X}_L, t)$$

is dynamically conserved, $\frac{d\mathscr{V}}{dt} = 0$. Next, note that the first two terms in Eq. 1.36 resemble a nonlinear diffusion equation with density variable H and diffusion coefficient $-\left(\frac{1+\chi}{1+\chi H}\right)^2 \frac{H^2}{2}$. Since the diffusion coefficient is negative, this thermocapillary term drives H like a diffusion process operating in reverse, leading to fluid accumulation. This is the source of the instability of flat film profiles. The capillary term, which does not have a diffusive analog since it involves higher order spatial derivatives, acts qualitatively to oppose highly curved interfaces and thereby promotes flattening. Backwards diffusion alone leads to blow up of solutions in finite time, but the addition of the capillary term makes a balance between the two possible which can prevent blow up.

Motivated by the similarity with diffusive problems such as the problem of spinodal decomposition, Oron and Rosenau [18, 19] derived a Lyapunov energy functional by analogy with the Cahn Hilliard equation [20]. They cast the thin film equation into a variational form, which greatly simplifies the stability analysis of steady states. This variational structure follows whenever some evolution equation can be expressed in the form

$$\frac{\partial H}{\partial t} - \nabla_L \cdot \left(Q_1(H) \nabla_L \frac{\delta F}{\delta H} \right) = 0, \tag{1.37}$$

where $Q_1(H) \geq 0$ is some positive mobility function, $F = F[H]$ is a functional of H and its spatial derivatives, and $\frac{\delta}{\delta H}$ is the functional derivative with respect to H. Recall that the functional derivative is found by comparing $F[H]$ and $F[H + \delta H]$ for infinitesimal functional perturbations δH. For example, when $F[H] = \int \mathrm{d}^2X\ \mathcal{F}(H, \nabla_L H)$, it follows that $\frac{\delta F}{\delta H} = \frac{\partial \mathcal{F}}{\partial H} - \nabla_L \cdot \frac{\partial \mathcal{F}}{\partial \nabla_L H}$, which is the familiar Euler operator appearing in the Euler-Lagrange equations. Assume that the domain of support of the fluid is infinite and that boundary terms that arise from integration by parts vanish identically, e.g. by taking periodic boundary conditions. After using Eq. 1.37 and integrating by parts, a functional version of the chain rule, $\frac{dF}{dt} = \int \mathrm{d}^2X\ \frac{\delta F}{\delta H}\frac{\partial H}{\partial t}$, yields

$$\frac{dF}{dt} = \int \mathrm{d}^2X\ \frac{\delta F}{\delta H}\nabla_L \cdot \left(Q_1(H)\nabla_L \frac{\delta F}{\delta H}\right) = -\int \mathrm{d}^2X Q_1(H)\left|\nabla_L \frac{\delta F}{\delta H}\right|^2 \leq 0,$$

where the final inequality follows because $Q_1(H) \geq 0$. When a functional which never increases as time increases can be found, it is termed a Lyapunov function or energy, and its existence can be helpful in establishing the stability of steady state solutions. The existence of a Lyapunov function fundamentally reflects that a system undergoes irreversible processes during its evolution.

In the specific case of Eq. 1.36, take $Q_1(H) = \frac{H^3}{(4\pi)^2}$ and

$$F[H] \equiv \int \mathrm{d}^2X\ \mathcal{F}\ (H, \nabla_L H) \tag{1.38}$$
$$\mathcal{F}\ (H, \nabla_L H) \equiv \frac{1}{2}|\nabla_L H|^2 - \frac{(4\pi)^2}{2}(1+\chi)^2 H \log\frac{H}{1+\chi H},$$

which defines a Cahn-Hilliard Lyapunov energy. From this definition, it follows that

$$\begin{aligned} Q_1(H)\nabla_L \frac{\delta F}{\delta H} &= -\frac{H^3}{(4\pi)^2}\nabla_L\left(\nabla_L^2 H + \frac{(4\pi)^2}{2}(1+\chi)^2\left(\log\frac{H}{1+\chi H} + \frac{1}{1+\chi H}\right)\right) \\ &= -\left(\frac{H^3}{(4\pi)^2}\nabla_L\nabla_L^2 H + \left(\frac{1+\chi}{1+\chi H}\right)^2 \frac{H^2}{2}\nabla_L H\right). \end{aligned}$$

Thus Eq. 1.36 is indeed of the form of Eq. 1.37. Although the term Lyapunov energy is used, the functional in Eq. 1.38 does not have any obvious relationship with the physical conserved energy or a thermodynamic free energy. The first capillary term in Eq. 1.38 does resemble the expected energy for a surface tension, but the second Marangoni term does not have an obvious energetic interpretation. The hot and cold substrates are two heat baths which continuously exchange heat through the film, and so thermodynamic entropy is constantly decreasing and the entire system

is not in thermodynamic equilibrium. There does not exist a general free-energy description for such non-equilibrium systems, and the fact that such a Lyapunov energy exists for this hydrodynamic system is something of a mystery.

1.2 A non-local equation for a thin film coupled to a thick viscous layer

Several different geometries and models of heat transport have been considered for the thermocapillary driven thin film. The earliest models considered only a single fluid layer and used simplified models for heat transport away from the film [21–23]. The equation described above was based on a two layer model in which the layer above the fluid film is an inviscid, conductive fluid [13, 14]. A more recent and elaborate model of Merkt et al. [24] treats both layers as thin viscous and conductive fluids. Here we consider a new regime in which the relative thickness of the two films differs significantly, as depicted in Fig. 1.2.

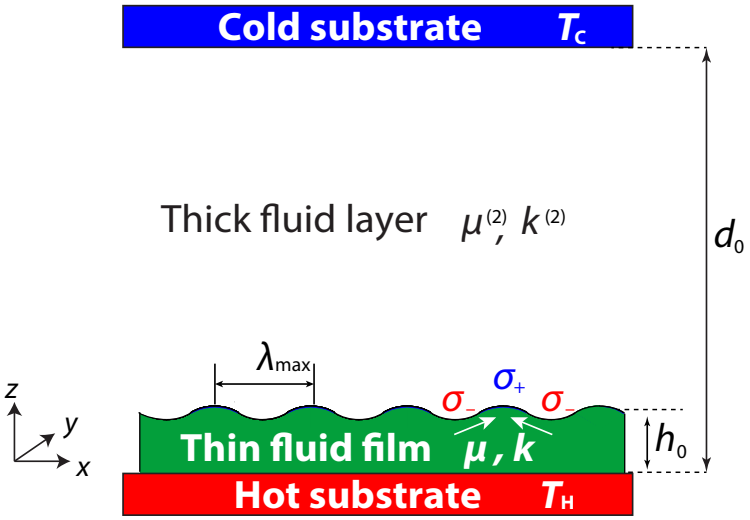

Figure 1.2: A thin fluid film with thickness h_0, viscosity μ, and conductivity k is confined between a hot substrate below at temperature T_H and a cold substrate a distance d_0 above at temperature T_C with a thick layer of viscous fluid above it with viscosity $\mu^{(2)}$ and conductivity $k^{(2)}$. Cooler portions of the film have larger surface tension σ which pull more fluid towards the cold substrate, driving the growth of protrusions.

Let the density, viscosity, and conductivity of the thick layer fluid be denoted $\rho^{(2)}$, $\mu^{(2)}$ and $k^{(2)}$. Similarly, let the lateral and vertical fluid velocity in the thick layer be denoted $\mathbf{u}_L^{(2)}$ and $u_z^{(2)}$ and let the temperature and pressure in the thick layer fluid be denoted $T^{(2)}$ and $p^{(2)}$. Under the assumption that the viscosities and conductivities of the thick layer are smaller or comparable to those of the thin layer, the momentum and temperature gradients at the film interface in the thick layer are much smaller

than those in the thin layer and the resulting surface forces become negligible, so that one of the previous models in the literature is appropriate. However, under the assumption that $\mu^{(2)} \gg \mu$ and $k^{(2)} \gg k$, all surface forces may be relevant and more interesting equations result. In particular, there is a qualitative difference in the transport in the thick layer since gradients can be large in both the lateral and surface normal directions, as depicted in Fig. 1.3. As we will show later, the resulting film evolution equation must be non-local to account for such processes, unlike all the previous models described here. The relevant non-dimensional numbers for this derivation are

$$\bar{\mu} \equiv \epsilon \frac{\mu^{(2)}}{\mu}, \quad \bar{k} \equiv \epsilon \frac{k^{(2)}}{k}, \quad \bar{D}_0 \equiv \epsilon \frac{d_0}{h_0},$$

which will all be assumed to be $O(1)$. The unperturbed film temperature from Eq. 1.2 is, to leading order,

$$\bar{T}_0 \equiv T_C + \frac{\bar{D}_0 (T_H - T_C)}{\bar{D}_0 + \bar{k}}, \tag{1.39}$$

and the surface tension again is assumed to decrease linearly with temperature

$$\sigma = \sigma_0 - \sigma_T (T - \bar{T}_0). \tag{1.40}$$

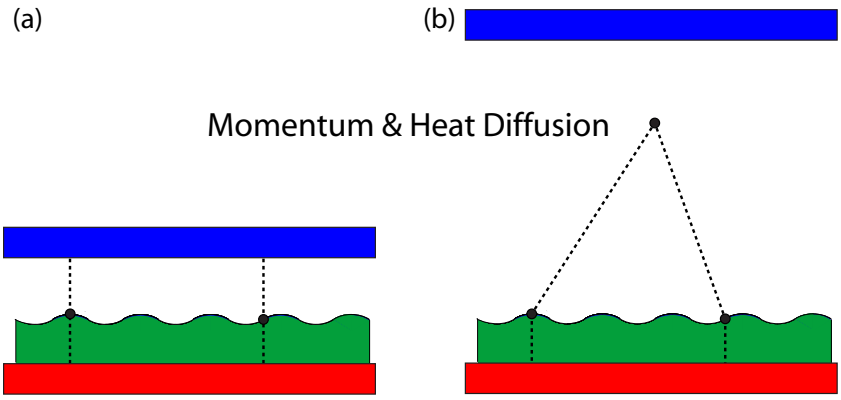

Figure 1.3: Diffusion of heat and momentum in bilayer of differing thickness. (a) In two thin layers, the diffusion is dominated by the gradients normal to the film and coupling between surface points only occurs through derivatives of the film thickness. (b) When a thick layer is present, lateral heat and momentum diffusion couples far away surface points leading to a non-local film equation.

In the thick layer, the transport of momentum is governed by the Navier-Stokes

equations,

$$\rho^{(2)}\left(\frac{\partial u_z^{(2)}}{\partial \bar{t}} + \left(\mathbf{u}_L^{(2)} \cdot \bar{\nabla}_L\right) u_z^{(2)} + u_z^{(2)} \frac{\partial u_z^{(2)}}{\partial z}\right) = -\frac{\partial p^{(2)}}{\partial z} + \mu^{(2)}\left(\left(\bar{\nabla}_L\right)^2 u_z^{(2)} + \frac{\partial^2 u_z^{(2)}}{\partial z^2}\right),$$

$$\rho^{(2)}\left(\frac{\partial \mathbf{u}_L^{(2)}}{\partial \bar{t}} + \left(\mathbf{u}_L^{(2)} \cdot \bar{\nabla}_L\right) \mathbf{u}_L^{(2)} + u_z \frac{\partial \mathbf{u}_L^{(2)}}{\partial z}\right) = -\bar{\nabla}_L p^{(2)} + \mu^{(2)}\left(\left(\bar{\nabla}_L\right)^2 \mathbf{u}_L^{(2)} + \frac{\partial^2 \mathbf{u}_L^{(2)}}{\partial z^2}\right).$$

Furthermore, we assume the this layer fluid is incompressible,

$$\bar{\nabla}_L \cdot \mathbf{u}_L^{(2)} + \frac{\partial u_z^{(2)}}{\partial z} = 0.$$

No slip boundary conditions are specified at the cool substrate,

$$u_z^{(2)}\Big|_{z=d_0} = 0, \quad \mathbf{u}_L^{(2)}\Big|_{z=d_0} = \mathbf{0}.$$

The same non-dimensional lateral coordinates $\mathbf{X}_L$ and the same non-dimensional time t are used in both layers. The same lateral velocity scale u_c and lateral length scale L as in the thin layer are used to define thick layer scales

$$Z^{(2)} \equiv \frac{z}{L}, \quad \mathbf{U}_L^{(2)} \equiv \frac{\mathbf{u}_L^{(2)}}{u_c}, \quad U_Z^{(2)} \equiv \frac{u_z^{(2)}}{u_c}, \quad P^{(2)} \equiv \frac{p^{(2)} - p_0}{(\mu^{(2)} u_c / L)}.$$

Assuming that the thick layer Reynolds' number is small $\mathrm{Re}^{(2)} \equiv \rho^{(2)} L u_c / \mu^{(2)} \ll 1$, the leading order non-dimensional thick layer momentum transport and continuity equations are

$$\begin{aligned}
\nabla_L^2 \mathbf{U}_L^{(2)} + \frac{\partial \mathbf{U}_L^{(2)}}{\partial Z^{(2)}} - \nabla_L P^{(2)} &= 0, \\
\nabla_L^2 U_Z^{(2)} + \frac{\partial U_Z^{(2)}}{\partial Z^{(2)}} - \frac{\partial P^{(2)}}{\partial Z^{(2)}} &= 0, \\
\nabla_L \cdot \mathbf{U}_L^{(2)} + \frac{\partial U_Z^{(2)}}{\partial Z^{(2)}} &= 0.
\end{aligned} \tag{1.41}$$

Unlike the leading order equations in the thin film in Eqns. 1.14-1.16, real space integration of the thick layer momentum equations is not possible. Given the lateral translational invariance of the problem, taking the Fourier transform in the $\mathbf{X}_L$ variables is a good first step. Let the Fourier transforms be denoted

$$\begin{aligned}
\mathbf{U}_L^{(2)} &= \int \frac{\mathrm{d}^2 q}{(2\pi)^2} \, \mathrm{e}^{i\mathbf{q}\cdot\mathbf{X}_L} \left(-\frac{i\mathbf{q}}{q^2}\tilde{U}_1 - \frac{i\,(\star\mathbf{q})}{q^2}\tilde{U}_2\right), \\
U_Z^{(2)} &= \int \frac{\mathrm{d}^2 q}{(2\pi)^2} \, \mathrm{e}^{i\mathbf{q}\cdot\mathbf{X}_L} \tilde{U}_Z, \\
P^{(2)} &= \int \frac{\mathrm{d}^2 q}{(2\pi)^2} \, \mathrm{e}^{i\mathbf{q}\cdot\mathbf{X}_L} \tilde{P}.
\end{aligned}$$

The linear operator $\star$ is the dual two-dimensional vector, defined by its action on the basis vectors $\star\hat{\mathbf{x}} = -\hat{\mathbf{y}}$ and $\star\hat{\mathbf{y}} = \hat{\mathbf{x}}$. Given any nonzero vector $\mathbf{q}$, that vector $\mathbf{q}$ and its dual $\star\mathbf{q}$ can serve as an orthogonal basis for the two-dimensional vector space, and vectors will often be decomposed this way. This operator is related to the Hodge dual of differential geometry. Taking the divergence $\nabla_L \cdot$ and the dual divergence $\star\nabla_L \cdot$ of the first equation in Eq. 1.41 and then taking the Fourier transform, the thick layer momentum transport equations are

$$\begin{aligned} -q^2\tilde{U}_1 + \frac{\partial^2 \tilde{U}_1}{\partial (Z^{(2)})^2} + q^2\tilde{P} &= 0, \\ -q^2\tilde{U}_2 + \frac{\partial^2 \tilde{U}_2}{\partial (Z^{(2)})^2} &= 0, \\ -q^2\tilde{U}_Z + \frac{\partial^2 \tilde{U}_Z}{\partial (Z^{(2)})^2} - \frac{\partial \tilde{P}}{\partial Z^{(2)}} &= 0, \\ \tilde{U}_1 + \frac{\partial \tilde{U}_Z}{\partial Z^{(2)}} &= 0. \end{aligned} \tag{1.42}$$

Using the first and fourth equations in Eq. 1.42 to eliminate $\tilde{U}_1$ and $\tilde{P}$ in favor of $\tilde{U}_Z$ in the third equation gives a fourth order ordinary differential equation governing $\tilde{U}_Z$,

$$q^4\tilde{U}_Z - 2q^2\frac{\partial^2 \tilde{U}_Z}{\partial (Z^{(2)})^2} + \frac{\partial^4 \tilde{U}_Z}{\partial (Z^{(2)})^4} = 0.$$

Combined with the second order ordinary differential equation in the second line in Eq. 1.42, the equations can be solved in terms of six integration constants. Choosing these constants to be encoded in two two-dimensional vectors $\mathbf{a}$ and $\mathbf{b}$ and two scalars a_Z and b_Z, the solution can be written

$$\begin{aligned} \mathbf{U}_L^{(2)} = \int \frac{\mathrm{d}^2 q}{(2\pi)^2}\, \mathrm{e}^{i\mathbf{q}\cdot\mathbf{X}_L} \Bigg(& \left(\mathbf{a} - \frac{i\mathbf{q}}{q}\left(qa_Z + i\mathbf{q}\cdot\mathbf{b}\right)\left(Z^{(2)} - \bar{D}_0\right)\right)\cosh\left(q\left(Z^{(2)} - \bar{D}_0\right)\right) \\ & + \left(\mathbf{b} - \frac{i\mathbf{q}}{q}\left(qb_Z + i\mathbf{q}\cdot\mathbf{a}\right)\left(Z^{(2)} - \bar{D}_0\right)\right)\sinh\left(q\left(Z^{(2)} - \bar{D}_0\right)\right)\Bigg), \\ U_Z^{(2)} = \int \frac{\mathrm{d}^2 q}{(2\pi)^2}\, \mathrm{e}^{i\mathbf{q}\cdot\mathbf{X}_L} \Bigg(& \left(a_Z - \left(qb_Z + i\mathbf{q}\cdot\mathbf{a}\right)\left(Z^{(2)} - \bar{D}_0\right)\right)\cosh\left(q\left(Z^{(2)} - \bar{D}_0\right)\right) \\ & + \left(b_Z - \left(qa_Z + i\mathbf{q}\cdot\mathbf{b}\right)\left(Z^{(2)} - \bar{D}_0\right)\right)\sinh\left(q\left(Z^{(2)} - \bar{D}_0\right)\right)\Bigg), \\ P^{(2)} = \int \frac{\mathrm{d}^2 q}{(2\pi)^2}\, \mathrm{e}^{i\mathbf{q}\cdot\mathbf{X}_L} \Bigg(& \left(qa_Z + i\mathbf{q}\cdot\mathbf{b}\right)\cosh\left(q\left(Z^{(2)} - \bar{D}_0\right)\right) \\ & + \left(qb_Z + i\mathbf{q}\cdot\mathbf{a}\right)\sinh\left(q\left(Z^{(2)} - \bar{D}_0\right)\right)\Bigg). \end{aligned} \tag{1.43}$$

In the thin film, the lubrication approximation can be made in the bulk as in the previous section. In particular, the solution in Eqns. 1.24-1.26, repeated here for convenience, remain valid

$$\begin{aligned}\mathbf{U}_L &= \frac{Z^2}{2}\nabla_L P + Z\mathbf{A},\\ U_Z &= -\frac{Z^3}{6}\nabla_L^2 P - \frac{Z^2}{2}\nabla_L\cdot\mathbf{A},\\ P &= B.\end{aligned} \tag{1.44}$$

The nine integration constant $\mathbf{a}$, $\mathbf{b}$, a_Z, b_Z, $\mathbf{A}$ and B must next be eliminated using appropriate boundary conditions. First the no-slip boundary condition on the cold substrate requires $\mathbf{U}_L^{(2)}\big|_{Z^{(2)}=\bar{D}_0} = \mathbf{0}$ and $U_Z^{(2)}\big|_{Z^{(2)}=\bar{D}_0} = 0$, which implies

$$\mathbf{a} = \mathbf{0} \;\text{ and }\; a_Z = 0. \tag{1.45}$$

Next is continuity of the velocity at the interface

$$\mathbf{U}_L|_{Z=H} = \mathbf{U}_L^{(2)}\big|_{Z^{(2)}=\epsilon H}, \qquad \epsilon\, U_Z|_{Z=H} = U_Z^{(2)}\big|_{Z^{(2)}=\epsilon H}.$$

Defining

$$\tilde{\mathbf{A}} \equiv H\mathbf{A} + \frac{1}{2}H^2\nabla_L B \tag{1.46}$$

and inserting Eq. 1.43 and Eq. 1.44 into the velocity continuity boundary condition, the equations are solved for $\mathbf{b} = \frac{\mathbf{q}}{q^2}\mathbf{q}\cdot\mathbf{b} + \frac{\star\mathbf{q}}{q^2}(\star\mathbf{q})\cdot\mathbf{b}$ and b_Z to zeroth order in ϵ,

$$\begin{aligned} b_Z &= \frac{i\bar{D}_0\sinh\left(q\bar{D}_0\right)}{\sinh\left(q\bar{D}_0\right) - q^2\bar{D}_0^2}\int \mathrm{d}^2X\; \mathrm{e}^{-i\mathbf{q}\cdot\mathbf{X}_L}\mathbf{q}\cdot\tilde{\mathbf{A}},\\ \mathbf{q}\cdot\mathbf{b} &= \frac{q\bar{D}_0\cosh\left(q\bar{D}_0\right) - \sinh\left(q\bar{D}_0\right)}{\sinh\left(q\bar{D}_0\right) - q^2\bar{D}_0^2}\int \mathrm{d}^2X\; \mathrm{e}^{-i\mathbf{q}\cdot\mathbf{X}_L}\mathbf{q}\cdot\tilde{\mathbf{A}},\\ (\star\mathbf{q})\cdot\mathbf{b} &= -\frac{1}{\sinh\left(q\bar{D}_0\right)}\int \mathrm{d}^2X\; \mathrm{e}^{-i\mathbf{q}\cdot\mathbf{X}_L}(\star\mathbf{q})\cdot\tilde{\mathbf{A}}. \end{aligned} \tag{1.47}$$

The stress balance conditions at the interface require slight modification of the results in Eqns. 1.21-1.22. The terms on the left hand sides of those equations remain leading order, but in addition we must check any contributions $\hat{\mathbf{n}}\cdot\mathbf{T}^{(2)}$ in Eqns. 1.11-1.12 from the thick layer stress tensor $\mathbf{T}^{(2)} = 2\mu^{(2)}\mathbf{E}^{(2)} - p^{(2)}\mathbb{I}$, with $\mathbf{E}^{(2)}$ the thick fluid symmetric rate of strain tensor as in Eq. 1.9. The largest additional contributions from Eq. 1.11 after non-dimensionalizing by multiplying by the factor $\epsilon^2 L/\mu u_c$ is

$$\epsilon\bar{\mu}\left(P^{(2)} - 2\frac{\partial U_Z}{\partial Z^{(2)}}\right),$$

which is sub-leading. Thus the normal stress balance is

$$\left(P + \bar{\mathrm{Ca}}^{-1}\nabla_L^2 H\right)\Big|_{Z=H} = 0,$$

from which we conclude that the integration constant B is given by

$$B = -\bar{\mathrm{Ca}}^{-1}\nabla_L^2 H. \tag{1.48}$$

On the other hand, the largest additional contribution in the tangential stress balance in Eq. 1.12 after non-dimensionalizing by multiplying by the factor $\epsilon L/\mu u_c$ is

$$\bar{\mu}\left(\frac{\partial \mathbf{U}_L^{(2)}}{\partial Z^{(2)}} + \nabla_L U_Z^{(2)}\right)\cdot\hat{\mathbf{x}}_i\Bigg|_{Z^{(2)}=\epsilon H},$$

which does contributes at leading order in ϵ. The tangential stress balance is then

$$\left(\frac{\partial \mathbf{U}_L}{\partial Z} - \bar{\mathrm{Ma}}\nabla_L\Sigma\right)\Bigg|_{Z=H} = \bar{\mu}\left(\frac{\partial \mathbf{U}_L^{(2)}}{\partial Z^{(2)}} + \nabla_L U_Z^{(2)}\right)\Bigg|_{Z^{(2)}=\epsilon H}.$$

Inserting the solutions in Eqns. 1.43-1.48 into this tangential stress balance and simplifying, the result is

$$\begin{aligned}\tilde{\mathbf{A}} = {}& \frac{1}{2}H^2\bar{\mathrm{Ca}}^{-1}\nabla_L\nabla_L^2 H + \bar{\mathrm{Ma}}H\nabla_L\Sigma \\ & + \bar{\mu}H\int \mathrm{d}^2X'\frac{\mathrm{d}^2q}{(2\pi)^2}\,\mathrm{e}^{i\mathbf{q}\cdot(\mathbf{X}_L-\mathbf{X}'_L)}\Bigg(-\coth\left(q\bar{D}_0\right)\frac{(\star\mathbf{q})\cdot\tilde{\mathbf{A}}(\mathbf{X}'_L)}{q}\star\mathbf{q} \\ & \qquad + \frac{2\left(q\bar{D}_0 - \sinh\left(q\bar{D}_0\right)\cosh\left(q\bar{D}_0\right)\right)}{\sinh\left(q\bar{D}_0\right)^2 - q^2\bar{D}_0^2}\frac{\mathbf{q}\cdot\tilde{\mathbf{A}}(\mathbf{X}'_L)}{q}\mathbf{q}\Bigg),\end{aligned} \tag{1.49}$$

which is a Fredholm integral equation determining $\tilde{\mathbf{A}}$. Given a solution to Eq. 1.49, all the integration constants from the momentum transport are determined.

The heat transport through the bilayer proceeds analogously to the momentum transport. The thick layer is governed by the heat transport equation

$$\rho^{(2)}c^{(2)}\left(\frac{\partial T^{(2)}}{\partial \bar{t}} + \mathbf{u}_L^{(2)}\cdot\bar{\nabla}_L T^{(2)} + u_z^{(2)}\frac{\partial T^{(2)}}{\partial z}\right) = k^{(2)}\left(\bar{\nabla}_L^2 T^{(2)} + \frac{\partial^2 T^{(2)}}{\partial z^2}\right),$$

and Dirichlet boundary conditions on the cold substrate are used,

$$T^{(2)}\Big|_{Z^{(2)}=\bar{D}_0} = T_C.$$

The previous non-dimensional temperature in the thin film and surface tension are used and a new non-dimensional thick film temperature is defined

$$\Theta \equiv \frac{T-\bar{T}_0}{T_H-\bar{T}_0}, \quad \Sigma \equiv \frac{\sigma-\sigma_0}{\sigma_T(T_H-\bar{T}_0)} = -\,\Theta|_{Z=H}\,, \quad \Theta^{(2)} \equiv \frac{T^{(2)}-T_C}{\bar{T}_0-T_C}.$$

On non-dimensionalization of the heat transport equation, the group

$$\mathrm{Pe}_T^{(2)} \equiv \rho^{(2)} c^{(2)} L u_c / k^{(2)}$$

appears, and we assume $\mathrm{Pe}_T^{(2)} \ll 1$. The leading order heat transport equation in the thick layer is then

$$\nabla_L^2 \Theta^{(2)} + \frac{\partial^2 \Theta^{(2)}}{\partial (Z^{(2)})^2} = 0.$$

The Fourier transform is used once again

$$\Theta^{(2)} = \int \frac{\mathrm{d}^2 q}{(2\pi)^2} \, \mathrm{e}^{i\mathbf{q}\cdot\mathbf{X}_L} \tilde{\Theta},$$

and the leading order thick film heat transport equation is

$$-q^2 \tilde{\Theta} + \frac{\partial^2 \tilde{\Theta}}{\partial (Z^{(2)})^2} = 0,$$

subject to the Dirichlet boundary conditions for the temperature at the cold substrate $T^{(2)}\Big|_{z=d_0} = T_C$ which non-dimensionalize to $\Theta^{(2)}\Big|_{Z^{(2)}=\bar{D}_0} = 0$. The solution is then

$$\Theta^{(2)} = \int \frac{\mathrm{d}^2 q}{(2\pi)^2} \, \mathrm{e}^{i\mathbf{q}\cdot\mathbf{X}_L} e \sinh\left(q\left(Z^{(2)} - \bar{D}_0\right)\right), \tag{1.50}$$

where e is an integration constant depending only on $\mathbf{X}_L$ and not $Z^{(2)}$. In the thin film, the lubrication approximation can be made in the bulk as in the previous section. In particular, Eq. 1.30, repeated here for convenience, remains valid,

$$\Theta = 1 + CZ. \tag{1.51}$$

The integration constants C and e must next be eliminated using appropriate boundary conditions. The temperature continuity condition $T|_{z=d_0} = T^{(2)}\Big|_{z=d_0}$ non-dimensionalizes to

$$\bar{T}_0 + (T_H - \bar{T}_0)\, \Theta|_{Z=H} = T_C + (\bar{T}_0 - T_C)\, \Theta^{(2)}\Big|_{Z^{(2)}=\epsilon H}.$$

Inserting the solution in Eq. 1.50, the constant e can be eliminated to leading order

$$e = -\int \mathrm{d}^2 X' \, \mathrm{e}^{-i\mathbf{q}\cdot\mathbf{X}'_L} \frac{T_H - T_C + (T_H - \bar{T}_0) C(\mathbf{X}'_L) H(\mathbf{X}'_L)}{(\bar{T}_0 - T_C)\sinh(q\bar{D}_0)}. \tag{1.52}$$

Next the continuity of the heat flux across the interface requires

$$k\hat{\mathbf{n}} \cdot \left(\nabla_L T + \hat{\mathbf{z}} \frac{\partial T}{\partial z}\right)\Bigg|_{z=d_0} = k^{(2)} \hat{\mathbf{n}} \cdot \left(\nabla_L T^{(2)} + \hat{\mathbf{z}} \frac{\partial T^{(2)}}{\partial z}\right)\Bigg|_{z=d_0}.$$

which non-dimensionalizes to leading order to

$$(T_H - \bar{T}_0)\frac{\partial \Theta}{\partial Z}\bigg|_{Z=H} = \bar{k}\ (\bar{T}_0 - T_C)\frac{\partial \Theta^{(2)}}{\partial Z^{(2)}}\bigg|_{Z^{(2)}=\epsilon H}.$$

Inserting the solutions in Eqns. 1.50-1.52, keeping leading order terms only, and simplifying using the $\bar{T}_0$ in Eq. 1.39 results in

$$C = -\frac{\bar{D}_0 + \bar{k}}{\bar{D}_0} - \bar{k}\int \mathrm{d}^2X' \frac{\mathrm{d}^2q}{(2\pi)^2} \mathrm{e}^{i\mathbf{q}\cdot(\mathbf{X}_L - \mathbf{X}'_L)} q \coth\left(q\bar{D}_0\right) H(\mathbf{X}'_L) C(\mathbf{X}'_L), \quad (1.53)$$

which is another Fredholm integral equation determining C. Given a solution to Eq. 1.53, all the integration constants from the heat transport are determined. Using the relation between the temperature and the surface tension in Eq. 1.40, an equivalent Fredholm integral equation in the non-dimensional surface tension can be easily derived,

$$\Sigma = H - 1 - \bar{k}H\int \mathrm{d}^2X' \frac{\mathrm{d}^2q}{(2\pi)^2}\ \mathrm{e}^{i\mathbf{q}\cdot(\mathbf{X}_L - \mathbf{X}'_L)} q \coth\left(q\bar{D}_0\right) \Sigma(\mathbf{X}'_L). \quad (1.54)$$

The only remaining equation is the non-dimensionalized kinematic boundary condition in Eq. 1.23, repeated here for convenience,

$$\left(\frac{\partial H}{\partial t} + \nabla_L H \cdot \mathbf{U}_L - U_Z\right)\bigg|_{Z=H} = 0.$$

Using the thin film solution in Eqns. 1.44 and Eq. 1.48 and the definition of $\tilde{\mathbf{A}}$ in Eq. 1.46, the kinematic boundary condition governing the film evolution is

$$\frac{\partial H}{\partial t} + \nabla_L \cdot \left(\frac{\bar{\mathrm{Ca}}^{-1}}{12} H^3 \nabla_L \nabla_L^2 H + \frac{1}{2} H \tilde{\mathbf{A}}\right) = 0, \quad (1.55)$$

along with the two integral equations in Eq. 1.49 and Eq. 1.54, repeated here for convenience,

$$\begin{aligned}
\Sigma &= H - 1 - \quad \bar{k}H\int \mathrm{d}^2X' \frac{\mathrm{d}^2q}{(2\pi)^2}\ \mathrm{e}^{i\mathbf{q}\cdot(\mathbf{X}_L - \mathbf{X}'_L)} q \coth\left(q\bar{D}_0\right) \Sigma(\mathbf{X}'_L), \\
\tilde{\mathbf{A}} &= \frac{1}{2} H^2 \bar{\mathrm{Ca}}^{-1} \nabla_L \nabla_L^2 H + \bar{\mathrm{Ma}} H \nabla_L \Sigma \\
&\quad + \bar{\mu} H \int \mathrm{d}^2X' \frac{\mathrm{d}^2q}{(2\pi)^2}\ \mathrm{e}^{i\mathbf{q}\cdot(\mathbf{X}_L - \mathbf{X}'_L)} \Bigg(- \coth\left(q\bar{D}_0\right) \frac{(\star\mathbf{q})\cdot\tilde{\mathbf{A}}(\mathbf{X}'_L)}{q} \star \mathbf{q} \\
&\qquad + \frac{2\left(q\bar{D}_0 - \sinh\left(q\bar{D}_0\right)\cosh\left(q\bar{D}_0\right)\right)}{\sinh\left(q\bar{D}_0\right)^2 - q^2\bar{D}_0^2} \frac{\mathbf{q}\cdot\tilde{\mathbf{A}}(\mathbf{X}'_L)}{q}\mathbf{q}\Bigg).
\end{aligned} \quad (1.56)$$

Equations 1.55 and 1.56 together form the analog of the thin film equation in Eq. 1.34. The major qualitative difference between Eqns. 1.55-1.56 and Eq. 1.34 is the non-local contribution arising from the integral equations, which can be understood in terms of the lateral diffusion of mometum and heat as depicted in Fig. 1.3.

Liouville-Neumann series

A formal solution for $\tilde{\mathbf{A}}$ and Σ in Eq. 1.56 can be generated by using successive approximations by initially neglecting the integral terms. The result is called the Liouville-Neumann series. Define operators

$$\mathcal{L}_{\tilde{\mathbf{A}}}\left[\tilde{\mathbf{A}}\right] \equiv H\int \mathrm{d}^2X' \frac{\mathrm{d}^2q}{(2\pi)^2}\,\mathrm{e}^{i\mathbf{q}\cdot(\mathbf{X}_L-\mathbf{X}'_L)}\Bigg(-\coth\left(q\bar{D}_0\right)\frac{(\star\mathbf{q})\cdot\tilde{\mathbf{A}}(\mathbf{X}'_L)}{q}\star\mathbf{q} + \frac{2\left(q\bar{D}_0-\sinh\left(q\bar{D}_0\right)\cosh\left(q\bar{D}_0\right)\right)}{\sinh\left(q\bar{D}_0\right)^2-q^2\bar{D}_0^2}\frac{\mathbf{q}\cdot\tilde{\mathbf{A}}(\mathbf{X}'_L)}{q}\mathbf{q}\Bigg),$$

and

$$\mathcal{L}_{\Gamma}\left[\Sigma\right] \equiv H\int \mathrm{d}^2X' \frac{\mathrm{d}^2q}{(2\pi)^2}\,\mathrm{e}^{i\mathbf{q}\cdot(\mathbf{X}_L-\mathbf{X}'_L)}q\coth\left(q\bar{D}_0\right)\Sigma(\mathbf{X}'_L),$$

and let $\mathcal{L}^n_{\tilde{\mathbf{A}}}$ and $\mathcal{L}^n_{\Gamma}$ denote the nth iterated operations. Then the Liouville-Neumann series solution to the integral equations in Eq. 1.56 are

$$\begin{aligned}\Sigma &= \sum_{n=0}^{\infty}\left(-\bar{k}\right)^n\mathcal{L}^n_{\Gamma}\left[H-1\right],\\ \tilde{\mathbf{A}} &= \sum_{n=0}^{\infty}(\bar{\mu})^n\,\mathcal{L}^n_{\tilde{\mathbf{A}}}\left[\frac{1}{2}\bar{\mathrm{Ca}}^{-1}H\nabla_L\nabla_L^2H+\bar{\mathrm{Ma}}H\nabla_L\Sigma\right].\end{aligned}\tag{1.57}$$

The formal solutions in Eq. 1.57 can then be substituted into Eq. 1.55 to generate the film evolution equation. The formal nature of the Liouville-Neumann series should be emphasized – unless the terms decrease in magnitude sufficiently fast, the series will not converge. This operator series is very much analogous to the Taylor series $\frac{1}{1-x}=\sum_{n=0}^{\infty}x^n$ for $|x|<1$, and some operator norms on $\mathcal{L}_{\tilde{\mathbf{A}}}$ and $\mathcal{L}_{\Gamma}$ could ensure convergence, though we will not pursue such bounds. Furthermore, both operators are invertible,

$$\mathcal{L}^{-1}_{\tilde{\mathbf{A}}}\left[\tilde{\mathbf{A}}\right] \equiv H\int \mathrm{d}^2X' \frac{\mathrm{d}^2q}{(2\pi)^2}\,\mathrm{e}^{i\mathbf{q}\cdot(\mathbf{X}_L-\mathbf{X}'_L)}\Bigg(-\tanh\left(q\bar{D}_0\right)\frac{(\star\mathbf{q})\cdot\tilde{\mathbf{A}}(\mathbf{X}'_L)}{q^3H(\mathbf{X}'_L)}\star\mathbf{q} + \frac{\sinh\left(q\bar{D}_0\right)^2-q^2\bar{D}_0^2}{2\left(q\bar{D}_0-\sinh\left(q\bar{D}_0\right)\cosh\left(q\bar{D}_0\right)\right)}\frac{\mathbf{q}\cdot\tilde{\mathbf{A}}(\mathbf{X}'_L)}{q^3H(\mathbf{X}'_L)}\mathbf{q}\Bigg),$$

and

$$\mathcal{L}^{-1}_{\Gamma}\left[\Gamma\right] = \int \mathrm{d}^2X' \frac{\mathrm{d}^2q}{(2\pi)^2}\mathrm{e}^{i\mathbf{q}\cdot(\mathbf{X}_L-\mathbf{X}'_L)}\frac{\tanh(q\bar{D}_0)}{qH(\mathbf{X}'_L)}\Sigma(\mathbf{X}'_L).$$

If the Liouville-Neumann series fails to converge, the Liouville-Neumann series for the inverse equations

$$\Sigma = -\sum_{n=1}^{\infty} \left(-\bar{k}\right)^{-n} \mathcal{L}_{\Gamma}^{-n} \left[H - 1\right],$$
$$\tilde{\mathbf{A}} = -\sum_{n=1}^{\infty} \left(\bar{\mu}\right)^{-n} \mathcal{L}_{\tilde{\mathbf{A}}}^{-n} \left[\frac{1}{2}\bar{\mathrm{Ca}}^{-1} H \nabla_L \nabla_L^2 H + \bar{\mathrm{Ma}} H \nabla_L \Sigma\right], \tag{1.58}$$

may be expected to converge, just as $\frac{1}{1-x} = -\frac{1/x}{1-1/x} = -\sum_{n=1}^{\infty} x^{-n}$ for $|x| > 1$. In a numerical study of Eq. 1.55, a truncated version of Eq. 1.58 or Eq. 1.57 could be easily implemented in finite element simulations.

Linear stability analysis

As a first application of Eqns. 1.55-1.44, we perform a linear stability analysis of a flat base state $H_0(\mathbf{X}_L) = 1$. Consider a modal perturbation

$$H(\mathbf{X}_L) = 1 + \delta H \mathrm{e}^{bt + i\mathbf{p}\cdot\mathbf{X}_L}$$

with $\delta H \ll 1$ and $\mathbf{p}$ a wave vector. First we will consider the solutions to the integral equations in Eq. 1.56. The iterated operators $\mathcal{L}_{\Gamma}^{n}\left[\delta H \mathrm{e}^{bt+i\mathbf{p}\cdot\mathbf{X}_L}\right]$ is evaluated inductively. Suppose

$$\mathcal{L}_{\Gamma}^{n}\left[\delta H \mathrm{e}^{bt+i\mathbf{p}\cdot\mathbf{X}_L}\right] = \delta H \mathrm{e}^{bt+i\mathbf{p}\cdot\mathbf{X}_L} \left(|\mathbf{p}| \coth(|\mathbf{p}|\bar{D}_0)\right)^n.$$

Then it follows that

$$\begin{aligned}
\mathcal{L}_{\Gamma}^{n+1}\left[\delta H \mathrm{e}^{bt+i\mathbf{p}\cdot\mathbf{X}_L}\right] &= \mathcal{L}_{\Gamma}\left[\delta H \mathrm{e}^{bt+i\mathbf{p}\cdot\mathbf{X}_L} \quad \left(|\mathbf{p}| \quad \coth(|\mathbf{p}|\bar{D}_0)\right)^n\right] \\
&= (1 + \delta H \mathrm{e}^{bt+i\mathbf{p}\cdot\mathbf{X}_L}) \int \quad \mathrm{d}^2X' \frac{\mathrm{d}^2 q}{(2\pi)^2} \mathrm{e}^{i\mathbf{q}\cdot(\mathbf{X}_L - \mathbf{X}'_L)} q \coth\left(q\bar{D}_0\right) \\
&\qquad\qquad \times \delta H \mathrm{e}^{bt+i\mathbf{p}\cdot\mathbf{X}'_L} \left(|\mathbf{p}| \coth(|\mathbf{p}|\bar{D}_0)\right)^n \\
&= \delta H \mathrm{e}^{bt+i\mathbf{p}\cdot\mathbf{X}_L} \left(|\mathbf{p}| \coth(|\mathbf{p}|\bar{D}_0)\right)^{n+1},
\end{aligned}$$

to leading order in δH. The base case for $n = 0$ is immediate, so that the induction is complete. Inserting this in the Liouville-Neumann series in Eq. 1.57 and evaluating the sum, the dimensionless surface tension is

$$\Sigma = \frac{\delta H \mathrm{e}^{bt+i\mathbf{p}\cdot\mathbf{X}_L}}{1 + \bar{k}|\mathbf{p}| \coth\left(|\mathbf{p}|\bar{D}_0\right)}.$$

Next, the argument in the second line in Eq. 1.56 is evaluated,

$$\frac{1}{2}\bar{\mathrm{Ca}}H^2\nabla_L\nabla_L^2 H+\bar{\mathrm{Ma}}H\nabla_L\Sigma=\left(-\frac{\bar{\mathrm{Ca}}^{-1}}{2}|\mathbf{p}|^2+\frac{\bar{\mathrm{Ma}}}{1+\bar{k}|\mathbf{p}|\coth\left(|\mathbf{p}|\bar{D}_0\right)}\right)i\mathbf{p}\delta H\mathrm{e}^{bt+i\mathbf{p}\mathbf{X}_L}.$$

The iteratred operator in the second line of Eq. 1.57 can be evaluated inductively in the same fashion, and the result can be summed to give

$$\tilde{\mathbf{A}}=\frac{-\frac{1}{2}\bar{\mathrm{Ca}}^{-1}|\mathbf{p}|^2+\frac{\bar{\mathrm{Ma}}}{1+\bar{k}|\mathbf{p}|\coth\left(|\mathbf{p}|\bar{D}_0\right)}}{1-\bar{\mu}\frac{2|\mathbf{p}|\left(|\mathbf{p}|\bar{D}_0-\sinh\left(|\mathbf{p}|\bar{D}_0\right)\cosh\left(|\mathbf{p}|\bar{D}_0\right)\right)}{\sinh\left(|\mathbf{p}|\bar{D}_0\right)^2-|\mathbf{p}|^2\bar{D}_0^2}}i\mathbf{p}\delta H\mathrm{e}^{bt+i\mathbf{p}\mathbf{X}_L}.$$

Finally, the solution for $\tilde{\mathbf{A}}$ is inserted into Eq. 1.55 and the equation is solved for $b(|\mathbf{p}|)$ to give the dispersion relation

$$b(|\mathbf{p}|)=|\mathbf{p}|^2\left(\frac{1}{2}\frac{-\frac{1}{2}\bar{\mathrm{Ca}}^{-1}|\mathbf{p}|^2+\frac{\bar{\mathrm{Ma}}}{1+\bar{k}|\mathbf{p}|\coth\left(|\mathbf{p}|\bar{D}_0\right)}}{1-\bar{\mu}\frac{2|\mathbf{p}|\left(|\mathbf{p}|\bar{D}_0-\sinh\left(|\mathbf{p}|\bar{D}_0\right)\cosh\left(|\mathbf{p}|\bar{D}_0\right)\right)}{\sinh\left(|\mathbf{p}|\bar{D}_0\right)^2-|\mathbf{p}|^2\bar{D}_0^2}}-\frac{1}{12}\bar{\mathrm{Ca}}^{-1}|\mathbf{p}|^2\right) \tag{1.59}$$

This dispersion relation has the qualitative shape of a type II instability, having $b(0)=0$, a positive unstable band of $b(|\mathbf{p}|)$ for $0<|\mathbf{p}|<|\mathbf{p}|_c$ for some $|\mathbf{p}|_c>0$, and a maximum at some $b(2\pi/\lambda_{\max})=b_{\max}$, but the shape of the curves vary with the parameters $\bar{k}$, $\bar{\mu}$, and $\bar{D}_0$. The curves can be easily compared by plotting $b/b_{\max}$ vs. $|\mathbf{p}|\lambda_{\max}$, which eliminates the dependence on the parameters $\bar{\mathrm{Ca}}$ and $\bar{\mathrm{Ma}}$, as shown in Fig. 1.4 for a selection of $\bar{k}$, $\bar{\mu}$, and $\bar{D}_0$.

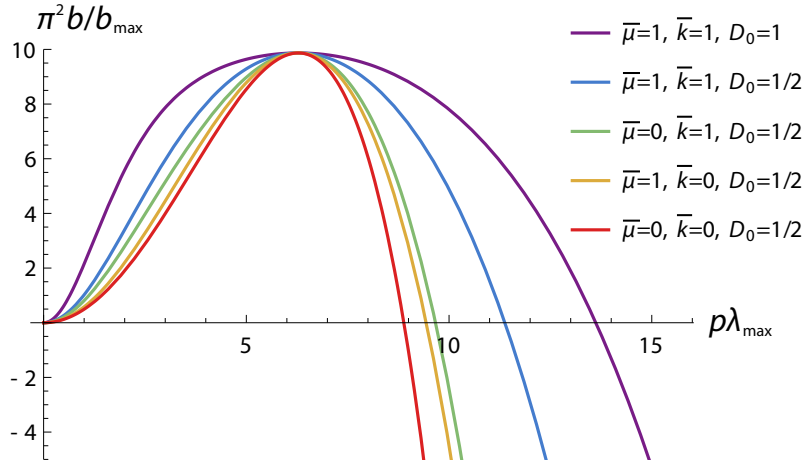

Figure 1.4: Linear stability dispersion relation of the thick-thin bilayer. Larger values of $\bar{\mu}$, $\bar{k}$, and $\bar{D}_0$ tend to make the unstable band flatter and wider.

Lastly, it is interesting to note the effects of varying the parameters $\bar{k}$ and $\bar{\mu}$ on the maximum growth rate $b_{\max}$ and the wavelength of the fastest growing mode $\lambda_{\max}$ for fixed $\bar{\text{Ma}}$ and $\bar{\text{Ca}}$. Larger values of the conductivity ratio $\bar{k}$ and the viscosity ratio $\bar{\mu}$ tend to increases the wavelength of the most unstable mode and tend to decrease the growth rate of the unstable modes. On the other hand, larger values of the gap width ratio $\bar{D}_0$ tend to decrease the wavelength of the most unstable mode and tend to increase the growth rate of the unstable modes. It should be emphasized here that since our definition of $\bar{\text{Ma}} \equiv \frac{\epsilon\sigma_T(T_H - T_0)}{\mu u_c}$ involves the temperature at the unperturbed interface T_0 rather than the temperature at the cold substrate T_C, varying $\bar{D}_0$ at fixed $\bar{\text{Ma}}$ entails simultaneously changing the dimensionful gap width d_0 and the applied temperature gradient. Contour plots of the wavelength of the fastest growing modes $\lambda_{\max}$ and its growth rate $b_{\max}$ are shown in Fig. 1.5 below for $\bar{\text{Ca}} = 1$ and $\bar{\text{Ma}} = 1$.

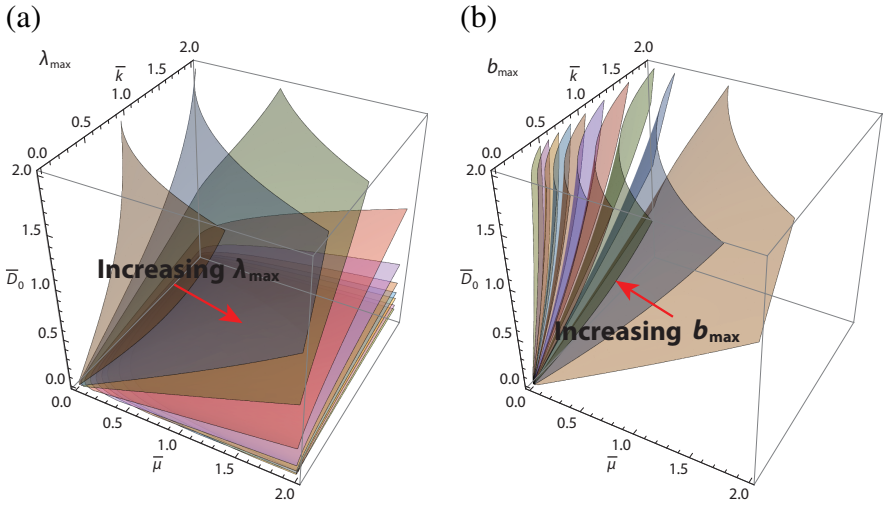

Figure 1.5: Contour plots of (a) the wavelength of the fastest growing mode and (b) the growth rate of the fastest growing mode for $\bar{\text{Ca}} = 1$ and $\bar{\text{Ma}} = 1$. Contour values increase in the direction of the red arrow. The wavelength $\lambda_{\max}$ increases with increasing $\bar{k}$ and $\bar{\mu}$ and with decreasing $\bar{D}_0$. The growth rate $b_{\max}$ decreases with increasing $\bar{k}$ and $\bar{\mu}$ and with decreasing $\bar{D}_0$.

Limiting Behavior

Here we consider the limiting behavior of Eqns. 1.55-1.56 for $\bar{D}_0 \ll 1$. In this limit the approximations $\coth\left(|\mathbf{p}|\bar{D}_0\right) \approx \frac{1}{|\mathbf{p}|\bar{D}_0}$ and $\frac{2(|\mathbf{p}|\bar{D}_0 - \sinh(|\mathbf{p}|\bar{D}_0)\cosh(|\mathbf{p}|\bar{D}_0))}{\sinh(|\mathbf{p}|\bar{D}_0)^2 - |\mathbf{p}|^2\bar{D}_0^2} \approx -\frac{4}{|\mathbf{p}|\bar{D}_0}$

puts Eq. 1.49 in the form

$$\tilde{\mathbf{A}} = \frac{1}{2}H^2\bar{\mathrm{Ca}}^{-1}\nabla_L\nabla_L^2 H + \bar{\mathrm{Ma}}H\nabla_L\Sigma \\ - \frac{\bar{\mu}}{\bar{D}_0}H\int \mathrm{d}^2X' \frac{\mathrm{d}^2q}{(2\pi)^2}\,\mathrm{e}^{i\mathbf{q}\cdot(\mathbf{x}_L-\mathbf{x}'_L)}\left(\frac{(\star\mathbf{q})\cdot\tilde{\mathbf{A}}(\mathbf{X}'_L)}{q^2}\star\mathbf{q} + 4\frac{\mathbf{q}\cdot\tilde{\mathbf{A}}(\mathbf{X}'_L)}{q^2}\mathbf{q}\right). \tag{1.60}$$

Solving Eq. 1.60 takes a little work. First, divide by H and take the divergence, noting that in the integral term a factor $i\mathbf{q}\cdot$ will fall out and cancel the denominator allowing the integral to be performed with a Dirac delta function,

$$\nabla_L\cdot\frac{\tilde{\mathbf{A}}}{H} = \nabla_L\cdot\left(\frac{1}{2}\bar{\mathrm{Ca}}H\nabla_L\nabla_L^2 H + \bar{\mathrm{Ma}}\nabla_L\Sigma\right) - 4\frac{\bar{\mu}}{\bar{D}_0}\nabla_L\cdot\tilde{\mathbf{A}}.$$

Collecting all terms together,

$$\nabla_L\cdot\left(\left(\frac{1}{H}+4\frac{\bar{\mu}}{\bar{D}_0}\right)\tilde{\mathbf{A}} - \left(\frac{1}{2}\bar{\mathrm{Ca}}H\nabla_L\nabla_L^2 H + \bar{\mathrm{Ma}}\nabla_L\Sigma\right)\right) = 0.$$

Since the quantity in parenthesis has zero divergence, it can be expressed in terms in a stream function f as $\frac{6\bar{\mu}}{\bar{D}_0^2}(\star\nabla_L)f$ with the multiplicative factor chosen here for later comparison with work in the literature. Thus

$$\tilde{\mathbf{A}} = \frac{\frac{1}{2}\bar{\mathrm{Ca}}H\nabla_L\nabla_L^2 H + \bar{\mathrm{Ma}}\nabla_L\Sigma}{1+4\frac{\bar{\mu}}{\bar{D}_0}H} + \frac{6\bar{\mu}H\,(\star\nabla_L)\,f}{\bar{D}_0^2\left(1+4\frac{\bar{\mu}}{\bar{D}_0}H\right)}. \tag{1.61}$$

Next, the dual divergence $(\star\nabla_L)\cdot$ of Eq. 1.60 is taken noting that a factor $i\,(\star\mathbf{q})\cdot$ falls out in the integral term which allows the integral to be performed,

$$(\star\nabla_L)\cdot\frac{\tilde{\mathbf{A}}}{H} = (\star\nabla_L)\cdot\left(\frac{1}{2}\bar{\mathrm{Ca}}H\nabla_L\nabla_L^2 H + \bar{\mathrm{Ma}}\nabla_L\Sigma\right) - \frac{\bar{\mu}}{\bar{D}_0}(\star\nabla_L)\cdot\tilde{\mathbf{A}}.$$

Substituting the solution in Eq. 1.61 and simplifying into a form that will be convenient shortly, the stream function f is specified by

$$(\star\nabla_L)\cdot\left(\frac{12\bar{\mu}\left(\bar{D}_0+\bar{\mu}H\right)}{\bar{D}_0^3\left(\bar{D}_0+4\bar{\mu}H\right)}(\star\nabla_L)\,f\right) = (\star\nabla_L)\cdot\left(\bar{\mathrm{Ma}}\frac{6\bar{\mu}H}{\bar{D}_0\left(\bar{D}_0+4\bar{\mu}H\right)}\nabla_L\Sigma \right. \\ \left. - \bar{\mathrm{Ca}}\left(1-\frac{3\bar{\mu}H^2}{\bar{D}_0\left(\bar{D}_0+\bar{\mu}H\right)}\right)\nabla_L\nabla_L^2 H\right). \tag{1.62}$$

Next, substituting the solution in Eq. 1.61 into Eq. 1.55 and simplifying the result, a limiting thin film equation is derived,

$$0 = \frac{\partial H}{\partial t} - \nabla_L \cdot \left(\frac{\bar{\mathrm{Ca}}^{-1}}{3} \frac{\bar{D}_0 + \bar{\mu} H}{\bar{D}_0 + 4\bar{\mu} H} H^3 \nabla_L \nabla_L^2 H + \frac{\bar{\mathrm{Ma}}}{2} \frac{H^2}{\bar{D}_0 + 4\bar{\mu} H} \nabla_L \Sigma + \frac{3\bar{\mu} H^2}{\bar{D}_0 \left(\bar{D}_0 + 4\bar{\mu} H \right)} \left(\star \nabla_L \right) f \right). \tag{1.63}$$

The surface tension in Eq. 1.54 is also approximated using $\cosh\left(|\mathbf{p}|\bar{D}_0\right) \approx \frac{1}{|\mathbf{p}|\bar{D}_0}$

$$\Sigma = H - 1 - \frac{\bar{k}}{\bar{D}_0} H \int \mathrm{d}^2 X' \frac{\mathrm{d}^2 q}{(2\pi)^2} \, \mathrm{e}^{i\mathbf{q}\cdot(\mathbf{X}_L - \mathbf{X}'_L)} \Sigma(\mathbf{X}'_L),$$

which can be integrated and solved as

$$\Sigma = \frac{\bar{D}_0}{\bar{D}_0 + \bar{k}} \left(H - 1 \right). \tag{1.64}$$

In summary, Eqns. 1.62-1.64 are the coupled equations in the $\bar{D}_0 \ll 1$ limit. Taking the small $\bar{D}_0$ limit of the equations causes the non-local nature of the evolution equations to break down and allows the integral equations to be re-expressed as the differential equation Eq. 1.62. This is to be expected since in the small $\bar{D}_0$ limit the non-local transport mechanism in Fig. 1.3 is invalidated as the thick layer becomes thin. As noted at the beginning of this section, the evolution of a doubly thin viscous bilayer has been considered by Merkt et al. [24]. In fact, the doubly thin bilayer evolution equations derived by Merkt et al. matches exactly with Eqns. 1.62-1.64 in the limit of a large gap ratio, viscosity ratio, and conductivity ratio. This matching between models is entirely analogous to matched asymptotics – these models are appropriate for distinct parameter regimes and their limiting behavior must coincide as one moves between these regimes.

1.3 Other variants of thin film equations

We have focused on the case where the only interfacial forces are capillary and thermocapillary ones, but a much wider class of thin film equations can be derived with analogous methods. Consider the interface between a gas (with negligible viscous stresses) and a thin viscous fluid film (incompressible and with constant viscosity) evolving on a flat substrate under the influence of a body force potential Φ, an external interfacial shear stress $\boldsymbol{\tau}_{\mathrm{ext}}$, an external interfacial normal stress Π, varying surface tension Σ, and slip coefficient β, with all variables being appro-

priately non-dimensionalized[1]. Such a film [23] can be modeled with the partial differential equation

$$\frac{\partial H}{\partial t} + \nabla_L \cdot \left(\left(\boldsymbol{\tau}_{\text{ext}} + \bar{\text{Ma}} \nabla_L \Sigma \right) \left(\frac{1}{2} H^2 + \beta H \right) - \left(\frac{1}{3} H^3 + \beta H^2 \right) \nabla_L P \right) = 0, \quad (1.65)$$

where

$$P = \Phi|_{Z=H} - \bar{\text{Ca}}^{-1} \nabla_L^2 H - \Pi. \quad (1.66)$$

Note that Eq. 1.65 is a local conservation equation – changes in the film height H, and hence the total volume $\mathscr{V}[H]$, are directly related to the divergence of a volumetric flux $\mathbf{Q}_L$,

$$\frac{\partial H}{\partial t} + \nabla_L \cdot \mathbf{Q}_L = 0, \quad (1.67)$$

where

$$\mathscr{V}[H] \equiv \int \mathrm{d}^2 X \; H(\mathbf{X}_L, t),$$
$$\mathbf{Q}_L \equiv \left(\boldsymbol{\tau}_{\text{ext}} + \bar{\text{Ma}} \nabla_L \Sigma \right) \left(\frac{1}{2} H^2 + \beta H \right) - \left(\frac{1}{3} H^3 + \beta H^2 \right) \nabla_L P.$$

Assuming the flux $\mathbf{Q}_L$ vanishes appropriately at the boundary of the wetted domain, this implies that the total volume $\mathscr{V}[H]$ is a conserved quantity.

In the important special case where the external forces depend on space and time only implicitly through H as $\boldsymbol{\tau}_{\text{ext}} = \frac{\partial \tau_{\text{ext}}}{\partial H} \nabla_L H$, $\Phi|_{Z=H} = \Phi(H)$, $\Pi = \Pi(H)$, and $\Sigma = \Sigma(H)$, Eq. 1.65 can be cast in the form

$$\frac{\partial H}{\partial t} + \nabla_L \cdot \left(Q_1(H) \nabla_L \left(\bar{\text{Ca}}^{-1} \nabla_L^2 H - W'(H) \right) \right) = 0, \quad (1.68)$$

where

$$Q_1(H) \equiv \frac{1}{3} H^3 + \beta H^2,$$
$$W''(H) \equiv \frac{\partial \Phi}{\partial H} - \frac{\partial \Pi}{\partial H} - \frac{3H^2 + 6\beta H}{2H^3 + 6\beta H^2} \left(\frac{\partial \tau_{\text{ext}}}{\partial H} + \bar{\text{Ma}} \frac{\partial \Sigma}{\partial H} \right).$$

The form of Eq. 1.68 is called the Cahn-Hilliard type and is significant because of its variational structure,

$$\frac{\partial H}{\partial t} - \nabla_L \cdot \left(Q_1(H) \nabla_L \frac{\delta F}{\delta H} \right) = 0, \quad (1.69)$$

[1] In [23], the authors use a dimensionless surface tension $\tilde{\Sigma} \equiv \frac{\epsilon \sigma}{\mu u_c}$. We opt to use a dimensionless surface tension $\Sigma \equiv \frac{\sigma - \sigma_0}{\Delta \sigma}$ where $\Delta\sigma$ is a scale of variations in surface tension, as was done in Section 1.1. The two are related by $\nabla_L \tilde{\Sigma} = \bar{\text{Ma}} \nabla_L \Sigma$ where $\bar{\text{Ma}} \equiv \frac{\Delta \sigma}{\mu u_c}$.

where the Lyapunov energy is

$$F[H] \equiv \int \mathrm{d}^2X\, \mathcal{F}(\mathbf{X}_L, t)$$
$$\mathcal{F}(\mathbf{X}_L, t) \equiv \frac{\bar{\mathrm{Ca}}^{-1}}{2} |\nabla_L H|^2 + W(H).$$

In the remainder of this thesis, we will study a variety of such film equations. Although fluid slip is important for modelling moving contact lines, the only focus on contact lines will be energetic rather than dynamic, so we will always take $\beta = 0$. The purely thermocapillary case in Section 1.1 affects the surface tension $\Sigma_{\mathrm{TC}} = -1 + \frac{(D_0+\kappa-1)H}{D_0+(\kappa-1)H}$ as in Eq. 1.33 and contributes to Lyapunov potential through a term

$$W_{\mathrm{TC}} = -\frac{3\bar{\mathrm{Ma}}}{2}(1+\chi) H \log\left(\frac{H}{1+\chi H}\right). \tag{1.70}$$

In addition, we will occasionally consider additional body forces including a vertical gravitational force with non-dimensionalized body force potentials $\Phi_{\mathrm{G}} = \bar{G}Z$ where $\bar{G} \equiv \epsilon\rho g h_0^2/\mu u_c$ is the non-dimensional thin film gravitational number. The gravitational contribution to the Lyapunov energy is

$$W_{\mathrm{G}} \equiv \frac{\bar{G}}{2}H^2. \tag{1.71}$$

Additionally, an electrohydrodynamic problem with an interfacial normal force resulting from an applied electric voltage ΔV across the top and bottom substrates will be considered for a dielectric fluid. The resulting normal interfacial force is $\Pi_{\mathrm{EHD}} = \frac{1}{2}\frac{\varepsilon_{\mathrm{EHD}}(\varepsilon_{\mathrm{EHD}}-1)\mathcal{V}^2}{(D_0+(\varepsilon_{\mathrm{EHD}}-1)H)^2}$ where $\varepsilon_{\mathrm{EHD}} \equiv \varepsilon_{\mathrm{air}}/\varepsilon$ is the ratio of the relative permittivity of the air $\varepsilon_{\mathrm{air}}$ to the relative permittivity of the film ε and $\mathcal{V} \equiv \sqrt{\epsilon\varepsilon_0\varepsilon/\mu u_c h_0}\Delta V$ is the dimensionless voltage magnitude, with ε_0 the vacuum permittivity [24]. An appropriate Lyapunov potential for the electrohydrodynamic contribution is

$$W_{\mathrm{EHD}} \equiv -\frac{\bar{\mathrm{E}}}{2}\frac{\chi_{\mathrm{EHD}}H}{1+\chi_{\mathrm{EHD}}H}, \tag{1.72}$$

where $\chi_{\mathrm{EHD}} \equiv \frac{\varepsilon_{\mathrm{EHD}}-1}{D_0}$ is a dimensionless dielectric and gap ratio number and $\bar{\mathrm{E}} \equiv \frac{\varepsilon_{\mathrm{EHD}}}{D_0}\mathcal{V}^2$ is a dimensionless electrohydrodynamic number. This Lyapunov contribution differs from that of [24] by a constant such that $W_{\mathrm{EHD}}(0) = 0$ for reasons that will be emphasized in Chapter 3. Another commonly introduced force is a retarded body force potential accounting for Van der Waals interactions $\Phi_{\mathrm{VdW}} = A_{\mathrm{VdW}}/Z^3$ where $A_{\mathrm{VdW}} \equiv \epsilon A'_{\mathrm{VdW}}/6\pi\mu u_c h_0^2$ is the non-dimensional Hamaker constant. Such

interactions become important near film rupture, but will generally be neglected in this thesis for the sake of simplicity.

We will also consider a more complicated case which involves more than one independent variable. When an insoluble surfactant spreads on the film, the surface tension is a function of the surfactant concentration γ. The surface tension is assumed to decrease linearly with the surfactant concentration $\sigma = \sigma_0 - \sigma_\gamma (\gamma - \gamma_\mathrm{m})$. In terms of the dimensionless surfactant concentration $\Gamma \equiv \gamma/\gamma_\mathrm{m}$, the dimensionless surface tension is $\Sigma = 1 - \Gamma$. A second transport equation in addition to Eq. 1.65 is required to model the transport of the surfactant concentration Γ. Assuming the surfactant is advectively transported on the surface with an additional surface diffusion term, the appropriate equations are [25]

$$\begin{aligned} 0 &= \frac{\partial H}{\partial t} + \nabla_L \cdot \left(\frac{\bar{\mathrm{Ca}}^{-1}}{3} H^3 \nabla_L \nabla_L^2 H - \frac{\bar{\mathrm{Ma}}}{2} H^2 \nabla_L \Gamma \right), \\ 0 &= \frac{\partial \Gamma}{\partial t} + \nabla_L \cdot \left(\frac{\bar{\mathrm{Ca}}^{-1}}{2} H^2 \Gamma \nabla_L \nabla_L^2 H - \bar{\mathrm{Ma}} H \Gamma \nabla_L \Gamma - \bar{\mathrm{Pe}} \nabla_L \Gamma \right), \end{aligned} \tag{1.73}$$

where $\bar{\mathrm{Pe}} \equiv \epsilon L u_c / \mathcal{D}$ is the thin film Peclet number with $\mathcal{D}$ the surface diffusion constant for the surfactant. Thiele, Archer, and Plapp [26] uncovered the Cahn-Hilliard form of the surfactant spreading problem of Eq. 1.73,

$$\begin{aligned} 0 &= \frac{\partial H}{\partial t} - \nabla_L \cdot \left(\frac{H^3}{3} \nabla_L \frac{\delta F_\mathrm{SS}}{\delta H} + \frac{H^2 \Gamma}{2} \nabla_L \frac{\delta F_\mathrm{SS}}{\delta \Gamma} \right), \\ 0 &= \frac{\partial \Gamma}{\partial t} - \nabla_L \cdot \left(\frac{H^2 \Gamma}{2} \nabla_L \frac{\delta F_\mathrm{SS}}{\delta H} + \left(H \Gamma^2 + \frac{\bar{\mathrm{Pe}}}{\bar{\mathrm{Ma}}} \Gamma \right) \nabla_L \frac{\delta F_\mathrm{SS}}{\delta \Gamma} \right), \end{aligned}$$

where the Lyapunov function in this case is

$$\begin{aligned} F_\mathrm{SS}[H, \Gamma] &\equiv \int \mathrm{d}^2 X \, \mathcal{F}_\mathrm{SS}(\mathbf{X}_L, t), \\ \mathcal{F}_\mathrm{SS} &\equiv \frac{\bar{\mathrm{Ca}}^{-1}}{2} |\nabla_L H|^2 + \bar{\mathrm{Ma}} \Gamma \log \Gamma. \end{aligned}$$

The proof of that the Lyapunov energy decreases in time relies on the fact that the mobility matrix $\begin{pmatrix} \frac{H^3}{3} & \frac{H^2\Gamma}{2} \\ \frac{H^2\Gamma}{2} & H\Gamma^2 + \frac{\bar{\mathrm{Pe}}}{\bar{\mathrm{Ma}}}\Gamma \end{pmatrix}$ is positive definite for $H > 0$ and $\Gamma > 0$, as can be easily verified by considering its determinant and trace.

The Cahn-Hilliard form of Eq. 1.73 has only recently been derived, and as far as the author is aware general methods for deriving such forms for more complicated cases are not well known in the field. The necessary mathematical tools do exist,

however, and will be outlined in the remainder of this section. Suppose we are given a set of coupled evolution equations in some number of dependent variables u^i which depend on $\mathbf{X}_L$ and t like

$$\frac{\partial u^i}{\partial t} + \nabla_L \cdot \left(\mathbf{Q}_L^i\right) = 0, \tag{1.74}$$

where $\mathbf{Q}_L^i$ are some known set of fluxes that corresponds to u^i. The Cahn-Hilliard form will be generalized to

$$\frac{\partial u^i}{\partial t} - \frac{\partial}{\partial X^j}\left(Q_1^{ijkl}\frac{\partial \delta F}{\partial X^l \delta u^k}\right) = 0, \tag{1.75}$$

where the matrix of mobility factors Q_1^{ijkl} is appropriately positive-definite. By an argument identical to the one given in Section 1.1, it follows from appropriate assumptions on the boundary conditions that

$$\frac{dF}{dt} = -\int \mathrm{d}^2X \; \frac{\partial \delta F}{\partial X^j \delta u^i} Q_1^{ijkl} \frac{\partial \delta F}{\partial X^l \delta u^k} \leq 0,$$

where the inequality follows from the positive-definite assumption on Q_1, so that F is a Lyapunov functional. Clearly Eq. 1.74 is of the form in Eq. 1.75 if the fluxes can be expressed as

$$\mathbf{Q}_L^i = -Q_1^{ijkl}\frac{\partial \delta F}{\partial X^l \delta u^k}\hat{\mathbf{x}}_j.$$

The key observation here is that this can be interpreted as an exactness condition in differential geometry such that $\left(Q_1^{-1}\right)_{ijkl}\left(\hat{\mathbf{x}}^j \cdot \mathbf{Q}_L^i\right)\hat{\mathbf{x}}^l = -\nabla_L \psi_k$, where Q_1^{-1} is the inverse mobility matrix and $\psi_k = \frac{\delta F}{\delta u^k}$. Under some mild assumptions, the Poincare lemma [27] guarantees such an exactness is equivalent to a closedness condition, which can be written

$$(\star \nabla_L) \cdot \left(\left(Q_1^{-1}\right)_{ijkl}\left(\hat{\mathbf{x}}^j \cdot \mathbf{Q}_L^i\right)\hat{\mathbf{x}}^l\right) = 0. \tag{1.76}$$

Equation 1.76 can be regarded as a collection of partial differential equations that the mobility factors Q_1^{ijkl} must satisfy. In the usual case, we require that Q_1 depend only on space and time implicitly through the dependent variables u^i and not their derivatives, though this assumption could be relaxed if no such Cahn-Hilliard form exists. Under that assumption, Eq. 1.76 can be expanded in a Taylor series in the derivatives of u^i and the coefficient of each term is a partial differential equation which the mobility factors must satisfy. This expansion is analogous to the method of finding point symmetries of differential equations that we will discuss in Section 2.2 below. Finding some collection of mobility factors that form a solution to Eq. 1.76 is

the first step to putting Eq. 1.74 into the form in Eq. 1.75. Once the mobility factors have been determined, the quantities ψ_k can be found using a homotopy operator as

$$\psi_k\left(\mathbf{X}'_L\right) = -\int_0^1 \frac{\mathrm{d}\lambda}{\lambda}\ \left(X^l\left(Q_1^{-1}\right)_{ijkl}\hat{\mathbf{x}}^j\cdot\mathbf{Q}^i_L\right)\Big|_{\mathbf{X}_L=\lambda\mathbf{X}'_L}. \tag{1.77}$$

We won't detail homotopy operators here, but refer the reader to [28]. Furthermore it is not always necessary to employ the homotopy formula as it is often easy to deduce ψ_k from the fluxes and mobilities. Once ψ_k is known, there is yet another exactness condition which needs to be satisfied, namely a functional one $\psi_k = \frac{\delta F}{\delta u^k}$. There exist yet another functional closedness condition analogous to Eq. 1.76, this time that the Fréchet derivative of ψ_k is self-adjoint $\mathbb{D}_\psi = \mathbb{D}^*_\psi$, where the Fréchet derivative and its adjoint are discussed in Section 2.1 and defined in Eq. 2.6 and Eq. 2.9 below. If this functional closedness condition is not satisfied for any possible mobility factor solutions to Eq. 1.76, we have proven that no such Lyapunov function exists. On the other hand when the functional closedness condition is satisfied, the Lyapunov functional F can be constructed using a functional homotopy operator analogous to Eq. 1.77, namely

$$F[\tilde{u}] = \int\left(\int_0^1 \frac{\mathrm{d}\lambda}{\lambda}\ \left(u^k\ \psi_k\right)\Big|_{u=\lambda\tilde{u}}\right)\mathrm{d}^2X. \tag{1.78}$$

Note that the Lyapunov energy is only uniquely defined up to the addition of a null Lagrangian, and thus the form in Eq. 1.78 may need to be integrated by parts to put it in a familiar form. This functional homotopy machinery is part of the variational or bivariational complex and is a relatively modern development which stems from the study of the inverse problem in the calculus of variations. A more complete description is available in [28].

The use of Eq. 1.76-1.78 in determining Lyapunov functions provides a powerful general method. For example, the author has applied this procedure to the surfactant spreading problem in Eq. 1.73 and revealed a Cahn-Hilliard form depending on a function $W_{\mathrm{SS}}(\Gamma)$ with more general mobility factors

$$\begin{aligned}
0 &= \frac{\partial H}{\partial t} - \nabla_L\cdot\left(\frac{H^3}{3}\nabla_L\frac{\delta F_{\mathrm{SS}}}{\delta H} + \frac{H^2\Gamma}{2W''_{\mathrm{SS}}(\Gamma)}\nabla_L\frac{\delta F_{\mathrm{SS}}}{\delta\Gamma}\right),\\
0 &= \frac{\partial\Gamma}{\partial t} - \nabla_L\cdot\left(\frac{H^2\Gamma}{2}\nabla_L\frac{\delta F_{\mathrm{SS}}}{\delta H} + \frac{1}{W''_{\mathrm{SS}}(\Gamma)}\left(H\Gamma^2 + \frac{\bar{\mathrm{Pe}}}{\bar{\mathrm{Ma}}}\Gamma\right)\nabla_L\frac{\delta F_{\mathrm{SS}}}{\delta\Gamma}\right),
\end{aligned} \tag{1.79}$$

with an associated family of Lyapunov functionals

$$F_{\mathrm{SS}}[H,\Gamma] \equiv \int \mathrm{d}^2X\, \mathcal{F}\,(\mathbf{X}_L,t)\,,$$
$$\mathcal{F}_{\mathrm{SS}} \equiv \frac{\bar{\mathrm{Ca}}^{-1}}{2}\,|\nabla_L H|^2 + \bar{\mathrm{Ma}} W_{\mathrm{SS}}(\Gamma), \tag{1.80}$$

where the positive definiteness condition is met only if $1/3 < \Gamma W''_{\mathrm{SS}}(\Gamma) < 3$. One particular class with $W_{\mathrm{SS}}(\Gamma) = \Gamma \log \Gamma^s$, where $1/3 < s < 3$, generalizes the Lyapunov function of Thiele, Archer, and Plapp noted above.

1.4 Notes

The quantitative study of thin films of viscous fluids is well over a century old, beginning with Reynolds' description of the fluid flow of an oil layer lubricating a rotating journal bearing [29]. The parallel study of fluid convection driven by heating has a particularly rich history originating with Bénard's first observations of cellular convection at the start of the twentieth century [30]. Lord Rayleigh's seminal description of buoyancy driven convection [31] had enormous influence on physics, and the study of pattern formation that developed is currently an active area of research [32]. The identification of surface tension variations as the relevant driving force for many thin films, including those observed by Bénard, was uncovered in the middle of the twentieth century [33–37], and a variety of linear stability results were established then. The study of thin films with a free interface was extensively explored in the late 20th century. During that time, Davis in the United States [22, 38] and Kopbosynov and Pukhnachev in the Soviet Union [21] independently introduced the use of Reynolds' lubrication theory in deriving an evolution equation for the film thickness. Oron and Rosenau first described the use of Lyapunov functions for thin film equations [18]. Later, Van Hook [14, 39] compared simulations with experiments and recognized an important difference (the sign of his two-layer Biot number) between fluid films which are placed in a confined geometry and fluid films which are unconfined above the free interface. An review article detailing many of these developments in the study of thin films is also available [23].

Much of the recent work on the thermocapillary instability in thin films is motivated by the prospect of generating micro- and nano-scale patterns for the purpose of manufacturing devices such as optical arrays. Experiments from Chou et al. [5, 6], Schäffer et al. [7–9], Peng et al. [10], and Troian et al. [11–13] demonstrated this possibility and highlight advantages over existing lithographic manufacturing processes. In this same vein, the possibility of driving instabilities using electric

fields rather than temperature gradients has been explored by Steiner et al. and Pease and Russel, among others [40–43]. The use of the lubrication approximation to model the elecrohydrodynamic problem with leaky dielectrics came more recently in the work of Shankar and Sharma [44], Craster and Matar [45], and Merk et al. [24]. A model with a perfect dielectric and with negligible viscosity in the top fluid layer using the film equation in Eq. 1.68 with the Lyapunov contribution in Eq. 1.72 will suffice for the purposes of this thesis. The inclusion of Van der Waals interactions is frequently introduced to model thin film rupture and contact line motion, as the Van der Waals interaction is known to become increasingly relevant for ultra thin films. DeGennes' review [46] is a classic account of many aspects of contact lines. Early numerical work on thin film equations such as the paper of Oron et al. [18, 47] often encountered numerical singularities during film rupture events. More recently, Thiele et al. have demonstrated how a repulsive Van der Waals interaction leads to ultra thin precursor films rather than rupture and allowed more extensive numerical analysis of thin film equations [24, 48, 49]. The most frequently employed model of Van der Waals interactions utilizes a retarded potential which is predominantly phenomenological, and a satisfactory theoretical hydrodynamics which includes Van der Waals interactions consistently is wanting. Since we do not require Van der Waals interactions to regulate numerics in this thesis, they will generally be neglected. The study of the spreading of an insoluble surfactant on a thin viscous film has an alternate motivation and history in medicine as human respiratory and ocular systems rely on surfactants to reduce surface tension [25]. The most recent major elaboration of the thin film equation in the literature is the thin viscous bilayer model of Merkt et al. noted in Section 1.2 [24]. The related problem of a two layer fluid film with a free interface between the layers and at a second interface with the overhead air has also received significant attention recently [50–53].

The first original contribution to the field from this thesis is the coupled thick-thin bilayer model in Eqns.1.55-1.56 in Section 1.2. This model exhibited a non-local character that is not present in other thin film equations. We further showed how the limit of a thin top layer in this model matches with the thin bilayer model of Merkt et al. [24]. This thin-thick film equation should also be compared with the boundary element method [54], which permits two-dimensional modeling of three-dimensional fluid flows by monitoring quantities and fluxes only at the boundary of a domain. The boundary element method shares the non-local character of Eq. 1.55, but requires many more dependent variables, including one for each component of

momentum, one for heat, and even more for the fluxes of these variables rather than the single dependent variable H of Eq. 1.55. The second original contribution to the field from this thesis is the description of homotopy methods in deriving Lyapunov functions in Section 1.3. This work complements recent work by Thiele et al. putting surfactant and solute transport equations into gradient form [26, 55]. The homotopy methods developed for use in the inverse problem of the calculus of variations have a very long and interesting history [28]. As far as the author is aware, the description of additional Lyapunov functionals for the surfactant spreading problem in Eq. 1.80 is new. The author has not discovered any application of these additional Lyapunov functionals to the surfactant spreading problem, but has noted the use of multiple Lyapunov functions in rigorously establishing convergence to steady states from arbitrary initial conditions in some mathematical works [56, 57].

Chapter 2

SYMMETRY ANALYSES

The purpose of this chapter is to discuss symmetry analysis methods in the study of partial differential equations. First among them is the study of self-similar solutions. The method of reducing the number of independent variables in partial differential equations by seeking similarity variables is ubiquitous in fluid mechanics. This procedure is usually carried out in hopes of finding a particular solution which is believed to at least approximate the evolution of a physical system. In Section 2.1 we argue for a deeper mathematical motivation for this fundamental analysis: such solutions provide important geometrical information about the system's general solution space. Next in Section 2.2 we derive the point symmetries of various thin film equations with the aid of the symbolic computation package zgnsymmetry.m which the author wrote for Mathematica. The package is included in full in Appendix A. Finally, Section 2.3 contains a discussion of the history and literature in the field, with an attempt to place the new research contained in this chapter in a wider context.

2.1 Geometrical interpretations of self-similar solutions

To develop motivation for the study of self-similar solutions of partial differential equations, consider first a simpler dynamical systems example of a set of ordinary differential equations,

$$\frac{\partial u^1}{\partial x^0} = u^2, \quad \frac{\partial u^2}{\partial x^0} = -(u^1)^3 + u^1, \tag{2.1}$$

where superscripts are indices enumerating dependent and independent variables, not exponents. These are the evolution equations for a one-dimensional anharmonic oscillator in phase space, where the independent variables are the displacement u^1 and its conjugate momentum u^2 and the dependent variable x^0 is time (this notation is used here to be consistent with later notation). Since Eq. 2.1 is autonomous, its fixed points can be studied. There are three such fixed points, a hyperbolic fixed point at $(u^1, u^2) = (0, 0)$ and two elliptic fixed points at $(u^1, u^2) = (\pm 1, 0)$. The stable and unstable manifolds of the hyperbolic fixed point coincide as a homoclinic separatrix, depicted as a red line in the phase portrait on the (u^1, u^2) coordinate plane in Fig. 2.1 below.

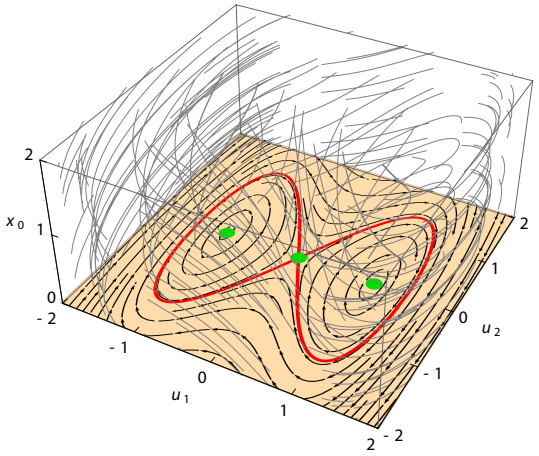

Figure 2.1: The extended phase space of Eq. 2.1. One-dimensional solution trajectories (gray lines) foliate this space. Projection onto the (u^1, u^2) phase plane reveals the geometric structure of the foliation characterized by the green fixed points and the red separatrix.

In this simple example, the charateristics of the fixed points, i.e., their stability and the separatrices eminating from them, have important implications regarding the geometric structure of the phase space as a whole. Many other examples of fixed points having important influence on the topology of solutions in phase space are known in dynamical systems, including their relevance in the emergence of chaos. In the language of symmetry analysis, the fact that Eq. 2.1 is autonomous is a time-translational symmetry of the differential system. Furthermore, the fixed points of Eq. 2.1 are simply the group-invariant solutions of this equation under this symmetry. These concepts can be generalized in a straightforward manner to partial differential equations. In order to make this generalization concrete, we introduce briefly here some of the language of jet bundles that aid in the symmetry analysis of partial differential equations. This discussion is introductory and pedagogical – more formal developments are available in the mathematics literature [28, 58].

Suppose we want to study n coupled partial differential equations with $m + 1$ independent variables and n dependent variables, denoted as $x = (x^0, x^1, \ldots, x^m)$ and $u = (u^1, u^2, \ldots, u^n)$, respectively. Partial derivatives of dependent variables will be denoted by $u^j_{(\nu)} \equiv \frac{\partial^{|\nu|} u^j}{\partial (x^0)^{\nu_0} \partial (x^1)^{\nu_1} \cdots \partial (x^m)^{\nu_m}}$, where ν is a multi-index and $|\nu| = \nu_0 + \nu_1 + \cdots + \nu_m$, and the system of partial differential equations under study will be written $\Delta_j(x, u; u_{(\nu)}) = 0$, where Δ_j is a set of differential functions depending on the dependent and independent variables and the partial derivatives of the dependent variables. Forget for the moment that we ultimately regard the dependent variables

as functions of the independent variables, and instead consider them as just variables which can take on values in some domain like $\mathbb{R}$. In fact, rather than considering u and x simply as variables, it is advantageous to consider them as coordinates on manifolds. Let $\mathcal{U}$ be an n-dimensional manifold with coordinates $(u^1, u^2, \ldots, u^n)$ and $\mathcal{X}$ an $(m+1)$-dimensional manifold with coordinates $(x^0, x^1, \ldots, x^m)$, and consider the $(m+n+1)$-dimensional manifold $\mathcal{M} = \mathcal{U} \otimes \mathcal{X}$. We will avoid technical issues like the distinction between a local coordinate patch and the entire manifold itself by assuming that these coordinate systems cover the entire manifold which is Cartesian, i.e. $\mathcal{M} = \mathbb{R}^{m+n+1}$. One reason this geometric interpretation is preferred is because it is often advantageous to change coordinates on $\mathcal{M}$ to various combinations of the original independent and dependent variables in order to simplify the system of differential equations, and a coordinate independent understanding of the system is desired. A solution to the system of equations under study is a set of function $f^j(x^0, x^1, \ldots, x^m)$ which renders the equations an identity when $u = f$, so that $\Delta_j \left(x, f(x); \frac{\partial^{|\nu|} f(x)}{\partial (x^0)^{\nu_0} \partial (x^1)^{\nu_1} \cdots \partial (x^m)^{\nu_m}} \right) = 0$ holds identically. Geometrically, a solution of the partial differential equations is its graph, an $m+1$-dimensional submanifold $\mathcal{S} \subset \mathcal{M}$,

$$\mathcal{S} = \left\{ (x, u) \in \mathcal{M} \mid u^j = f^j(x^0, x^1, \ldots x^m) \right\}.$$

Next is a somewhat abstract conceptual leap – consider the manifold $\mathcal{U}^{(s)}$ whose coordinates are all the partial derivatives $(u_{(\nu)})$ of order $|\nu| < s$ including the zeroth order partial derivatives which are simply the dependent variables themselves, and let $\mathcal{M}^{(s)} = \mathcal{U}^{(s)} \otimes \mathcal{X}$. This construction is called the sth order jet bundle [58]. Such fiber bundles are generalizations of the more familiar tangent and cotangent bundles of coordinate manifolds in Hamiltonian mechanics. If the set of differential equations $\Delta_j = 0$ contain at most sth order partial derivatives, then the equations $\Delta_j(x, u; u_{(\nu)}) = 0$ are simply algebraic equations in the jet bundle which define some subvariety $\mathscr{S}^{(s)}_{\Delta} \subset \mathcal{M}^{(s)}$,

$$\mathscr{S}^{(s)}_{\Delta} = \left\{ (x, u; u_{(\nu)}) \in \mathcal{M}^{(s)} \mid \Delta_j(x, u; u_{(\nu)}) = 0 \right\}.$$

The distinction between a smooth manifold and a variety is not particularly important for our discussion – only note that varieties may have singularities such as cusps where they are not locally diffeomorphic to a Cartesian space. Mapping out such singularities of $\mathscr{S}^{(s)}_{\Delta}$ is another geometrical aspect which will not be discussed for the moment. Mathematical objects like functions and vector fields on $\mathcal{M}$ are said to prolong to corresponding objects in the jet bundle $\mathcal{M}^{(s)}$. These prolonged objects

are found by requiring the natural differential relations between the coordinates of the jet bundle are satisfied. For example, the manifold $\mathcal{S}$ associated to a solution $u = f(x)$ prolongs to the manifold

$$\mathcal{S}^{(s)} = \left\{ (x, u; u_{(\nu)}) \in \mathcal{M}^{(s)} \,\middle|\, u^j_{(\nu)} = \frac{\partial^{|\nu|} f^j(x)}{\partial (x^0)^{\nu_0} \partial (x^1)^{\nu_1} \cdots \partial (x^m)^{\nu_m}} \forall\, |\nu| \leq s \right\}.$$

For ordinary differential equations, the space $\mathscr{S}^{(s)}_\Delta$ is the extended phase space which is foliated by the prolongation of solutions as in Fig. 2.1. There is, however, one caveat when generalizing to more independent variables – in contrast to ordinary differential equations, for partial differential equations there may be multiple solution manifolds which pass through a point of $\mathscr{S}^{(s)}_\Delta$, so a single foliation of $\mathscr{S}^{(s)}_\Delta$ could never enumerate all possible solutions to a partial differential equation. This is best illustrated through an example. Consider the linear partial differential equation $\Delta_1 \equiv \frac{\partial u^1}{\partial x^0} + \frac{\partial u^1}{\partial x^1} = 0$ with general solution $u^1 = f(x^0 - x^1)$ for any smooth function $f : \mathbb{R} \to \mathbb{R}$. If f_1 and f_2 are two such solutions with corresponding prolonged manifolds $\mathcal{S}^{(1)}_1$ and $\mathcal{S}^{(1)}_2$ in the first order jet bundle $\mathcal{M}^{(1)}$ and if there are constants $A, B, C \in \mathbb{R}$ such that $f_1(C) = f_2(C) = A$ and $f_1'(C) = f_2'(C) = B$, then the curve in the first order jet bundle parameterized by x^0

$$\left\{ (x, u; u_{(\nu)}) \in \mathcal{M}^{(1)} \,\middle|\, x^1 = x^0 - C,\ u^1 = A, u^1_{(1,0)} = -u^1_{(0,1)} = B \right\}$$

lies in both $\mathcal{S}^{(1)}_1$ and $\mathcal{S}^{(1)}_2$, so that these manifolds have a non-empty intersection. We cannot then unambiguously associate a solution leaf to each point in $\mathscr{S}^{(s)}_\Delta$ as was done in Fig. 2.1. One way to resolve this ambiguity is to consider prolonging $\mathscr{S}^{(s)}_\Delta$ to another subvariety $\mathscr{S}^{(k)}_\Delta$ which resides in a higher order jet bundle $\mathcal{M}^{(k)}$ with $k > s$ by imposing in addition to $\Delta_j = 0$ that all the partial derivatives of Δ_j which involve partial derivatives of the dependent variables of order less than or equal to k also vanish. If $f_1''(C) \neq f_2''(C)$, then it is clear that in the second-order jet bundle the prolongations $\mathcal{S}^{(2)}_1$ and $\mathcal{S}^{(2)}_2$ would no longer intersect. To fully resolve all ambiguities, we can consider the prolongation to the infinite order jet bundle [58]. A related observation is that since the general solution of this partial differential equation involves an arbitrary function f, an infinite number of integration constants such as the coefficients in the Taylor series of f are required to enumerate all solutions, so the codimensional of a solution leaf must therefore be infinite.

The symbol $\mathscr{S}_\Delta$ will be used to denote the infinite prolongation of the differential system under study, and it will be called the extended phase space of the system

of partial differential equations. For ordinary differential equations, this infinite prolongation actually remains finite-dimensional – for each prolongation to the next order jet bundle, n new derivative coordinates are introduced and n new constraints are imposed by taking one more derivative of each the n equations $\Delta_j = 0$, so the dimension of $\mathscr{S}_\Delta^{(k)}$ does not increase as k increases and all the $\mathscr{S}_\Delta^{(k)}$ and $\mathscr{S}_\Delta$ are isomorphic. Thus, for example, the extendend phase space $\mathscr{S}_\Delta$ for Eq. 2.1 is the three-dimensional space depicted in Fig. 2.1. On the other hand, for partial differential equations the space $\mathscr{S}_\Delta$ will be infinite-dimensional. The local solvability and uniqueness of analytic partial differential equations of interest here is provided by the Cauchy-Kovalevski theorem [28]. This result permits us to consider a local foliation of the infinite-dimensional space $\mathscr{S}_\Delta$ by solutions of the differential equaiton.

A qualitative study of a system of partial differential equations should aim to understand the structure of the foliation of the extended phase space by solutions. What exactly do we mean by the structure of this foliation? Locally we expect the infinitely prolonged space $\mathscr{S}_\Delta$ to be quite homogenously sliced into $m+1$-dimensional submanifolds by the foliation. Let us return to the example in Eq. 2.1 for concreteness - the extended phase space for this system can be coordinatized by (x^0, u^1, u^2) and is depicted in Fig. 2.1 above. Through each point passes a leaf of the foliation which is the one-dimensional trajectory that describes a solution. Because of the time translational symmetry of Eq. 2.1, translating any such leaf vertically maps it onto another leaf. The quotient space formed by projecting out time is the usual phase space shown on the (u^1, u^2) coordinate plane in Fig. 2.1, and the structure of the foliation becomes clear only after this projection. Note that solutions which are themselves invariant under time translations project down to zero-dimensional fixed points rather than lines.

The procedure of forming a quotient space of the extended phase space is a general one given any symmetry of a differential system. Formally, a vector field on $\mathcal{M}$,

$$\vec{v} = \xi^i_{\text{sym}}(x,u)\frac{\partial}{\partial x^i} + \phi^j_{\text{sym}}(x,u)\frac{\partial}{\partial u^j}, \tag{2.2}$$

generates a point symmetry of the differential system if $\mathscr{S}_\Delta$ is invariant under the flow generated by its prolongation. Details about the prolongation of vector fields can be found in [28], and an analytic statement of this condition is given below in Eq. 2.7. Any solution to $\Delta = 0$ is mapped onto another solution to $\Delta = 0$ under the flow generated by a symmetry. Given a generator of some symmetry $\vec{v}$, it is

generally possible to consider $n+m$ independent invariants of $\vec{v}$, which are functions $\eta^k(x,u)$ on $\mathcal{M}$ such that

$$\vec{v}(\eta^k) = \xi^i_{\text{sym}}(x,u)\frac{\partial \eta^k}{\partial x^i} + \phi^j_{\text{sym}}(x,u)\frac{\partial \eta^k}{\partial u^j} = 0. \tag{2.3}$$

To find invariants, we can consider Eq. 2.3 as a linear partial differential equation that needs to be solved for the unknown η^k, and the method of characteristics can be used to find a full set of independent invariants. Similarly, we can consider another special function η^0 that satisfies the linear partial differential equation

$$\vec{v}(\eta^0) = \xi^i_{\text{sym}}(x,u)\frac{\partial \eta^0}{\partial x^i} + \phi^j_{\text{sym}}(x,u)\frac{\partial \eta^0}{\partial u^j} = 1. \tag{2.4}$$

If we change coordinates on $\mathcal{M}$ to $(\eta^0, \eta^1, \ldots, \eta^{n+m})$, we will straighten out the generator of the symmetry to $\vec{v} = \frac{\partial}{\partial \eta^0}$. Since $\vec{v}$ is a symmetry of $\Delta(x,u) = 0$, this implies that in these new coordinates, the transformed set of equations

$$\tilde{\Delta}(\eta^0, \eta^1, \ldots, \eta^{n+m}) = 0$$

does not depend on η^0, and the equations are autonomous with respect to η^0 if we take η^0 to be one of the independent variables. The extended phase space $\mathscr{S}_\Delta$ can then be projected along the η^0 axis to form a quotient manifold $\mathscr{S}_\Delta/G$ with coordinates $(\eta^1, \eta^2, \ldots, \eta^{n+m})$, where G is the Lie group with generator $\vec{v}$. This quotient manifold is analogous to the phase space of autonomous ordinary differential equations. General solutions $\mathcal{S}^{(s)} \subset \mathscr{S}_\Delta$ project down to $m+1$-dimensional manifolds on $\mathscr{S}_\Delta/G$ analogous to the phase space trajectories of an ordinary differential equation. However, solutions which are themselves invariant under G will project down to m-dimensional manifolds in $\mathscr{S}_\Delta/G$ analogous to fixed points. Such solutions are called self-similar or group-invariant solutions. When searching for self-similar solutions, we need only solve a system of partial differential equations in m independent variables and n dependent variables which is derived from $\tilde{\Delta}(\eta^0, \eta^1, \ldots, \eta^{n+m}) = 0$ by simply setting all η^0 derivatives to zero. Further symmetries of these reduced equations permit further projections of the space of self-similar solutions, and in practice most special solutions to partial differential equations are found through such reductions.

There exists a general procedure to find all the point symmetries of a given set of partial differential equations. The invariance condition that the phase space $\mathscr{S}_\Delta$ be invariant under the flow generated by the prolongation of $\vec{v}$ is equivalent to a set of

linear differential conditions on the generator coefficients. Define the characteristic of the generator

$$Q^j_{\vec{v}}\left(x,u;u_{(\nu)}\right) \equiv \phi^j_{\text{sym}}\left(u,x\right) - \xi^i_{\text{sym}}\left(u,x\right) u^j_{(\hat{\nu}_i)}, \tag{2.5}$$

where $\hat{\nu}_i$ is the multi-index with a one in the ith entry and a zero in every other entry and ϕ_{sym} and ξ_{sym} are the coefficients of the generator in Eq. 2.2. Also define the Fréchet derivative of Δ, $\mathbb{D}_\Delta$, which acts on differential functions f^j depending on the independent variables, the dependent variables, and the partial derivatives of the dependent variables,

$$(\mathbb{D}_\Delta)_{j_1 j_2}(f^{j_2}) \equiv \sum_\nu \frac{\partial \Delta_{j_1}}{\partial u^{j_2}_{(\nu)}} \left(\frac{d}{dx^0}\right)^{\nu_0} \left(\frac{d}{dx^1}\right)^{\nu_1} \cdots \left(\frac{d}{dx^m}\right)^{\nu_m} (f^{j_2}), \tag{2.6}$$

where the sum ranges over all multi-indices and the total derivative is

$$\frac{d}{dx^i} = \frac{\partial}{\partial x^i} + \sum_\nu u^j_{(\nu+\hat{\nu}_i)} \frac{\partial}{\partial u^j_{(\nu)}}.$$

The Fréchet derivative of Δ is sometimes called the linearized equation since it is the linear operator that appears when considering perturbations of solutions. The symmetry condition that is satisfied when $Q_{\vec{v}}$ is the characteristic of a symmetry of Δ is

$$(\mathbb{D}_\Delta)_{j_1 j_2}(Q^{j_2}_{\vec{v}})\Big|_{\mathscr{S}_\Delta} = 0, \tag{2.7}$$

where the result is evaluated only on the extended phase space [28]. Any choice of ξ_{sym} and ϕ_{sym} which satisfies Eq. 2.7 generates a symmetry of Δ. The crucial observation is the while ξ_{sym} and ϕ_{sym} depend only on u and x, the various derivatives $u_{(\nu)}$ also appear in Eq. 2.7. Thus the coefficient of every monomial in these derivatives must vanish independently. In this manner, Eq. 2.7 corresponds to a large number of generally over-determined linear determining equations which we must solve to enumerate all the point symmetries of Δ. Finally, aside from the characterization that self-similar solutions $u = f$ depend only on invariants of the symmetry generated by $\vec{v}$, another characterization [28] of self-similar solutions is that the characteristics vanish,

$$Q^j_{\vec{v}}\left(x,u;u_{(\nu)}\right)\Big|_{u=f(x)} = 0 \text{ when } f(x) \text{ is invariant under } \vec{v}. \tag{2.8}$$

In addition to $\Delta = 0$, self similar solutions must satisfy Eq. 2.8 which is another set of partial differential equations. The compatibility conditions between this new set of equations and $\Delta = 0$ are guaranteed by the symmetry condition in Eq. 2.7.

In searching for self-similar solutions to some set of partial differential equations, we can hope to map out structures in the phase spaces of the solution set to gain a qualitative understanding of the possible behaviors of solutions. Furthermore, given any particular self-similar solution, a local analysis can be carried out for nearby solutions by finding eigenvalues and eigenfunctions of a linearized problem. By numerically solving the equation in the direction of the eigenfunctions, we could try to map out the separatrices in these phase spaces as well. In practice, this is a fairly daunting task for even very simple nonlinear partial differential equations, and we will only partially complete such analyses for a few thin film equations in the remainder of this thesis. In closing this discussion, we emphasize that many concepts from dynamical systems can be applied to partial differential equations with this geometric perspective in mind. For example, what could we learn from the Poincaré sections of these projections of the extended phase space? For what equations and under what circumstances do fractal sets appear in these phase spaces, and does this inform us at all about systems with spatio-temporal chaos? For Hamiltonian systems, is there an invariant tori structure around self-similar solutions, and if so what can be said about its structual stability to perturbations? Such investigations seem a promising direction in this very challenging field.

Lastly before closing this section, another important aspect of symmetry analyses is their connection to conservation laws. For variational problems with an action functional, the celebrated Noethers' theorem guarantees a conservation law for every symmetry of the action. The thin film equations of interest here, however, do not minimize an action, and thus the classic form of Noethers' theorem does not apply. There is a more modern generalization which applies to all partial differential equations, however. The statement of this result requires the adjoint of the Fréchet derivative

$$(\mathbb{D}^*_\Delta)_{j_1 j_2}(f^{j_2}) \equiv \sum_\nu \left(-\frac{d}{dx^0}\right)^{\nu_0} \left(-\frac{d}{dx^1}\right)^{\nu_1} \cdots \left(-\frac{d}{dx^m}\right)^{\nu_m} \left(\frac{\partial \Delta_{j_2}}{\partial u^{j_1}_{(\nu)}} f^{j_2}\right). \tag{2.9}$$

The general condition [28, 59] that guarantees a conservation law is that there exist a set of multipliers Λ^j such that

$$(\mathbb{D}^*_\Delta)_{j_1 j_2}(\Lambda^{j_2}) + (\mathbb{D}^*_\Lambda)_{j_1}{}^{j_2}(\Delta_{j_2}) = 0. \tag{2.10}$$

The Λ here is not restricted to depend only on the u and x but may depend on arbitrarily high derivatives $u_{(\nu)}$, and we call the highest order derivative on which Λ depends the order of the multiplier. This condition can be related to an adjoint

symmetry condition by restricting the result to the extended phase space

$$(\mathbb{D}^*_\Delta)_{j_1 j_2}(\Lambda^{j_2})\Big|_{\mathscr{S}_\Delta} = 0, \tag{2.11}$$

where the second term in Eq. 2.10 vanishes because $\Delta = 0$ on $\mathscr{S}_\Delta$. As for point symmetries, Eq. 2.11 generates a large number of adjoint determining equations through the coefficients of the monomials involving derivatives of dependent variables for which Λ does not depend. Not every adjoint symmetry solution to Eq. 2.11 is a multiplier for a conservation law, but every multiplier for a conservation law satisfies Eq. 2.11. Once the multipliers are known, there is a closed form expression for the conserved current of the conservation law [59]. One can solve Eq. 2.11 for any order $|\nu|$ to systematically enumerate the adjoint symmetries, and then find which adjoint symmetries satisfy Eq. 2.10 to enumerate all the conservation laws. Note also that in the case that the Fréchet derivative is self-adjoint, the symmetries and the adjoint symmetries of Δ coincide and the symmetries of Δ correspond to conservation laws just as in Noether's theorem. As noted in Section 1.3, the exactness of the variational complex implies that the Fréchet derivative of Δ is self adjoint if and only if Δ is the functional derivative of some action functional. Thus we see that Noethers' theorem is a special case of this connection between conservation laws and adjoint symmetries.

2.2 Calculations of symmetries and reductions of thin film equations

[1] Z. G. Nicolaou and S. M. Troian. "Embedded symmetries and classes of self-similar solutions of the thin film equations". In: *Phys. Rev. Fluids* (preparing for submission 2016).

In this section, we will carry out symmetry analyses of the some of thin film equations described in Chapter 1. First we will consider a driven film with one dependent variable H. Then we will consider the surfactant spreading problem with two dependent variables H and Γ. Our calculations rely on computational assistance from the Mathematica package zgnsymmetry.m, which is included in full in Appendix A.

Thin film equations with a single dependent variable H

Here we consider the symmetries of the general thin film equation in Eq. 1.68 with no fluid slip, namely

$$\Delta_1 = \frac{\partial H}{\partial t} + \nabla_L \cdot \left(\frac{H^3}{3} \nabla_L \left(\bar{\mathrm{Ca}}^{-1} \nabla_L^2 H - W'(H) \right) \right) = 0. \tag{2.12}$$

To find symmetries of Eq. 2.12, we must solve Eq. 2.7 for the generators $\xi_{\rm sym}$ and $\phi_{\rm sym}$. Since Eq. 2.12 is fourth order in space and depends on two spatial independent variables, the invariance condition in Eq. 2.7 turns out to be an enormous equation, consisting of 3071 individual terms! Dealing with such large expressions by hand is not feasible. However, as noted above this large equation actually generates a large list of simpler equations which must be satisfied, namely the coefficients of the derivatives of H in this expression. Some of these equations are very simple and can be readily solved. To aid in our analysis, we have written a Mathematica package to isolate simple terms in the invariance condition. The package file zgnsymmetry.m is included in Appendix A, and a digital version can be supplied by the author upon request. Once the package file zgnsymmetry.m is placed in the Applications folder in the Mathematic user base directory, it can be included in a Mathematica notebook with the command

```
<< zgnsymmetry`
```

To use the package, we must define Mathematica functions of the independent variables for the differential equations Δ

```
Delta1[t_,x_,y_]:=D[H[t,x,y],t]+Div[1/3*H[t,x,y]^3*(Grad[Laplacian[H[t,x,y],{x,y}]\
-W'[H[t,x,y]],{x,y}]),{x,y}];
```

Similarly the characteristics $Q_{\vec{v}} = \phi_{\rm sym} - \xi^i_{\rm sym} H_{(v_i)}$ are defined as Mathematica functions of the independent variables

```
Q1[t_,x_,y_]:=Phi1[t,x,y,H[t,x,y]]-Xi0[t,x,y,H[t,x,y]]*D[H[t,x,y],t]\
-Xi1[t,x,y,H[t,x,y]]*D[H[t,x,y],x]-Xi2[t,x,y,H[t,x,y]]*D[H[t,x,y],y];
```

The equations and characteristics are put into lists

```
Delta = {Delta1};
Q = {Q1};
```

We next define a list of independent and dependent variables and a list of variables which will be eliminated when solving $\Delta = 0$,

```
var = {{t, x, y}, {H}};
solvefor = {Derivative[1, 0, 0][H]};
```

The function FindInvariance returns the invariance condition in Eq. 2.7. For example, we can see the number of terms in the invariance condition with

```
Plus @@ Length /@ FindInvariance[Delta,var,Q,solvefor]
```

which returns 3071, as claimed before. The zgnsymmetry.m package contains a function FindEquations which returns a list consisting of the number of equations, the equations themselves, and the monomials to which that equation corresponds for equations with a specified number of terms. By solving equations involving only a small number of terms first, we can effectively find all the symmetries of Eq. 2.12.

We first run FindEquations, looking for equations with 1 term.

```
FindEquations[Delta, var, Q, solvefor, 1]
```

This reveals that there are 316 equations in the determining system, including

$$\frac{\partial \xi^0_{\text{sym}}}{\partial X} = 0,$$
$$\frac{\partial \xi^0_{\text{sym}}}{\partial Y} = 0,$$
$$\frac{\partial \xi^0_{\text{sym}}}{\partial H} = 0,$$

appearing as coefficients for multiple monomial terms, including $H_{(0,7,0)}$, $H_{(0,0,7)}$, and $H_{(0,1,0)}H_{(0,7,0)}$, respectively. We can thus conclude that that

$$\xi^0_{\text{sym}}(t, X, Y, H) = \xi^0_{\text{sym}_1}(t),$$

where $\xi^0_{\text{sym}_1}$ is a new function which depends only on t. We then define this in Mathematica.

```
Xi0[t_,x_,y_,H_]:=Xi01[t];
```

We next run FindEquations, again looking for equations with 1 term.

```
FindEquations[Delta, var, Q, solvefor, 1]
```

This reveals that there are 78 equations in the determining system, including

$$\frac{\partial \xi^1_{\text{sym}}}{\partial H} = 0,$$
$$\frac{\partial \xi^2_{\text{sym}}}{\partial H} = 0,$$

appearing as coefficients for multiple monomial terms, including $H_{(0,4,0)}H_{(0,1,0)}$ and $H_{(0,0,4)}H_{(0,0,1)}$, respectively. We can thus conclude that

$$\xi^1_{\text{sym}}(t, X, Y, H) = \xi^1_{\text{sym}_1}(t, X, Y),$$
$$\xi^2_{\text{sym}}(t, X, Y, H) = \xi^2_{\text{sym}_1}(t, X, Y).$$

We then define this in Mathematica.

```
Xi1[t_,x_,y_,H_]:=Xi11[t,x,y];
Xi2[t_,x_,y_,H_]:=Xi21[t,x,y];
```

We next run FindEquations, again looking for equations with 1 term.

```
FindEquations[Delta, var, Q, solvefor, 1]
```

This reveals that there are 31 equations in the determining system, including

$$\frac{\partial^2 \phi^1_{\text{sym}}}{\partial H^2} = 0,$$

appearing as a coefficient for multiple monomial terms, including $H^2_{(0,2,0)}$. We can thus conclude that

$$\phi^1_{\text{sym}}(t, X, Y, H) = \phi^1_{\text{sym}_1}(t, X, Y) + H\phi^1_{\text{sym}_2}(t, X, Y).$$

We then define this in Mathematica.

```
Phi1[t_,x_,y_,H_]:=Phi11[t,x,y]+H*Phi12[t,x,y];
```

We next run FindEquations, now looking for equations with 4 terms.

```
FindEquations[Delta, var, Q, solvefor, 4]
```

This reveals that there are 26 equations in the determining system, including

$$2\phi^1_{\text{sym}_1} + H\left(3\phi^1_{\text{sym}_2} + \frac{\partial \xi^0_{\text{sym}_1}}{\partial t} - 4\frac{\partial \xi^1_{\text{sym}_1}}{\partial X}\right) = 0,$$
$$3\phi^1_{\text{sym}_1} + H\left(3\phi^1_{\text{sym}_2} + \frac{\partial \xi^0_{\text{sym}_1}}{\partial t} - 4\frac{\partial \xi^1_{\text{sym}_1}}{\partial X}\right) = 0,$$

appearing as coefficients for the monomials $H_{(0,1,0)}H_{(0,3,0)}$ and $H_{(0,4,0)}$, respectively. These equations imply that $\phi^1_{\text{sym}_1} = 0$. We then define this in Mathematica.

```
Phi11[t_,x_,y_]:=0;
```

We next run FindEquations, again looking for equations with 4 terms.

```
FindEquations[Delta, var, Q, solvefor, 4]
```

This reveals that there are 23 equations in the determining system, including

$$3\phi^1_{\text{sym}_2} + \frac{\partial \xi^0_{\text{sym}_1}}{\partial t} - 2\left(\frac{\partial \xi^1_{\text{sym}_1}}{\partial X} + \frac{\partial \xi^2_{\text{sym}_1}}{\partial Y}\right) = 0,$$

appearing as coefficients for multiple monomial terms, including $H_{(0,2,2)}$. This imples

$$\phi^1_{\mathrm{sym}_2} = \frac{1}{3}\left(2\left(\frac{\partial \xi^1_{\mathrm{sym}_1}}{\partial X} + \frac{\partial \xi^2_{\mathrm{sym}_1}}{\partial Y}\right) - \frac{\partial \xi^0_{\mathrm{sym}_1}}{\partial t}\right).$$

We then define this in Mathematica.

```
Phi12[t_,x_,y_]:=1/3*(2*(D[Xi11[t,x,y],x]+D[Xi21[t,x,y],y])-D[Xi01[t],t]);
```

We next run FindEquations, now looking for equations with 2 terms.

```
FindEquations[Delta, var, Q, solvefor, 2]
```

This reveals that there are 21 equations in the determining system, including

$$\begin{aligned}
2\frac{\partial^2 \xi^1_{\mathrm{sym}_1}}{\partial X \partial Y} &= \frac{\partial^2 \xi^2_{\mathrm{sym}_1}}{\partial Y^2},\\
2\frac{\partial^2 \xi^2_{\mathrm{sym}_1}}{\partial X \partial Y} &= \frac{\partial^2 \xi^1_{\mathrm{sym}_1}}{\partial X^2},\\
\frac{\partial \xi^1_{\mathrm{sym}_1}}{\partial X} &= \frac{\partial \xi^2_{\mathrm{sym}_1}}{\partial Y},
\end{aligned}$$

appearing as coefficients for multiple monomial terms, including $H_{(0,1,0)}H_{(0,0,2)}$, $H_{(0,2,0)}H_{(0,0,1)}$, and $H_{(0,4,0)}$, respectively. Differentiating the third equation with respect to Y and substracting the first equation reveals that $\frac{\partial^2 \xi^1_{\mathrm{sym}_1}}{\partial X \partial Y} = 0$. Likewise, differentiating the third equation with respect to X and subtracting the second equation reveal that $\frac{\partial^2 \xi^2_{\mathrm{sym}_1}}{\partial X \partial Y} = 0$. It follows that

$$\begin{aligned}
\xi^1_{\mathrm{sym}_1}(t,X,Y) &= \xi^1_{\mathrm{sym}_2}(t,X) + \xi^1_{\mathrm{sym}_3}(t,Y),\\
\xi^2_{\mathrm{sym}_1}(t,X,Y) &= \xi^2_{\mathrm{sym}_2}(t,X) + \xi^2_{\mathrm{sym}_3}(t,Y).
\end{aligned}$$

We then define this in Mathematica.

```
Xi11[t_,x_,y_]:=Xi12[t,x]+Xi13[t,y];
Xi21[t_,x_,y_]:=Xi22[t,x]+Xi23[t,y];
```

We next run FindEquations, again looking for equations with 1 term.

```
FindEquations[Delta, var, Q, solvefor, 1]
```

This reveals that there are 21 equations in the determining system, including

$$\begin{aligned}
\frac{\partial^2 \xi^1_{\mathrm{sym}_2}}{\partial X^2} &= 0,\\
\frac{\partial^2 \xi^2_{\mathrm{sym}_3}}{\partial Y^2} &= 0,
\end{aligned}$$

appearing as coefficients for monomial terms $H_{(0,0,2)}H_{(0,1,0)}$ and $H_{(0,0,1)}H_{(0,2,0)}$, respectively. It follows that

$$\xi^1_{\mathrm{sym}_2}(t,X) = \xi^1_{\mathrm{sym}_4}(t) + X\xi^1_{\mathrm{sym}_5}(t),$$
$$\xi^2_{\mathrm{sym}_3}(t,Y) = \xi^2_{\mathrm{sym}_4}(t) + Y\xi^2_{\mathrm{sym}_5}(t).$$

We then define this in Mathematica.

```
Xi12[t_,x_]:=Xi14[t]+x*Xi15[t];
Xi23[t_,y_]:=Xi24[t]+y*Xi25[t];
```

We next run FindEquations, again looking for equations with 1 term.

```
FindEquations[Delta, var, Q, solvefor, 1]
```

This reveals that there are 13 equations in the determining system, including

$$\frac{\partial^2 \xi^1_{\mathrm{sym}_3}}{\partial Y^2} = 0,$$
$$\frac{\partial^2 \xi^2_{\mathrm{sym}_2}}{\partial X^2} = 0,$$

appearing as coefficients for multiple monomial terms, including $H_{(0,3,0)}$ and $H_{(0,0,3)}$, respectively. It follows that

$$\xi^1_{\mathrm{sym}_3}(t,Y) = Y\xi^1_{\mathrm{sym}_6}(t),$$
$$\xi^2_{\mathrm{sym}_2}(t,X) = X\xi^2_{\mathrm{sym}_6}(t),$$

where we absorb the integration constants into the previous terms $\xi^1_{\mathrm{sym}_4}(t)$ and $\xi^2_{\mathrm{sym}_4}(t)$. We then define this in Mathematica.

```
Xi13[t_,y_]:=y*Xi16[t];
Xi22[t_,x_]:=x*Xi26[t];
```

We next run FindEquations, again looking for equations with 2 term.

```
FindEquations[Delta, var, Q, solvefor, 2]
```

This reveals that there are 11 equations in the determining system, including

$$\xi^2_{\mathrm{sym}_5}(t) = \xi^1_{\mathrm{sym}_5}(t),$$
$$\xi^2_{\mathrm{sym}_6}(t) = -\xi^1_{\mathrm{sym}_6}(t),$$

appearing as coefficients for multiple monomial terms, including $H_{(0,4,0)}$ and $H_{(0,3,0)}H_{(0,0,1)}$. We then define this in Mathematica.

```
Xi25[t_]:=Xi15[t];
Xi26[t_]:=-Xi16[t];
```

We next run FindEquations, now looking for equations with 3 terms.

```
FindEquations[Delta, var, Q, solvefor, 3]
```

This reveals that there are 5 equations in the determining system, including

$$Y\frac{\partial \xi^1_{\text{sym}_5}}{\partial t} + \frac{\partial \xi^2_{\text{sym}_4}}{\partial t} - X\frac{\partial \xi^1_{\text{sym}_6}}{\partial t} = 0,$$
$$Y\frac{\partial \xi^1_{\text{sym}_6}}{\partial t} + \frac{\partial \xi^1_{\text{sym}_4}}{\partial t} + X\frac{\partial \xi^1_{\text{sym}_5}}{\partial t} = 0,$$

appearing as coefficients for monomial terms $H_{(0,0,1)}$ and $H_{(0,1,0)}$, respectively. Noting that the functions here depend only on t and not X or Y, the each term must vanish independently, so that

$$\xi^1_{\text{sym}_5}(t) = \xi^1_{\text{sym}_7},$$
$$\xi^1_{\text{sym}_6}(t) = \xi^1_{\text{sym}_8},$$
$$\xi^1_{\text{sym}_4}(t) = \xi^1_{\text{sym}_9},$$
$$\xi^2_{\text{sym}_4}(t) = \xi^2_{\text{sym}_9},$$

where the right hand sides are all constants. We then define this in Mathematica.

```
Xi15[t_]:=Xi17;
Xi16[t_]:=Xi18;
Xi14[t_]:=Xi19;
Xi24[t_]:=Xi29;
```

We next run FindEquations, again looking for equations with 1 term.

```
FindEquations[Delta, var, Q, solvefor, 1]
```

This reveals that there are 3 equations in the determining system, including

$$\frac{\partial^2 \xi^0_{\text{sym}_1}}{\partial t^2} = 0,$$

appearing as coefficients for the constant monomial term. This implies that

$$\xi^0_{\text{sym}_1}(t) = \xi^0_{\text{sym}_2} + t\xi^0_{\text{sym}_3}.$$

We then define this in Mathematica.

```
Xi01[t_]:=Xi02+t*Xi03;
```

We next run FindEquations, again looking for equations with 3 term.

```
FindEquations[Delta, var, Q, solvefor , 3]
```

This reveals 2 equations in the determining system, including

$$6\xi^1_{\text{sym}_7}\frac{\partial^2 W}{\partial H^2} - H\left(\xi^0_{\text{sym}_3} - 4\xi^1_{\text{sym}_7}\right)\frac{\partial^3 W}{\partial H^3} = 0, \tag{2.13}$$

appearing as a coefficient for multiple monomial terms, including $H_{(0,0,2)}$.

Here the symmetry consideration depends on the function $W(H)$. In the general case, Eq. 2.20 is satisfied only for $\xi^1_{\text{sym}_7} = \xi^0_{\text{sym}_3} = 0$. However, when W has a power law form

$$W(H) = \begin{cases} \frac{W_0}{\alpha(\alpha-1)}H^\alpha + W_1 H + W_2, & \text{if } \alpha \neq 0 \text{ and } \alpha \neq 1 \\ W_0 H \log(H) + W_1 H + W_2, & \text{if } \alpha = 1, \\ W_0 \log(H) + W_1 H + W_2, & \text{if } \alpha = 0, \end{cases} \tag{2.14}$$

for some constants W_0, W_1, W_2, and α, Eq. 2.13 can be solved with $\xi^0_{\text{sym}_3} = \frac{4\alpha-2}{\alpha-2}\xi^1_{\text{sym}_7}$. Lastly for purely capillary films with the power law form with $W_0 = 0$, Eq. 2.13 is satisfied with both $\xi^1_{\text{sym}_7}$ and $\xi^0_{\text{sym}_3}$ free parameters. We note that the terms $W_1 H$ and W_2 do not actually contribute any driving terms to the film equation. Thus there there are four, five, or six symmetries of Eq. 2.12 parameterized by $\xi^0_{\text{sym}_2}$, $\xi^1_{\text{sym}_9}$, $\xi^2_{\text{sym}_9}$, $\xi^1_{\text{sym}_8}$, and possibly $\xi^1_{\text{sym}_7}$ and $\xi^0_{\text{sym}_3}$, which correspond to time translations, spatial X translations, spatial Y translations, rotations, scalings, and scalings, respectively. These symmetries are summarized in Table 2.1.

Having enumerated the symmetries of Eq. 2.12, we now describe its reductions by one independent variable. As noted in Section 2.1, this is accomplished by seeking the invariants of an arbitrary symmetry using Eq. 2.3. Listing all the unique one-variable reductions requires finding an optimal system of one-dimensional Lie subalgebras [28]. This involves considering how an arbitrary linear combination of the vectors in Table 2.1 can be simplified under a finite symmetry transformation and is carried out with the adjoint representation of the group. Any one-variable reduction is related to one in the optimal system after a finite symmetry transformation such as a change in the origin or the Cartesian coordinates. The one-variable reductions of Eq. 2.12 are listed in Table 2.2. Similarly, to reduce Eq. 2.12 by two independent variables and hence find an ODE reduction, an optimal system of

Generators

Time translations: $\vec{v}^{\,1} = \frac{\partial}{\partial t}$
Spatial translations: $\vec{v}^{\,2} = \frac{\partial}{\partial X}$
Spatial translations: $\vec{v}^{\,3} = \frac{\partial}{\partial Y}$
Spatial rotations: $\vec{v}^{\,4} = -Y\frac{\partial}{\partial X} + X\frac{\partial}{\partial Y}$
Scalings: $\vec{v}_\alpha^{\,5} = -2H\frac{\partial}{\partial H} + (4\alpha - 2)t\frac{\partial}{\partial t} + (\alpha - 2)X\frac{\partial}{\partial X} + (\alpha - 2)Y\frac{\partial}{\partial Y}$

Lie Brackets

	$\vec{v}^{\,1}$	$\vec{v}^{\,2}$	$\vec{v}^{\,3}$	$\vec{v}^{\,4}$	$\vec{v}^{\,5}$
$\vec{v}^{\,1}$	0	0	0	0	$(4\alpha - 2)\vec{v}^{\,1}$
$\vec{v}^{\,2}$	0	0	0	$\vec{v}^{\,3}$	$(\alpha - 2)\vec{v}^{\,2}$
$\vec{v}^{\,3}$	0	0	0	$-\vec{v}^{\,2}$	$(\alpha - 2)\vec{v}^{\,3}$
$\vec{v}^{\,4}$	0	$-\vec{v}^{\,3}$	$\vec{v}^{\,2}$	0	0
$\vec{v}_\alpha^{\,5}$	$-(4\alpha - 2)\vec{v}^{\,1}$	$-(\alpha - 2)\vec{v}^{\,2}$	$-(\alpha - 2)\vec{v}^{\,3}$	0	0

Table 2.1: Generators of symmetries of Eq. 2.12 and their Lie brackets. The scaling $\vec{v}_\alpha^{\,5}$ are symmetries only for the power law form in Eq. 2.14. For purely capillary case with $W_0 = 0$, there are two independent scaling symmetries $\vec{v}_\alpha^{\,5}$ and $\vec{v}_{\alpha'}^{\,5}$ with any distinct values of α and α'.

two-dimensional Lie subalgebras must be found. The two-variable reductions of Eq. 2.12 are listed in Table 2.3.

(i-1) Rotating wave solutions are invariant under $\vec{v}^{\,1} + \omega\vec{v}^{\,4}$ with invariants

$$\begin{aligned}\tilde{H} &= H,\\ \tilde{X} &= X\cos(\omega t) + Y\sin(\omega t),\\ \tilde{Y} &= -X\sin(\omega t) + Y\cos(\omega t).\end{aligned}$$

Denoting here $\mathbf{X}_L = (\tilde{X}, \tilde{Y})$ as independent variables and $\tilde{H}$ as the dependent variable, the reduced equation is

$$0 = \omega\mathbf{X}_L \cdot \left(\star\nabla_L\tilde{H}\right) + \nabla_L \cdot \left(\frac{\tilde{H}^3}{3}\nabla_L\left(\bar{\mathrm{Ca}}^{-1}\nabla_L^2\tilde{H} - W'(\tilde{H})\right)\right).$$

(i-2) Travelling wave solutions are invariant under $\vec{v}^{\,1} + v\vec{v}^{\,2}$ with invariants

$$\begin{aligned}\tilde{H} &= H,\\ \tilde{X} &= X - vt,\\ \tilde{Y} &= Y.\end{aligned}$$

Denoting here $\mathbf{X}_L = (\tilde{X}, \tilde{Y})$ as independent variables and $\tilde{H}$ as the dependent variable, the reduced equation is

$$0 = -v\frac{\partial\tilde{H}}{\partial\tilde{X}} + \nabla_L \cdot \left(\frac{\tilde{H}^3}{3}\nabla_L\left(\bar{\mathrm{Ca}}^{-1}\nabla_L^2\tilde{H} - W'(\tilde{H})\right)\right).$$

(i-3) Rotationally invariant solutions are invariant under $\vec{v}^{\,4}$ with invariants

$$\begin{aligned}\tilde{H} &= H,\\ \tilde{R} &= \sqrt{X^2 + Y^2},\\ \tilde{t} &= t.\end{aligned}$$

Choosing $\tilde{R}$ and $\tilde{t}$ as independent variables and $\tilde{H}$ as the dependent variable, the reduced equation is

$$0 = \frac{\partial\tilde{H}}{\partial\tilde{t}} + \frac{1}{\tilde{R}}\frac{\partial}{\partial\tilde{R}}\left(\tilde{R}\frac{\tilde{H}^3}{3}\frac{\partial}{\partial\tilde{R}}\left(\bar{\mathrm{Ca}}^{-1}\frac{1}{\tilde{R}}\frac{\partial}{\partial\tilde{R}}\left(\tilde{R}\frac{\partial\tilde{H}}{\partial\tilde{R}}\right) - W'(\tilde{H})\right)\right).$$

(i-4) Translationally invariant solutions are invariant under $\vec{v}^{\,3}$ with invariants

$$\begin{aligned}\tilde{H} &= H,\\ \tilde{X} &= X,\\ \tilde{t} &= t.\end{aligned}$$

Choosing $\tilde{X}$ and $\tilde{t}$ as independent variables and $\tilde{H}$ as the dependent variable, the reduced equation is

$$0 = \frac{\partial \tilde{H}}{\partial \tilde{t}} + \frac{\partial}{\partial \tilde{X}}\left(\frac{\tilde{H}^3}{3}\frac{\partial}{\partial \tilde{X}}\left(\bar{\mathrm{Ca}}^{-1}\frac{\partial^2 \tilde{H}}{\partial \tilde{X}^2} - W'(\tilde{H})\right)\right).$$

(i-5) For the power-law case in Eq. 2.14, the rotating scale invariant solutions are invariant under $\vec{v}_\alpha^{\,5} + \omega\vec{v}^{\,4}$ with invariants

$$\begin{aligned}
\tilde{H} &= (\pm t)^{\frac{1}{2\alpha-1}} H, \\
\tilde{X} &= (\pm t)^{\frac{-\alpha+2}{4\alpha-2}}\left(X\cos\left(\omega\log(\pm t)^{\frac{-1}{4\alpha-2}}\right) + Y\sin\left(\omega\log(\pm t)^{\frac{-1}{4\alpha-2}}\right)\right), \\
\tilde{Y} &= (\pm t)^{\frac{-\alpha+2}{4\alpha-2}}\left(-X\sin\left(\omega\log(\pm t)^{\frac{-1}{4\alpha-2}}\right) + Y\cos\left(\omega\log(\pm t)^{\frac{-1}{4\alpha-2}}\right)\right).
\end{aligned}$$

Denoting here $\mathbf{X}_L = (\tilde{X}, \tilde{Y})$ as the independent variables and $\tilde{H}$ as the dependent variable, the reduced equation is

$$\begin{aligned}
0 = \pm\Bigg(&-\frac{\tilde{H}}{2\alpha-1} - \frac{\alpha-2}{4\alpha-2}\mathbf{X}_L\cdot\nabla_L\tilde{H} + \omega\mathbf{X}_L\cdot\left(\star\nabla_L\tilde{H}\right)\Bigg) \\
&+ \nabla_L\cdot\left(\frac{\tilde{H}^3}{3}\nabla_L\left(\bar{\mathrm{Ca}}^{-1}\nabla_L^2\tilde{H} - W'(\tilde{H})\right)\right).
\end{aligned}$$

The choice of invariants above is only valid for $\alpha \neq \frac{1}{2}$. A different choice can be made for $\alpha \neq 2$,

$$\begin{aligned}
\tilde{H} &= R^{\frac{2}{\alpha-2}} H, \\
\tilde{t} &= R^{-\frac{4\alpha-2}{\alpha-2}} t, \\
\tilde{\theta} &= \theta + \omega\log\left(R^{\frac{1}{\alpha-2}}\right),
\end{aligned}$$

where $R = \sqrt{X^2+Y^2}$ and $\theta = \arctan\frac{Y}{X}$ are the usual polar coordinates. The reduced equation using these invariants is rather complicated and will be omitted for brevity.

Table 2.2: There are up to five one-variable reductions of Eq. 2.12, including (i-1) the rotating wave solutions, (i-2) the travelling wave solutions, (i-3) the rotationally invariant solutions, (i-4) the translationally invariant solutions, and (i-5) the scale invariant solutions.

(ii-1) Rotationally invariant steady solutions are invariant under $\vec{v}^{\,1}$ and $\vec{v}^{\,4}$ with invariants

$$\tilde{H} = H,$$
$$\tilde{R} = \sqrt{X^2 + Y^2}.$$

Choosing $\tilde{R}$ as the independent variable and $\tilde{H}$ as the dependent variable, the reduced equation is

$$0 = \frac{1}{\tilde{R}}\frac{\partial}{\partial \tilde{R}}\left(\tilde{R}\frac{\tilde{H}^3}{3}\frac{\partial}{\partial \tilde{R}}\left(\bar{\mathrm{Ca}}^{-1}\frac{1}{\tilde{R}}\frac{\partial}{\partial \tilde{R}}\left(\tilde{R}\frac{\partial \tilde{H}}{\partial \tilde{R}}\right) - W'(\tilde{H})\right)\right).$$

(ii-2) Translationally invariant travelling wave solutions are invariant under $\vec{v}^{\,3}$ and $\vec{v}^{\,1} + v\vec{v}^{\,2}$ with invariants

$$\tilde{H} = H,$$
$$\tilde{X} = X - vt.$$

Choosing $\tilde{X}$ as independent variable and $\tilde{H}$ as the dependent variable, the reduced equation is

$$0 = -v\frac{\partial \tilde{H}}{\partial \tilde{X}} + \frac{\partial}{\partial \tilde{X}}\left(\frac{\tilde{H}^3}{3}\frac{\partial}{\partial \tilde{X}}\left(\bar{\mathrm{Ca}}^{-1}\frac{\partial^2 \tilde{H}}{\partial \tilde{X}^2} - W'(\tilde{H})\right)\right).$$

(ii-3) Constant solutions are invariant under $\vec{v}^{\,2}$ and $\vec{v}^{\,3}$ with invariants

$$\tilde{H} = H,$$
$$\tilde{t} = t.$$

Choosing $\tilde{t}$ as the independent variable and $\tilde{H}$ as the dependent variable, the reduced equation is

$$0 = \frac{\partial \tilde{H}}{\partial \tilde{t}}.$$

(ii-4) For the power-law case in Eq. 2.14, the rotationally invariant scale invariant solutions are invariant under $\vec{v}_\alpha^{\,5}$ and $\vec{v}^{\,4}$ with invariants

$$\tilde{H} = (\pm t)^{\frac{1}{2\alpha-1}} H,$$
$$\tilde{R} = (\pm t)^{-\frac{\alpha-2}{4\alpha-2}}\sqrt{X^2 + Y^2}.$$

Choosing $\tilde{R}$ as the independent variable and $\tilde{H}$ as the dependent variable, the reduced equation is

$$0 = \pm\left(-\frac{\tilde{H}}{2\alpha-1} - \frac{\alpha-2}{4\alpha-2}\tilde{H}\frac{\partial\tilde{H}}{\partial\tilde{R}}\right) + \frac{1}{\tilde{R}}\frac{\partial}{\partial\tilde{R}}\left(\tilde{R}\frac{\tilde{H}^3}{3}\frac{\partial}{\partial\tilde{R}}\left(\bar{\mathrm{Ca}}^{-1}\frac{1}{\tilde{R}}\frac{\partial}{\partial\tilde{R}}\left(\tilde{R}\frac{\partial\tilde{H}}{\partial\tilde{R}}\right) - W'(\tilde{H})\right)\right).$$

The choice of invariants above is only valid for $\alpha \neq \frac{1}{2}$. A different choice can be made for $\alpha = \frac{1}{2}$,

$$\tilde{H} = R^{-4/3}H,$$
$$\tilde{t} = t.$$

Choosing $\tilde{t}$ as the independent variable and $\tilde{H}$ as the dependent variable, the reduced equation is

$$0 = \bar{\mathrm{Ca}}\frac{\partial\tilde{H}}{\partial\tilde{t}} - \frac{320}{243}\tilde{H}^4 - \frac{40}{27}\bar{\mathrm{Ca}}W_0\tilde{H}^{5/2}.$$

(ii-5) For the power-law case in Eq. 2.14, the translationally invariant scale invariant solutions are invariant under $\vec{v}_\alpha^{\,5}$ and $\vec{v}^{\,3}$ and with invariants

$$\tilde{H} = (\pm t)^{\frac{1}{2\alpha-1}}H,$$
$$\tilde{X} = (\pm t)^{-\frac{\alpha-2}{4\alpha-2}}X.$$

Choosing $\tilde{X}$ as the independent variable and $\tilde{H}$ as the dependent variable, the reduced equation is

$$0 = \pm\left(-\frac{\tilde{H}}{2\alpha-1} - \frac{\alpha-2}{4\alpha-2}\tilde{X}\frac{\partial\tilde{H}}{\partial\tilde{X}}\right) + \frac{\partial}{\partial\tilde{X}}\left(\frac{\tilde{H}^3}{3}\frac{\partial}{\partial\tilde{X}}\left(\bar{\mathrm{Ca}}^{-1}\frac{\partial^2\tilde{H}}{\partial\tilde{X}^2} - W'(\tilde{H})\right)\right).$$

The choice of invariants above is only valid for $\alpha \neq \frac{1}{2}$. A different choice can be made for $\alpha = \frac{1}{2}$,

$$\tilde{H} = X^{-4/3}H,$$
$$\tilde{t} = t.$$

Choosing $\tilde{t}$ as the independent variable and $\tilde{H}$ as the dependent variable, the reduced equation is

$$0 = \bar{\mathrm{Ca}}\frac{\partial\tilde{H}}{\partial\tilde{t}} - \frac{56}{243}\tilde{H}^4 - \frac{28}{27}W_0\bar{\mathrm{Ca}}\tilde{H}^{5/2}.$$

(ii-6) For the power-law case in Eq. 2.14, the scale invariant steady solutions are invariant under $\vec{v}^{\,1}$ and $\vec{v}_{\alpha}^{\,5} + \omega\vec{v}^{\,4}$ with invariants

$$\tilde{H} = R^{\frac{2}{\alpha-2}} H,$$
$$\tilde{\theta} = \theta + \omega \log\left(R^{\frac{1}{\alpha-2}}\right).$$

Choosing $\tilde{\theta}$ as the independent variable and $\tilde{H}$ as the dependent variable, the reduced equation is

$$\begin{aligned}
0 = {} & \frac{16}{3}\left(\alpha^2+\alpha-2\right)\tilde{H}^4 + \tilde{H}^2\left((\alpha-2)^2+\omega^2\right)^2 \frac{\partial\tilde{H}}{\partial\tilde{\theta}}\frac{\partial^3\tilde{H}}{\partial\tilde{\theta}^3} \\
& - 2(\alpha+1)\omega\tilde{H}^2\left((\alpha-2)^2+\omega^2\right)\frac{\partial\tilde{H}}{\partial\tilde{\theta}}\frac{\partial^2\tilde{H}}{\partial\tilde{\theta}^2} \\
& + 4\tilde{H}^2\left((2\alpha-1)\omega^2+(\alpha-2)^2\right)\left(\frac{\partial\tilde{H}}{\partial\tilde{\theta}}\right)^2 - \frac{8}{3}(\alpha(2\alpha+7)-6)\omega\tilde{H}^3\frac{\partial\tilde{H}}{\partial\tilde{\theta}} \\
& + \frac{4}{3}\tilde{H}^3\left(\left(\alpha^2+\alpha-1\right)(\alpha-2)^2+(\alpha(\alpha+5)+1)\omega^2\right)\frac{\partial^2\tilde{H}}{\partial\tilde{\theta}^2} \\
& - \frac{2}{3}(2\alpha+3)\omega\tilde{H}^3\frac{\partial^3\tilde{H}}{\partial\tilde{\theta}^3}\left((\alpha-2)^2+\omega^2\right) + \frac{1}{3}\tilde{H}^3\frac{\partial^4\tilde{H}}{\partial\tilde{\theta}^4}\left((\alpha-2)^2+\omega^2\right)^2 \\
& - \frac{4\bar{\mathrm{Ca}}W_0}{3}(\alpha-2)^2\alpha\left(\alpha^2+\alpha-2\right)\tilde{H}^{\alpha+1}\left(\tilde{H}-\omega\frac{\partial\tilde{H}}{\partial\tilde{\theta}}\right) \\
& - \frac{\bar{\mathrm{Ca}}W_0}{3}(\alpha-2)^2(\alpha-1)\alpha\left((\alpha-2)^2+\omega^2\right)\tilde{H}^{\alpha}\left(\tilde{H}\frac{\partial^2\tilde{H}}{\partial\tilde{\theta}^2}+(\alpha+1)\frac{\partial\tilde{H}}{\partial\tilde{\theta}}^2\right).
\end{aligned}$$

These invariants are only valid for $\alpha \neq 2$, but for $\alpha = 2$, the invariants turn out to not depend on H and there is therefore no such reduction.

(ii-7) For the power-law case in Eq. 2.14 with $\alpha = \frac{1}{2}$, the scale invariant rotating wave solutions are invariant under $\vec{v}^{\,1} + \omega\vec{v}^{\,4}$ and $\vec{v}_{1/2}^{\,5}$ with invariants

$$\tilde{H} = R^{-4/3} H,$$
$$\tilde{\theta} = \theta - \omega t.$$

Choosing $\tilde{\theta}$ as the independent variable and $\tilde{H}$ as the dependent variable, the reduced equation is

$$\begin{aligned}
0 = {} & -\bar{\mathrm{Ca}}\omega\frac{\partial\tilde{H}}{\partial\tilde{\theta}} - \frac{320}{243}\tilde{H}^4 - \frac{4}{27}\tilde{H}^3\frac{\partial^2\tilde{H}}{\partial\tilde{\theta}^2} + \frac{16}{9}\tilde{H}^2\left(\frac{\partial\tilde{H}}{\partial\tilde{\theta}}\right)^2 + \tilde{H}^2\frac{\partial^3\tilde{H}}{\partial\tilde{\theta}^3}\frac{\partial\tilde{H}}{\partial\tilde{\theta}} \\
& + \frac{1}{3}\tilde{H}^3\frac{\partial^4\tilde{H}}{\partial\tilde{\theta}^4} + \frac{10\bar{\mathrm{Ca}}W_0}{27}\tilde{H}^{5/2} + \frac{\bar{\mathrm{Ca}}W_0}{12}\tilde{H}^{3/2}\frac{\partial^2\tilde{H}}{\partial\tilde{\theta}^2} + \frac{\bar{\mathrm{Ca}}W_0}{8}\tilde{H}^{1/2}\left(\frac{\partial\tilde{H}}{\partial\tilde{\theta}}\right)^2.
\end{aligned}$$

(ii-8) For the power-law case in Eq. 2.14 with $\alpha = 0$, the scale invariant travelling wave solutions are invariant under $\vec{v}^{\,1} + v\vec{v}^{\,2}$ and $\vec{v}_0^{\,5}$ with invariants

$$\tilde{H} = (X - vt)^{-1} H,$$
$$\tilde{\theta} = \arctan\left(\frac{Y}{X - vt}\right).$$

Choosing $\tilde{\theta}$ as the independent variable and $\tilde{H}$ as the dependent variable, the reduced equation is

$$\begin{aligned}
0 = &-v\bar{\mathrm{Ca}}\tilde{H} + v\bar{\mathrm{Ca}}\sin(\tilde{\theta})\cos(\tilde{\theta})\frac{\partial\tilde{H}}{\partial\tilde{\theta}} - 2\tilde{H}^2\cos^4(\tilde{\theta})\left(\frac{\partial\tilde{H}}{\partial\tilde{\theta}}\right)^2 \\
&- 3\tilde{H}^2\sin(\tilde{\theta})\cos^3(\tilde{\theta})\frac{\partial\tilde{H}}{\partial\tilde{\theta}}\frac{\partial^2\tilde{H}}{\partial\tilde{\theta}^2} + \tilde{H}^2\frac{\partial^3\tilde{H}}{\partial\tilde{\theta}^3}\cos^4(\tilde{\theta})\frac{\partial\tilde{H}}{\partial\tilde{\theta}} \\
&+ 4\tilde{H}^3\sin(\tilde{\theta})\cos^3(\tilde{\theta})\frac{\partial\tilde{H}}{\partial\tilde{\theta}} + \frac{1}{3}\tilde{H}^3\cos^2(\tilde{\theta})(1 - 8\cos(2\tilde{\theta}))\frac{\partial^2\tilde{H}}{\partial\tilde{\theta}^2} \\
&- \frac{7}{3}\tilde{H}^3\frac{\partial^3\tilde{H}}{\partial\tilde{\theta}^3}\sin(\tilde{\theta})\cos^3(\tilde{\theta}) + \frac{1}{3}\tilde{H}^3\frac{\partial^4\tilde{H}}{\partial\tilde{\theta}^4}\cos^4(\tilde{\theta}) \\
&+ \frac{\bar{\mathrm{Ca}}W_0}{3}\left(\tilde{H}\left(\tilde{H} - 2\sin(2\tilde{\theta})\frac{\partial\tilde{H}}{\partial\tilde{\theta}}\right) + \cos^2(\tilde{\theta})\left(\tilde{H}\frac{\partial^2\tilde{H}}{\partial\tilde{\theta}^2} + \left(\frac{\partial\tilde{H}}{\partial\tilde{\theta}}\right)^2\right)\right).
\end{aligned}$$

(ii-9) For the purely capillary case, the scale invariant scale invariant solutions are invariant under $\vec{v}_{1/2}^{\,5} + \omega\vec{v}^{\,4}$ and $\vec{v}_\alpha^{\,5}$ with $\alpha \neq 1/2$ with invariants

$$\tilde{H} = R^{-4/3}(\pm t)^{1/3} H,$$
$$\tilde{\theta} = \theta - \omega\log\left((\pm t)^{\frac{2(\alpha-2)}{3(4\alpha-2)}} R^{-2/3}\right).$$

Choosing $\tilde{\theta}$ as the independent variable and $\tilde{H}$ as the dependent variable, the reduced equation is

$$\begin{aligned}
0 = \bar{\mathrm{Ca}}&\left(-\frac{\tilde{H}}{3} + \frac{(\alpha-2)\omega}{3-6\alpha}\frac{\partial\tilde{H}}{\partial\tilde{\theta}}\right) + \frac{16}{9}\tilde{H}^2\frac{\partial\tilde{H}}{\partial\tilde{\theta}}^2 + \frac{4}{27}\omega\left(4\omega^2+9\right)\tilde{H}^2\frac{\partial\tilde{H}}{\partial\tilde{\theta}}\frac{\partial^2\tilde{H}}{\partial\tilde{\theta}^2} \\
&+ \frac{1}{81}\left(4\omega^2+9\right)^2\tilde{H}^2\frac{\partial^3\tilde{H}}{\partial\tilde{\theta}^3}\frac{\partial\tilde{H}}{\partial\tilde{\theta}} - \frac{256}{243}\omega\tilde{H}^3\frac{\partial\tilde{H}}{\partial\tilde{\theta}} + \frac{4}{81}\left(20\omega^2-3\right)\tilde{H}^3\frac{\partial^2\tilde{H}}{\partial\tilde{\theta}^2} \\
&+ \frac{32}{243}\omega\left(4\omega^2+9\right)\tilde{H}^3\frac{\partial^3\tilde{H}}{\partial\tilde{\theta}^3} + \frac{1}{243}\left(4\omega^2+9\right)^2\tilde{H}^3\frac{\partial^4\tilde{H}}{\partial\tilde{\theta}^4} - \frac{320}{243}\tilde{H}^4.
\end{aligned}$$

For $\alpha = \frac{1}{2}$, the scale invariant scale invariant solutions are invariant under $\vec{v}_2^{\,5} + \omega\vec{v}^{\,4}$ and $\vec{v}_{1/2}^{\,5}$ with invariants

$$\tilde{H} = R^{-4/3}(\pm t)^{1/3} H,$$
$$\tilde{\theta} = \theta - \omega\log\left((\pm t)^{1/6}\right).$$

Choosing $\tilde{\theta}$ as the independent variable and $\tilde{H}$ as the dependent variable, the reduced equation is

$$0 = \bar{\mathrm{Ca}}\left(-\frac{\tilde{H}}{3} - \frac{1}{6}\omega\frac{\partial\tilde{H}}{\partial\tilde{\theta}}\right) + \frac{16}{9}\tilde{H}^2\frac{\partial\tilde{H}}{\partial\tilde{\theta}}^2 - \frac{4}{27}\tilde{H}^3\frac{\partial^2\tilde{H}}{\partial\tilde{\theta}^2} + \tilde{H}^2\frac{\partial^3\tilde{H}}{\partial\tilde{\theta}^3}\frac{\partial\tilde{H}}{\partial\tilde{\theta}} + \frac{1}{3}\tilde{H}^3\frac{\partial^4\tilde{H}}{\partial\tilde{\theta}^4} - \frac{320}{243}\tilde{H}^4.$$

Table 2.3: There are up to nine two-variable reductions of Eq. 2.12, including (ii-1) the rotationally invariant steady solutions, (ii-2) the translationally invariant travelling wave solutions, (ii-3) the constant solutions, (ii-4) the rotationally invariant scale invariant solutions, (ii-5) the translationally invariant scale invariant solutions, (ii-6) the steady scale invariant solutions, (ii-7) the rotating wave scale invariant solutions, (ii-8) the travelling wave scale invariant solutions, and (ii-9) the scale invariant scale invariant solutions.

For the cases of the scale invariant solutions which involved invariants related to the angular θ, the reductions are somewhat complicated. This is a consequence of the fourth spatial order of Eq. 2.12. Some numerical solutions for these reductions are presented in Section 4.2 below.

Surfactant spreading

We previously detailed how the Mathematica package zgnsymmetry.m was used to find the symmetries of Eq. 2.12. A similar analysis has been performed for the surfactant spreading problem of Eq. 1.73, namely

$$\begin{aligned} 0 &= \frac{\partial H}{\partial t} + \nabla_L\cdot\left(\frac{\bar{\mathrm{Ca}}^{-1}}{3}H^3\nabla_L\nabla_L^2 H - \frac{\bar{\mathrm{Ma}}}{2}H^2\nabla_L\Gamma\right), \\ 0 &= \frac{\partial\Gamma}{\partial t} + \nabla_L\cdot\left(\frac{\bar{\mathrm{Ca}}^{-1}}{2}H^2\Gamma\nabla_L\nabla_L^2 H - \bar{\mathrm{Ma}}H\Gamma\nabla_L\Gamma - \bar{\mathrm{Pe}}\nabla_L\Gamma\right). \end{aligned} \tag{2.15}$$

The need for computer assistance in this case is even greater – the symmetry condition in Eq. 2.7 contains 18814 terms! Rather than present the each step in the derivation here, we will simply state the results. The symmetries generators of Eq. 2.15 include the first four in Table 2.1, namely time translations $\vec{v}^{\,1} = \frac{\partial}{\partial t}$, spatial translations $\vec{v}^{\,2} = \frac{\partial}{\partial X}$ and $\vec{v}^{\,3} = \frac{\partial}{\partial Y}$, and rotations $\vec{v}^{\,4} = -Y\frac{\partial}{\partial X} + X\frac{\partial}{\partial Y}$. In addition, there are scaling symmetries

$$\vec{v}^{\,6}_{(\alpha_1,\alpha_2)} = X\frac{\partial}{\partial X} + Y\frac{\partial}{\partial Y} + (2-\alpha_1-\alpha_2)t\frac{\partial}{\partial t} + \alpha_1 H\frac{\partial}{\partial H} + \alpha_2\Gamma\frac{\partial}{\partial\Gamma},$$

where α_1 and α_2 are two scaling exponents. In general, the scaling $\vec{v}^{\,6}_{(\alpha_1,\alpha_2)}$ is a symmetry of Eq. 2.15 only for $\alpha_1 = 2/3$ and $\alpha_2 = -2/3$. If, however, the diffusive forces are negligible and $\bar{\text{Pe}} \ll 1$, then the scaling $\vec{v}^{\,6}_{(\alpha_1,\alpha_2)}$ is a symmetry of Eq. 2.15 whenever for $\alpha_2 = 2\alpha_1 - 2$. On the other hand, if capillary forces are negligible and $\bar{\text{Ca}} \ll 1$, then the scaling $\vec{v}^{\,6}_{(\alpha_1,\alpha_2)}$ is a symmetry of Eq. 2.15 whenever $\alpha_2 = -\alpha_1$. Lastly, if both capillary and diffusive forces are negligible, then the scaling $\vec{v}^{\,6}_{(\alpha_1,\alpha_2)}$ is a symmetry of Eq. 2.15 for any values of α_1 and α_2. We are particularly interested in the case when both capillary and diffusive forces are negligible, both because the symmetry is extraordinarily large and because these conditions are satisfied for a certain physical system that we will discuss in Chapter 4. For the remainder of this section, the $\bar{\text{Ca}} \ll 1$ and $\bar{\text{Pe}} \ll 1$ equations will be studied. After a simple rescaling of t, the dependence on $\bar{\text{Ma}}$ can be eliminated and the equations are put in the form

$$\begin{aligned} 0 &= \frac{\partial H}{\partial t} + \nabla_L \cdot \left(-\frac{1}{2} H^2 \nabla_L \Gamma \right), \\ 0 &= \frac{\partial \Gamma}{\partial t} + \nabla_L \cdot \left(-H \Gamma \nabla_L \Gamma \right). \end{aligned} \tag{2.16}$$

We will consider rotationally invariant solutions which are also invariant under the scaling symmetry generated by $\vec{v}^{\,6}_{(\alpha_1,\alpha_2)}$ to illustrate some of the geometrical ideas discussed in Section 2.1. This is also a preview of Section 4.1 below, where more detailed calculations are carried out. The symmetry leads to the new set of variables $\tilde{\theta} \equiv \tan^{-1}\left(\frac{Y}{X}\right)$, $\eta \equiv \log(\pm t)/(2-\alpha_1-\alpha_2)$, $\tilde{R} \equiv \sqrt{X^2+Y^2}/(\pm t)^{1/(2-\alpha_1-\alpha_2)}$, $\tilde{H} \equiv H/(\pm t)^{\alpha_1/(2-\alpha_1-\alpha_2)}$, and $\tilde{\Gamma} \equiv \Gamma/(\pm t)^{\alpha_2/(2-\alpha_1-\alpha_2)}$. The variables $\tilde{\theta}$ and η are the η_0 variables that satisfy Eq. 2.4 for the rotational and scaling symmetries, respectively, while the variables $\tilde{R}$, $\tilde{H}$, $\tilde{\Gamma}$ are mutual invariants to both symmetries that satisfy Eq. 2.3. In these new variables, the system is

$$\begin{aligned} \tilde{\Delta}_1 &= \pm \frac{\frac{\partial \tilde{H}}{\partial \eta} + \alpha_1 \tilde{H} - \tilde{R}\frac{\partial \tilde{H}}{\partial \tilde{R}}}{2-\alpha_1-\alpha_2} + \frac{1}{\tilde{R}}\frac{\partial}{\partial \tilde{R}}\left(-\frac{\tilde{R}\tilde{H}^2}{2}\frac{\partial \tilde{\Gamma}}{\partial \tilde{R}} \right) + \frac{1}{\tilde{R}}\frac{\partial}{\partial \tilde{\theta}}\left(-\frac{\tilde{H}^2}{2\tilde{R}}\frac{\partial \tilde{\Gamma}}{\partial \tilde{\theta}} \right) = 0, \\ \tilde{\Delta}_2 &= \pm \frac{\frac{\partial \tilde{\Gamma}}{\partial \eta} + \alpha_2 \tilde{\Gamma} - \tilde{R}\frac{\partial \tilde{\Gamma}}{\partial \tilde{R}}}{2-\alpha_1-\alpha_2} + \frac{1}{\tilde{R}}\frac{\partial}{\partial \tilde{R}}\left(-\tilde{R}\tilde{H}\tilde{\Gamma}\frac{\partial \tilde{\Gamma}}{\partial \tilde{R}} \right) + \frac{1}{\tilde{R}}\frac{\partial}{\partial \tilde{\theta}}\left(-\frac{\tilde{H}\tilde{\Gamma}}{\tilde{R}}\frac{\partial \tilde{\Gamma}}{\partial \tilde{\theta}} \right) = 0. \end{aligned} \tag{2.17}$$

Because of scaling and rotational symmetries generated by $\frac{\partial}{\partial \eta}$ and $\frac{\partial}{\partial \tilde{\theta}}$, respectively, these equations are autonomous with respect to $\tilde{\theta}$ and η.

Self-similar solutions can be found by taking $\tilde{H}$ and $\tilde{\Gamma}$ as dependent variables which depend only on the independent variable $\tilde{R}$, which reduces Eq. 2.16 to a set of ordinary differential equations. Because of the remnant scaling symmetries from

$\vec{v}^{\,6}_{(\alpha_1,\alpha_2)}$ for different values of α_1 and α_2, it is possible to further integrate the resulting ordinary differential equations twice by changing coordinates yet again so that one of the new dependent variables is the η_0 of these remnant symmetries. Since the equations then depend only on derivatives of this dependent variable, an integration by quadrature is performed [28]. Details of this reduction can be found in Section 4.1 below. The final result is a set of planar autonomous ordinary differential equations in new dependent variables ζ_2 and ζ_1 with a new independent variables τ,

$$\begin{aligned}\frac{\partial\zeta_1}{\partial\tau} &= \zeta_1\left(\zeta_1(3\zeta_2+2\alpha_1-\alpha_2-4)+2\zeta_2(\zeta_2-1)\right),\\ \frac{\partial\zeta_2}{\partial\tau} &= 3\zeta_2^3+6\zeta_2^2\zeta_1+2\zeta_2\zeta_1(\zeta_1+\alpha_1-\alpha_2)-2b\zeta_1^2,\end{aligned} \tag{2.18}$$

Each self-similar solution with exponents α_1 and α_2 corresponds to a trajectory in a planar dynamical system which satisfies Eq. 2.18. A sample phase portrait for this planar system is depicted in Fig. 2.2 below. In addition to the system in Eq. 2.18,

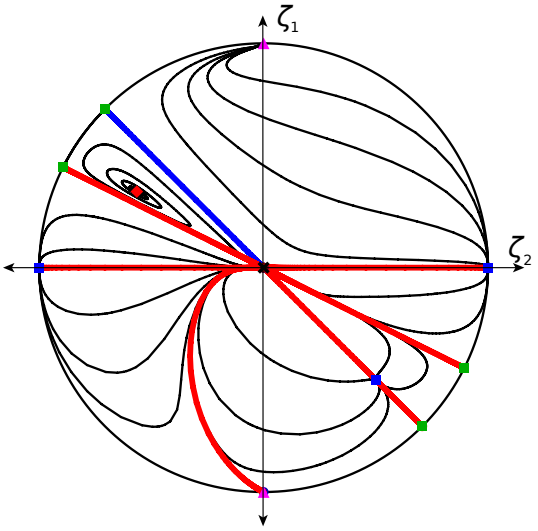

Figure 2.2: Planar system in Eq. 2.18 with $\alpha_1 = 0$ and $\alpha_2 = -2$. The (ζ_2, ζ_1) plane has been compactified in this image so that the boundary of the disk corresponds to infinity. Each black line is a solution, the various colored symbols are fixed points, and the colored lines are the separatrices. The blue separatrix is the special self-similar solution in Eq. 2.20.

there is a transformation back to the original variables

$$\begin{aligned}\tilde{R} &= \sqrt{|(2-\alpha_1-\alpha_2)H_0\Gamma_0\zeta_1|}\,\mathrm{e}^{-\frac{1}{2}\int_0^\tau\left((2\alpha_1-\alpha_2)\zeta_1+\zeta_2(2\zeta_2+3\zeta_1)\right)\,\mathrm{d}\tau},\\ H &= H_0(\pm t)^{\frac{\alpha_1}{2-\alpha_1-\alpha_2}}\mathrm{e}^{-\int_0^\tau\left((2\alpha_1-\alpha_2)\zeta_1+\zeta_2(\zeta_2+\zeta_1)\right)\,\mathrm{d}\tau},\\ \Gamma &= \Gamma_0(\pm t)^{\frac{\alpha_2}{2-\alpha_1-\alpha_2}}\mathrm{e}^{-\int_0^\tau\left(\zeta_2(\zeta_2+2\zeta_1)\right)\,\mathrm{d}\tau}.\end{aligned} \tag{2.19}$$

The quantities H_0 and Γ_0 here are the integration constants from the quadratures. Given a solution of Eq. 2.18, one must invert the first line of Eq. 2.19 to eliminate τ in favor of $\tilde{R}$ to finally recover the solution in the original variables. It is interesting to note how self-similar solutions fall into different categories depending on which class of trajectories in the planar system they correspond to. This is one reflection of the very complex geometric structure in the foliation of $\mathscr{S}_\Delta$ by solutions to Eq. 2.16.

The special solution represented by the blue curve in Fig. 2.2 has a particularly simple form. In the invariant variables, this solution is

$$\tilde{H} = \tilde{H}_0(\tilde{R}) \equiv 2\tilde{R}^2, \ \tilde{\Gamma} = \tilde{\Gamma}_0(\tilde{R}) \equiv -\frac{1}{8}\log(\tilde{R}), \tag{2.20}$$

valid for $0 < \tilde{R} < 1$. By taking the ansatz $\tilde{H} = \tilde{H}_0(\tilde{R}) + \delta\tilde{H}(\tilde{R},\eta)\cos(n\tilde{\theta})$ and $\tilde{\Gamma} = \tilde{\Gamma}_0(\tilde{R}) + \delta\tilde{\Gamma}(\tilde{R},\eta)\cos(n\tilde{\theta})$ and taking $\delta\tilde{H}$ and $\delta\tilde{\Gamma}$ small, a linear problem is derived from Eq. 2.17,

$$\begin{aligned}
0 &= \pm\frac{\frac{\partial\delta\tilde{H}}{\partial\eta} + \alpha_1\delta\tilde{H} - \tilde{R}\frac{\partial\delta\tilde{H}}{\partial\tilde{R}}}{2-\alpha_1-\alpha_2} - \frac{1}{\tilde{R}}\frac{\partial}{\partial\tilde{R}}\left(\tilde{R}\left(\tilde{H}_0\delta\tilde{H}\frac{\partial\tilde{\Gamma}_0}{\partial\tilde{R}} + \frac{\tilde{H}_0^2}{2}\frac{\partial\delta\tilde{\Gamma}}{\partial\tilde{R}}\right)\right) + \frac{n^2}{2\tilde{R}^2}\tilde{H}_0^2\delta\tilde{\Gamma}, \\
0 &= \pm\frac{\frac{\partial\delta\tilde{\Gamma}}{\partial\eta} + \alpha_2\delta\tilde{\Gamma} - \tilde{R}\frac{\partial\delta\tilde{\Gamma}}{\partial\tilde{R}}}{2-\alpha_1-\alpha_2} - \frac{1}{\tilde{R}}\frac{\partial}{\partial\tilde{R}}\left(\tilde{R}\left(\delta\tilde{H}\tilde{\Gamma}_0\frac{\partial\tilde{\Gamma}_0}{\partial\tilde{R}} + \tilde{H}_0\delta\tilde{\Gamma}\frac{\partial\tilde{\Gamma}_0}{\partial\tilde{R}} + \tilde{H}_0\tilde{\Gamma}_0\frac{\partial\delta\tilde{\Gamma}}{\partial\tilde{R}}\right)\right) \\
&\quad + \frac{n^2}{\tilde{R}^2}\tilde{H}_0\tilde{\Gamma}_0\delta\tilde{\Gamma}.
\end{aligned} \tag{2.21}$$

Since the equations are autonomous with respect to η (as guaranteed by the symmetry), $\frac{\partial\delta\tilde{H}}{\partial\eta}$ and $\frac{\partial\delta\tilde{\Gamma}}{\partial\eta}$ are equal to a linear operator which depends only on $\tilde{R}$, and the eigenvalues and eigenvectors of this linear operator characterize the η-evolution of all perturbations. Eigenvalues of a discretized approximation to this linear operator are depicted in Fig. 2.3 below. Ensuring that the discretization of Eq. 2.21 is sufficiently fine to resolve these eigenvalues would be necessary for a more quantitative study. The eigenvalue with largest real part in Fig. 2.3, for example, is clearly converging to the exact value, which is $\lambda_0 = 0$ with $n = 0$. This mode results from the remnant scaling symmetries and has simple eigenfunctions $\delta\tilde{H}_0(\tilde{R},\eta) = 2\tilde{R}^2$ and $\delta\tilde{\Gamma}_0(\tilde{R},\eta) = \frac{1}{8}\log\tilde{R}$. However, a subtle convergence issue was observed. As the grid is refined, two eigenvalues from the complex branches may come together on the real axis and then move apart on the real axis. Two of non-zero, real eigenvalues in Fig. 2.3, for example, had imaginary components for a coarser grid before becoming real at a finer grid. This issue makes it difficult to determine how many real eigenvalues there are and their signs in the continuum limit, but it appears that no eigenvalues for Eq. 2.21 have a positive real part in this limit. The numerical

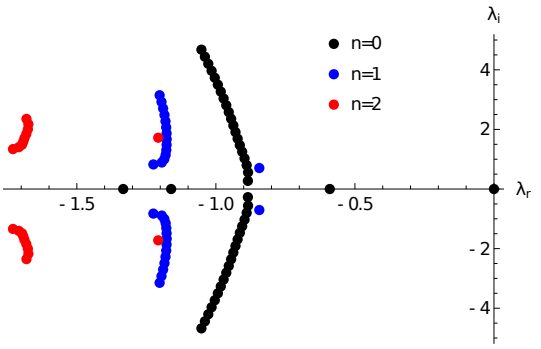

Figure 2.3: Eigenvalues $\lambda = \lambda_r + i\lambda_i$ corresponding to the η direction for the special solution in Eq. 2.20. For this particular solution, all the eigenvalues have non-positive real parts, and the solution corresponds to a stable fixed point.

eigenfunctions associated to the four real eigenvalues are depicted in Fig. 2.4 below. A more complete analysis would strive to find both eigenvalues and eigenfunctions for each trajectory in Fig. 2.2, and would further do so for all values of the exponents α_1 and α_2. For "hyperbolic" self-similar solutions, the eigenfunctions could also be used as initial conditions from which one could numerically trace out phase space "separatrices." These potential analyses are quite formidable, but could be carried out given current computational methods.

One important simplification in the eigenvalue analysis that we made above was the restriction of the domain to $\tilde{R} \leq 1$. This choice was made because the base state surfactant mass vanished there $\tilde{\Gamma}_0|_{\tilde{R}=1} = 0$. This is a singular point (sometimes called a degenerate point) of Eq. 2.17 since the highest order derivatives have vanishing coefficients there. This singularity corresponds to the leading edge shock front in a spreading droplet, and capillary forces need to be reintroduced to properly model it. This is an example of the other general geometrical feature of singularites of $\mathscr{S}_\Delta$ that should be understood in a qualitative study, as noted in Section 2.1.

Aside from this interesting structure for fixed values of α_1 and α_2, we can consider how the planar system in Eq. 2.18 varies as the exponents α_1 and α_2 vary. This corresponds to varying the direction in the extended phase space $\mathscr{S}_\Delta$ which we choose to project along, which is possible because of the very large symmetry of Eq. 2.16. As we vary α_1 and α_2, the various fixed points of Eq. 2.18 move. For certain values of α_1 and α_2 these fixed points undergo bifurcations. The local bifurcations that occur as the real part of one of the eigenvalues of the fixed points pass through zero are depicted in Fig. 2.5(a) below. These local bifurcations do not even exhaust all bifurcations that are present – global bifurcations are also known

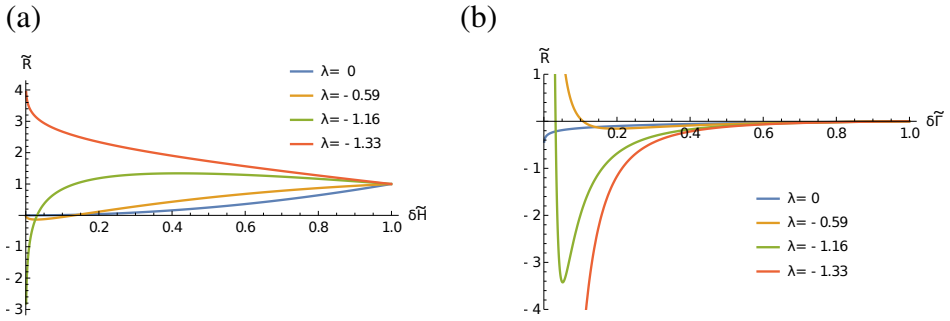

Figure 2.4: Eigenfunctions for the real eigenvalues in Fig. 2.3. Since all the eigenvalues are negative for this solution, these eigenfunctions do not represent separatrices in the extended phase space.

to exist, as depicted in Fig 2.5(b)-(c). This is yet another interesting geometric structure that is present in $\mathscr{S}_\Delta$. Each bifurcation in Fig. 2.5 corresponds to a change in the asymptotic behavior of some class of self-similar solutions.

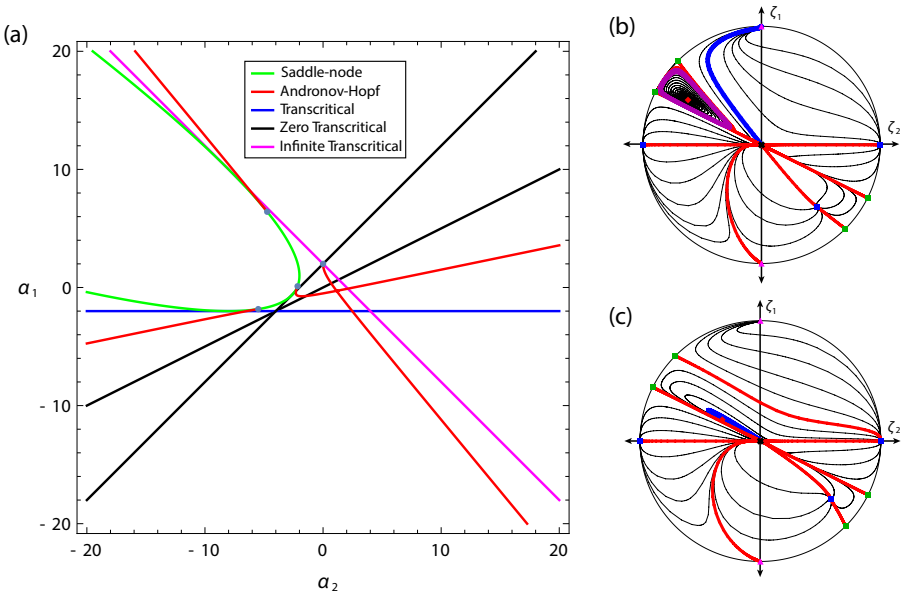

Figure 2.5: (a) Local bifurcations in the self-similar planar system as the exponents α_1 and α_2 vary. There are also global bifurcations like that occurring at $\alpha_1 = -1$ and $\alpha_2 = -2$ depicted in (b) in (c) in which the purple limit cycle collides with blue heteroclinic orbit and the separatrices rearrange themselves. The scaling exponents were $\alpha_1 = -0.8$ and $\alpha_2 = -1.6$ in (b) and $\alpha_1 = -1.5$ and $\alpha_2 = -3.0$ in (c).

Finally, to close this section we will enumerate the other two variable reductions of Eq. 2.16 in Table 2.4 below. These reductions have the same form as those for the film with a single dependent variable, but since the equations are only second order in space, they are somewhat simpler. The above description of the eigenvalues and

eigenfunctions in Figs. 2.3-2.4 and the bifurcations in Fig. 2.5 were carried out only for the rotationally invariant scale invariant solutions in reduction (ii-4) in Table 2.4. An analogous analysis is readilly made for the translationally invariant scale invariant reductions in (ii-5), and interesting studies of the other four scale invariant solutions may be possible. Indeed we have only begun to reveal the complex and remarkably rich structure in the reductions of the apparently simple Eq. 2.16.

(ii-1) Rotationally invariant steady solutions are invariant under $\vec{v}^{\,1}$ and $\vec{v}^{\,4}$ and with invariants

$$\tilde{H} = H,$$
$$\tilde{\Gamma} = \Gamma,$$
$$\tilde{R} = \sqrt{X^2 + Y^2}.$$

Choosing $\tilde{R}$ as the independent variable and $\tilde{H}$ and $\tilde{\Gamma}$ as the dependent variables, the reduced equations are

$$0 = \frac{1}{\tilde{R}}\frac{\partial}{\partial \tilde{R}}\left(-\frac{\tilde{R}\tilde{H}^2}{2}\frac{\partial \Gamma}{\partial \tilde{R}}\right),$$
$$0 = \frac{1}{\tilde{R}}\frac{\partial}{\partial \tilde{R}}\left(-\tilde{R}\tilde{H}\tilde{\Gamma}\frac{\partial \Gamma}{\partial \tilde{R}}\right).$$

(ii-2) Translationally invariant travelling wave solutions are invariant under $\vec{v}^{\,3}$ and $\vec{v}^{\,1} + v\vec{v}^{\,2}$ with invariants

$$\tilde{H} = H,$$
$$\tilde{\Gamma} = \Gamma,$$
$$\tilde{X} = X - vt.$$

Choosing $\tilde{X}$ as the independent variable and $\tilde{H}$ and $\tilde{\Gamma}$ as the dependent variables, the reduced equations are

$$0 = -v\frac{\partial \tilde{H}}{\partial \tilde{X}} + \frac{\partial}{\partial \tilde{X}}\left(-\frac{\tilde{H}^2}{2}\frac{\partial \Gamma}{\partial \tilde{X}}\right),$$
$$0 = -v\frac{\partial \tilde{\Gamma}}{\partial \tilde{X}} + \frac{\partial}{\partial \tilde{X}}\left(-\tilde{H}\tilde{\Gamma}\frac{\partial \Gamma}{\partial \tilde{X}}\right).$$

(ii-3) Constant solutions are invariant under $\vec{v}^{\,2}$ and $\vec{v}^{\,3}$ and with invariants

$$\tilde{H} = H,$$
$$\tilde{\Gamma} = \Gamma,$$
$$\tilde{t} = t.$$

Choosing $\tilde{t}$ as the independent variable and $\tilde{H}$ and $\tilde{\Gamma}$ as the dependent variables, the reduced equation are

$$0 = \frac{\partial \tilde{H}}{\partial \tilde{t}},$$
$$0 = \frac{\partial \tilde{\Gamma}}{\partial \tilde{t}}.$$

(ii-4) Rotationally invariant scale invariant solutions are invariant under $\vec{v}^{\,6}_{(\alpha_1,\alpha_2)}$ and $\vec{v}^{\,4}$ with invariants

$$\tilde{H} = (\pm t)^{-\frac{\alpha_1}{2-\alpha_1-\alpha_2}} H,$$
$$\tilde{\Gamma} = (\pm t)^{-\frac{\alpha_2}{2-\alpha_1-\alpha_2}} \Gamma,$$
$$\tilde{R} = (\pm t)^{-\frac{1}{2-\alpha_1-\alpha_2}} \sqrt{X^2+Y^2}.$$

Choosing $\tilde{R}$ as the independent variable and $\tilde{H}$ and $\tilde{\Gamma}$ as the dependent variables, the reduced equation are

$$0 = \pm\frac{\alpha_1\tilde{H} - \tilde{R}\frac{\partial\tilde{H}}{\partial\tilde{R}}}{2-\alpha_1-\alpha_2} + \frac{1}{\tilde{R}}\frac{\partial}{\partial\tilde{R}}\left(-\frac{\tilde{R}\tilde{H}^2}{2}\frac{\partial\tilde{\Gamma}}{\partial\tilde{R}}\right),$$
$$0 = \pm\frac{\alpha_2\tilde{\Gamma} - \tilde{R}\frac{\partial\tilde{\Gamma}}{\partial\tilde{R}}}{2-\alpha_1-\alpha_2} + \frac{1}{\tilde{R}}\frac{\partial}{\partial\tilde{R}}\left(-\tilde{R}\tilde{H}\tilde{\Gamma}\frac{\partial\tilde{\Gamma}}{\partial\tilde{R}}\right).$$

The choice of invariants above is only valid for $2-\alpha_1-\alpha_2 \neq 0$. For brevity this special case will be omitted.

(ii-5) Translationally invariant scale invariant solutions are invariant under $\vec{v}^{\,6}_{(\alpha_1,\alpha_2)}$ and $\vec{v}^{\,3}$ with invariants

$$\tilde{H} = (\pm t)^{-\frac{\alpha_1}{2-\alpha_1-\alpha_2}} H,$$
$$\tilde{\Gamma} = (\pm t)^{-\frac{\alpha_2}{2-\alpha_1-\alpha_2}} H,$$
$$\tilde{X} = (\pm t)^{-\frac{1}{2-\alpha_1-\alpha_2}} X.$$

Choosing $\tilde{X}$ as the independent variable and $\tilde{H}$ and $\tilde{\Gamma}$ as the dependent variables, the reduced equations are

$$0 = \pm\frac{\alpha_1\tilde{H} - \tilde{X}\frac{\partial\tilde{H}}{\partial\tilde{X}}}{2-\alpha_1-\alpha_2} + \frac{\partial}{\partial\tilde{X}}\left(-\frac{\tilde{H}^2}{2}\frac{\partial\tilde{\Gamma}}{\partial\tilde{X}}\right),$$
$$0 = \pm\frac{\alpha_2\tilde{\Gamma} - \tilde{X}\frac{\partial\tilde{\Gamma}}{\partial\tilde{X}}}{2-\alpha_1-\alpha_2} + \frac{\partial}{\partial\tilde{X}}\left(-\tilde{H}\tilde{\Gamma}\frac{\partial\tilde{\Gamma}}{\partial\tilde{X}}\right).$$

The choice of invariants above is only valid for $2-\alpha_1-\alpha_2 \neq 0$. For brevity this special case will be omitted.

(ii-6) Scale invariant steady solutions are invariant under $\vec{v}^{\,1}$ and $\vec{v}^{\,6}_{(\alpha_1,\alpha_2)} + \omega\vec{v}^{\,4}$ with invariants

$$\tilde{H} = R^{-\alpha_1} H,$$
$$\tilde{\Gamma} = R^{-\alpha_2}\Gamma,$$
$$\tilde{\theta} = \theta - \omega\log\left(R^{-1}\right).$$

Choosing $\tilde{\theta}$ as the independent variable and $\tilde{H}$ and $\tilde{\Gamma}$ as the dependent variables, the reduced equations are

$$\begin{aligned}
0 &= \tilde{H}\left(2\omega(\alpha_1+\alpha_2)\frac{\partial\tilde{\Gamma}}{\partial\tilde{\theta}} + \alpha_2(2\alpha_1+\alpha_2)\tilde{\Gamma} + \left(\omega^2+1\right)\frac{\partial^2\tilde{\Gamma}}{\partial\tilde{\theta}^2}\right) \\
&\quad + 2\frac{\partial\tilde{H}}{\partial\tilde{\theta}}\left(\alpha_2\omega\tilde{\Gamma} + \left(\omega^2+1\right)\frac{\partial\tilde{\Gamma}}{\partial\tilde{\theta}}\right), \\
0 &= \tilde{H}\left(\tilde{\Gamma}\left(\omega(\alpha_1+4\alpha_2)\frac{\partial\tilde{\Gamma}}{\partial\tilde{\theta}} + \left(\omega^2+1\right)\frac{\partial^2\tilde{\Gamma}}{\partial\tilde{\theta}^2}\right) + \alpha_2(\alpha_1+2\alpha_2)\tilde{\Gamma}^2\right) \\
&\quad + \tilde{\Gamma}\frac{\partial\tilde{H}}{\partial\tilde{\theta}}\left(\alpha_2\omega\tilde{\Gamma} + \left(\omega^2+1\right)\frac{\partial\tilde{\Gamma}}{\partial\tilde{\theta}}\right) + \left(\omega^2+1\right)\tilde{H}\left(\frac{\partial\tilde{\Gamma}}{\partial\tilde{\theta}}\right)^2.
\end{aligned}$$

(ii-7) For $\alpha_2 = 2-\alpha_1$, scale invariant rotating wave solutions are invariant under $\vec{v}^{\,1} + \omega\vec{v}^{\,4}$ and $\vec{v}^{\,6}_{(\alpha_1,2-\alpha_1)}$ with invariants

$$\begin{aligned}
\tilde{H} &= R^{-\alpha_1}H, \\
\tilde{\Gamma} &= R^{-(2-\alpha_1)}\Gamma, \\
\tilde{\theta} &= \theta - \omega t.
\end{aligned}$$

Choosing $\tilde{\theta}$ as the independent variable and $\tilde{H}$ and $\tilde{\Gamma}$ as the dependent variables, the reduced equations are

$$\begin{aligned}
0 &= \tilde{H}^2\left(\frac{\partial^2\tilde{\Gamma}}{\partial\tilde{\theta}^2} - \left(\alpha_1^2-4\right)\tilde{\Gamma}\right) + 2\tilde{H}\frac{\partial\tilde{H}}{\partial\tilde{\theta}}\frac{\partial\tilde{\Gamma}}{\partial\tilde{\theta}} + 2\omega\frac{\partial\tilde{H}}{\partial\tilde{\theta}}, \\
0 &= \tilde{H}\left(\left(\alpha_1^2-6\alpha_1+8\right)\tilde{\Gamma}^2 + \tilde{\Gamma}\frac{\partial^2\tilde{\Gamma}}{\partial\tilde{\theta}^2} + \left(\frac{\partial\tilde{\Gamma}}{\partial\tilde{\theta}}\right)^2\right) + \frac{\partial\tilde{\Gamma}}{\partial\tilde{\theta}}\left(\tilde{\Gamma}\frac{\partial\tilde{H}}{\partial\tilde{\theta}} + \omega\right).
\end{aligned}$$

(ii-8) For $\alpha_2 = 1-\alpha_1$, scale invariant travelling wave solutions are invariant under $\vec{v}^{\,1} + v\vec{v}^{\,2}$ and $\vec{v}^{\,6}_{(\alpha_1,1-\alpha_1)}$ with invariants

$$\begin{aligned}
\tilde{H} &= (X-vt)^{-\alpha_1}H, \\
\tilde{\Gamma} &= (X-vt)^{-(1-\alpha_1)}\Gamma, \\
\tilde{\theta} &= \tan^{-1}\left(\frac{Y}{X-vt}\right).
\end{aligned}$$

Choosing $\tilde{\theta}$ as the independent variable and $\tilde{H}$ and $\tilde{\Gamma}$ as the dependent vari-

ables, the reduced equations are

$$0 = v\left(\sin(\tilde{\theta})\cos(\tilde{\theta})\frac{\partial \tilde{H}}{\partial \tilde{\theta}} - \alpha_1 \tilde{H}\right) - \cos^2(\tilde{\theta})\tilde{H}\frac{\partial \tilde{H}}{\partial \tilde{\theta}}\left((\alpha_1 - 1)\tilde{\Gamma}\tan(\tilde{\theta}) + \frac{\partial \tilde{\Gamma}}{\partial \tilde{\theta}}\right)$$
$$+ \frac{1}{2}\tilde{H}^2\left((\alpha_1 - 1)\alpha_1\tilde{\Gamma} + \cos(\tilde{\theta})\left(2\sin(\tilde{\theta})\frac{\partial \tilde{\Gamma}}{\partial \tilde{\theta}} - \cos(\tilde{\theta})\frac{\partial^2 \tilde{\Gamma}}{\partial \tilde{\theta}^2}\right)\right),$$
$$0 = v\left((\alpha_1 - 1)\tilde{\Gamma} + \sin(\tilde{\theta})\cos(\tilde{\theta})\frac{\partial \tilde{\Gamma}}{\partial \tilde{\theta}}\right) - \cos^2(\tilde{\theta})\tilde{\Gamma}\frac{\partial \tilde{H}}{\partial \tilde{\theta}}\left((\alpha_1 - 1)\tilde{\Gamma}\tan(\tilde{\theta}) + \frac{\partial \tilde{\Gamma}}{\partial \tilde{\theta}}\right)$$
$$- \tilde{H}\left(\tilde{\Gamma}\left((3\alpha_1 - 4)\sin(\tilde{\theta})\cos(\tilde{\theta})\frac{\partial \tilde{\Gamma}}{\partial \tilde{\theta}} + \frac{\partial^2 \tilde{\Gamma}}{\partial \tilde{\theta}^2}\right) + (\alpha_1 - 1)^2\tilde{\Gamma}^2 + \cos^2(\tilde{\theta})\frac{\partial \tilde{\Gamma}}{\partial \tilde{\theta}}^2\right).$$

(ii-9) Scale invariant scale invariant solutions are invariant under $\vec{v}_{(\alpha_3, 2-\alpha_3)}^{\,6} + \omega\vec{v}^{\,4}$ and $\vec{v}_{(\alpha_1,\alpha_2)}^{\,6}$ with invariants

$$\tilde{H} = (\pm t)^{\frac{\alpha_3 - \alpha_1}{2-\alpha_1-\alpha_2}} R^{-\alpha_3} H,$$
$$\tilde{\Gamma} = (\pm t)^{\frac{2-\alpha_3-\alpha_2}{2-\alpha_1-\alpha_2}} R^{-2+\alpha_3}\Gamma,$$
$$\tilde{\theta} = \theta + \omega\log\left((\pm t)^{-\frac{1}{2-\alpha_1-\alpha_2}} R\right).$$

Choosing $\tilde{\theta}$ as the independent variable and $\tilde{H}$ and $\tilde{\Gamma}$ as the dependent variables, the reduced equations are

$$0 = \pm\left(\frac{(\alpha_3 - \alpha_1)\tilde{H} + \omega\frac{\partial \tilde{H}}{\partial \tilde{\theta}}}{\alpha_1 + \alpha_2 - 2}\right) + \tilde{H}\left(\frac{\partial \tilde{H}}{\partial \tilde{\theta}}\left((\alpha_1 - 2)\omega\tilde{\Gamma} - \left(\omega^2 + 1\right)\frac{\partial \tilde{\Gamma}}{\partial \tilde{\theta}}\right)\right),$$
$$+ \frac{1}{2}\tilde{H}\left(\tilde{H}\left(\left(\alpha_3^2 - 4\right)\tilde{\Gamma} - \left(\omega^2 + 1\right)\frac{\partial^2 \tilde{\Gamma}}{\partial \tilde{\theta}^2} - 4\omega\frac{\partial \tilde{\Gamma}}{\partial \tilde{\theta}}\right)\right),$$
$$0 = \pm\left(\frac{\omega\frac{\partial \tilde{\Gamma}}{\partial \tilde{\theta}} - (\alpha_3 + \alpha_2 - 2)\tilde{\Gamma}}{\alpha_1 + \alpha_2 - 2}\right) + \tilde{\Gamma}\frac{\partial \tilde{H}}{\partial \tilde{\theta}}\left((\alpha_3 - 2)\omega\tilde{\Gamma} - \left(\omega^2 + 1\right)\frac{\partial \tilde{\Gamma}}{\partial \tilde{\theta}}\right)$$
$$- \tilde{H}\left(\tilde{\Gamma}\left((8 - 3\alpha_3)\omega\frac{\partial \tilde{\Gamma}}{\partial \tilde{\theta}} + \left(\omega^2 + 1\right)\frac{\partial^2 \tilde{\Gamma}}{\partial \tilde{\theta}^2}\right) + (\alpha_3 - 4)(\alpha_3 - 2)\tilde{\Gamma}^2\right)$$
$$- \left(\omega^2 + 1\right)\tilde{H}\left(\frac{\partial \tilde{\Gamma}}{\partial \tilde{\theta}}\right)^2.$$

The choice of invariants above is only valid for $2 - \alpha_1 - \alpha_2 \neq 0$. For brevity this special case will be omitted.

Table 2.4: There are up to nine two-variable reductions of Eq. 2.16, including (ii-1) the rotationally invariant steady solutions, (ii-2) the translationally invariant travelling wave solutions, (ii-3) the constant solutions, (ii-4) the rotationally invariant scale invariant solutions, (ii-5) the translationally invariant scale invariant solutions, (ii-6) the steady scale invariant solutions, (ii-7) the rotating wave scale invariant solutions, (ii-8) the travelling wave scale invariant solutions, and (ii-9) the scale invariant scale invariant solutions.

2.3 Notes

The theory of symmetry analysis of partial differential equations developed with the entirety of physics over the last 150 years. We will not attempt a survey of the history, but acknowledge the foundational work of Sophus Lie in the late 19th century. Our primary reference is the excellent book by P. J. Olver [28], where a detailed survey of the history of the field is presented. In Section 2.1, we presented an argument for the central role of jet space geometry in a qualitative study of partial differential equations. Our presentation is original but parallels many modern ideas in the mathematics. In contrast to much of those works, we attempted to present these ideas in a manner accessible to working physicists and applied mathematicians. The analogy between fixed points of dynamical systems and group invariant solutions was an original development for this purpose. Details on technical aspects of jet bundles which we avoided discussing can be found in [58]. There the important concept of the contact structure should be noted, which played an important historical role in the development of the method of characteristics for first order quasilinear equations in one dependent variable [60]. The idea of passing to the infinite prolongation in jet space to define our extended phase $\mathscr{S}_\Delta$ has also been considered in many technical works. Central in these studies are homological methods such as the variational (bi)complex mentioned in Section 1.4. An alternative but similar approach is the theory of diffieties (a play on the words "differential" and "variety") and the secondary calculus of Vinogradov et al. [61, 62]. The other important modern development noted in Section 2.1 was the generalization of Noethers' theorem to non-variational problems through adjoint symmetries. Aspects of this connection were noted in [28], but Bluman and Anco expounded the idea and gave explicit formulas for calculating conserved currents [59, 63, 64].

The application of symmetry methods to thin film equations was presented in Section 2.2. The enumeration of symmetries for a variety of thin film equations in only

one spatial dimension exists in the literature [65–67]. However, the full equation in two spatial dimensions has not been considered in the literature as far as the author is aware. This is not surprising, given the large number of terms in the symmetry invariance condition noted in Section 2.2. The package zgnsymmetry.m, included in the Appendix A, was created specifically to deal with this difficulty. Other mathematical computer packages for deriving symmetries exist such as that expounded in [68], but the author found it easier to create his own package tailored to extracting simple equations from a large list of equations than to use existing software. Since previous studies have focused only on one spatial dimension or rotationally invariant solutions, the various rotating solutions reductions noted in Tables 2.2-2.3 were previously, to the authors knowledge, unrecognized. Some scale invariant solutions with the power law form in Eq. 2.14 find applications in modeling the rupture of thin film with Van der Waals body forces [69, 70], but the travelling wave, rotating wave, and steady scale-invariant solutions have not been previously applied to spreading phenomena. The scale invariant scale invariant solutions for the purely capillary film are also, to the authors knowledge, new. In Section 4.2 below, we consider some numerical solutions to these novel scale-invariant reductions for capillary driven films. The rotationally invariant scale invariant solutions and the translationally invariant scale invariant solutions for the surfactant spreading problem were studied by Jensen [71], and the presentation of them as a planar dynamical system was derived there as well. The enumeration of the local bifurcations of this planar system, detailed in Section 4.1 below, is new, as are the additional four scale-invariant reductions of the surfactant spreading problem listed in Table 2.4.

The zgnsymmetry.m package is capable of calculating adjoint symmetries as well. Examples of calculations of symmetries and adjoint symmetries for the KdV equation, Burgers' equation, the heat equation, the wave equation, and the Euler equations for an inviscid incompressible fluid have been carried out by the author and have reproduced the known conserved quantities. The adjoint symmetries of the thin film equations did not turn out to produce any new conserved quantities aside from the obvious volume and surfactant mass conservation. We have only considered fourth order adjoint symmetries for the film with a single dependent variable and first order adjoint symmetries for the surfactant problem, however. Higher order considerations are possible but can become computationally expensive. The lack of additional conserved quantities is perhaps not surprising since we do not expect any of the thin film equations to be integrable. In this regard, the reductions of the

thin film equation do not satisfy the Painlevé criteria [72], as the contact line is a movable singularity which is not a simple pole. The contact line singularity will be discussed in detail in Chapter 3 below. The Painlevé conjecture would then implies that the thin film equations are not integrable by the inverse scattering method [72].

Generalizations to the procedure of finding group-invariant solutions should be noted as well. The non-classical method of Bluman and Cole relies on conditional symmetries which include Eq. 2.8 as well as $\Delta = 0$ in the constraints in its definition in Eq. 2.7 [73]. Adding this condition causes the determining equations to become nonlinear, reduces their number, and in some cases affords new reductions. In addition to Eq. 2.8, the compatibility conditions with $\Delta = 0$ and prolongations of all these equations can be included resulting in weak symmetries [73]. We have not attempted to seek such conditional symmetries, but it would not take great effort to incorporate this functionality into the zgnsymmetry.m package.

Chapter 3

STEADY STATES AND STABILITY

In this chapter, we will carry out analyses of one of the simplest and physically most important classes of the reductions of the thin film equations that were discussed in Section 2.2 above, namely the rotationally invariant steady solutions. Our focus here is on stability which ultimately requires solving a linearized eigenvalue problem as discussed in Section 2.2. However, because of the existence of the Lyapunov functional discussed in Section 1.3, a simpler problem which is second order in spatial derivatives rather than fourth order can be solved. An important subtlety in these problems is the consideration of the contact line, where the film height H becomes zero. This is an example of the other general geometrical feature of nonlinear partial differential equations discussed in Section 2.1, singularities. We will carefully consider how these singularities complicate some basic assumption. In Section 3.1, we consider some general results but focus on the stability of droplets in the thermocapillary problem. In Section 3.2, we will consider droplets under gravitational and thermocapillary or gravitational and electrohydrodynamic forces. Finally, Section 3.3 contains a discussion of the history and literature in the field, with an attempt to place the new research contained in this chapter in a wider context.

3.1 Stability of rotationally invariant, thermocapillary driven droplets

[1] Z. G. Nicolaou. “Stability and instability of axisymmetric droplets in thermocapillary-driven thin films”. In: *Nonlinearity* (under review 2016).

The evolution of a thin viscous fluid film has been of theoretical and technological interest for decades. Often in such systems, a flat fluid film is prepared and some driving force is then applied that causes the film to deform. Figure 3.1 depicts two possible scenarios for the structures that might develop from such a film. One promising application of such an instability is as an alternative to lithography in the manufacture of micro- and nano- scale optical devices: frozen arrays of smooth droplets in polymer films similar to those depicted in Fig. 3.1(a) have potential uses as microlens arrays, for example. On the other hand, the possibility depicted in Fig. 3.1(b) that a jet or spray of fluid forms because no droplet state exists that can accommodate the fluid in a growing protrusion has not previously received as

much attention. Such jets may offer the possibility of application in manufacture of other structures with very sharp and smooth profiles. Linear stability analyses give valuable information about the film deformations shortly after the driving force is applied, but determining the longer time evolution requires a more sophisticated study. Here we consider this possibility by studying the stability properties of axisymmetric, steady droplet states in driven thin films. One particular system of

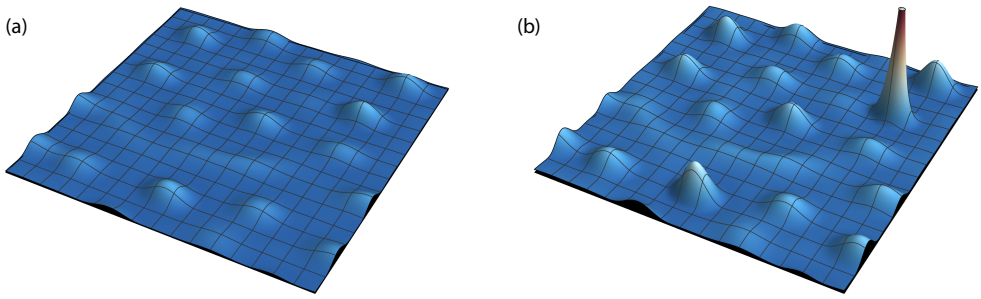

Figure 3.1: An initially flat, unstable film may (a) develop into a collection of nearly steady, nearly isolated droplets or may (b) develop a secondary instability resulting in jet formation if no droplet states exists to accommodate the fluid in the protrusions.

current interest is a thin film destabilized by a surface-normal temperature gradient, like that depicted in Fig. 3.2. Thermocapillary (or Marangoni) forces have been recognized as driving this instability [11–13]. These are forces resulting from variations in the surface tension across the film. The surface tension σ varies with temperature, and colder portions tend to have higher surface tension and consequently pull fluid closer towards the cold substrate. We shall see that this system is one example in which both steady droplet formation and jet formation are possible[1].

The basic partial differential equation noted in Eq. 1.65 for driven thin fluid films is

[1]Note that since the cold substrate confines the fluid above in this system, such a jet will result in the formation of a column of fluid between the hot and cold substrates.

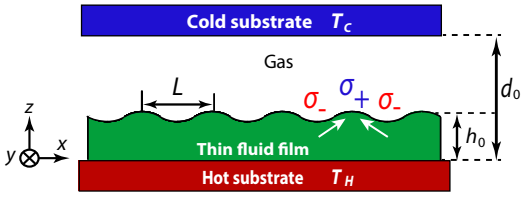

Figure 3.2: A liquid film of thickness h_0 is supported on a hot substrate at temperature T_H, and a cold substrate at temperature T_C is suspended a distance d_0 above. The surface tension σ increases with decreasing temperature, resulting in the spontaneous growth of long-wavelength protrusions.

repeated here for convenience:

$$\begin{aligned} 0 &= \frac{\partial H}{\partial t} + \nabla_L \cdot \left(Q_1(H) \nabla_L \left(\bar{\mathrm{Ca}}^{-1} \nabla_L^2 H - W'(H) \right) \right), \\ Q_1(H) &\equiv \frac{1}{3} H^3 + \beta H^2, \\ W''(H) &\equiv \frac{\partial \Phi}{\partial H} - \frac{\partial \Pi}{\partial H} - \frac{3H^2 + 6\beta H}{2H^3 + 6\beta H^2} \left(\frac{\partial \tau_{\mathrm{ext}}}{\partial H} + \bar{\mathrm{Ma}} \frac{\partial \Sigma}{\partial H} \right), \end{aligned} \tag{3.1}$$

as are the fundamental conservation form for volume:

$$\begin{aligned} 0 &= \frac{\partial H}{\partial t} + \nabla_L \cdot \mathbf{Q}_L, \\ \mathbf{Q}_L &\equiv \left(\boldsymbol{\tau}_{\mathrm{ext}} + \bar{\mathrm{Ma}} \nabla_L \Sigma \right) \left(\frac{1}{2} H^2 + \beta H \right) - \left(\frac{1}{3} H^3 + \beta H^2 \right) \nabla_L P, \\ \mathscr{V}[H] &\equiv \int \mathrm{d}^2 X \; H(\mathbf{X}_L, t). \end{aligned} \tag{3.2}$$

and the Cahn-Hilliard form:

$$\begin{aligned} 0 &= \frac{\partial H}{\partial t} - \nabla_L \cdot \left(Q_1(H) \nabla_L \frac{\delta F}{\delta H} \right), \\ F[H] &\equiv \int \mathrm{d}^2 X \; \mathcal{F}(\mathbf{X}_L, t) \\ \mathcal{F}(\mathbf{X}_L, t) &\equiv \frac{\bar{\mathrm{Ca}}^{-1}}{2} |\nabla_L H|^2 + W(H). \end{aligned} \tag{3.3}$$

For the thermocapillary system described in Fig. 3.2, important dimensionless parameters are the ratio of the thermal conductivity of the gas to the fluid $\kappa \equiv k_{\mathrm{gas}}/k$ and the liquid-gap width aspect ratio $D_0 \equiv d_0/h_0 > 1$. Although $\kappa > 1$ is possible for light molecular weight gases or highly insulating fluids, it will be assumed throughout this section that the thermal conductivity of the gas is strictly less than that of the

liquid film, so that $\kappa < 1$, unless otherwise noted. For very thin films, gravitational effects are negligible, and additionally we neglect fluid slip and other interactions between the fluid and the substrates for the sake of simplicity. We noted in Section 1.1 Eq. 1.35 that the specification of $\bar{\text{Ca}} = (4\pi)^2/3$ and $\bar{\text{Ma}} = (D_0 + \kappa - 1)/D_0$ is equivalent to choosing appropriate scales for the lateral velocity scale and the lateral legnth scale and reduces the dependence of the thin film equation to a single parameter $\chi \equiv \frac{\kappa-1}{D_0}$,

$$\frac{\partial H}{\partial t} + \nabla_L \cdot \left(\frac{H^3}{(4\pi)^2} \nabla_L \nabla_L^2 H + \frac{H^2}{2} \left(\frac{1+\chi}{1+\chi H} \right)^2 \nabla_L H \right) = 0. \tag{3.4}$$

In this case, yet another rescaling simplifies the problem further. Using rescaled variables $H' = -H/\chi$, $t' = -\chi \left(1 + \chi^4\right) t$ and $\mathbf{X}'_L = \sqrt{-\chi}\,(1+\chi)\,\mathbf{X}_L$ allows us to eliminate all dependence on the parameter χ. When discussing this system, these rescaled variables will be used for the remainder of the section, but the primes will be dropped in order to achieve more concise notation. The author apologizes for this abuse of notation, but the advantage of eliminating χ from the problem is great. The rescaled film equation in this case is

$$\frac{\partial H}{\partial t} + \nabla_L \cdot \left(\frac{H^3}{(4\pi)^2} \nabla_L \nabla_L^2 H + \frac{H^2}{2} \frac{1}{(1-H)^2} \nabla_L H \right) = 0. \tag{3.5}$$

The Lyapunov energy can be rescaled in an analogous manner to eliminate the dependence on χ and the relevant functions are

$$\begin{aligned} \mathcal{F}(H, \nabla_L H) &\equiv \frac{1}{2} |\nabla_L H|^2 + W(H) \\ W(H) &\equiv -\frac{(4\pi)^2}{2} H \log \frac{H}{1-H}, \\ Q_1(H) &\equiv \frac{H^3}{3}. \end{aligned} \tag{3.6}$$

The functions in Eq. 3.6 will be used as a specific example to illustrate some stability results in what follows. Elaborations taking other effects into account are relatively straightforward, and it is expected that other researchers can adapt the methods presented here to their purposes.

Outline of results

Given all the previous results indicating film rupture and evolution towards droplet states in such driven films, the focus of this study is on finite volumes of fluid supported on compact domains. To aid understanding and readability, it will be

everywhere assumed that functions are sufficiently regular to allow the operations performed, and more technical aspects of the mathematics will be avoided. As a consequence, we do not claim to prove any theorems with complete mathematical rigor, but only to provide strong evidence for several propositions which could be formalized. In general, states may be assumed to be infinitely differentiable in the interior of their support (the wetted domain) Ω and only become singular on the boundary of their support $\partial\Omega$ (the contact line). When considering possible perturbation that may destabilize a state, volume should be independently conserved in each connected component of such a domain Ω since fluid cannot physically tranport across the dry regions. Technical complications, such as cases in which the boundaries of disjoint, connected components of the wetted domain intersect, will not be considered. Since each connected component then evolves independently, it is convenient and sufficient to consider the support Ω to be a single, connected, compact region throughout.

The Lyapunov energy functional $F[H]$ from Eq. 3.3 derives its significance from its time evolution. Assuming periodic boundary conditions or a stationary contact line so that no boundary contributions appear, a functional version of the chain rule implies that the Lyapunov energy strictly decreases in time,

$$\frac{dF[H]}{dt} = \int \mathrm{d}^2X \, \frac{\delta F}{\delta H}\frac{\partial H}{\partial t} = -\int \mathrm{d}^2X \, Q_1(H)\left|\nabla_L \frac{\delta F}{\delta H}\right|^2 \leq 0, \tag{3.7}$$

as first noted by Oron and Rosenau and Deissler and Oron [18, 74]. In the subsection **Lyapunov function for states with finite support** below this calculation is considered more carefully in the case that the film profile H is supported on a compact domain Ω with a time-dependent boundary $\partial\Omega$. There it is shown that boundary terms cannot be generally neglected, a complication which, to the author's knowledge, has not been fully appreciated. An additional assumption will be required throughout:

Assumption 1 *Consider a stable, steady, weak solution $H_0(\mathbf{X}_L)$ of Eq. 3.3 with compact support Ω. For any weak solution $H(\mathbf{X}_L, t) = H_0(\mathbf{X}_L) + \delta H(\mathbf{X}_L, t)$ of Eq. 3.3 with δH sufficiently small and regular, the Lyapunov energy is a non-increasing function of time, $\frac{dF[H]}{dt} \leq 0$.*

Recall that weak solutions are those with moving contact lines which are found through regularized equations, as described in [75–77]. The restriction to perturbations of steady, weak solutions is all that is required here, though we expect the

conclusions to hold for all weak solutions. The general validity of Assumption 1 is unknown, but arguments supporting it are given in the subsection **Lyapunov function for states with finite support**.

The existence of a Lyapunov energy functional aids in the study of stability of steady states. In particular, states that are not local minima (among states of the same volume) of the Lyapunov energy are necessarily unstable as some small perturbation then exists that decreases the energy. This perturbation cannot decay with time since the energy can never increase to its previous value. States that are local minima of the Lyapunov energy are termed energy-stable and enjoy a degree of asymptotic stability [78, 79]. In the subsection **Steady solutions**, the following proposition is easily established as a result.

Proposition 1 *Any stable, steady state of Eq. 3.3 $H(\mathbf{X}_L)$ has everywhere vanishing volumetric flux $\mathbf{Q}_L = \mathbf{0}$ and satisfies the partial differential equation*

$$C_1 = \nabla_L^2 H - W'(H) \tag{3.8}$$

for some constant C_1 in the interior of its support.

Next, in the subsection **A "thermodynamic" relation**, two important results are demonstrated as consequences of a thermodynamic-like relation derived in Lemma 1. First, it is shown that among the solutions to Eq. 3.8, only those that satisfy a certain contact slope criterion can be stable. The tangent of the familiar contact angle is the contact slope, which plays a more prominent role than the contact angle in the thin film limit of interest here.

Proposition 2 *Let $H(\mathbf{X}_L)$ be a compactly supported solution of Eq. 3.8 and denote the support of H by Ω. The boundary of Ω will be denoted $\partial\Omega$ and will be referred to as the contact line. Define the contact slope*

$$C_c(\mathbf{X}_c) = \lim_{(\mathbf{X}_L \in \Omega) \to \mathbf{X}_c} |\nabla_L H(\mathbf{X}_L)| \tag{3.9}$$

at a point $\mathbf{X}_c \in \partial\Omega$. If H is energy-stable, then $C_c(\mathbf{X}_c) = 2\bar{\mathrm{C}}\mathrm{a}W(0)$ everywhere on the contact line.

Note that the Lyapunov energy density in Eq. 3.3 can always be modified by the addition of a global constant without altering the thin film equation, since only derivatives of F appear in Eq. 3.3. However, according to Proposition 2, the addition

of such a constant alters the potentially stable steady contact slope. The derivation of Eq. 3.1 assumes that a thin fluid film exists that wets the surface, and the contact line is precisely where this assumption breaks down. Consequently, the integration region in the definition of $F[H]$ in Eq. 3.3 has been restricted to the wetted domain, where $H > 0$. Equivalently, $\mathcal{F} \equiv 0$ has been defined wherever H is identically zero, but $\mathcal{F} \to W(0)$ as $H \to 0$ from above, and $W(0)$ represents the difference in Lyapunov energy density between an infinitesimal film and a dry region. It is evident that additional physical considerations and modelling are necessary to conclusively determine $W(0)$, and hence to determine the stable steady contact slope for any specific system.

In any case, for a given $W(H)$, analysis can proceed, and among those solutions to Eq. 3.8 that satisfy the contact slope criterion in Proposition 2, a relationship between the volume and the Lyapunov energy is established.

Proposition 3 *Let $H_\varepsilon(\mathbf{X}_L)$ be a family of compactly supported solutions of Eq. 3.8 with supports $\Omega(\varepsilon)$ and $C_c(\mathbf{X}_c) = 2\bar{\mathrm{C}}\mathrm{a}W(0)$ for all $\mathbf{X}_c \in \partial\Omega(\varepsilon)$. Assume that H_ε is sufficiently smooth with respect to ε. Then*

$$\frac{dF[H_\varepsilon]}{d\varepsilon} + C_1 \frac{d\mathscr{V}[H_\varepsilon]}{d\varepsilon} = 0. \tag{3.10}$$

It follows that if $0 < |\frac{F + C_1\mathscr{V}}{\mathscr{V}^2}| < \infty$ for all ε, then the critical points of $\mathscr{V}[H_\varepsilon]$ and $F[H_\varepsilon]/\mathscr{V}[H_\varepsilon]$ coincide. Furthermore, the relation between volume and free energy per unit volume is monotonic.

Proposition 3 has interesting implications regarding the long-time evolution of the film. If the droplets' Lyapunov energy per unit volume decreases with increasing droplet volume, it implies that droplet coarsening (the combining of smaller droplets to form larger droplets) is energetically favorable. These assumptions appear to hold in the usual settings, as corroborated by the numerical droplet-coarsening observations of Thiele et al. [24, 48, 49]. Cheung and Chou also noted this result in the case of Eq. 3.100 by observing that "configurations of droplets" are "energy unstable," meaning that the Lyapunov energy can always be decreased by combining droplets to form a single droplet of larger volume. However, we note that if true film rupture does occur, fluid cannot transfer across dry regions, so that droplets may not have the opportunity to combine and coarsening may cease.

Next, in the subsection **Energy stability in the thermocapillary case of Eq. 3.6**, the stability of rotationally invariant droplets in the thermocapillary problem in Eq. 3.6

is considered. This discussion proceeds first by finding numerical, rotationally-invariant solutions of Eq. 3.8 in the subsection **Rotationally invariant solutions for steady state profiles**, then by dividing the change in Lyapunov energy under small perturbations into interior and boundary contributions in the subsection **The separation of the interior and boundary contributions**. The interior contribution reduces to an eigenvalue problem that is solved numerically in the subsection **The interior contribution to the energy stability analysis and the eigenvalue problem** while the boundary contribution reduces to a problem in asymptotic analysis in the subsection **The boundary contribution to the energy stability analysis and the stable contact slope**. The conclusions are summarized in the following proposition.

Proposition 4 *Fix* $\mathcal{F} = \frac{1}{2}|\nabla_L H|^2 + W(H)$ *and* $W(H) = -\frac{(4\pi)^2}{2} H \log \frac{H}{1-H}$ *as in Eq. 3.6, and let* $H_0(R)$ *be a rotationally invariant solution of Eq. 3.8 with compact support and everywhere zero contact slope. It follows that* H_0 *attains its maximum at* $R = R_{\max} = 0$*; denote* $H_0(0) = H_{\max}$*. Then* $H_0(R)$ *is energy stable if and only if* $H_{\max} \lesssim 0.81113$*. Furthermore, for the one-parameter family of solutions* H_ε *with zero contact slope parameterized by* $\varepsilon = H_{\max}$*, the volume* $\mathscr{V}[H_\varepsilon]$ *is maximized and the free energy per unit volume* $F[H_\varepsilon]/\mathscr{V}[H_\varepsilon]$ *is minimized for* $\varepsilon = H_{\max} \approx 0.81113$*.*

The simultaneous critical point $\varepsilon \approx 0.81113$ of $\mathscr{V}[H_\varepsilon]$ and $F[H_\varepsilon]/\mathscr{V}[H_\varepsilon]$ established by Proposition 3 gains further significance in this case as also indicating a change in droplet stability. Whether a more formal connection can be established for general $Q_1(H)$ and $W(H)$ is a promising direction for future research.

Results for general driving forces

Here we discuss results that can be established without specifying the mobility factor $Q_1(H)$ or the Lyapunov potential $W(H)$.

Lyapunov function for states with finite support and Assumption 1

The demonstration that the Lyapunov energy in Eq. 3.3 strictly decreases with time (i.e., that it is a Lyapunov function) is complicated when the wetted domain is not infinite and boundary contributions are nonnegligible. Consider a solution $H(\mathbf{X}_L, t)$ of Eq. 3.3 with support on some finite, compact domain $\Omega(t) \subset \mathbb{R}^2$ and the Lyapunov energy in Eq. 3.3. The rate of change of $F[H]$ can be found using the Reynolds'

transport theorem for 2-forms in 2 dimensions [80],

$$\frac{dF[H]}{dt} = \int_{\Omega(t)} \mathrm{d}^2X \left(\bar{\mathrm{Ca}}^{-1}\nabla_L H \cdot \nabla_L \frac{\partial H}{\partial t} + W'(H)\frac{\partial H}{\partial t}\right) + \int_{\partial\Omega(t)} \mathrm{d}X \left(\frac{\bar{\mathrm{Ca}}^{-1}}{2}|\nabla_L H|^2 + W(H)\right)\mathbf{V}_c \cdot \hat{\mathbf{n}}_c, \tag{3.11}$$

where $\partial\Omega$ is the boundary of Ω, $\mathbf{V}_c = \frac{d\mathbf{X}_c}{dt}$ is the velocity of the boundary point $\mathbf{X}_c \in \partial\Omega$, and $\hat{\mathbf{n}}_c$ is the outward-pointing, lateral unit normal vector on the contact line. Substituting $\frac{\partial H}{\partial t}$ from Eq. 3.3 and rearranging terms into a total divergence, this can be reexpressed as

$$\begin{aligned}
\frac{dF[H]}{dt} &= -\int_{\Omega(t)} \mathrm{d}^2X\, Q_1(H)\left|\nabla_L \frac{\delta F}{\delta H}\right|^2 \\
&\quad + \int_{\Omega(t)} \mathrm{d}^2X\, \nabla_L \cdot \left(\bar{\mathrm{Ca}}^{-1}\frac{\partial H}{\partial t}\nabla_L H + \frac{\delta F}{\delta H}Q_1(H)\nabla_L \frac{\delta F}{\delta H}\right) \\
&\quad + \int_{\partial\Omega(t)} \mathrm{d}X \left(\frac{\bar{\mathrm{Ca}}^{-1}}{2}|\nabla_L H|^2 + W(H)\right)\mathbf{V}_c \cdot \hat{\mathbf{n}}_c \\
&= -\int_{\Omega(t)} \mathrm{d}^2X\, Q_1(H)\left|\nabla_L \frac{\delta F}{\delta H}\right|^2 \\
&\quad + \int_{\partial\Omega(t)} \mathrm{d}X \left(\bar{\mathrm{Ca}}^{-1}\frac{\partial H}{\partial t}\nabla_L H + \frac{\delta F}{\delta H}Q_1(H)\nabla_L \frac{\delta F}{\delta H}\right)\cdot \hat{\mathbf{n}}_c \\
&\quad + \int_{\partial\Omega(t)} \mathrm{d}X \left(\frac{\bar{\mathrm{Ca}}^{-1}}{2}|\nabla_L H|^2 + W(H)\right)\mathbf{V}_c \cdot \hat{\mathbf{n}}_c,
\end{aligned} \tag{3.12}$$

where the divergence theorem was used to arrive at the second equality.

Next, consider the conservation of the volume in Eq. 3.2, again using Reynolds' transport theorem and the divergence theorem,

$$\begin{aligned}
\frac{d\mathscr{V}[H]}{dt} &= \int_{\Omega(t)} \mathrm{d}^2X\, \frac{\partial H}{\partial t} + \int_{\partial\Omega(t)} \mathrm{d}X\, H\mathbf{V}_c \cdot \hat{\mathbf{n}}_c \\
&= \int_{\Omega(t)} \mathrm{d}^2X\, \nabla_L \cdot \left(Q_1(H)\nabla_L \frac{\delta F}{\delta H}\right) + \int_{\partial\Omega(t)} \mathrm{d}X\, H\mathbf{V}_c \cdot \hat{\mathbf{n}}_c \\
&= \int_{\partial\Omega(t)} \mathrm{d}X \left(Q_1(H)\nabla_L \frac{\delta F}{\delta H} + H\mathbf{V}_c\right)\cdot \hat{\mathbf{n}}_c.
\end{aligned} \tag{3.13}$$

The integrand here is the volumetric flux of fluid across the moving contact line. Since the contact line is generally not expected to be a source or sink of fluid mass, this flux must vanish everywhere on $\partial\Omega$,

$$\left(Q_1(H)\nabla_L \frac{\delta F}{\delta H} + H\mathbf{V}_c\right)\cdot \hat{\mathbf{n}}_c \Big|_{\partial\Omega(t)} = 0, \tag{3.14}$$

which of course implies that $\frac{d\mathscr{V}[H]}{dt} = 0$. Also, note that if $\mathbf{X}_c \in \partial\Omega(t)$ is a boundary point, then $H(\mathbf{X}_c(t), t) = 0$. This relation can be differentiated with respect to t to find

$$\left(\nabla_L H \cdot \mathbf{V}_c + \frac{\partial H}{\partial t}\right) \Big|_{\partial\Omega(t)} = 0. \tag{3.15}$$

Lastly, the outward-pointing unit normal vector on the contact line $\partial\Omega(t)$, where $H = 0$, is

$$\hat{\mathbf{n}}_c = -\frac{\nabla_L H}{|\nabla_L H|}, \tag{3.16}$$

since the contact line is the zero level set of the film height function $H(\mathbf{X}_L, t)$. Combining Eqns. 3.12-3.16, the rate change of the Lyapunov energy can be written

$$\begin{aligned}\frac{dF[H]}{dt} = &-\int_{\Omega(t)} \mathrm{d}^2X\, Q_1(H) \left|\nabla_L \frac{\delta F}{\delta H}\right|^2 \\ &-\int_{\partial\Omega(t)} \mathrm{d}X\, \left(\bar{\mathrm{Ca}}^{-1}\left(\frac{1}{2}|\nabla_L H|^2 - H\nabla_L^2 H\right) + HW'(H) - W(H)\right)\mathbf{V}_c \cdot \hat{\mathbf{n}}_c.\end{aligned} \tag{3.17}$$

The boundary contribution here was neglected in the derivation in Section 1.3, and furthermore, it is apparently not negative definite. Thus it does not yet follow that $F[H]$ is actually a Lyapunov function. Of course, on $\partial\Omega(t)$, the film height vanishes $H \to 0$, so provided the Lyapunov potential $W(H)$ and $\nabla_L^2 H$ are not too singular on the contact line, the terms $H\nabla_L^2 H$ and $HF'(H)$ will vanish. However, the other terms $\frac{\bar{\mathrm{Ca}}^{-1}}{2}|\nabla_L H|^2 - W(0)$ involving the contact slope $C_c = |\nabla_L H|$ and the Lyapunov potential $W(0)$ will not generally vanish, and the sign of $\mathbf{V}_c \cdot \hat{\mathbf{n}}_c$ is apparently unconstrained.

The exact conditions on H, $Q_1(H)$ and $W(H)$ necessary to ensure $\frac{dF[H]}{dt} \leq 0$ will not be derived here, and instead Assumption 1 will be taken for the remainder of the section. It seems likely that the correct notion of weak solutions will automatically entail this assumption, although this would require both a precise mathematical definition and a physical justification to be satisfactory. There is a promising, albeit somewhat technical, approach that we will briefly outline now. First, regulate Eq. 3.3 so as to remove the $H \to 0$ degeneracy, for example, by using $Q_1^\varepsilon(H) = Q_1(H) + \varepsilon > 0$ in place of $Q_1(H)$. This allows regularity results from the standard theory of parabolic partial differential equations to be used, and is in fact used in the construction of weak solutions [75, 76]. Next, consider a disk $D \in \mathbb{R}^2$ with $\Omega(t) \subset D$. Let $H_\varepsilon(\mathbf{x})$ be a sequence of solutions of the regulated problem with

support on D and with $H_\varepsilon \to H(\mathbf{X}_L)$ as $\varepsilon \to 0$ for all $\mathbf{X}_L \in D$, and choose H_ε such that $\mathbf{V}_c = \mathbf{0}$ at time t on ∂D, so that the boundary contributions in Eq. 3.17 vanish and $\frac{dF[H_\varepsilon]}{dt} \leq 0$ follows. It is not yet guaranteed that $0 \geq \frac{dF[H_\varepsilon]}{dt} \to \frac{dF[H]}{dt}$ as $\varepsilon \to 0$, but this is expected to follow from the Ascoli-Arzelà theorem given the regularity of the regulated solution (equicontinuity in time) and the uniform boundedness above zero of the functions $\frac{dF[H_\varepsilon]}{dt}$. The restriction in Assumption 1 to small perturbation of steady states is weaker than $\frac{dF[H]}{dt} \leq 0$ for all weak solutions, but it is the only necessary requirement for the remainder of the section.

Steady solutions and Proposition 1

Here Proposition 1 will be demonstrated. As noted in Section 1.3, assuming the Lyapunov energy in Eq. 3.3 strictly decreases with time, any stable, steady state must locally minimize it. It was also mentioned there that the total volume is dynamically conserved, so a Lagrange multiplier should be included in the Lyapunov energy when extremizing it to search for stable, steady states. If H is a local minimum, it must satisfy the Euler-Lagrange equations with Lagrange multiplier C_1 constraining the volume

$$0 = \frac{\delta F}{\delta H} + C_1 \frac{\delta \mathscr{V}}{\delta H} = C_1 - \left(\nabla_L^2 H - W'(H)\right), \tag{3.18}$$

which is indeed equivalent to Eq. 3.8.

A more direct approach to study the steady state solutions of Eq. 3.3 is to set $\frac{\partial H}{\partial t} = 0$ so that the equation reduces to $\nabla_L \cdot \mathbf{Q}_L = 0$, where $\mathbf{Q}_L$ is the volumetric flux in Eq. 3.2. This equation can be integrated with a stream function using a form of the Poincaré Lemma of differential geometry: $\nabla_L \cdot \mathbf{Q}_L = 0$ if and only if $\mathbf{Q}_L = (\star \nabla_L)\psi$ for some function ψ, where $\star\nabla_L \equiv \hat{\mathbf{X}} \frac{\partial}{\partial Y} - \hat{\mathbf{Y}} \frac{\partial}{\partial X}$ is the Hodge dual gradient operator. Note that H may be a steady state even if the flux does not vanish everywhere, as is often the case in hydrodynamical problems. However, for states with vanishing flux, it follows that

$$\mathbf{Q}_L = Q_1(H) \nabla_L \left(\nabla_L^2 H - W'(H)\right) = \mathbf{0}. \tag{3.19}$$

This is equivalent to Eq. 3.8 after a trivial integration, so that the solutions of Eq. 3.8 do indeed have everywhere vanishing volumetric flux. Those steady states with non-vanishing flux therefore cannot be stable.

The fundamental relation of thermodynamics and Propositions 2 and 3

Here, Propositions 2 and 3 will be demonstrated using a thermodynamic-like relation for systems that extremize a functional under some constraint. While analogues date back to the birth of thermodynamics, as far as the author is aware, this relationship has not been recognized in the context of free boundary problems, like the determination of a droplet profile and its contact line explored here. A general statement is derived first for general functionals in D dimensions, and later specialized to the Lyapunov energy functional in Eq. 3.3 in $D = 2$ dimensions. Consider an energy functional $F[u] = \int_\Omega \mathrm{d}^D X \; \mathcal{F}\left(u(\mathbf{X}), \boldsymbol{\nabla} u(\mathbf{X})\right)$, where $u(\mathbf{X})$ is an field variable and Ω is a bounded, D-dimensional domain in $\mathbb{R}^D$ on which $u(\mathbf{X})$ has support. Assume that $u(\mathbf{X}) \geq 0$ for $\mathbf{X} \in \Omega$ and $u(\mathbf{X}_c) = 0$ for $\mathbf{X}_c \in \partial\Omega$, where $\partial\Omega$ is the boundary of Ω. Also assume that another functional $\mathscr{V}[u] = \int_\Omega \mathrm{d}^D X \; \mathcal{V}\left(u(\mathbf{X}), \boldsymbol{\nabla} u(\mathbf{X})\right)$ exists that is constrained to take some specified value. The free boundary problem is to extremize $F[u]$ under the constraint on $\mathscr{V}[u]$ to determine simultaneously the profile $u(\mathbf{X})$ and the domain of support Ω. For concreteness, we have assumed that $\mathcal{F}$ and $\mathcal{V}$ both depend on $\mathbf{X}$ only implicitly through $u(\mathbf{X})$ and $\boldsymbol{\nabla} u(\mathbf{X})$. It follows that any solution $u(\mathbf{X})$ must satisfy the constrained Euler-Lagrange equations

$$\begin{aligned} \frac{\partial \mathcal{F}}{\partial u} - \boldsymbol{\nabla} \cdot \frac{\partial \mathcal{F}}{\partial \boldsymbol{\nabla} u} + C\left(\frac{\partial \mathcal{V}}{\partial u} - \boldsymbol{\nabla} \cdot \frac{\partial \mathcal{V}}{\partial \boldsymbol{\nabla} u}\right) = 0 \text{ for } \mathbf{X} \in \Omega, \\ u(\mathbf{X}) \geq 0 \text{ for } \mathbf{X} \in \Omega, \\ u(\mathbf{X}_c) = 0 \text{ for } \mathbf{X}_c \in \partial\Omega, \end{aligned} \tag{3.20}$$

where C is the Lagrange multiplier that is used to fix $\mathscr{V}[u]$.

Lemma 1 *Let $u_\varepsilon(\mathbf{X})$ be a family of solutions of Eq. 3.20 with compact supports $\Omega(\varepsilon)$. Assume that $u_\varepsilon(\mathbf{X})$ is differentiable with respect to ε for every $\mathbf{X} \in \Omega(\varepsilon)$. Then*

$$\frac{dF}{d\varepsilon} + C\frac{d\mathscr{V}}{d\varepsilon} = \int_{\partial\Omega(\varepsilon)} \mathrm{d}^{D-1} X \left(\mathcal{F} + C\mathcal{V} - \boldsymbol{\nabla} u_\varepsilon \cdot \left(\frac{\partial \mathcal{F}}{\partial \boldsymbol{\nabla} u_\varepsilon} + C\frac{\partial \mathcal{V}}{\partial \boldsymbol{\nabla} u_\varepsilon}\right)\right) \frac{\partial \mathbf{X}_c}{\partial \varepsilon} \cdot \hat{\mathbf{n}}_c, \tag{3.21}$$

where $\mathbf{X}_c \in \partial\Omega$ denotes the boundary integration variable and $\hat{\mathbf{n}}_c$ is the outward-pointing normal vector to the boundary.

Lemma 1 is shown using the Reynolds' transport theorem for D-forms in D dimensions [80]:

$$\frac{dF}{d\varepsilon} + C\frac{d\mathscr{V}}{d\varepsilon} = \int_{\Omega(\varepsilon)} \mathrm{d}^D X \left[\left(\frac{\partial \mathcal{F}}{\partial u_\varepsilon} + C\frac{\partial \mathcal{V}}{\partial u_\varepsilon} \right) \frac{\partial u_\varepsilon}{\partial \varepsilon} + \left(\frac{\partial \mathcal{F}}{\partial \boldsymbol{\nabla} u_\varepsilon} + C\frac{\partial \mathcal{V}}{\partial \boldsymbol{\nabla} u_\varepsilon} \right) \cdot \boldsymbol{\nabla} \frac{\partial u_\varepsilon}{\partial \varepsilon} \right] + \int_{\partial\Omega(\varepsilon)} \mathrm{d}^{D-1} X \ (\mathcal{F} + C\mathcal{V}) \frac{\partial \mathbf{X}_c}{\partial \varepsilon} \cdot \hat{\mathbf{n}}_c. \tag{3.22}$$

Rearranging slightly,

$$\frac{dF}{d\varepsilon} + C\frac{d\mathscr{V}}{d\varepsilon} = \int_{\Omega(\varepsilon)} \mathrm{d}^D X \left[\left(\frac{\partial \mathcal{F}}{\partial u_\varepsilon} + C\frac{\partial \mathcal{V}}{\partial u_\varepsilon} - \boldsymbol{\nabla} \cdot \frac{\partial \mathcal{F}}{\partial \boldsymbol{\nabla} u_\varepsilon} - C\boldsymbol{\nabla} \cdot \frac{\partial \mathcal{V}}{\partial \boldsymbol{\nabla} u_\varepsilon} \right) \frac{\partial u_\varepsilon}{\partial \varepsilon} + \boldsymbol{\nabla} \cdot \left(\left(\frac{\partial \mathcal{F}}{\partial \boldsymbol{\nabla} u_\varepsilon} + C\frac{\partial \mathcal{V}}{\partial \boldsymbol{\nabla} u_\varepsilon} \right) \frac{\partial u_\varepsilon}{\partial \varepsilon} \right) \right] + \int_{\partial\Omega(\varepsilon)} \mathrm{d}^{D-1} X \ (\mathcal{F} + C\mathcal{V}) \frac{\partial \mathbf{X}_c}{\partial \varepsilon} \cdot \hat{\mathbf{n}}_c. \tag{3.23}$$

Applying Eq. 3.20 and the divergence theorem results in

$$\frac{dF}{d\varepsilon} + C\frac{d\mathscr{V}}{d\varepsilon} = \int_{\partial\Omega(\varepsilon)} \mathrm{d}^{D-1} X \left[(\mathcal{F} + C\mathcal{V}) \frac{\partial \mathbf{X}_c}{\partial \varepsilon} + \left(\frac{\partial \mathcal{F}}{\partial \boldsymbol{\nabla} u_\varepsilon} + C\frac{\partial \mathcal{V}}{\partial \boldsymbol{\nabla} u_\varepsilon} \right) \frac{\partial u_\varepsilon}{\partial \varepsilon} \right] \cdot \hat{\mathbf{n}}_c. \tag{3.24}$$

It is remarkable that the particular combination of derivatives on the left-hand side depends only on the boundary integral on the right-hand side and not on any volume integrals. Next, the condition defining being on the boundary, $u_\varepsilon(\mathbf{X}_c(\varepsilon)) = 0$ when $\mathbf{X}_c \in \partial\Omega(\varepsilon)$, can be differentiated with respect to ε to find

$$\boldsymbol{\nabla} u_\varepsilon \cdot \frac{\partial \mathbf{X}_c}{\partial \varepsilon} + \frac{\partial u_\varepsilon}{\partial \varepsilon} \Big|_{\partial\Omega(\varepsilon)} = 0, \tag{3.25}$$

and the outward-pointing unit normal vector to the boundary $\partial\Omega(t)$ defined by the zero level set $u = 0$ is

$$\hat{\mathbf{n}}_c = -\frac{\boldsymbol{\nabla} u_\varepsilon}{|\boldsymbol{\nabla} u_\varepsilon|}. \tag{3.26}$$

Equations 3.25 and 3.26 are used to eliminate $\frac{\partial u_\varepsilon}{\partial \varepsilon}$ to find

$$\frac{dF}{d\varepsilon} + C\frac{d\mathscr{V}}{d\varepsilon} = \int_{\partial\Omega(\varepsilon)} \mathrm{d}^{D-1} X \left(\mathcal{F} + C\mathcal{V} - \boldsymbol{\nabla} u_\varepsilon \cdot \left(\frac{\partial \mathcal{F}}{\partial \boldsymbol{\nabla} u_\varepsilon} + C\frac{\partial \mathcal{V}}{\partial \boldsymbol{\nabla} u_\varepsilon} \right) \right) \frac{\partial \mathbf{X}_c}{\partial \varepsilon} \cdot \hat{\mathbf{n}}_c, \tag{3.27}$$

which completes the derivation.

Equation 3.21 should be regarded as an analogue of the fundamental relation of thermodynamics. Expressed in terms of the Helmholtz free energy A, this is a relation among differentials

$$\mathrm{d}A = -S\mathrm{d}T - p\mathrm{d}V, \tag{3.28}$$

where S is the entropy, T is the temperature, p is the pressure, and V is the volume of some thermodynamic system in equilibrium. Since the parameter ε in Eq. 3.21 was entirely arbitrary, the "denominators" of the derivatives with respect to ε can be "multiplied through" and thus this relation can be regarded as a relation among differentials as well. Furthermore, recall from statistical mechanics that the pressure p, for example, is the generalized force conjugate to the volume V which arises as a Lagrange multiplier, just as C is the Lagrange multiplier fixing $\mathscr{V}[u]$ in Eq. 3.21. In Eq. 3.21, the generalized force conjugate to the boundary position $\mathbf{X}_c$ is apparently $\mathcal{F} + C\mathcal{V} - \boldsymbol{\nabla} u_\varepsilon \cdot \left(\frac{\partial \mathcal{F}}{\partial \boldsymbol{\nabla} u_\varepsilon} + C\frac{\partial \mathcal{V}}{\partial \boldsymbol{\nabla} u_\varepsilon}\right)$. Lastly, it is well known that the Helmholtz free energy strictly decreases during irreversible processes and is minimized at equilibrium, which is entirely analogous to the Lyapunov energy's time evolution. It should be stressed, however, that Eq. 3.21 is not a thermodynamic relationship, as thermodynamics only applies to systems at thermodynamic equilibrium. There is a heat flux across this system due to the fixed temperature difference between the hot and cold substrates and hence a generation of entropy; the thin film, even under stationary conditions, is not in thermodynamic equilibrium. The origin of these relations is in the existence of irreversible dynamics (i.e., the existence of a Lyapunov function) and a conserved quantity, and in the mathematics of constrained optimization rather than in the physics of thermodynamics.

Specializing to the thin film equations with $u = H$, $C = C_1$, and $D = 2$, the volume takes the form in Eq. 3.2 with $\mathcal{V} = H$ and the free energy takes the form in Eq. 3.3 with $\mathcal{F} = \frac{\bar{\mathrm{Ca}}^{-1}}{2}|\nabla_L H|^2 + W(H)$. Then Eq. 3.21 becomes

$$\frac{dF[H_\varepsilon]}{d\varepsilon} + C_1\frac{d\mathscr{V}[H_\varepsilon]}{d\varepsilon} = \int_{\partial\Omega(\varepsilon)} \mathrm{d}X \left(-\frac{\bar{\mathrm{Ca}}^{-1}}{2}C_c(\mathbf{X}_c)^2 + W(0)\right)\frac{\partial \mathbf{X}_c}{\partial \varepsilon}\cdot\hat{\mathbf{n}}_c. \tag{3.29}$$

Propositions 2 and 3 can now be easily demonstrated. First, consider a family of steady droplet profiles with varying contact lines but constant volume. Then Eq. 3.29 becomes

$$\frac{dF[H_\varepsilon]}{d\varepsilon} = \int_{\partial\Omega(\varepsilon)} \mathrm{d}X \left(-\frac{\bar{\mathrm{Ca}}^{-1}}{2}C_c(\mathbf{X}_c)^2 + W(0)\right)\frac{\partial \mathbf{X}_c}{\partial \varepsilon}\cdot\hat{\mathbf{n}}_c. \tag{3.30}$$

If $-\frac{\bar{\text{Ca}}^{-1}}{2}C_c(\mathbf{X}_c)^2 + W(0)$ is nonzero near any $\mathbf{X}_c \in \partial\Omega$, the family can be chosen such that $\frac{\partial \mathbf{X}_c}{\partial \varepsilon} \cdot \hat{\mathbf{n}}_c$ is nonzero only near $\mathbf{X}_c$. Then it follows that $\frac{dF[H_\varepsilon]}{d\varepsilon} \neq 0$, so that any droplet with $C_c^2 \neq 2\bar{\text{Ca}}W(0)$ cannot be a local minimum of the Lyapunov energy among states of the same volume, as claimed in Proposition 2. Next, consider a family of steady states H_ε for which $C_c^2 = 2\bar{\text{Ca}}W(0)$ for all ε. Note that the right-hand side of Eq. 3.29 then vanishes, and Eq. 3.10 is established. The final claim in Proposition 3 follows by noting that Eq. 3.10 implies that

$$\frac{d(F/\mathscr{V})}{d\varepsilon} = \frac{1}{\mathscr{V}}\frac{dF}{d\varepsilon} - \frac{F}{\mathscr{V}^2}\frac{d\mathscr{V}}{d\varepsilon} = -\left(\frac{F + C_1\mathscr{V}}{\mathscr{V}^2}\right)\frac{d\mathscr{V}}{d\varepsilon}. \tag{3.31}$$

Between each pair of critical points of $\mathscr{V}$, the implicit function theorem guarantees that the relation between $\mathscr{V}$ and ε can be inverted, and then on each branch

$$\frac{d(F/\mathscr{V})}{d\mathscr{V}} = \frac{d(F/\mathscr{V})}{d\varepsilon}\left(\frac{d\mathscr{V}}{d\varepsilon}\right)^{-1} = -\left(\frac{F + C_1\mathscr{V}}{\mathscr{V}^2}\right). \tag{3.32}$$

By the assumption in Proposition 3 that $0 < |\frac{F+C_1\mathscr{V}}{\mathscr{V}^2}| < \infty$, it follows that the right-hand side never changes sign, and thus the monotonic relation between $F/\mathscr{V}$ and $\mathscr{V}$ is established.

Energy stability in the thermocapillary-driven case and Proposition 4

In this section, the stability of steady axisymmetric droplet states in the thermocapillary driven film described by Eq. 3.6 will be considered, as described in Proposition 4.

Rotationally invariant solutions for steady state profiles

Consider the steady state condition Eq. 3.8 with the specified $W(H)$ in Eq. 3.6, and seek solutions $H_0(R)$ that depend only on the radial coordinate $R = \sqrt{X^2 + Y^2}$. The resulting one-dimensional ordinary differential equation is

$$C_1 = \frac{1}{R}\frac{\partial}{\partial R}\left(R\frac{\partial H_0}{\partial R}\right) + \frac{(4\pi)^2}{2}\left(\log\frac{H_0}{1-H_0} + \frac{1}{1-H_0}\right). \tag{3.33}$$

Note that $H = 1$ is a singular point of Eq. 3.33 since the logarithm term diverges there. In fact, $H < 1$ is required since the argument of the logarithm must be positive. There is another, more physical constraint as well since the fluid interface cannot penetrate the solid cold substrate in Fig. 3.2. Given the scalings described above, this requires

$$H < 1 - \kappa. \tag{3.34}$$

Since $\kappa > 0$, this physical constraint is more stringent than $H < 1$, and solutions with $1 - \kappa < H < 1$ must be regarded as unphysical.

The classes of physically relevant, rotationally invariant solutions will now be described. Since solutions are bounded above by Eq. 3.34, they will either achieve a maximum somewhere or approach a maximum as $R \to \infty$. In the former case, since there are no singular points of Eq. 3.33 in the interval $0 < H < 1$, the solution must be differentiable at this maximum. The maximum for such solutions will be denoted $H_{\max}$ and the position of the maximum $R = R_{\max}$, so that

$$H_0|_{R=R_{\max}} = H_{\max}, \quad \frac{\partial H_0}{\partial R}|_{R=R_{\max}} = 0, \tag{3.35}$$

which are the two boundary conditions necessary to integrate Eq. 3.33. One more parameter is required to eliminate C_1 in Eq. 3.33, and the curvature (in the thin-film limit) at $R = R_{\max}$ is appropriate

$$k \equiv \frac{1}{R}\frac{\partial}{\partial R}\left(R\frac{\partial H_0}{\partial R}\right)\Big|_{R=R_{\max}}, \tag{3.36}$$

where $k < 0$ since $H_{\max}$ is a local maximum. Evaluating Eq. 3.33 at $R = R_{\max}$, C_1 can be eliminated in favor of $H_{\max}$ and k,

$$C_1 = k + \frac{(4\pi)^2}{2}\left(\log\frac{H_{\max}}{1 - H_{\max}} + \frac{1}{1 - H_{\max}}\right). \tag{3.37}$$

Finally, Eq. 3.33 is integrated numerically starting at any $R = R_{\max}$ for any given $0 < H_{\max} < 1$ and $k < 0$.

A few subtleties should be noted here. First, as we integrates between either $0 < R < R_{\max}$ or $R_{\max} < R < \infty$, the profile may or may not achieve $H_0 = 0$. Since the logarithm in Eq. 3.33 becomes singular at $H_0 = 0$, this is a singular point of the differential equation. Furthermore, a negative film height would penetrate the solid hot substrate, which is clearly unphysical, so there is expected to be some singular behavior as $H_0 \to 0$. The lines in space $R = R_c$ at which H_0 first attains zero are termed the contact lines, and there is technically a loss of uniqueness in solutions beyond the contact lines. There may be multiple wetted domains, where $H_0 > 0$, separated by dry regions, where H_0 is identically zero. However, each connected component of the wetted domain can be considered independently in the stability analysis. A single wetted domain may terminate with zero, one, or two contact lines (which are always circles centered at the origin for rotationally invariant solutions), or even a single contact point if H_0 should achieve zero at $R = 0$. Second, while

an arbitrary choice of the parameters will guarantee that $H_{\max}$ is a local maximum, it will not generally be the global maximum. If this is not the case, however, the solution will be identical to a solution with another set of the parameters $H_{\max}$, $R_{\max}$, and k for which $H_{\max}$ is the global maximum. Lastly, the possibility that the solution only attains its global maximum as $R \to \infty$ apparently only occurs for the flat film solution, and hence is not of additional interest. Depending on the number and position of the contact lines, there are four possible classes of solutions, and example of such solutions are depicted in Fig. 3.3.

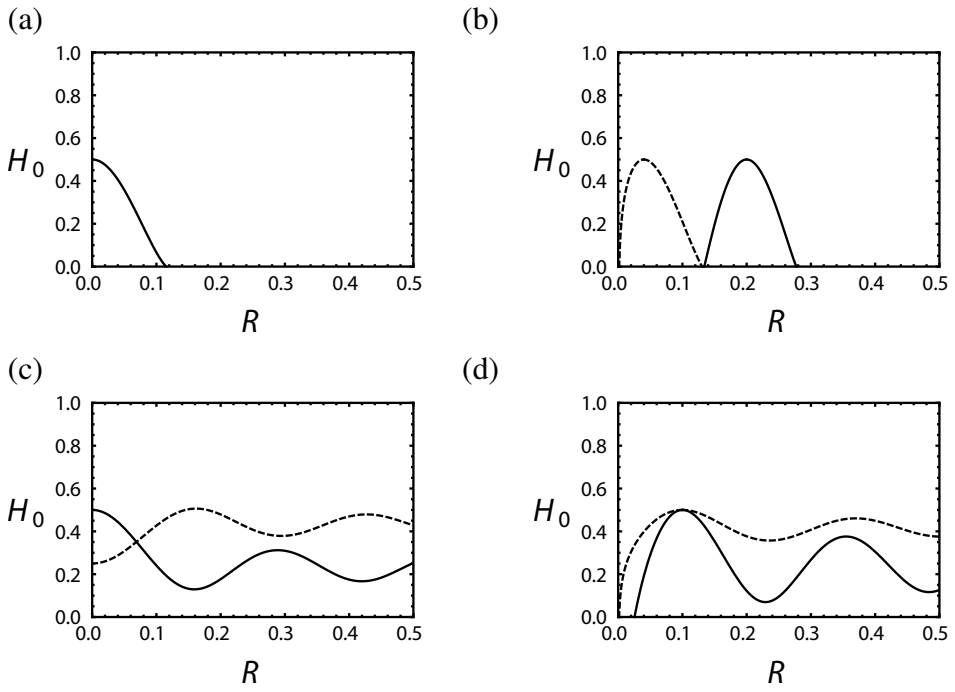

Figure 3.3: Examples solutions of Eq. 3.33 with $H_{\max} = 0.5$. (a) A droplet solution with $R_{\max} = 0$, and $k = -250$, (b) two ring-shaped droplet solutions with $R_{\max} = 0.2$, and $k = -250$ (solid line) and $R_{\max} = 0.04$, and $k = -250$ (dashed line), (c) two smooth solutions with $R_{\max} = 0$, and $k = -150$ (solid line) and $R_{\max} \approx 0.16$, and $k \approx -41$ (dashed line), and (d) two hole solutions with $R_{\max} = 0.1$ and $k = -150$ (solid line), and $R_{\max} = 0.1$ and $k = -50$ (dashed line). The smooth solutions and hole solutions in (c) and (d) have non-compact support that extends to $R \to \infty$ beyond the depicted region.

The droplet solutions in Fig. 3.3(a) attain their maximum at $R = R_{\max} = 0$ and have a single wetted domain which is a disc centered about the origin that is terminated by a contact line $R = R_c$. The ring-shaped droplet solutions in Fig. 3.3(b) attain their maximum at $R = R_{\max} > 0$, have a dry region around the origin, either a single

point (as in the dashed line) or a disc centered at the origin (as in the solid line), and also possess a second contact line at larger R and a second dry region that is the complement of a disc centered at the origin. The smooth solutions in Fig. 3.3(c) are everywhere differentiable and approach a flat film solution as $R \to \infty$. They may achieve their global maxima either at $R = R_{\max} = 0$ (as in the solid line) or at $R = R_{\max} > 0$ (as in the dashed line), and in the latter case, the origin must be a local minimum of the solution. The hole solutions in Fig. 3.3(d) have a dry region around the origin and approach a flat film solution as $R \to \infty$. This dry region may be a single point (as in the dashed line) or it may be a disc centered at the origin (as in the solid line).

Although there is a rich variety of rotationally invariant steady state profiles, only the droplet solutions of Fig. 3.3(a) will be discussed in detail for the remainder of the section. The ring-shaped droplet solutions in Fig. 3.3(b) have two contact lines, and the contact slope at the larger contact line is always observed to be smaller than that of the smaller contact line. The criterion of zero contact slope in Proposition 2 for stable solutions then precludes their stability. Intuition suggests that the solutions with non-compact support in Fig. 3.3(c)-(d) cannot be stable either, given first the analogous results in one-dimensional models [78] and the development of rupture in three-dimensional numerical models [47]. This establishes the first claim in Proposition 4, that the stable droplets achieve their maxima at $R = 0$. In the case of a fluid film contained in a finite apparatus like a circular petri dish, it may be possible to restrict the non-compactly supported solutions in Fig. 3.3(c)-(d) to some compact domain $0 < R < R_c$ by specifying some additional boundary condition at the lateral boundary R_c. Such considerations are left open for future research.

Next, consider the family H_ε of droplet solutions with zero contact slope and varying height $\varepsilon = H_{\max}$. Such solutions are found using a numerical shooting scheme, iteratively increasing k for fixed $H_{\max}$ until $C_c = 0$ is acheived. This was performed for several values of $H_{\max}$ between 0 and 1, and the volume $\mathscr{V}$ and the Lyapunov energy per unit volume $F/\mathscr{V}$ was computed for each solution. These results are shown with interpolations in Fig. 3.4. Numerically computing the extrema of the interpolation reveals a simultaneous maximum of $\mathscr{V}$ and minimum of $F/\mathscr{V}$ near $H_{\max} \approx 0.81113$, as claimed in Proposition 4.

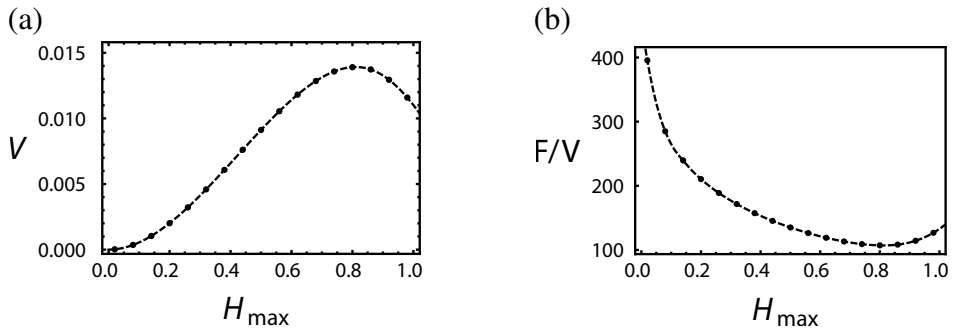

Figure 3.4: Droplet volume and Lyapunov energy per unit volume as a function of height $H_{\max}$ with $C_c = 0$. The largest volume droplet occurs around $H_{\max} \approx 0.81113$ and it minimizes the Lyapunov energy per unit volume among all droplet solutions.

The separation of the interior and boundary contributions

To study the stability of a droplet base state $H = H_0(R)$ where H_0 satisfies Eq. 3.33, consider "infinitesimal perturbations" of that state. More precisely, consider a family of states $H_\varepsilon(R, \theta)$ such that $H_{\varepsilon=0} = H_0$ and consider the limit $\varepsilon \to 0$. Some continuity or smoothness in the ε variable is clearly implied to restrict this family of states. Since dynamical excitations that may destabilize the droplet do not add or remove fluid from the system, it is required that the volume given by Eq. 3.2 for each state in the family does not vary with ε,

$$\int_0^{2\pi} \mathrm{d}\theta \int_0^{\infty} R\mathrm{d}R\, H_\varepsilon(R, \theta) = 2\pi \int_0^{R_c} R\mathrm{d}R\, H_0(R). \tag{3.38}$$

Now, define $\delta H_\varepsilon(R, \theta) \equiv H_\varepsilon(R, \theta) - H_0(R)$. As $\varepsilon \to 0$, it is assumed to be the case that $\delta H_\varepsilon \to 0$. In many problems, it is possible to assume that ε is sufficiently small so that $H_0 \gg \delta H_\varepsilon$ everywhere, and such perturbations are deemed infinitesimal. However, in the study of droplets, the existence of a contact line $R = R_c$, where $H_0(R_c) = 0$, makes such an assumption unjustifiable. Whenever the contact lines of H_0 and H_ε differ, it is clear that $\delta H_\varepsilon \ll H_0$ will not hold sufficiently close to $R = R_c$. In order to overcome the difficulty with the boundary, separate an interior region $0 < R < R_\varepsilon^-$, where

$$\delta H_\varepsilon|_{R \le R_\varepsilon^-} = (H_\varepsilon - H_0)\,|_{R \le R_\varepsilon^-} \ll H_0|_{R \le R_\varepsilon^-}, \tag{3.39}$$

and a boundary region $R_\varepsilon^- < R < R_\varepsilon^+$ (in which this approximation may fail), where R_ε^+ is the perturbed contact line, $H_\varepsilon|_{R=R_\varepsilon^+} = 0$. Since the $\varepsilon \to 0$ limit is being

considered, assume that $R_\varepsilon^-, R_\varepsilon^+ \to R_c$ as $\varepsilon \to 0$. This separation of the domain into a boundary region and an interior region is depicted in Fig. 3.5.

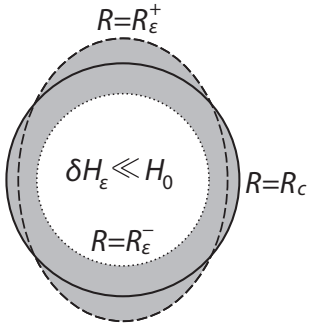

Figure 3.5: Separation of domain into boundary region (grey) and interior region (white). The unperturbed contact line $R = R_c$ is shown as a solid circle, the perturbed contact line $R = R_\varepsilon^+$ is shown as a dashed ellipse, and the separation between the interior and boundary regions $R = R_\varepsilon^-$ is shown as a dotted line. The perturbative condition in Eq. 3.39 holds only in the interior region, while the boundary region becomes increasingly small as $\varepsilon \to 0$.

Consider the difference in the Lyapunov energy in Eq. 3.3 between the states H_ε and H_0, and specifically consider the asymptotic form of this expression as $\varepsilon \to 0$,

$$\delta F_\varepsilon \equiv F[H_\varepsilon] - F[H_0] = \int_0^{2\pi} \mathrm{d}\theta \int_0^{R_\varepsilon^+} R\mathrm{d}R \left(\frac{1}{2} |\nabla_L H_\varepsilon|^2 + \frac{(4\pi)^2}{2} H_\varepsilon \log \frac{H_\varepsilon}{1 - H_\varepsilon} \right) - \int_0^{2\pi} \mathrm{d}\theta \int_0^{R_c} R\mathrm{d}R \left(\frac{1}{2} |\nabla_L H_0|^2 + \frac{(4\pi)^2}{2} H_0 \log \frac{H_0}{1 - H_0} \right). \tag{3.40}$$

Next, divide each contribution into an interior contribution where R ranges from 0 to R_ε^- and a boundary contribution, where R ranges from R_ε^- to R_ε^+,

$$\begin{aligned} \delta F_\varepsilon = & \int_0^{2\pi} \mathrm{d}\theta \int_0^{R_\varepsilon^-} R\mathrm{d}R \left(\frac{1}{2} |\nabla_L H_\varepsilon|^2 + \frac{(4\pi)^2}{2} H_\varepsilon \log \frac{H_\varepsilon}{1 - H_\varepsilon} \right) \\ & - \int_0^{2\pi} \mathrm{d}\theta \int_0^{R_\varepsilon^-} R\mathrm{d}R \left(\frac{1}{2} |\nabla_L H_0|^2 + \frac{(4\pi)^2}{2} H_0 \log \frac{H_0}{1 - H_0} \right) \\ & + \int_0^{2\pi} \mathrm{d}\theta \int_{R_\varepsilon^-}^{R_\varepsilon^+} R\mathrm{d}R \left(\frac{1}{2} |\nabla_L H_\varepsilon|^2 + \frac{(4\pi)^2}{2} H_\varepsilon \log \frac{H_\varepsilon}{1 - H_\varepsilon} \right) \\ & - \int_0^{2\pi} \mathrm{d}\theta \int_{R_\varepsilon^-}^{R_c} R\mathrm{d}R \left(\frac{1}{2} |\nabla_L H_0|^2 + \frac{(4\pi)^2}{2} H_0 \log \frac{H_0}{1 - H_0} \right). \end{aligned} \tag{3.41}$$

In the interior region, since $H_\varepsilon = H_0 + \delta H_\varepsilon$ and $\delta H_\varepsilon \ll H_0$, it is possible to expand the first integrand in a power series with respect to δH_ε up to second order,

$$\begin{aligned}\delta F_\varepsilon = &\int_0^{2\pi} \mathrm{d}\theta \int_0^{R_\varepsilon^-} R\mathrm{d}R \left(\nabla_L H_0 \cdot \nabla_L \delta H_\varepsilon - \frac{(4\pi)^2}{2}\left(\log\frac{H_0}{1-H_0} + \frac{1}{1-H_0}\right)\delta H_\varepsilon\right)\\ &+ \int_0^{2\pi} \mathrm{d}\theta \int_0^{R_\varepsilon^-} R\mathrm{d}R \left(\frac{1}{2}|\nabla_L \delta H_\varepsilon|^2 - \frac{(4\pi)^2}{4}\frac{\delta H_\varepsilon^2}{H_0(1-H_0)^2}\right) + \cdots\\ &+ \int_0^{2\pi} \mathrm{d}\theta \int_{R_\varepsilon^-}^{R_\varepsilon^+} R\mathrm{d}R \left(\frac{1}{2}|\nabla_L H_\varepsilon|^2 + \frac{(4\pi)^2}{2} H_\varepsilon \log\frac{H_\varepsilon}{1-H_\varepsilon}\right)\\ &- \int_0^{2\pi} \mathrm{d}\theta \int_{R_\varepsilon^-}^{R_c} R\mathrm{d}R \left(\frac{1}{2}|\nabla_L H_0|^2 + \frac{(4\pi)^2}{2} H_0 \log\frac{H_0}{1-H_0}\right).\end{aligned} \tag{3.42}$$

In the first integral, the first term is integrated by parts and Eq. 3.33 is applied to simplify it to

$$\int_0^{2\pi} \mathrm{d}\theta \left(\frac{\partial H_0}{\partial R}\delta H_\varepsilon\right)\Big|_{R=0}^{R_\varepsilon^-} - \int_0^{2\pi} \mathrm{d}\theta\, C_1 \int_0^{R_\varepsilon^-} R\mathrm{d}R\, \delta H_\varepsilon. \tag{3.43}$$

Furthermore, the volume conservation constraint in Eq. 3.38 and the fact that $\frac{\partial H_0}{\partial R}|_{R=0} = 0$ can be used to reexpress this as another boundary contribution

$$\int_0^{2\pi} \mathrm{d}\theta \left(\frac{\partial H_0}{\partial R}(H_0 - H_\varepsilon)\right)\Big|_{R=R_\varepsilon^-} - \int_0^{2\pi} \mathrm{d}\theta\, C_1 \left(\int_{R_\varepsilon^-}^{R_c} R\mathrm{d}R\, H_0 - \int_{R_\varepsilon^-}^{R_\varepsilon^+} R\mathrm{d}R\, H_\varepsilon\right). \tag{3.44}$$

So, collecting all terms, the leading order change in the Lyapunov energy consists of an interior contribution δF_ε^i and a boundary contribution δF_ε^b,

$$\begin{aligned}\delta F_\varepsilon &= \delta F_\varepsilon^i + \delta F_\varepsilon^b,\\ \delta F_\varepsilon^i &= \int_0^{2\pi} \mathrm{d}\theta \int_0^{R_\varepsilon^-} R\mathrm{d}R \left(\frac{1}{2}|\nabla_L \delta H_\varepsilon|^2 - \frac{(4\pi)^2}{4}\frac{\delta H_\varepsilon^2}{H_0(1-H_0)^2}\right) + \cdots,\\ \delta F_\varepsilon^b &= \int_0^{2\pi} \mathrm{d}\theta \left(R\frac{\partial H_0}{\partial R}(H_\varepsilon - H_0)\right)\Big|_{R=R_\varepsilon^-}\\ &\quad - \int_0^{2\pi} \mathrm{d}\theta\, C_1 \left(\int_{R_\varepsilon^-}^{R_c} R\mathrm{d}R\, H_0 - \int_{R_\varepsilon^-}^{R_\varepsilon^+} R\mathrm{d}R\, H_\varepsilon\right)\\ &\quad + \int_0^{2\pi} \mathrm{d}\theta \int_{R_\varepsilon^-}^{R_\varepsilon^+} R\mathrm{d}R \left(\frac{1}{2}|\nabla_L H_\varepsilon|^2 - \frac{(4\pi)^2}{2} H_\varepsilon \log\frac{H_\varepsilon}{1-H_\varepsilon}\right)\\ &\quad - \int_0^{2\pi} \mathrm{d}\theta \int_{R_\varepsilon^-}^{R_c} R\mathrm{d}R \left(\frac{1}{2}|\nabla_L H_0|^2 - \frac{(4\pi)^2}{2} H_0 \log\frac{H_0}{1-H_0}\right).\end{aligned} \tag{3.45}$$

The interior contribution to the energy stability analysis and the eigenvalue problem

First consider the leading order ε interior contribution in Eq. 3.45 for the rotationally invariant droplets with $C_c = 0$, and ignore any possible movement of the contact line, which will be considered later in the subsection **The boundary contribution to the energy stability analysis and the stable contact slope**. Define ε to be the leading order scale of the perturbation in the interior region, so that $\delta H_\varepsilon(R,\theta) \equiv \varepsilon\delta H(R,\theta) + \cdots$. Because δH must be 2π periodic in θ, it can be decomposed in a Fourier series

$$\delta H(R,\theta) = \frac{1}{\sqrt{2}}\delta H_0(R) + \sum_{n=1}^{\infty} \delta H_n(R)\cos(n\theta) + \widetilde{\delta H}_n(R)\sin(n\theta). \tag{3.46}$$

For simplicity of notation, define $\widetilde{\delta H}_0 \equiv 0$. The leading order contribution to the perturbed energy is

$$\begin{aligned}
E[\delta H] &\equiv \lim_{\varepsilon\to 0}\frac{\delta F^i_\varepsilon}{\varepsilon^2} \\
&= \pi\sum_{n=0}^{\infty}\int_0^{R_c} R\mathrm{d}R\left(\frac{1}{2}\left(\frac{\partial\delta H_n}{\partial R}\right)^2 + \frac{n^2\delta H_n^2}{2R^2} - \frac{(4\pi)^2\delta H_n^2}{4H_0(1-H_0)^2}\right) \\
&\quad + \int_0^{R_c} R\mathrm{d}R\left(\frac{1}{2}\left(\frac{\partial\widetilde{\delta H}_n}{\partial R}\right)^2 + \frac{n^2\widetilde{\delta H}_n^2}{2R^2} - \frac{(4\pi)^2\widetilde{\delta H}_n^2}{4H_0(1-H_0)^2}\right) \\
&= \pi\sum_{n=0}^{\infty}\int_0^{R_c} R\mathrm{d}R\,\delta H_n\left(-\frac{1}{2R}\frac{\partial}{\partial R}\left(R\frac{\partial\delta H_n}{\partial R}\right) + \frac{n^2\delta H_n}{2R^2} - \frac{(4\pi)^2\delta H_n}{4H_0(1-H_0)^2}\right) \\
&\quad + \int_0^{R_c} R\mathrm{d}R\,\widetilde{\delta H}_n\left(-\frac{1}{2R}\frac{\partial}{\partial R}\left(R\frac{\partial\widetilde{\delta H}_n}{\partial R}\right) + \frac{n^2\widetilde{\delta H}_n}{2R^2} - \frac{(4\pi)^2\widetilde{\delta H}_n}{4H_0(1-H_0)^2}\right) \\
&= \pi\sum_{n=0}^{\infty}\int_0^{R_c} R\mathrm{d}R\,\delta H_n\mathcal{E}_n[\delta H_n] + \int_0^{R_c}\widetilde{\delta H}_n\mathcal{E}_n[\widetilde{\delta H}_n],
\end{aligned} \tag{3.47}$$

where an integration by parts was performed to arrive at the third equality, and

$$\mathcal{E}_n[\delta H_n] \equiv -\frac{1}{2R}\frac{\partial}{\partial R}\left(R\frac{\partial\delta H_n}{\partial R}\right) + \frac{n^2}{2R^2}\delta H_n - \frac{(4\pi)^2}{4H_0(1-H_0)^2}\delta H_n \tag{3.48}$$

is a linear operator. The volume conservation constraint from Eq. 3.38 implies a constraint only on δH_0,

$$\int_0^{2\pi}\mathrm{d}\theta\int_0^{R_\varepsilon^+} R\mathrm{d}R\,\delta H(R,\theta) = \sqrt{2}\pi\int_0^{R_c} R\mathrm{d}R\,\delta H_0(R) = 0. \tag{3.49}$$

If $E[\delta H] < 0$ for any δH satisfying Eq. 3.49, then H_0 will not be a local minimum of the Lyapunov energy, and the droplet will be deemed unstable. Otherwise, H_0 will be considered stable. To determine which is the case, the problem of determining the infimum of $E[\delta H]$ over normalized δH satisfying Eq. 3.49 is considered. By the standard argument, this is equivalent to considering the infimum over n of the infima of $\int R\mathrm{d}R\ \delta H_n \mathcal{E}_n[\delta H_n]$ where each δH_n is normalized and δH_0 satisfies Eq. 3.49. Thus, without loss of generality, it will be henceforth assumed that either $\delta H(R,\theta) = \frac{1}{\sqrt{2}}\delta H_0(R)$ or $\delta H(R,\theta) = \cos(n\theta)\delta H_n(R)$.

An exact analytic solution of this problem seems intractable, so this analysis will be carried out numerically. First, the linear operator $\mathcal{E}_n$ is approximated on a finite space. Space is discretized into $M+1$ grid points $\{R_i\}_{i=0}^{M}$ with $R_0 = 0$, $R_M = R_c$, and $R_i < R_j$ for $i < j$, and a vector $\{v_i = \delta H_n(R_i)\}_{i=0}^{M}$ is associated with the perturbation. Boundary conditions are applied by defining the values of v_0 and v_M. Since movement of the contact line will be considered in the subsection **The boundary contribution to the energy stability analysis and the stable contact slope** below, take the simple Diriclet boundary condition $v_M \equiv 0$ at the contact line. The second boundary condition is more subtle. For $n \neq 0$, there will be a discontinuity in δH_n at the origin unless $v_0 \equiv 0$, but for the $n = 0$ case, a Neumann boundary condition $\frac{\partial \delta H_0}{\partial R}|_{R=0} = 0$ is possible, which can be approximated with $v_0 \equiv v_1$. In fact, since the Lyapunov energy increases with curvature, any gradients around $R = 0$ will tend to increase $E[\delta H]$. It is then more natural to take this Neumann boundary condition at $R = 0$ for the $n = 0$ modes. That this Neumann boundary condition at $R = 0$ is appropriate (i.e., that it leads to smaller eigenvalues below than other possible boundary conditions) has also been numerically verified.

Now, introduce the approximation

$$\mathcal{E}_n(\delta H_n)|_{R=R_i} \approx \sum_j A_{i,j} v_j, \tag{3.50}$$

where A is the appropriate matrix using a symmetric finite difference approximation for the derivatives with respect to R,

$$\begin{aligned} A_{i,j} \equiv -\frac{1}{2}\left(\frac{\frac{\delta_{i+1,j}-\delta_{i,j}}{R_{i+1}-R_i} - \frac{\delta_{i,j}-\delta_{i-1,j}}{R_i-R_{i-1}}}{\frac{R_{i+1}-R_{i-1}}{2}}\right) - \frac{1}{2R_i}\frac{\delta_{i+1,j}-\delta_{i-1,j}}{R_{i+1}-R_{i-1}} + \frac{n^2\delta_{i,j}}{2R_i^2} \\ - \frac{(4\pi)^2\delta_{i,j}}{4H_0(R_i)\left(1-H_0(R_i)\right)^2}. \end{aligned} \tag{3.51}$$

Integrals are approximated with Riemann sums of the form

$$\int g(R)\ R\mathrm{d}R \approx \sum_i g(R_i)\frac{R_i}{2}(R_{i+1} - R_{i-1}), \tag{3.52}$$

for any function g. The perturbation energy in Eq. 3.47 is then approximated

$$E\left[\delta H\right] \approx \pi \sum_{i,j} v_i A_{i,j} v_j \frac{R_i}{2}(R_{i+1} - R_{i-1}). \tag{3.53}$$

There exists an elegant way to absorb the metric factors into A and v that simultaneously converts the non-symmetric matrix A to a symmetric $\tilde{A}$. This is accomplished with

$$\begin{aligned}\tilde{v}_i &= v_i\sqrt{\frac{R_i}{2}(R_{i+1} - R_{i-1})},\\ \tilde{A}_{i,j} &= A_{i,j}\sqrt{\frac{R_i(R_{i+1} - R_{i-1})}{R_j(R_{j+1} - R_{j-1})}}.\end{aligned} \tag{3.54}$$

It follows that

$$\begin{aligned}\tilde{E}[\tilde{v}] &\equiv \sum_{ij} \tilde{v}_i \tilde{A}_{i,j} \tilde{v}_j\\ &= \sum_{i,j} v_i\sqrt{\frac{R_i}{2}(R_{i+1} - R_{i-1})}A_{i,j}\sqrt{\frac{R_i(R_{i+1} - R_{i-1})}{R_j(R_{j+1} - R_{j-1})}}v_j\sqrt{\frac{R_j}{2}(R_{j+1} - R_{j-1})}\\ &= \sum_{i,j} v_i A_{i,j} v_j \frac{R_i}{2}(R_{i+1} - R_{i-1})\\ &\approx \frac{E\left[\delta H\right]}{\pi}.\end{aligned} \tag{3.55}$$

To verify that $\tilde{A}$ is indeed symmetric, it is only necessary to consider the off-diagonal part, which after a little simplification,

$$\begin{aligned}\tilde{A}_{i,j\neq i} &= \left(-\frac{1}{2}\left(\frac{\frac{\delta_{i+1,j}}{R_{i+1}-R_i} - \frac{-\delta_{i-1,j}}{R_i-R_{i-1}}}{\frac{R_{i+1}-R_{i-1}}{2}}\right) - \frac{1}{2R_i}\frac{\delta_{i+1,j} - \delta_{i-1,j}}{R_{i+1} - R_{i-1}}\right)\sqrt{\frac{R_i(R_{i+1} - R_{i-1})}{R_j(R_{j+1} - R_{j-1})}}\\ &= \frac{-\frac{R_i}{R_{i+1}-R_i}\delta_{i+1,j} - \frac{R_i}{R_i-R_{i-1}}\delta_{i-1,j} - \frac{1}{2}(\delta_{i+1,j} - \delta_{i-1,j})}{\sqrt{R_iR_j(R_{i+1} - R_{i-1})(R_{j+1} - R_{j-1})}}\\ &= -\frac{1}{2}\frac{\frac{R_{i+1}+R_i}{R_{i+1}-R_i}\delta_{i+1,j} + \frac{R_i+R_{i-1}}{R_i-R_{i-1}}\delta_{i-1,j}}{\sqrt{R_iR_j(R_{i+1} - R_{i-1})(R_{j+1} - R_{j-1})}}\\ &= -\frac{1}{2}\frac{\frac{R_{i+1}+R_i}{R_{i+1}-R_i}\delta_{i+1,j} + \frac{R_{j+1}+R_j}{R_{j+1}-R_j}\delta_{i,j+1}}{\sqrt{R_iR_j(R_{i+1} - R_{i-1})(R_{j+1} - R_{j-1})}},\end{aligned} \tag{3.56}$$

is clearly symmetric. Later the eigenvalues of $\tilde{A}$ or a related matrix will be needed, and besides guaranteeing an orthonormal eigenbasis, symmetric matrices are better suited for numerical eigenvalue methods than non-symmetric ones.

Before seeking to minimize the energy, the volume conservation constraint Eq. 3.49 must be considered. For $n \neq 0$, the θ integral in Eq. 3.49 evaluates to zero, and this constraint is satisfied without imposing any on δH. For $n = 0$, on the other hand, there is a real constraint. When the integral approximation Eq. 3.52 is applied, this constraint is approximated as

$$0 \approx \sum_i \frac{R_i}{2}(R_{i+1} - R_{i-1})v_i, \tag{3.57}$$

which can be re-expressed in terms on $\tilde{v}_i$ from Eq. 3.54 as

$$0 \approx \sum_i \tilde{v}_i a_i \quad \text{where} \quad a_i \equiv \sqrt{\frac{R_i}{2}(R_{i+1} - R_{i-1})}. \tag{3.58}$$

The problem is now to find the vectors $\tilde{v}$ that extremize the quadratic form in Eq. 3.55, subject to the linear constraint in Eq. 3.58 when $n = 0$. As usual, this extremization is considered only over normalized vectors, since the quadratic form scales with the normalization squared. The problem is then to extremize the function

$$\phi[\tilde{v}] \equiv \begin{cases} \sum_{i,j} \tilde{v}_i \tilde{A}_{i,j} \tilde{v}_j - \lambda \left(\sum_i \tilde{v}_i^2 - 1 \right) & \text{if } n \neq 0, \\ \sum_{i,j} \tilde{v}_i \tilde{A}_{i,j} \tilde{v}_j - \lambda \left(\sum_i \tilde{v}_i^2 - 1 \right) - \mu \sum_i \tilde{v}_i a_i & \text{if } n = 0, \end{cases} \tag{3.59}$$

where λ is a Lagrange multiplier that imposes normalization on $\tilde{v}$ and μ is a Lagrange multiplier that imposes the volume conservation constraint Eq. 3.58. The stationary values of ϕ are found by equating the derivatives with respect to $\tilde{v}_i$, λ, and μ (in the $n = 0$ case) to zero. For the $n \neq 0$ case, the resulting problem is

$$\begin{aligned} \sum_j \tilde{A}_{j,i} \tilde{v}_j + \sum_j \tilde{A}_{i,j} \tilde{v}_j = 2 \sum_j \tilde{A}_{i,j} \tilde{v}_j = 2\lambda \tilde{v}_i, \\ \sum_i \tilde{v}_i^2 = 1, \end{aligned} \tag{3.60}$$

where the fact that $\tilde{A}$ is symmetric was used. Equation 3.60 is simply the problem of finding the normalized eigenvalues and eigenvectors of $\tilde{A}$, which is easily accomplished numerically. The energy associated to an eigenvector $\tilde{v}$ with eigenvalue λ is simply

$$\tilde{E}[\tilde{v}] = \sum_{i,j} \tilde{v}_i \tilde{A}_{i,j} \tilde{v}_j = \lambda \sum_i \tilde{v}_i \tilde{v}_i = \lambda. \tag{3.61}$$

It follows that the base state H_0 is unstable to an $n > 0$ mode if the smallest eigenvalue of the corresponding $\tilde{A}$ is negative.

For the $n = 0$ case, the problem is

$$\sum_j \tilde{A}_{j,i}\tilde{v}_j + \sum_j \tilde{A}_{i,j}\tilde{v}_j + \mu a_i = 2\sum_j \tilde{A}_{i,j}\tilde{v}_j + \mu a_i = 2\lambda\tilde{v}_i,$$
$$\sum_i \tilde{v}_i^2 = 1,$$
$$\sum_i a_i\tilde{v}_i = 0. \tag{3.62}$$

To simplify Eq. 3.62, we follow the method of Golub [81]. The first equation in Eq. 3.62 is multiplied by a_i and the result is summed over all i

$$2\sum_{i,j} a_i\tilde{A}_{i,j}\tilde{v}_i + \mu\sum_i a_i^2 = 2\lambda\sum_i a_i\tilde{v}_i = 0, \tag{3.63}$$

where the last equation in Eq. 3.62 was used to arrive at the final equality. Using Eq. 3.63, the Lagrange multiplier μ is eliminated and substituted back into the first equation in Eq. 3.62,

$$\sum_j \tilde{A}_{i,j}\tilde{v}_j - \frac{\sum_{j,k} a_k\tilde{A}_{k,j}\tilde{v}_j}{\sum_l a_l^2}a_i = \lambda\tilde{v}_i.$$
$$\sum_i \tilde{v}_i^2 = 1.$$
$$\sum_i a_i\tilde{v}_i = 0. \tag{3.64}$$

Next, define a new Hermitian matrix $\mathscr{P}$

$$\mathscr{P}_{i,k} \equiv \delta_{i,k} - \frac{a_i a_k}{\sum_l a_l^2}, \tag{3.65}$$

and re-express the first equation in Eq. 3.64 in terms of $\mathscr{P}$,

$$\sum_{j,k} \mathscr{P}_{i,k}\tilde{A}_{k,j}\tilde{v}_j = \lambda\tilde{v}_i. \tag{3.66}$$

Note that the matrix $\mathscr{P}$ is actually a projection operator

$$\sum_k \mathscr{P}_{i,k}\mathscr{P}_{k,j} = \sum_k \left(\delta_{i,k} - \frac{a_i a_k}{\sum_l a_l^2}\right)\left(\delta_{k,j} - \frac{a_k a_j}{\sum_l a_l^2}\right) = \delta_{i,j} - \frac{a_i a_j}{\sum_l a_l^2} = \mathscr{P}_{i,j}. \tag{3.67}$$

It follows from the last line in Eq. 3.64 that

$$\sum_l \mathscr{P}_{i,k}\tilde{v}_k = \sum_l \mathscr{P}_{k,i}\tilde{v}_k = \tilde{v}_i - \frac{a_i}{\sum_l a_l^2}\sum_k a_k\tilde{v}_k = \tilde{v}_i. \tag{3.68}$$

Equation 3.68 is substituted back into the left-hand side of Eq. 3.66 to arrive at the final problem to be solved

$$\sum_{j,k,l} \mathscr{P}_{i,k} \tilde{A}_{k,j} \mathscr{P}_{j,l} \tilde{v}_l = \lambda \tilde{v}_i,$$
$$\sum_i \tilde{v}_i^2 = 1. \tag{3.69}$$

Equation 3.69 is simply the problem of finding the eigenvalues and normalized eigenvectors of the symmetric matrix $\tilde{K} \equiv \mathscr{P}\tilde{A}\mathscr{P}$. Note that final condition in Eq. 3.64 has been omitted in Eq. 3.69. This is permissible because a_i is an eigenvector of $\tilde{K}$ since $\sum_j \mathscr{P}_{j,i} a_i = 0$. This eigenvector does not satisfy the constraint $\sum_i a_i \tilde{v}_i = 0$ and should thus be discarded, but all other eigenvectors of $\tilde{K}$ will be orthogonal to a since $\tilde{K}$ is symmetric, and they will therefore satisfy this condition. The energy associated to an eigenvector $\tilde{v}$ with eigenvalue λ is (using Eq. 3.68 twice)

$$\tilde{E}[\tilde{v}] = \sum_{i,j} \tilde{v}_i \tilde{A}_{i,j} \tilde{v}_j = \sum_{i,j,k,l} \tilde{v}_k \mathscr{P}_{k,i} \tilde{A}_{i,j} \mathscr{P}_{j,l} \tilde{v}_l = \lambda \sum_i \tilde{v}_i^2 = \lambda. \tag{3.70}$$

It follows that the base state H_0 is unstable to an $n = 0$ mode if the smallest eigenvalue of $\tilde{K}$ is negative.

Finally, the two smallest eigenvalues $\lambda_{n,0}^M$, and $\lambda_{n,1}^M$ for the $n = 0$, $n = 1$ and $n = 2$ cases were computed numerically for increasing grid size from $M = 5000$ to $M = 10000$ in increments of 100. These estimates have been calculated for three drops: a short drop with $H_{\max} = 0.7 < 0.81113$, the maximum volume drop with $H_{\max} = 0.81113$, and a tall drop with $H_{\max} = 0.9 > 0.81113$. The approximate eigenfunctions for the smallest eigenvalues for three droplets are shown in Fig. 3.6. The convergence of the numerical procedure with increasing grid size M has been verified as follows. Suppose that there is a power-law convergence of the eigenvalues, $\lambda_{n,m}^M \sim \lambda_{n,m} + cM^{-p}$ as $M \to \infty$. It then follows that in the plot of $\log \frac{d\lambda}{dM} \equiv \log\left(\frac{\lambda_{n,m}^{M_{i+1}} - \lambda_{n,m}^{M_i}}{M_{i+1} - M_i}\right)$ versus $\log M_i$, where $M_i = 5000 + 100i$, the values should lie on a straight line with slope $-p + 1$. This was verified for multiple spatial grids, and the grid that attained the fastest rate of convergence p was

$$R_i = R_c \sqrt{\frac{i}{M}}. \tag{3.71}$$

Noting that $R_i \approx \frac{R_{i+1} + R_{i-1}}{2}$ for small grid spacings, the area elements are approxi-

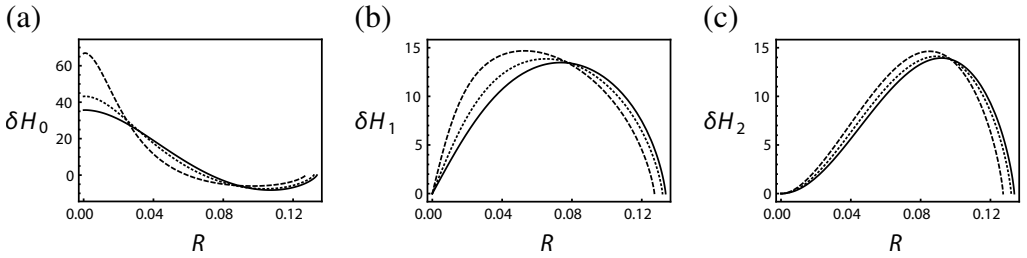

Figure 3.6: Eigenfunction interpolation δH with $M = 5000$ corresponding to the smallest eigenvalue for (a) $n = 0$, (b) $n = 1$, and (c) $n = 2$ modes. Solid lines correspond to $H_{\max} = 0.7$, dotted lines correspond to $H_{\max} = 0.81113$, and dashed lines correspond to $H_{\max} = 0.9$. The perturbations were normalized by $\int R\mathrm{d}R\ (\delta H)^2 = 1$.

mately constant for this grid,

$$R\mathrm{d}R \approx \frac{R_i}{2}(R_{i+1} - R_{i-1}) \approx \frac{(R_{i+1} + R_{i-1})(R_{i+1} - R_{i-1})}{4} = \frac{R_{i+1}^2 - R_{i-1}^2}{4} = \frac{R_c^2}{2M}. \tag{3.72}$$

The convergence of the eigenvalue estimates is depicted in Fig. 3.7.

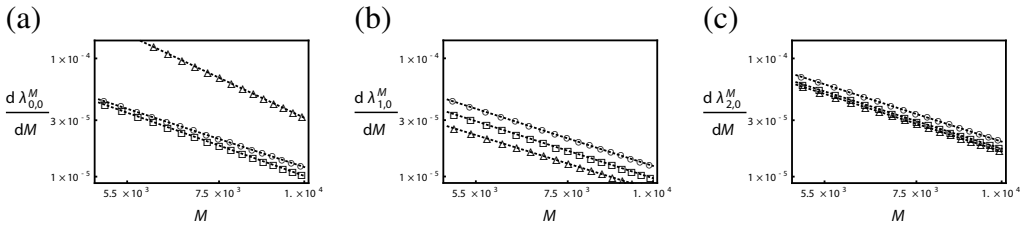

Figure 3.7: Convergence of direct numerical estimate of the smallest eigenvalues $\lambda_{n,0}^M$ for (a) $n = 0$, (b) $n = 1$, and (c) $n = 2$ modes. Circles correspond to $H_{\max} = 0.7$, squares corresponds to $H_{\max} = 0.81113$, and triangles corresponds to $H_{\max} = 0.9$. The rate of convergence p is estimated from the slope of the lines fitting the data.

Using the estimated power-law exponent p, it is possible to estimate the continuum eigenvalue as well by fitting the power-law curve to the data. This results in a direct estimate for the continuum eigenvalues, $\lambda_{n,0}^{\mathrm{dir}}$ for the smallest eigenvalue and $\lambda_{n,1}^{\mathrm{dir}}$ for the second smallest eigenvalue. Alternatively, the eigenvectors can be used to create an interpolation to approximate the perturbation $\delta H(R)$, which can then be used in Eq. 3.47 to estimate the eigenvalues. Again estimating the rate of convergence and computing a numerical fit, an interpolation estimate for the continuum eigenvalues is $\lambda_{n,0}^{\mathrm{int}}$ for the smallest eigenvalue and $\lambda_{n,1}^{\mathrm{int}}$ for the second smallest eigenvalue.

The results of this procedure are listed in Table 3.1. It is clear from Table 3.1

	$n = 0$	$n = 1$	$n = 2$
$H_{\max} = 0.7$	$\lambda_{0,0}^{\text{dir}} = 201.87$ $\lambda_{0,0}^{\text{int}} = 201.87$ $\lambda_{0,1}^{\text{dir}} = 1396.14$ $\lambda_{0,1}^{\text{int}} = 1396.13$	$\lambda_{1,0}^{\text{dir}} = -0.00$ $\lambda_{1,0}^{\text{int}} = 0.00$ $\lambda_{1,1}^{\text{dir}} = 793.19$ $\lambda_{1,1}^{\text{int}} = 793.19$	$\lambda_{2,0}^{\text{dir}} = 265.00$ $\lambda_{2,0}^{\text{int}} = 265.00$ $\lambda_{2,1}^{\text{dir}} = 1369.46$ $\lambda_{2,1}^{\text{int}} = 1369.44$
$H_{\max} = 0.81113$	$\lambda_{0,0}^{\text{dir}} = 0.01$ $\lambda_{0,0}^{\text{int}} = 0.00$ $\lambda_{0,1}^{\text{dir}} = 1338.68$ $\lambda_{0,1}^{\text{int}} = 1338.61$	$\lambda_{1,0}^{\text{dir}} = -0.00$ $\lambda_{1,0}^{\text{int}} = 0.00$ $\lambda_{1,1}^{\text{dir}} = 772.40$ $\lambda_{1,1}^{\text{int}} = 772.41$	$\lambda_{2,0}^{\text{dir}} = 293.39$ $\lambda_{2,0}^{\text{int}} = 293.39$ $\lambda_{2,1}^{\text{dir}} = 1402.82$ $\lambda_{2,1}^{\text{int}} = 1402.79$
$H_{\max} = 0.9$	$\lambda_{0,0}^{\text{dir}} = -658.21$ $\lambda_{0,0}^{\text{int}} = -658.23$ $\lambda_{0,1}^{\text{dir}} = 1218.84$ $\lambda_{0,1}^{\text{int}} = 1218.80$	$\lambda_{1,0}^{\text{dir}} = -0.00$ $\lambda_{1,0}^{\text{int}} = 0.01$ $\lambda_{1,1}^{\text{dir}} = 765.75$ $\lambda_{1,1}^{\text{int}} = 765.80$	$\lambda_{2,0}^{\text{dir}} = 341.59$ $\lambda_{2,0}^{\text{int}} = 341.59$ $\lambda_{2,1}^{\text{dir}} = 1515.46$ $\lambda_{2,1}^{\text{int}} = 1515.44$

Table 3.1: Numerical estimates for the two smallest eigenvalues of the first three angular modes for a short droplet, the maximum volume droplet, and a tall droplet. The direct and interpolations estimates agree up to the tens digit, where numerical errors become non-negligible.

that the direct and interpolation estimates are in good agreement whenever their magnitudes are larger than $O(10^{-1})$, where numerical errors apparently become relevant. Furthermore, the smallest eigenvalue for the rotationally invariant $n = 0$ is positive for $H_{\max} = 0.7$, approximately zero for $H_{\max} = 0.81113$, and negative for $H_{\max} = 0.9$, indicating that tall droplets are unstable and short ones may be stable, as claimed in Proposition 4. It is also clear that the smallest $n = 1$ eigenvalue $\lambda_{1,0}$ is approximately zero for all drops. In fact, this mode corresponds to a translation of the entire droplet without a change in shape. This can be demonstrated by taking the perturbed state to be the base state translated in the X direction by an amount ε as $\varepsilon \to 0$,

$$H_\varepsilon(R,\theta) = H_0\left(\sqrt{(X-\varepsilon)^2 + Y^2}\right) \approx H_0(R) - \varepsilon\cos\theta\frac{\partial H_0}{\partial R}(R). \tag{3.73}$$

A comparison of the interpolation estimate for δH and $\cos\theta\frac{\partial H_0}{\partial R}$ confirms that these $n = 1$ modes correspond to this translation. Indeed, since a translation of the droplet does not alter its energy, the continuum eigenvalue is exactly zero. This can also be easily analytically demonstrated by substituting the $n = 1$ perturbation $\delta H(R,\theta) = -\cos(\theta)\frac{\partial H_0}{\partial R}$ into Eq. 3.47 and applying the derivative of Eq. 3.33 with

respect to R. Lastly, besides $\lambda_{0,0}$ and $\lambda_{1,0}$, all other eigenvalues are strictly positive, and so they do not indicate any other instability or neutral modes. In fact, it is clear that for all $n \geq 2$, the eigenvalues will be strictly positive, since the energy $E[\delta H]$ in Eq. 3.47 for $n > 2$ is altered by a strictly positive perturbation $\int R\mathrm{d}R\, \frac{n^2-1}{2R^2}(\delta H)^2$ from the $n = 1$ case.

The boundary contribution to the energy stability analysis and the stable contact slope

It was shown in the subsection **The interior contribution to the energy stability analysis and the eigenvalue problem** that zero contact slope droplets are unstable to a rotationally invariant perturbation if $H_{\max} \gtrsim 0.81113$, as claimed in Proposition 4. However, to demonstrate the stability of droplets with $H_{\max} \lesssim 0.81113$, the boundary contribution must also be considered. Here the leading order contributions to the boundary perturbation δF_ε^b in Eq. 3.45 is considered for droplets with $C_c = 0$. Since the boundary region $(R_\varepsilon^-, R_\varepsilon^+)$ becomes increasingly small as $\varepsilon \to 0$, it is assumed that an asymptotic approximation of the perturbed state will suffice there. In particular, the perturbed state in the boundary region will be taken as a θ-dependent shift of the base state $H_0(R - \delta R_c(\theta, \varepsilon))$ plus a small linear change $\delta C_c(\theta, \varepsilon)(R_c + \delta R_c(\theta, \varepsilon) - R)$,

$$H_\varepsilon(R) = H_0(R - \delta R_c) + \delta C_c(R_c + \delta R_c - R) + \cdots, \tag{3.74}$$

where, for brevity, the θ and ε dependence of δR_c and δC_c has been omitted. It follows that the perturbed contact line is $R_\varepsilon^+(\theta, \varepsilon) = R_c + \delta R_c(\theta, \varepsilon) + \cdots$. The form in Eq. 3.74 is motivated by the assumption that as $\varepsilon \to 0$, the perturbed contact line tends to R_c, hence the small change δR_c. Since the boundary region is presumed to be small for small ε, it is also assumed that the change in the shape of H_ε from H_0 can be well approximated by the small linear change $\delta C_c(R_c + \delta R_c - R)$. While Eq. 3.74 can represent a very wide variety of boundary perturbations, it should be noted that some perturbations, such as those that change the nature of the singularity at the contact line, are excluded for simplicity here.

The division between the interior and boundary regions $R_\varepsilon^- = R_c - \delta R_\varepsilon^-$ must also be specified such that $\delta R_\varepsilon^- > 0$ and Eq. 3.39 is satisfied. On using Eq. 3.74, Eq. 3.39

requires

$$(H_\varepsilon - H_0)\,|_{R=R_c-\delta R_\varepsilon^-} \approx \left(-\delta R_c \frac{\partial H_0}{\partial R} + \delta C_c(\delta R_c + \delta R_\varepsilon^-)\right)\Big|_{R=R_c-\delta R_\varepsilon^-} \ll H_0|_{R=R_c-\delta R_\varepsilon^-}, \tag{3.75}$$

where the facts that δR_c is small and H_0 is differentiable at $R_c - \delta R_\varepsilon^-$ were used to approximate the difference $H_0(R_c - \delta R_\varepsilon^- - \delta R_c) - H_0(R_c - \delta R_\varepsilon^-)$ as a derivative using Taylor's theorem. This condition depends on the asymptotic form of H_0 near the unperturbed contact line, which is found by balancing the highest spatial derivative $\frac{\partial^2 H_0}{\partial R^2}$ with the singular term $\frac{(4\pi)^2}{2}\log(H_0)$ in Eq. 3.33 as $R \to R_c$ and $H_0 \to 0$,

$$H_0(R) = -\frac{(4\pi)^2}{2}(R_c - R)^2 \log(R_c - R) + \cdots. \tag{3.76}$$

Then Eq. 3.75 becomes

$$\delta R_c \delta R_\varepsilon^- \log \delta R_\varepsilon^- + \delta C_c(\delta R_c + \delta R_\varepsilon^-) \ll -\frac{(4\pi)^2}{2}(\delta R_\varepsilon^-)^2 \log(\delta R_\varepsilon^-), \tag{3.77}$$

so that

$$\delta R_c \ll \delta R_\varepsilon^- \text{ and } \delta C_c \ll -\delta R_\varepsilon^- \log(\delta R_\varepsilon^-) \tag{3.78}$$

is required. Then δR_ε^- must be chosen sufficiently large that Eq. 3.78 is satisfied for all θ.

Next, two results that will be used several times in the evaluation of δF_ε^b will be noted. First, multiply Eq. 3.33 by $\frac{\partial H_0}{\partial R}$ and simplify,

$$\frac{\partial}{\partial R}\left(\frac{1}{2}\left(\frac{\partial H_0}{\partial R}\right)^2 + \frac{(4\pi)^2}{2} H_0 \log\frac{H_0}{1-H_0} - C_1 H_0\right) = -\frac{1}{R}\left(\frac{\partial H_0}{\partial R}\right)^2. \tag{3.79}$$

The quantity in parentheses on the left-hand side of this equality will appear in several places below. It could be estimated by using the asymptotic form of H_0 in Eq. 3.76. However, this estimate turns out to be much larger than the actual value because of certain cancellations that occur when higher order terms are included in H_0. A better estimate can be derived by integrating Eq. 3.79,

$$\frac{1}{2}\left(\frac{\partial H_0}{\partial R}\right)^2 + \frac{(4\pi)^2}{2} H_0 \log\frac{H_0}{1-H_0} - C_1 H_0 = \int_R^{R_c} \frac{1}{R'}\left(\frac{\partial H_0}{\partial R'}\right)^2 \mathrm{d}R', \tag{3.80}$$

and then applying the base state approximation in Eq. 3.76 to the right-hand side. The second result used extensively below concerns differences of the form

$$\begin{aligned} I[g] &\equiv \int_{R_c-\delta R_\varepsilon^-}^{R_c+\delta R_c} Rg(R-\delta R_c)\,\mathrm{d}R - \int_{R_c-\delta R_\varepsilon^-}^{R_c} Rg(R)\,\mathrm{d}R \\ &= \int_{R_c-\delta R_\varepsilon^- -\delta R_c}^{R_c} (R+\delta R_c)g\,\mathrm{d}R - \int_{R_c-\delta R_\varepsilon^-}^{R_c} Rg\,\mathrm{d}R, \end{aligned} \tag{3.81}$$

where g is some arbitrary function and the integration variable in the first integral was shifted by δR_c and the functional dependence of $g(R)$ was omitted for brevity to arrive at the second equality. This will be expanded in a series around δR_c up to second order. The first integral is divided into two parts to cancel the second integral

$$I[g] = \delta R_c \int_{R_c-\delta R_\varepsilon^- -\delta R_c}^{R_c} g\,\mathrm{d}R + \int_{R_c-\delta R_\varepsilon^- -\delta R_c}^{R_c-\delta R_\varepsilon^-} Rg\,\mathrm{d}R. \tag{3.82}$$

Next, the Taylor series is formed up to second order:

$$I[g] = \delta R_c \int_{R_c-\delta R_\varepsilon^-}^{R_c} g\,\mathrm{d}R + \left(\delta R_c Rg + \frac{\delta R_c^2}{2}\left(g - R\frac{\partial g}{\partial R}\right)\right)\Big|_{R=R_c-\delta R_\varepsilon^-} + \cdots \tag{3.83}$$

The boundary contribution of Eq. 3.45 is now divided into five components:

$$\begin{aligned} \delta F_\varepsilon^b &= \delta F_1 + \delta F_2 + \delta F_3 + \delta F_\theta + \delta F_4, \\ \delta F_1 &= \int_0^{2\pi} \mathrm{d}\theta \left[R\frac{\partial H_0}{\partial R}\,(H_\varepsilon - H_0)\right]\Big|_{R=R_c-\delta R_\varepsilon^-}, \\ \delta F_2 &= \int_0^{2\pi} \mathrm{d}\theta\, C_1\Big[\int_{R_c-\delta R_\varepsilon^-}^{R_c+\delta R_c} H_\varepsilon\, R\mathrm{d}R - \int_{R_c-\delta R_\varepsilon^-}^{R_c} H_0\, R\mathrm{d}R\Big], \\ \delta F_3 &= \int_0^{2\pi} \mathrm{d}\theta\, \frac{1}{2}\Big[\int_{R_c-\delta R_\varepsilon^-}^{R_c+\delta R_c} \left(\frac{\partial H_\varepsilon}{\partial R}\right)^2 R\mathrm{d}R - \int_{R_c-\delta R_\varepsilon^-}^{R_c} \left(\frac{\partial H_0}{\partial R}\right)^2 R\mathrm{d}R\Big], \\ \delta F_\theta &= \int_0^{2\pi} \mathrm{d}\theta\, \frac{1}{2}\Big[\int_{R_c-\delta R_\varepsilon^-}^{R_c+\delta R_c} R\mathrm{d}R\,\frac{1}{R^2}\left(\frac{\partial H_\varepsilon}{\partial \theta}\right)^2\Big], \\ \delta F_4 &= \int_0^{2\pi} \mathrm{d}\theta\, -\frac{(4\pi)^2}{2}\Big[\int_{R_c-\delta R_\varepsilon^-}^{R_c+\delta R_c} H_\varepsilon \log\frac{H_\varepsilon}{1-H_\varepsilon}\, R\mathrm{d}R \\ &\quad - \int_{R_c-\delta R_\varepsilon^-}^{R_c} H_0 \log\frac{H_0}{1-H_0}\, R\mathrm{d}R\Big]. \end{aligned} \tag{3.84}$$

Next, H_ε from Eq. 3.74 is substituted in Eq. 3.84 and δF_1, δF_2, δF_3, and δF_4 (δF_θ is positive definite, and need not be considered until later) are expanded in a Taylor

series to second order in δC_c,

$$\begin{aligned}
\delta F_1 &= \int_0^{2\pi} \mathrm{d}\theta \left[R\frac{\partial H_0}{\partial R}\left(H_0(R-\delta R_c) - H_0(R) + \delta C_c(R_c+\delta R_c - R)\right)\right]\Big|_{R=R_c-\delta R_\varepsilon^-},\\
\delta F_2 &= \int_0^{2\pi} \mathrm{d}\theta\, C_1\Big[\int_{R_c-\delta R_\varepsilon^- - \delta R_c}^{R_c} H_0\,(R+\delta R_c)\mathrm{d}R - \int_{R_c-\delta R_\varepsilon^-}^{R_c} H_0\, R\mathrm{d}R\\
&\quad + \int_{R_c-\delta R_\varepsilon^- - \delta R_c}^{R_c} C_1\delta C_c(R_c-R)\,(R+\delta R_c)\mathrm{d}R\Big],\\
\delta F_3 &= \int_0^{2\pi} \mathrm{d}\theta\, \frac{1}{2}\Big[\int_{R_c-\delta R_\varepsilon^- - \delta R_c}^{R_c}\left(\frac{\partial H_0}{\partial R}\right)^2 (R+\delta R_c)\mathrm{d}R - \int_{R_c-\delta R_\varepsilon^-}^{R_c}\left(\frac{\partial H_0}{\partial R}\right)^2 R\mathrm{d}R\\
&\quad + \int_{R_c-\delta R_\varepsilon^- - \delta R_c}^{R_c}\left(-2\delta C_c\frac{\partial H_0}{\partial R} + \delta C_c^2\right)(R+\delta R_c)\mathrm{d}R\Big],\\
\delta F_4 &= \int_0^{2\pi} \mathrm{d}\theta\, -\frac{(4\pi)^2}{2}\Big[\int_{R_c-\delta R_\varepsilon^- - \delta R_c}^{R_c} H_0\log\frac{H_0}{1-H_0}\,(R+\delta R_c)\mathrm{d}R\\
&\quad - \int_{R_c-\delta R_\varepsilon^-}^{R_c} H_0\log\frac{H_0}{1-H_0}\,R\mathrm{d}R\\
&\quad + \int_{R_c-\delta R_\varepsilon^- - \delta R_c}^{R_c}\delta C_c(R_c-R)\left(\log\frac{H_0}{1-H_0} + \frac{1}{1-H_0}\right)(R+\delta R_c)\mathrm{d}R\\
&\quad + \int_{R_c-\delta R_\varepsilon^- - \delta R_c}^{R_c}\frac{\delta C_c^2(R_c-R)^2}{H_0\,(1-H_0)^2}\,(R+\delta R_c)\mathrm{d}R + \cdots\Big].
\end{aligned} \tag{3.85}$$

Before going any further, the δC_c and δC_c^2 parts will be simplified by finding their leading order parts in the small δR_c and δR_ε^- quantities. Collecting the δC_c terms in the sum $\delta F_1 + \delta F_2 + \delta F_3 + \delta F_4$ and denoting the contribution by $\delta F_C^{(1)}$,

$$\begin{aligned}
\delta F_C^{(1)} &= \int_0^{2\pi}\mathrm{d}\theta\,\delta C_c\Big[R(R_c+\delta R_c - R)\frac{\partial H_0}{\partial R}\Big|_{R=R_c-\delta R_\varepsilon^-}\\
&\quad - \int_{R_c-\delta R_\varepsilon^- - \delta R_c}^{R_c}\frac{\partial H_0}{\partial R}\,(R+\delta R_c)\mathrm{d}R + \int_{R_c-\delta R_\varepsilon^- - \delta R_c}^{R_c}(R_c-R)\\
&\quad \times\left(C_1 - \frac{(4\pi)^2}{2}\left(\log\frac{H_0}{1-H_0} + \frac{1}{1-H_0}\right)\right)(R+\delta R_c)\mathrm{d}R\Big].
\end{aligned} \tag{3.86}$$

Applying Eq. 3.33 to the third integral, this is

$$\begin{aligned}
\delta F_C^{(1)} &= \int_0^{2\pi}\mathrm{d}\theta\,\delta C_c\Big[R(R_c+\delta R_c - R)\frac{\partial H_0}{\partial R}\Big|_{R=R_c-\delta R_\varepsilon^-}\\
&\quad - \int_{R_c-\delta R_\varepsilon^- - \delta R_c}^{R_c}\frac{\partial H_0}{\partial R}\,(R+\delta R_c)\mathrm{d}R\\
&\quad + \int_{R_c-\delta R_\varepsilon^- - \delta R_c}^{R_c}(R_c-R)\left(\frac{\partial^2 H_0}{\partial R^2} + \frac{1}{R}\frac{\partial H_0}{\partial R}\right)(R+\delta R_c)\mathrm{d}R\Big].
\end{aligned} \tag{3.87}$$

The second derivative in the third integral is then integrated by parts

$$\begin{aligned}\delta F_C^{(1)} = \int_0^{2\pi} \mathrm{d}\theta\ \delta C_c \Big[& R(R_c + \delta R_c - R)\frac{\partial H_0}{\partial R}\Big|_{R=R_c-\delta R_\varepsilon^-} \\ & - \int_{R_c-\delta R_\varepsilon^- - \delta R_c}^{R_c} \frac{\partial H_0}{\partial R}\ (R+\delta R_c)\mathrm{d}R - (R_c - R)(R+\delta R_c)\frac{\partial H_0}{\partial R}\Big|_{R=R_c-\delta R_\varepsilon^- - \delta R_c} \\ & + \int_{R_c-\delta R_\varepsilon^- - \delta R_c}^{R_c} \left(-\frac{\partial H_0}{\partial R}(R_c - \delta R_c - 2R) + \frac{(R_c - R)}{R}\frac{\partial H_0}{\partial R}\ (R+\delta R_c)\right)\ \mathrm{d}R\Big].\end{aligned} \tag{3.88}$$

The first term in the first line is canceled by the $O((\delta R_c)^0)$ part of the term in the third line, leaving a leading order δR_c part, while the integrals combine to give

$$\begin{aligned}\delta F_C^{(1)} = \int_0^{2\pi} \mathrm{d}\theta\ \delta C_c \delta R_c \Big[& R_c(\delta R_\varepsilon^- + \delta R_c)\frac{\partial^2 H_0}{\partial R^2}\Big|_{R=R_c-\delta R_\varepsilon^-} \\ & + \int_{R_c-\delta R_\varepsilon^- - \delta R_c}^{R_c} \frac{R_c - R}{R}\frac{\partial H_0}{\partial R}\ \mathrm{d}R + \cdots \Big].\end{aligned} \tag{3.89}$$

Using the the asymptotic form in Eq. 3.76, and recalling from Eq. 3.78 that $\delta R_\varepsilon^- \gg \delta R_c$, the leading order result is

$$\delta F_C^{(1)} = \int_0^{2\pi} \mathrm{d}\theta\ \Big[-(4\pi)^2 R_c \delta C_c \delta R_c \delta R_\varepsilon^- \log \delta R_\varepsilon^- + \cdots \Big]. \tag{3.90}$$

The second order δC_c contribution to the sum $\delta F_1 + \delta F_2 + \delta F_3 + \delta F_4$, denoted $\delta F_C^{(2)}$, is simpler,

$$\begin{aligned}\delta F_C^{(2)} &= \int_0^{2\pi} \mathrm{d}\theta\ \delta C_c^2 \int_{R_c-\delta R_\varepsilon^- - \delta R_c}^{R_c} \left(\frac{R+\delta R_c}{2} - \frac{(4\pi)^2 (R_c - R)^2 (R+\delta R_c)}{2H_0(1-H_0)^2}\right)\ \mathrm{d}R \\ &= \int_0^{2\pi} \mathrm{d}\theta\ \Big[\frac{1}{2} R_c \delta C_c^2 \delta R_\varepsilon^- + \cdots \Big],\end{aligned} \tag{3.91}$$

to leading order.

Returning now to the $O(\delta C_c^0)$ in δF_ε^b, the quantities δF_1, δF_2, δF_3, and δF_4 in Eq. 3.84 are expanded to second order in δR_c by using the result in Eq. 3.83 for δF_2 with $g = H_0$, δF_3 with $g = \left(\frac{\partial H_0}{\partial R}\right)^2$, and δF_4 with $g = -H_0 \log \frac{H_0}{1-H_0}$, respectively.

The results are (excluding the δC_c and δC_c^2 terms already described above),

$$\begin{aligned}
\delta F_1 &= \int_0^{2\pi} \mathrm{d}\theta \left[R\frac{\partial H_0}{\partial R}\Big(- \delta R_c \frac{\partial H_0}{\partial R} + \frac{1}{2}(\delta R_c)^2 \frac{\partial^2 H_0}{\partial R^2}) \Big) + \cdots \right]_{R=R_c-\delta R_\varepsilon^-}, \\
\delta F_2 &= \int_0^{2\pi} \mathrm{d}\theta \; C_1 \Big[\delta R_c \int_{R_c-\delta R_\varepsilon^-}^{R_c} H_0 \, \mathrm{d}R + \Big(\delta R_c R H_0 \\
&\quad + \frac{\delta R_c^2}{2} \left(H_0 - R\frac{\partial H_0}{\partial R} \right) \Big) \Big|_{R=R_c-\delta R_\varepsilon^-} + \cdots \Big], \\
\delta F_3 &= \int_0^{2\pi} \mathrm{d}\theta \; \frac{1}{2} \Big[\delta R_c \int_{R_c-\delta R_\varepsilon^-}^{R_c} \left(\frac{\partial H_0}{\partial R} \right)^2 \mathrm{d}R + \Big(\delta R_c R \left(\frac{\partial H_0}{\partial R} \right)^2 \\
&\quad + \frac{\delta R_c^2}{2} \left(\left(\frac{\partial H_0}{\partial R} \right)^2 - 2R \frac{\partial H_0}{\partial R} \frac{\partial^2 H_0}{\partial R^2} \right) \Big) \Big|_{R=R_c-\delta R_\varepsilon^-} + \cdots \Big], \\
\delta F_4 &= \int_0^{2\pi} \mathrm{d}\theta \; -\frac{(4\pi)^2}{2} \Big[\delta R_c \int_{R_c-\delta R_\varepsilon^-}^{R_c} H_0 \log \frac{H_0}{1-H_0} \, \mathrm{d}R + \Big(\delta R_c R H_0 \log \frac{H_0}{1-H_0} \\
&\quad + \frac{\delta R_c^2}{2} \Big(H_0 \log \frac{H_0}{1-H_0} - R \left(\log \frac{H_0}{1-H_0} + \frac{1}{1-H_0} \right) \frac{\partial H_0}{\partial R} \Big) \Big|_{R=R_c-\delta R_\varepsilon^-} + \cdots \Big].
\end{aligned} \tag{3.92}$$

Collecting the δR_c terms in the sum $\delta F_1 + \delta F_2 + \delta F_3 + \delta F_4$ and denoting them $\delta F_R^{(1)}$ results in

$$\begin{aligned}
\delta F_R^{(1)} = \int_0^{2\pi} \mathrm{d}\theta \; \delta R_c \Big[\int_{R_c-\delta R_\varepsilon^-}^{R_c} \left(\frac{1}{2} \left(\frac{\partial H_0}{\partial R} \right)^2 - \frac{(4\pi)^2}{2} H_0 \log \frac{H_0}{1-H_0} + C_1 H_0 \right) \mathrm{d}R \\
- R \left(\frac{1}{2} \left(\frac{\partial H_0}{\partial R} \right)^2 + \frac{(4\pi)^2}{2} H_0 \log \frac{H_0}{1-H_0} - C_1 H_0 \right) \Big|_{R=R_c-\delta R_\varepsilon^-} \Big].
\end{aligned} \tag{3.93}$$

The second collection of terms in the big parentheses in the previous equation can be simplified using Eq. 3.80 and included in the integral

$$\begin{aligned}
\delta F_R^{(1)} &= \int_0^{2\pi} \mathrm{d}\theta \left[\delta R_c \int_{R_c-\delta R_\varepsilon^-}^{R_c} \Big(- \frac{R_c - \delta R_\varepsilon^-}{R} \left(\frac{\partial H_0}{\partial R} \right)^2 + \frac{1}{2} \left(\frac{\partial H_0}{\partial R} \right)^2 \right. \\
&\quad \left. - \frac{(4\pi)^2}{2} H_0 \log \frac{H_0}{1-H_0} + C_1 H_0 \Big) \mathrm{d}R \right] \\
&= \int_0^{2\pi} \mathrm{d}\theta \left[\delta R_c \int_{R_c-\delta R_\varepsilon^-}^{R_c} \Big(\frac{R + \delta R_\varepsilon^- - R_c}{R} \left(\frac{\partial H_0}{\partial R} \right)^2 - \frac{1}{2} \left(\frac{\partial H_0}{\partial R} \right)^2 \right. \\
&\quad \left. - \frac{(4\pi)^2}{2} H_0 \log \frac{H_0}{1-H_0} + C_1 H_0 \Big) \mathrm{d}R \right].
\end{aligned} \tag{3.94}$$

The last three terms can again be simplified using Eq. 3.80

$$\delta F_R^{(1)} = \int_0^{2\pi} \mathrm{d}\theta \left[\delta R_c \int_{R_c - \delta R_\varepsilon^-}^{R_c} \left(\frac{R + \delta R_\varepsilon^- - R_c}{R} \left(\frac{\partial H_0}{\partial R} \right)^2 - \int_R^{R_c} \frac{1}{R'} \left(\frac{\partial H_0}{\partial R} \right)^2 \mathrm{d}R' \right) \mathrm{d}R \right]. \tag{3.95}$$

Using the asymptotic form in Eq. 3.76 this becomes

$$\delta F_R^{(1)} = O\left(\frac{(4\pi)^4 \delta R_c (\delta R_\varepsilon^-)^4 (\log \delta R_\varepsilon^-)^2}{R_c} \right), \tag{3.96}$$

which is nonleading. The second order δR_c contribution to the sum $\delta F_1 + \delta F_2 + \delta F_3 + \delta F_4$, denoted $\delta F_R^{(2)}$, is again simpler. Using Eq. 3.33 and the asymptotic form in Eq. 3.76, the leading order is

$$\begin{aligned} \delta F_R^{(2)} &= \int_0^{2\pi} \mathrm{d}\theta \, \frac{1}{2} \left[\delta R_c^2 R_c \frac{\partial H_0}{\partial R} \left(\frac{(4\pi)^2}{2} \left(\log \frac{H_0}{1 - H_0} + \frac{1}{1 - H_0} \right) - C_1 \right) \Big|_{R = R_c - \delta R_\varepsilon^-} + \cdots \right] \\ &= \int_0^{2\pi} \mathrm{d}\theta \, \frac{1}{2} \left[\delta R_c^2 R_c \frac{\partial H_0}{\partial R} \left(-\frac{\partial^2 H_0}{\partial R^2} - \frac{1}{R} \frac{\partial H_0}{\partial R} \right) \Big|_{R = R_c - \delta R_\varepsilon^-} + \cdots \right] \\ &= \int_0^{2\pi} \mathrm{d}\theta \left[\frac{(4\pi)^4}{2} R_c \delta R_c^2 \delta R_\varepsilon^- (\log \delta R_\varepsilon^-)^2 + \cdots \right]. \end{aligned} \tag{3.97}$$

The completes the leading order derivation of δF_ε^b. Combining Eq. 3.84, Eq. 3.90, Eq. 3.91, and Eq. 3.97, after a little simplification, results in

$$\delta F_\varepsilon^b = \int_0^{2\pi} \mathrm{d}\theta \, \frac{1}{2} \left[R_c \delta R_\varepsilon^- \left(\delta C_c - (4\pi)^2 \delta R_c \log \delta R_\varepsilon^- \right)^2 + \int_{R_c - \delta R_\varepsilon^-}^{R_c + \delta R_c} R \mathrm{d}R \, \frac{1}{R^2} \left(\frac{\partial H_\varepsilon}{\partial \theta} \right)^2 + \cdots \right]. \tag{3.98}$$

The term from $\delta F_R^{(1)}$ from Eq. 3.96 has been neglected here because it is possible to choose δR_ε^- sufficiently small in accordance with Eq. 3.78 such that it is negligible compared to the terms retained. Finally, note that Eq. 3.98 is always non-negative, since $\delta R_\varepsilon^- > 0$. It follows that no boundary perturbation can lower the energy of the base state by dominating the interior contribution. Since ultimately δF_ε is to be minimized among all possible perturbations to search for instabilities, it follows that δR_c and δC_c should be chosen sufficiently small that the leading order contribution will come from the interior region δF_ε^i, as assumed in the subsection **The interior contribution to the the energy stability analysis and the eigenvalue problem**.

This implies that the zero contact slope droplets with $H_{\max} \lesssim 0.81113$ are indeed energy stable. This completes our demonstration of Proposition 4.

A few technical aspects concerning this demonstration will be noted now before closing this section. First, although we specialized to $C_c = 0$ earlier in view of Proposition 2, it is worth noting that when considering droplets with $C_c > 0$, the instability appears in the boundary contribution here as a lower order term that vanishes for $C_c = 0$ rather than as a negative eigenvalue in the interior contribution. Also, note that there is one technical complication if $\delta C_c = (4\pi)^2 \delta R_c \log \delta R_\varepsilon^-$ in Eq. 3.98. Since the leading order term then vanishes, the next leading order term should really be investigated before concluding that it is positive definite. Such an analysis seems excessive and has not been carried out. Lastly, the reader may wonder whether any of the higher order terms in δC_c or δR_c could dominate the terms that we have retained in Eq. 3.98. It was shown, for example, that the $\delta F_C^{(2)}$ and $\delta F_R^{(2)}$ terms can be comparable or dominate the $\delta F_C^{(1)}$ and $\delta F_R^{(1)}$ terms despite being higher order in δC_c and δR_c, respectively. However, note that there were terms of formally larger order in $\delta F_C^{(1)}$ and $\delta F_R^{(1)}$ that happened to cancel each other exactly after application of Eq. 3.33 or Eq. 3.80. This was in fact the only reason that it was possible for $\delta F_C^{(2)}$ and $\delta F_R^{(2)}$ to be comparable to these lower order terms. No such cancellation took place in the $\delta F_C^{(2)}$ and $\delta F_R^{(2)}$ terms, and so the higher order terms in δC_c and δR_c can never be comparable to them.

Discussion

Several propositions regarding the stability of compactly supported states have been described and supported in this section. The differential equation governing potentially stable, steady states described in Proposition 1 and the assessment of the stability of these solutions in Propositions 2-4 have relied essentially on the variational form of the governing equation in Eq. 3.3 and the fact that the Lyapunov energy strictly decreases in time, as described in Assumption 1. It is expected that physicists working in the field of thin films will be mostly satisfied with the assumptions made and the evidence provided herein. However, the exact conditions under which these propositions will hold and mathematically rigorous proofs of their validity have not been attempted, and future efforts to do so would certainly be valuable.

The most interesting and novel physical conclusion discussed was the destabilization of thermocapillary-driven droplets as their volume and height increases in the case

of Eq. 3.6. This result was likely not noted in previous numerical work because most studies have employed a convective model with the Lyapunov potential like

$$W(H) = H \log\left(\frac{H}{1+H}\right), \tag{3.99}$$

rather than the conductive one in Eq. 3.6, and there is no corresponding instability in the convective model. This Eq. 3.99 is also relevant in the unusual conductive case when $\kappa > 1$. Moreover, this instability result differs qualitatively from the one-dimensional power-law forcing considered in detail by mathematicians

$$\frac{\partial H}{\partial t} + \frac{\partial}{\partial X}\left(H^n \frac{\partial^3 H}{\partial X^3} + BH^m \frac{\partial H}{\partial X}\right) = 0, \tag{3.100}$$

with $Q_1(H) = H^n$ and $W'(H) = 0$ (unforced, $B = 0$) or $W''(H) = -BH^{m-n}$ (power-law forcing, $B > 0$). In this case, stability depends on the strength of the power law but not on the droplet size, as discussed in Section 3.3 below. Unlike the cases in Eq. 3.99 and Eq. 3.100, the driving force in Eq. 3.6 becomes increasingly dominant with increasing droplet height, since the thickness of the layer of insulating gas separating the hot and cold substrates in Fig. 3.2 decreases with increasing H and thus more heat is transported across taller films. This results in larger Marangoni stresses that consequently destabilize sufficiently large droplets. The correspondence in the case of Eq. 3.6 between droplet destabilization and the critical points of $\mathscr{V}$ and $F/\mathscr{V}$ described in Proposition 3 and Proposition 4 was an intriguing mathematical conclusion, which raises the question: Do the critical points of $\mathscr{V}$ and $F/\mathscr{V}$ always indicate a change in droplet stability for films governed by Eq. 3.3 with more general $Q_1(H)$ and $W(H)$?

Although stability of sufficiently short droplets governed by Eq. 3.6 has been established here, it has not been shown that a perturbed flat film will actually evolve towards a configuration consisting of such stable droplets in the large time limit. In fact, it can be easily demonstrated that the Lyapunov energy is unbounded below for any finite volume[2]. The stable droplet solutions are only local minima of the Lyapunov energy, and the flat film may or may not lie in the basin of attraction of droplet configurations. In fact, in past experimental studies, nanopillar growth has continued until contact with the cold substrate in Fig. 3.2 was achieved, but the development of an array of steady droplets is still likely possible given appropriate experimental parameters. Considering the physical constraint in Eq. 3.34

[2]Taking the $\kappa \to 0$ limit so that Eq. 3.34 can be satisfied, the profile $H_\infty(R) = 1 - \exp\left(-bR^{-a}\right)$ where $a > 2$ can easily be demonstrated to contain a finite volume $0 < \mathscr{V}[H_\infty] = b^{2/a}\Gamma\left(\frac{a-2}{a}\right)/2 < \infty$ but a divergent Lyapunov energy $F[H_\infty] = -\infty$, where Γ is the Gamma function.

and the conclusions in Proposition 4, it only follows for $\kappa \lesssim 0.18887$ that all stable droplets described here actually fit in the apparatus. Given the polymer melts and air used in a current experiment [13] with $k_{\text{air}} \approx 0.036\ \text{Wm}^{-1}\text{K}^{-1}$ and $k_{\text{PS}} \approx 0.130\ \text{Wm}^{-1}\text{K}^{-1}$ at $T = 443$ K, it follows that $\kappa \approx 0.28$, so that in fact the unstable tall droplets with height $H_{\max} \gtrsim 0.81113$ do not fit in this apparatus and are unphysical. However, κ can easily be lowered by using a heavier atomic mass gas instead of air above the fluid. For example, argon has a thermal conductivity $0.0224\ \text{Wm}^{-1}\text{K}^{-1} < k_{\text{Ar}} < 0.0265\ \text{Wm}^{-1}\text{K}^{-1}$ for $400\ \text{K} < T < 500\ \text{K}$, which could lead to sufficiently small value of κ when the fluid is the same polystyrene melt [82] . Such an experimental setup would be necessary to observe droplet instability. On the other hand, increasing κ will tend to stabilize more droplets and thus promote steady state formation. If helium, with thermal conductivity $0.1896\ \text{Wm}^{-1}\text{K}^{-1} < k_{\text{He}} < 0.2214\ \text{Wm}^{-1}\text{K}^{-1}$ for $400\ \text{K} < T < 500\ \text{K}$, were used, it would follow that $\kappa > 1$ with the same polystyrene melt [82]. In this case, Eq. 3.99 rather than Eq. 3.6 would be relevant, and all zero contact slope droplets would be stable.

Even if some of the supposedly stable droplets formed actually contact the cold substrate, the only requirement for forming a steady state droplets is that the droplets that do form are shorter than $H_{\max} = 1 - \kappa$. Given the total volume of fluid in initial flat film state, the most naive model assumes that a hexagonal lattice forms with the same volume of fluid and with lattice spacing equal to the wavelength of the most unstable mode of growth for the flat film. Carrying out the linear stability analysis of the flat film state, it can be shown that each droplet should contain a volume $\mathscr{V} = \sqrt{3}\chi^2(1+\chi)^2/2$, where $\chi = (\kappa - 1)/D_0$. On the other hand, the volume of the largest stable droplet in Fig. 3.4(a) is $\mathscr{V}_{\max} \approx 0.0139$. It follows that for $-0.851 \lesssim \chi \lesssim -0.149$, the largest stable droplet does not have enough volume to accommodate the volume in the initial state, so that $\chi \gtrsim -0.149$ is another requirement on steady state droplet formation ($\chi \lesssim -0.851$ also satisfies this criteria, but this situation corresponds to very small κ and D_0 and is not of experimental interest). Restated in terms of the gap width, the largest volume droplet contains enough volume to accommodate the hexagonal lattice when $D_0 \gtrsim (1-\kappa)/0.149$, but as noted above, this droplet only fits in the apparatus if $\kappa \lesssim 0.18887$. These bounds on steady droplet formations are not strict since the assumption that a perfect hexagonal lattice forms is obviously an idealization, but they may be of value in designing future experiments.

3.2 Long time evolution for driven films with gravitational forces

A detailed stability analysis for radially symmetric droplets was carried out in the previous section for a specific driving thermocapillary force, but the implications can be extended to a variety of other problems. Furthermore, many of the technical details considered in the previous sections can often be bypassed. To illustrate, we consider in this section the long time evolution and expected morphological development of an initially flat film under the influence of either thermocapillary and gravitational forces or electrohydrodynamic and gravitational forces.

We described in Eqns. 1.70-1.71 the appropriate Lyapunov potential in the thermocapillary and gravitation driven (TC) case

$$W_{\mathrm{TC}}(H) + W_{\mathrm{G}}(H) = -\frac{3\bar{\mathrm{Ma}}}{2}(1+\chi)H\log\left(\frac{H}{1+\chi H}\right) + \frac{\bar{G}}{2}H^2.$$

We also described in Eqns. 1.71-1.72 the appropriate Lyapunov potential in the electrohydrodynamic and gravitation driven (EHD) case,

$$W_{\mathrm{EHD}}(H) + W_{\mathrm{G}}(H) = -\frac{\bar{\mathrm{E}}}{2}\frac{\chi_{\mathrm{EHD}}H}{1+\chi_{\mathrm{EHD}}H} + \frac{\bar{G}}{2}H^2.$$

The resulting thin film equations in Eq. 3.3 in the TC case is

$$\frac{\partial H}{\partial t} + \nabla_L\cdot\left(\frac{\bar{\mathrm{Ca}}^{-1}H^3}{3}\nabla_L\nabla_L^2 H + \frac{\bar{\mathrm{Ma}}(1+\chi)H^2}{2\left(1+\chi H\right)^2}\nabla_L H - \frac{\bar{G}H^3}{3}\nabla_L H\right) = 0, \quad (3.101)$$

while in the EHD case, it is

$$\frac{\partial H}{\partial t} + \nabla_L\cdot\left(\frac{\bar{\mathrm{Ca}}^{-1}H^3}{3}\nabla_L\nabla_L^2 H + \frac{\bar{\mathrm{E}}\chi_{\mathrm{EHD}}^2H^3}{3\left(1+\chi_{\mathrm{EHD}}H\right)^3}\nabla_L H - \frac{\bar{G}H^3}{3}\nabla_L H\right) = 0. \quad (3.102)$$

As in Section 3.1, a rescaling of H, t and $\mathbf{X}_L$ can help collapse the dependencies on non-dimensional variables in Eqns. 3.101-3.102. For the TC case, we use the rescalings

$$\begin{aligned} H' &= (-\chi)\,H, \\ t' &= \left(\frac{3}{(4\pi)^2}\frac{(1+\chi)^2}{-\chi}\bar{\mathrm{Ma}}^2\bar{\mathrm{Ca}}\right)t, \\ \mathbf{X}_L' &= \left(\frac{3}{(4\pi)^2}\left(-\chi\left(1+\chi\right)\right)\bar{\mathrm{Ma}}\bar{\mathrm{Ca}}\right)^{1/2}\mathbf{X}_L, \end{aligned}$$

which, after dropping the primes, results in the rescaled equation

$$\frac{\partial H}{\partial t} + \nabla_L \cdot \left(\frac{H^3}{(4\pi)^2} \nabla_L \nabla_L^2 H + \frac{H^2}{2\,(1-H)^2} \nabla_L H - \frac{g_{\mathrm{TC}} H^3}{3} \nabla_L H \right) = 0, \tag{3.103}$$

where

$$g_{\mathrm{TC}} \equiv \frac{\bar{G}}{\bar{\mathrm{M}}\mathrm{a}\,(-\chi)\,(1+\chi)} = \frac{\rho g d_0^2}{\sigma_T\,(T_H - T_C)\,\kappa\,(1-\kappa)}$$

is the non-dimensional number quantifying the relative strength of gravitational and thermocapillary forces. Similarly for the EHD case, we use the rescalings

$$\begin{aligned} H' &= (-\chi_{\mathrm{EHD}})\, H, \\ t' &= \left(\frac{3}{(4\pi)^2} (-\chi_{\mathrm{EHD}}) \bar{\mathrm{E}}^2 \bar{\mathrm{C}}\mathrm{a} \right) t, \\ \mathbf{X}_L' &= \left(\frac{3}{(4\pi)^2}\,(-\chi_{\mathrm{EHD}})^2\, \bar{\mathrm{E}}\bar{\mathrm{C}}\mathrm{a} \right)^{1/2} \mathbf{X}_L, \end{aligned}$$

which, after dropping the primes, results in the rescaled equation

$$\frac{\partial H}{\partial t} + \nabla_L \cdot \left(\frac{H^3}{(4\pi)^2} \nabla_L \nabla_L^2 H + \frac{H^3}{3\,(1-H)^3} \nabla_L H - \frac{g_{\mathrm{EHD}} H^3}{3} \nabla_L H \right) = 0, \tag{3.104}$$

where

$$g_{\mathrm{EHD}} \equiv \frac{\bar{G}}{\bar{\mathrm{E}}\,(-\chi_{\mathrm{EHD}})^2} = \frac{\rho g d_0^3}{\varepsilon_0 \varepsilon \Delta V^2 \varepsilon_{\mathrm{EHD}}\,(1-\varepsilon_{\mathrm{EHD}})^2}$$

is the non-dimensional number quantifying the relative strength of gravitational and electrohydrodynamic forces. Note that both g_{TC} and g_{EHD} depend on various experimental parameters but not on the initial film thickness h_0.

To apply the conclusions from Section 3.1, we first consider the various radially symmetric steady droplet solutions to Eq. 3.103-3.104. As in the Proposition 1 of Section 3.1, because stable solution must minimize the relevant Lyapunov energies, the potentially stable radially symmetric droplets satisfy a second order spatial ordinary differential equation. For the TC problem, the droplets satisfy

$$C_1 = \frac{1}{R} \frac{\partial}{\partial R} \left(R \frac{\partial H}{\partial R} \right) + \frac{(4\pi)^2}{2} \left(\log\left(\frac{H}{1-H} \right) + \frac{1}{1-H} \right) - \frac{(4\pi)^2 g_{\mathrm{TC}}}{3} H, \tag{3.105}$$

while for the EHD problem, the droplets satisfy

$$C_1 = \frac{1}{R} \frac{\partial}{\partial R} \left(R \frac{\partial H}{\partial R} \right) + \frac{(4\pi)^2}{6} \frac{1}{(1-H)^2} - \frac{(4\pi)^2 g_{\mathrm{EHD}}}{3} H, \tag{3.106}$$

where C_1 is the Lagrange multiplier enforcing conservation of volume in both cases. Furthermore, since the relevant Lyapunov potentials vanish as $H \to 0$, Proposition 2

of Section 3.1 ensures that only those droplets with zero contact slope $C_c = \frac{\partial H}{\partial R}\Big|_{R=R_c}$ can be stable, where R_c is the radius of the contact line where $H|_{R=R_c} = 0$. Thus we can parameterize all the potentially stable droplet solutions with just the droplet height $H_{\max} = H|_{R=0}$. For each $H_{\max}$, we numerically solve Eqns. 3.105-3.106 while iteratively decreasing the droplet curvature in order to achieve the $C_c = 0$ condition, as was done in Section 3.1. Having carried out this procedure for several values of $H_{\max}$, the volume of each zero contact droplet solution was calculated for a number values of g_{TC} and g_{EHD} and plots of interpolations of $\mathscr{V}$ vs. $H_{\max}$ are depicted in Fig. 3.8.

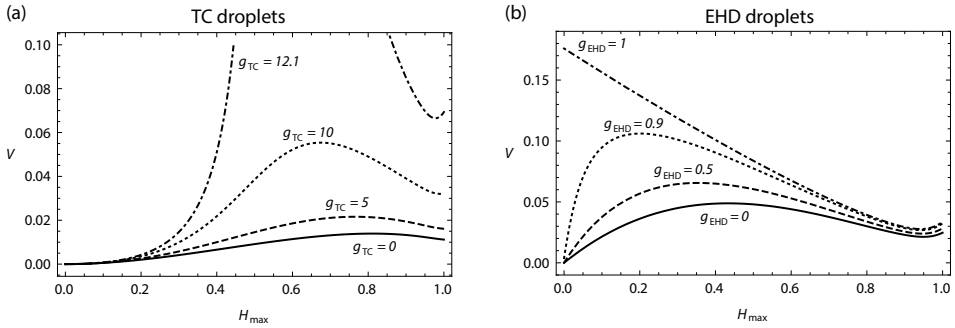

Figure 3.8: Volume of zero contact slope droplets for (a) thermocapillary driven films with $g_{\mathrm{TC}} = 0$ (solid line), $g_{\mathrm{TC}} = 5$ (dashed line), $g_{\mathrm{TC}} = 10$ (dotted line), and $g_{\mathrm{TC}} = 12.1$ (dash-dotted line) and (b) electrohydrodynamic films with $g_{\mathrm{EHD}} = 0$ (solid line), $g_{\mathrm{EHD}} = 0.5$ (dashed line), $g_{\mathrm{EHD}} = 0.9$ (dotted line), and $g_{\mathrm{EHD}} = 1$ (dash-dotted line). As the gravity numbers increase, the scaled height of the largest volume droplets decreases and the scaled volume of the largest volume droplets increases.

The relationship between stability and the plots of $\mathscr{V}$ vs. $H_{\max}$ for zero contact droplets was the subject of Proposition 3 and Proposition 4 in Section 3.1 in the thermocapillary case with $g_{\mathrm{TC}} = 0$. It was shown there the stable droplets were those with $H_{\max}$ between zero and the height of the droplet with maximum volume, which we denote here H_{LSD} (the subscript LSD denotes largest stable droplet). We conjecture here that this is true for all values of g_{TC} and also true for all values of g_{EHD} for the electrohydrodynamic droplets in Fig. 3.8(b). This claim is not proven but will be tested numerically later in this section for one case of EHD films. As g_{TC} increases, the volume of the largest stable droplet V_{LSD} increases while the height H_{LSD} decreases. This is possible only because the radius of the largest stable droplets R_{LSD} also increases with increasing g_{TC}. In fact, as g_{TC} approaches a critical number which is apparently a little larger than 12, the radius R_{LSD} and volume V_{LSD} appear to diverge while H_{LSD} approaches a constant that is a little larger than 0.5. This

is indicative of a bifurcation in which the droplet solutions merge into the flat film solutions. A similar bifurcation is apparent in the electrohydrodynamic droplets, but the critical number in that case is $g_{\mathrm{EHD}} = 1$. A qualitative difference in the EHD case is that the limiting maximum height H_{LSD} approaches zero as $g_{\mathrm{EHD}} \to 1$, while the volume V_{LSD} approaches a non-zero constant as the radius R_{LSD} diverges. This qualitative difference leads to some interesting physical differences between the thermocapillary and electrohydrodynamic films which we will discuss shortly.

The knowledge of the volume of the largest stable droplets V_{LSD} allows us to make important predictions about the long time evolution of an initially flat film. The first step in these predictions is the linear stability of an initially flat film. The film height was initially scaled by the initial film thickness h_0. After the rescaling described above, the initial TC film non-dimensionalizes to $H_0 = -\chi$ while the initial EHD film non-dimensionalizes to $H_0 = -\chi_{\mathrm{EHD}}$. The linear stability of Eqns. 3.103-3.104 is derived by linearizing with the ansatz $H = H_0 + \delta H \mathrm{e}^{bt + i\mathbf{p}\cdot\mathbf{X}_L}$ with $\delta H \ll H_0$. The resulting dispersion relation in the TC case is

$$b = -|\mathbf{p}|^2 \left(\frac{(-\chi)^3}{(4\pi)^2} |\mathbf{p}|^2 - \frac{(-\chi)^2}{2(1+\chi)^2} + \frac{g_{\mathrm{TC}}(-\chi)^3}{3} \right),$$

while in the EHD case, the dispersion relation is

$$b = -|\mathbf{p}|^2 \left(\frac{(-\chi_{\mathrm{EHD}})^3}{(4\pi)^2} |\mathbf{p}|^2 - \frac{(-\chi_{\mathrm{EHD}})^3}{3(1+\chi_{\mathrm{EHD}})^3} + \frac{g_{\mathrm{EHD}}(-\chi_{\mathrm{EHD}})^3}{3} \right).$$

The growth rate b is strictly negative for

$$g_{\mathrm{TC}} > \frac{3}{2} \frac{1}{(-\chi)(1+\chi)^2} \quad \text{or} \quad g_{\mathrm{EHD}} > \frac{1}{(1+\chi_{\mathrm{EHD}})^3}, \tag{3.107}$$

so that the flat films are stable in these cases. A type II instability results for smaller g_{TC} and g_{EHD} where a band of unstable wavenumbers with positive growth rates emergences starting at $|\mathbf{p}| = 0$. During the initial stages of the instability, the most important quantities are the growth rate $b_{\max}$ and the wavelength $\lambda_{\max}$ of the fastest growing mode. For the TC film, these are

$$\begin{aligned} b_{\max} &= \frac{4\pi^2(-\chi)^3}{9} \left(\frac{3}{2(-\chi)(1+\chi)^2} - g_{\mathrm{TC}} \right)^2, \\ \lambda_{\max} &= \sqrt{\frac{3}{2}} \left(\frac{3}{2(-\chi)(1+\chi)^2} - g_{\mathrm{TC}} \right)^{-1/2}. \end{aligned} \tag{3.108}$$

while for the EHD film they are

$$b_{\max} = \frac{4\pi^2(-\chi_{\mathrm{EHD}})^3}{9}\left(\frac{1}{(1+\chi_{\mathrm{EHD}})^3} - g_{\mathrm{EHD}}\right)^2,$$
$$\lambda_{\max} = \sqrt{\frac{3}{2}}\left(\frac{1}{(1+\chi_{\mathrm{EHD}})^3} - g_{\mathrm{EHD}}\right)^{-1/2}. \tag{3.109}$$

These quantities determine the size and growth rate of the initial protrusions that form in the flat film.

Long after the initial growth of an unstable film, one may expect that the protrusions will approach steady droplet states, and the film may rupture as the fluid is drawn out of the troughs between the protrusions. This will only be possible, however, if steady droplets solutions exists which can accomodate the volume in the initial film. In particular, if the growing pattern is a perfect hexagonal lattice with lattice constant of $\lambda_{\max}$, each protrusion must contain a volume of fluid $V_{\mathrm{protrusion}} = \frac{\sqrt{3}}{2}(\lambda_{\max})^2 H_0$ where $H_0 = -\chi$ in the TC case and $H_0 = -\chi_{\mathrm{EHD}}$ in the EHD case. This estimate for the volume in each protrusion is an underestimate, as a perfect hexagonal lattice will not generally occur. Nearby initial protrusions may combine during their growth, and a more realistic estimate for the volume the largest droplets must accomodate is $2V_{\mathrm{protrusion}}$. Whether such droplets exists depends on the volume of the largest stable droplet V_{LSD}. Taking the numerical values of V_{LSD} from the numerics described in Fig. 3.8, one can find the values of $\frac{D_0}{1-\kappa} = -\frac{1}{\chi}$ and $\frac{D_0}{1-\varepsilon_{\mathrm{EHD}}} = -\frac{1}{\chi_{\mathrm{EHD}}}$ which satisfy $V_{\mathrm{LSD}} = 2V_{\mathrm{protrusion}}$ and identify the boundary for which thicker initial films (and hence smaller gap ratio D_0) contain more volume per protrusion than the largest stable droplets. For films that are thicker than these, the protrusions are expected to grow until they make contact with the top substrate and form a column. If the gap width is very large, the growing protrusion may grow very thin and even break apart before making contact with the top substrate, thus producing a jet or spray or fluid instead. The thin film approximation is expected to fail prior to this outcome, and a singularity may be encountered in numerics. These predictions are plotted in Fig. 3.9 below.

One interesting feature of Fig. 3.9 is the difference between "triple point" where the droplet, flat film, and columns or jets domains all come together. For the thermocapillary films, this point lies around $g_{\mathrm{TC}} \approx 12.1$ and $\frac{D_0}{1-\kappa} \approx 5$, while for the electrohydrodynamic films, it lies at $g_{\mathrm{EHD}} = 1$ and $\frac{D_0}{1-\varepsilon_{\mathrm{EHD}}} = \infty$. The triple point is the bifurcation in which the radius R_c of largest stable droplet diverges and the largest stable droplets merge with the flat film solutions. The difference between

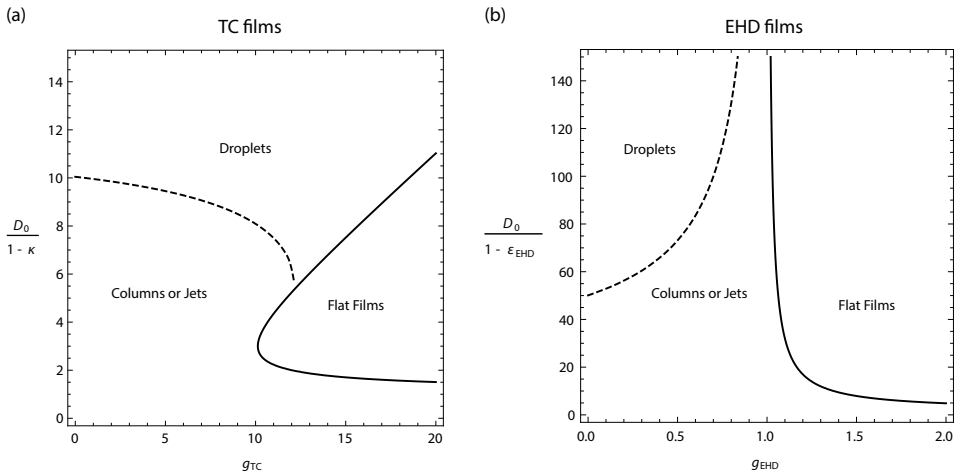

Figure 3.9: Expected long time morphology for (a) thermocapillary driven and (b) electrohydrodynamic driven films. The solid lines are the boundaries between stable and unstable flat films in Eq. 3.107, while the dotted lines are the boundaries determined by $V_{\mathrm{LSD}} = 2V_{\mathrm{protrusion}}$.

the character of the triple point in the TC and EHD case is the fact that the largest stable droplets have finite $H_{\max}$ as $g_{\mathrm{TC}} \to 12.1$ in the TC case but have vanishing $H_{\max}$ as $g_{\mathrm{EHD}} \to 1$ in the EHD case. The origin of this difference is apparently due to the fact that the thermocapillary force is a tangential interfacial force which has a H^2 coefficient in the film equation while the gravitational and electrohydrodynamic forces are body and surface normal forces which both have a H^3 coefficient in the film equation. Experimental implications about these predictions are discussed in Section 3.3 below.

Finally, to test our prediction about the morphological development, we implemented dynamical simulations to observe the morphological development of an initially flat film. We used Mathematica's method of lines discretization (with 100 points in each spatial direction) and a BDF integration method (specifically SUNDIALS IDA [83]) to numerically integrate the EHD driven film in Eq. 3.104 starting with an initially flat film with a small random initial perturbation one tenth the size of the initial film thickness. We used periodic boundary conditions and a domain that would accomodate a hexagonal lattice of 24 droplets with $\lambda_{\max}$ spacing. One simulation was carried out in the droplets domain in Fig. 3.9 with $g_{\mathrm{EHD}} = 0.5$ and initial film thickness $1/H_0 = \frac{D_0}{1-\varepsilon_{\mathrm{EHD}}} = 100$, while a second was carried out in the columns or jets domain with $g_{\mathrm{EHD}} = 0.5$ and initial film thickness $1/H_0 = \frac{D_0}{1-\varepsilon_{\mathrm{EHD}}} = 50$. The boundary between the droplet and columns or jets domain was predicted to be $\frac{D_0}{1-\varepsilon_{\mathrm{EHD}}} \approx 73$ for $g_{\mathrm{EHD}} = 0.5$. The first simulation was run for a time $5/b_{\max}$, five times

longer than the time scale determined by the the fastest growing mode. There we did observe the protrusions grow towards the steady droplet solutions. The second simulation reach a singularity shortly before a time $5/b_{\max}$, as a growing protrusion blew up into a jet formation. The results at the final time step are shown in Fig. 3.10 below. It should also be noted that for longer simulation in the droplet domain of parameters in Fig. 3.9, a different kind of numerical singularity was observed in which the film height became smaller than the precision of the integration in some of the interstitial regions between the droplets. This rupturing singularity has been noted by many other authors and can be mitigated with additional inclusion of Van der Waals forces, for example. In any case, these simulation confirm our prediction that for sufficiently thick initial films, there does not exist stable droplet states that can accomodate enough volume to support the development of droplets, and jets form instead.

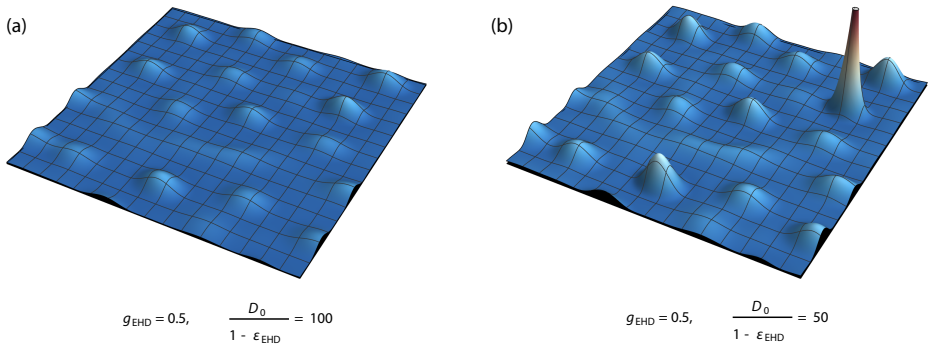

Figure 3.10: Final state of the simulations of electrohydrodynamic driven films in (a) the droplet forming domain and (b) the jet forming domain of Fig. 3.9. The formation of the prominent jet in (b) is expected to occur only for sufficiently thick initial films.

Over a longer course of development of a film in the droplet domain of Fig. 3.9, one may expect (with appropriate modeling of the contact lines or mitigation of rupture with Van der Waals forces) that the initial droplets that form will combine and coarsen slowly, as in spinodal decomposition. As this process continues, some droplets may attain volume in excess of V_{LSD} and would then be expected to develop into a jet or column. This very long time coarsening behavior is yet another interesting research direction for the future.

3.3 Notes

As noted in Section 3.1, the mathematical community has carried out several rigorous studies of equations of the form in Eq. 3.3 in the special case where H depends on only one of the two Cartesian coordinates (X, Y) and time t, as in Eq. 3.100. The degeneracy $Q_1(H) \to 0$ as $H \to 0$ is known to lead to singular behavior related to rupture, and Bernis and Friedman and later Bertozzi, Brenner, Dupont, and Kadanoff introduced weak, non-negative solutions to model the spreading of post-ruptured states and the moving contact line [75–77]. Important results regarding the $t \to \infty$ behavior of such solutions have also been established. First, in the unforced case, long-time strict positivity and convergence towards the uniform film have been establish by Beretta, Bertsch, Dal Passo, and Bertozzi [56, 57]. In the power-law forcing case, Bertozzi and Pugh showed that solutions remain bounded above for all t for $m < n + 2$, but can blow up in finite time otherwise [84, 85]. Laugesen and Pugh performed linear stability analyses of strictly positive periodic steady states and found instabilities when $m < n$ or $m > n + 1$ (or more generally, when $W^{(4)}(H) < 0$), and states were observed to numerically evolve towards ruptured arrays of droplets [78, 86, 87]. Recently, Cheung and Chou performed a stability analysis of droplet states for Eq. 3.100 and found stability of isolated droplets with zero contact slope for $n - 2 < m < n + 2$ but instability for $m > n + 3$ [79].

These mathematical results are significant and give an interesting perspective to complement the physics literature on the subject, but the specific form in Eq. 3.100 has limited physical application. First, although Eq. 3.100 is a valid reduction of Eq. 3.3 in which H does not depend on Y, the stability results described above neglect possible instabilities resulting from perturbations that vary with Y. On the other hand, the rotationally invariant solutions for which H depends only on R are expected to have greater physical significance, but the resulting reduction of Eq. 3.3 is not of the form in Eq. 3.100. Furthermore, perturbations that vary with the angular coordinate θ should be accounted for in the stability analysis. Another peculiarity in Eq. 3.100 resulting from the strict power-law forcing is the invariance under the scaling $H \to \lambda H$, $X \to \lambda^{(n-m)/2} X$, $t \to \lambda^{n-2m} t$. This symmetry allows droplets of differing volumes to be mapped to each other and implies that if a stable droplet exist for one volume, then a stable droplet exists for all volumes. For more general $W(H)$ and $Q_1(H)$, such a scaling will not be a symmetry of Eq. 3.3. Our results in Section 3.1 account for these complications. Proposition 1 characterized the potentially stable steady states as extrema of the Lyapunov energy, while Proposition 2 demonstrated that only those droplets with $C_c = 2\bar{C}aW(0)$ can

be stable. Analogous results appear in the one-dimensional study of Cheung and Chou [79]. However, several novel results were described as well. The coincidence of the extrema of $\mathscr{V}$ and $F/\mathscr{V}$ described in Proposition 3 relied on the analogue to the fundamental relation of thermodynamics in Lemma 1. This analog in Lemma 1 is rather general, applying to any family of functions which minimize a functional, and we expect it could find use in other problems involving free boundaries. The derivation of Lemma 1 relied on a form of the Reynolds' transport theorem which was generalized beyond the usual one. This generalized Reynolds' transport theorem is discussed and proven in Appendix B below. Finally, in Proposition 4, we studied one particular thermocapillary form for W and characterized stable droplets as those with $H_{\max} < 0.81113$. This particular droplet height was also a simultaneous critical point of $\mathscr{V}$ and $F/\mathscr{V}$ as discussed in Proposition 3, which allowed us to conjecture about stability of droplets with other Lyapunov potentials.

In the physics literature, several numerical studies have been carried out to predict the long time evolution of initially flat films. Deissler and Oron first described thin film droplet solutions in a thermocapillary film [74]. Oron and Rosenau and Boos and Thess have noted that in the absence of other stabilizing forces, the protrusions in the convectively cooled film tend to grow until film rupture occurs and the long time steady state is expected to consist of droplets of fluid separated by dry regions [18, 19, 47, 88]. More recently, Bestehorn, Pototsky, Thiele, and Knobloch studied the development and stability of droplet states in convectively cooled films, avoiding the difficulty of singularities during rupture by including a repulsive Van der Waals interaction with the hot substrate which prevented rupture from developing [48, 49]. They observed long time coarsening behavior, where small droplets combined or were depleted by larger droplets over time to eventually form a single, large, stable droplet state. Merkt, Pototsky, Bestehorn, and Thiele have also developed a thin film equation for two layer confined films which treated both the fluid and gas layer hydrodynamically and studied the development of droplet states numerically in a system with two layers of oil, again noting long time coarsening behavior [24].

In Section 3.2, we considered the long time evolution of an initially flat film in the presence of thermocapillary and gravitational forces and electrohydrodynamic and gravitational forces. There we utilized the new results of Section 3.1 by focusing on the simultaneous critical points of $\mathscr{V}$ and $F/\mathscr{V}$ for zero contact angle droplets, which significantly simplified the analysis. We found that the height of the largest stable droplets decreases while the volume increases with increasing gravitational

forces in both cases. Noting the size of the growing protrusions using linear stability, we characterized when stable droplets could accomodate the initial growth or, on the other hand, when columns or jets are expected to form instead, as summarized in Figure 3.9 which should be a useful guide to experiments in the future. Whether it is desirable to form steady droplets, or columns or jets depends on context, and a specification of the physical parameters necessary to achieve those states is significant. As far as the author is aware, the possibility of forming jets in the thermocapillary driven case has not been previously recognized. The portion of the parameter space in Figure 3.9 where jets might form is rather small, and since the gap widths are not especially large in this region, the more likely outcome seems to be the formation of columns when the growing protusion makes contact with the top substrate. It may be possible to design experiments to avoid this outcome, however, by leaving a gap in the top substrate for example.

The opposite is true in the electrohydrodynamic case – previous experiments seem to favor the formation of columns [40, 41]. Our results indicate that much larger gap widths are necessary to favor droplet formation than have been usually employed in experiments, but such droplet formation may be desirable. Finally, a particularly interesting domain of parameters in the electrohydrodynamic case is those films with large gap width and with $g_{\mathrm{EHD}} \lesssim 1$. Even for a very large ratio of gap width to initial film thickness, such films are expected to form jets rather than droplets. Furthermore, adjustment of g_{EHD} can be achieved by simply changing the applied voltage. However, since films with $g_{\mathrm{EHD}} \gtrsim 1$ are stable, the timescale of the linear instability for these films may be rather long, and tuning of various material and geometry parameters may be necessary to achieve such jet formation in an experimental setting. For reference, after undoing all the scalings described in Section 3.2, the dimensionful growth rate and wavelength of the most unstable modes are

$$\bar{b}_{\max} = \frac{\rho^2 g^2 h_0^3}{12\mu\sigma_0 g_{\mathrm{EHD}}^2}\left(\frac{1}{(1+\chi_{\mathrm{EHD}})^3} - g_{\mathrm{EHD}}\right)^2,$$
$$\bar{\lambda}_{\max} = \sqrt{\frac{8\pi^2\sigma_0 g_{\mathrm{EHD}}}{\rho g}}\left(\frac{1}{(1+\chi_{\mathrm{EHD}})^3} - g_{\mathrm{EHD}}\right)^{-1/2}.$$

A fluid with low viscosity and surface tension like ethanol, with $\rho \sim 790$ kg/m, $\sigma_0 \sim 22$ mN/m, $\mu \sim 1$ mPa $\cdot$ s, and relative permittivity $\varepsilon \sim 25$, with an initial film height of $h_0 = 20$ μm, a gap width of $d_0 = 2$ mm and with an applied voltage $\Delta V \sim 3.9$ kV would achieve $g_{\mathrm{EHD}} \approx 0.5$ with $\frac{D_0}{1-\varepsilon_{\mathrm{EHD}}} \approx 100$ as in Fig. 3.10(a), and

drop formation would be expected. Decreasing the gap width to $d_0 \sim 1$ mm and the applied voltage to $\Delta V \sim 1.4kV$ would achieve $g_{\mathrm{EHD}} \approx 0.5$ with $\frac{D_0}{1-\varepsilon_{\mathrm{EHD}}} \approx 50$ as in Fig. 3.10(b), and jet formation would be expected instead. The scales are reasonable in this case with a growth rate of $\bar{b}_{\max} \sim 0.002$ s^{-1} and a wavelength of $\bar{\lambda}_{\max} \sim 15$ mm. These are rather large voltages to apply to such a small gaps but are well below the breakdown voltage for air at standard temperature and pressure. This scenario was chosen such that the film is not so thin that Van der Waals forces dominate gravitational ones, the voltages are not unrealistically large, and the growth rate is not unreasonably small. To conclude, it seems likely that experiments to produce jets or droplets with the electrohydrodynamic instability are possible, though we note that leaky dielectric model may be more appropriate than the pure dielectric model we employed. An analogous analysis including Van der Waals forces for a leaky dielectric while neglecting gravitational forces for nanometer scale polymer melt thin films would be an interesting future direction for research.

Chapter 4

SCALE INVARIANT SELF-SIMILAR SOLUTIONS

We found in Chapter 2 that the thin film equations possess scaling symmetries in a number of special circumstances. In this chapter, we consider solutions which are invariant under these scaling symmetries. First, in Section 4.1, we will consider the problem of an insoluble surfactant spreading on a thin viscous film. When Marangoni forces dominate capillary and diffusive forces, as is the case in experiments shortly after deposition of a surfactant on a thin fluid film, the relevant evolution equations possess three independent scaling symmetries which lead to an extraordinary variety of scale-invariant solutions. Some of these scale-invariant solutions are well known, but we also demonstrate new scale-invariant solutions which describe the previously uncharacterized inner droplet portion of the spreading process. Next, in Section 4.2, we describe some scale-invariant solutions for a purely capillary spreading film which, to the authors knowledge, have not been previously studied. These include steady scale invariant solutions, traveling and rotating wave scale invariant solutions, and solutions which are invariant under two different scaling symmetries, with a rotating component as well. Finally, Section 4.3 contains a discussion of the history and literature in the field, with an attempt to place the new research contained in this chapter in a wider context.

4.1 Scale invariant spreading of an insoluble surfactant on a thin film

[1] Z. G. Nicolaou and S. M. Troian. "Scale Invariant Draining of the Inner Droplet in the Spreading of an Insoluble Surfactant on a Thin Viscous Film". In: *Phys. Rev. E* (preparing for submission 2016).

Consider an initially flat thin fluid film onto which a surfactant is deposited, as depicted in Fig. 4.1(a). Surface tension decreases with increasing surfactant concentration, so gradients in surfactant concentration result in surface tension gradients which are called Marangoni forces. Shortly after the initial deposition of the surfactant, a structure like that depicted in Fig. 4.1(b) has been observed to develop in both numerical and experimental work. The fluid and the surfactant with it are drawn out from the area of the initial deposition because of the Marangoni forces, and the fluid accumulates to forms a sharp ridge at the front of the spreading shock,

where the surfactant concentration vanishes. Closer to the initial deposition, an inner droplet of fluid with high surfactant concentration is trapped behind a drained region, where the film is very thin. The spreading ridge continues to expand while the inner droplet slowly drains with increasing time. Experiments with very thin films have also exhibited fingering instabilities which occur along the drained front. In these experiments, a finger of fluid protrudes and branches into finer fingers, resulting in a beautiful pattern. This pattern formation has not been theoretically understood, and it is hoped that the work characterizing the draining of the inner droplet contained in this section will help future researchers better understand this process.

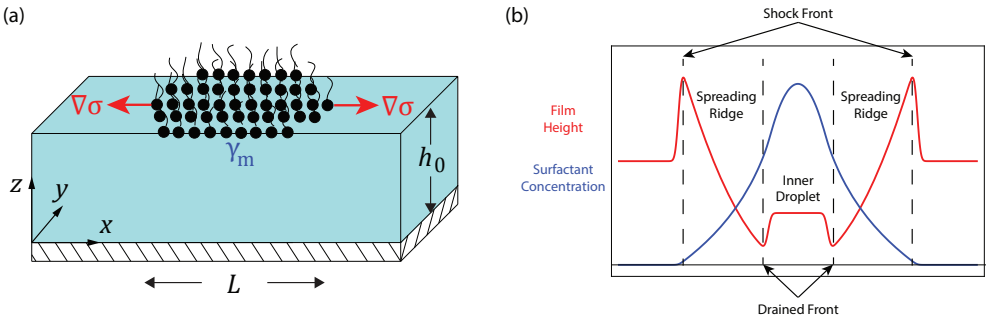

Figure 4.1: (a) An insoluble surfactant of concentration γ_m is deposited with a length scale L onto a flat visous fluid film of thickness h_0. Surface tension σ increases with decreasing surfactant concentration, and the resulting Marangoni forces (red arrows) pull fluid out from the region where the surfactant was deposited. After a short time, the structure shown in (b) develops and continues to spread.

The mathematical description of the spreading of an insoluble surfactant on a thin viscous fluid film was described in Section 1.3. The non-dimensionalized partial differential equations governing the evolution of the film height and surfactant concentration in Eq. 1.73 are repeated here for convenience,

$$\begin{aligned} \frac{\partial H}{\partial t} + \nabla_L \cdot \left(\frac{1}{3}\bar{\mathrm{Ca}}^{-1} H^3 \nabla_L \nabla_L^2 H - \frac{1}{2}\bar{\mathrm{Ma}} H^2 \nabla_L \Gamma \right) = 0, \\ \frac{\partial \Gamma}{\partial t} + \nabla_L \cdot \left(\frac{1}{2}\bar{\mathrm{Ca}}^{-1} H^2 \Gamma \nabla_L \nabla_L^2 H - \bar{\mathrm{Ma}} H \Gamma \nabla_L \Gamma - \bar{\mathrm{Pe}}^{-1} \nabla_L \Gamma \right) = 0, \end{aligned} \tag{4.1}$$

where $H \equiv h/h_0$ is the non-dimensionalized film thickness with h the dimensionful film thickness and h_0 the initial film thickness, $\Gamma \equiv \gamma/\gamma_\mathrm{m}$ is the non-dimensionalized surfactant concentration with γ the dimensionful surfactant concentration and γ_m the concentration in the initial deposition, $t \equiv \bar{t}u_c/L$ is the non-dimensionalized time

with $\bar{t}$ the dimensionful time, u_c the lateral velocity scale, and L the length scale of the initial surfactant deposition, $\nabla_L = \left(\frac{\partial}{\partial X}, \frac{\partial}{\partial Y}\right)$, where $\mathbf{X}_L = (X, Y) \equiv (x/L, y/L)$ are the non-dimensionalized Cartesian spatial coordinates in the directions lateral to the film with (x, y) the dimensionful Cartesian lateral coordinates, $\bar{\mathrm{Ca}} \equiv \mu u_c/\varepsilon^3\sigma_0$ is the thin-film capillary number with $\varepsilon \equiv h_0/L \ll 1$ is the thin film aspect ratio, μ is the fluid viscosity, and σ_0 the surface tension of the fluid in the absense of surfactant, $\bar{\mathrm{Ma}} \equiv \varepsilon\sigma_\gamma\gamma_\mathrm{m}/\mu u_c$ is the thin-film Marangoni number with σ_γ the coefficient describing the assumed linear relation $\sigma = \sigma_0 - \sigma_\gamma\gamma$ between the surface tension and the surfactant concentration, and $\bar{\mathrm{Pe}} \equiv \varepsilon L u_c/\mathcal{D}$ is the thin-film Peclet number with $\mathcal{D}$ the surface diffusion coefficient of the surfactant. For systems of interest, the Marangoni driving terms are much larger than the capillary and diffusive terms over for the portion of the domain closer to the initial surfactant deposition than the shock front. We therefore choose a Marangoni lateral velocity scale $u_c \equiv \varepsilon\sigma_\gamma\gamma_\mathrm{m}/\mu$ which fixes $\bar{\mathrm{Ma}} = 1$ and we assume $\bar{\mathrm{Ca}}^{-1} \ll 1$ and $\bar{\mathrm{Pe}}^{-1} \ll 1$. A valid approximation to Eq. 4.1 is then afforded by

$$\begin{aligned} 0 &= \frac{\partial H}{\partial t} + \nabla_L \cdot \left(-\frac{1}{2}H^2\nabla_L\Gamma\right), \\ 0 &= \frac{\partial \Gamma}{\partial t} + \nabla_L \cdot \left(-H\Gamma\nabla_L\Gamma\right). \end{aligned} \tag{4.2}$$

An extraordinary feature of Eq. 4.2 is the large degree of symmetry that it possess. Being spatially isotropic and homogeneous, the equations are invariant under the expected rotation in the (X, Y) plane and spatial translations in each direction, and being autonomous, the equations are invariant under translations in time. In addition, Eq. 4.2 possesses invariance under the scaling transformations

$$H \to \lambda_H H, \quad \Gamma \to \lambda_\Gamma \Gamma, \quad \mathbf{X}_L \to \lambda_{\mathbf{X}_L}\mathbf{X}_L, \quad t \to \frac{\lambda_{\mathbf{X}_L}^2}{\lambda_H\lambda_\Gamma}t, \tag{4.3}$$

parameterized by the independent scaling factors $\lambda_{\mathbf{X}_L}$, λ_H, and λ_Γ. Two scaling exponents α_1 and α_2 will specify a scale transformation in Eq. 4.3 with $\lambda_H = (\lambda_{\mathbf{X}_L})^{\alpha_1}$ and $\lambda_\Gamma = (\lambda_{\mathbf{X}_L})^{\alpha_2}$. In addition, a dimensionality variable n will be use that is $n = 0$ for translationally invariant solutions which depend on only one of the Cartesian variable X or Y and is $n = 1$ for rotationally invariant solutions which depend only on $R \equiv \sqrt{X^2 + Y^2}$. The similarity variable that is invariant under these scaling transformations and that used as an independent variable below is $\xi \equiv X/(\pm t)^{\frac{1}{2-\alpha_1-\alpha_2}}$ for $n = 0$ and $\xi \equiv R/(\pm t)^{\frac{1}{2-\alpha_1-\alpha_2}}$ for $n = 1$. The scaled dependent variables are $\tilde{H} \equiv H/(\pm t)^{\frac{\alpha_1}{2-\alpha_1-\alpha_2}}$ and $\tilde{\Gamma} \equiv \Gamma/(\pm t)^{\frac{\alpha_2}{2-\alpha_1-\alpha_2}}$, and a scale-invariant solution is one for which $\tilde{H}$ and $\tilde{\Gamma}$ depend on ξ alone. Generally we focus

only the $+t$ case, unless otherwise noted. The infinitestimal form of such a scaling symmetry with $\lambda_H = \lambda_{\mathbf{X}_L}^{\alpha_1}$ and $\lambda_\Gamma = \lambda_{\mathbf{X}_L}^{\alpha_2}$ is the vector $\vec{v}^6_{(\alpha_1,\alpha_2)} = X\frac{\partial}{\partial X} + Y\frac{\partial}{\partial Y} + (2-\alpha_1-\alpha_2)\frac{\partial}{\partial t} + \alpha_1 H\frac{\partial}{\partial H} + \alpha_2\Gamma\frac{\partial}{\partial\Gamma}$ discussed in Section 2.2.

Derivation of the planar system

One means to study Eq. 4.2 is to look for special solutions, and as discussed in Chapter 2, invariance of a solution under symmetries of a differential equations provides a general approach to finding such solutions. In the case of Eq. 4.2, Jensen [71] described solutions which are invariant either under spatial translations or spatial rotations and under the arbitrary scaling transformation of Eq. 4.3. Jensen showed that the scale invariant coupled equations can be recast as a planar system described by an autonomous pair of ordinary differential equations. Jensen's results can be summarized with the following differential system in the new dependent variables $U \equiv \tilde{H}\tilde{\Gamma}/\xi^2$ which is a scaled product of the film thickness and surfactant concentration and $V \equiv -\tilde{H}\frac{\partial\tilde{\Gamma}}{\partial\xi}/\xi$ which is the scaled surface velocity. Jensen used the independent variable $\phi \equiv \log(\xi)$, and derived the planar system,

$$\begin{aligned}\frac{\partial U}{\partial\phi} &= -\frac{U\,(2V+1-6\delta-3\alpha\,(1-2\delta))+V\,(2V-3\delta)}{V-2\delta},\\ \frac{\partial V}{\partial\phi} &= -\frac{U\,((n+1)V+(2\delta-1)(1-\alpha))+V(\delta-V)}{U},\end{aligned} \tag{4.4}$$

where $\delta \equiv 1/(2-\alpha_1-\alpha_2)$ and $\alpha \equiv \alpha_1/(\alpha_1+\alpha_2)$ are an arbitrary real scaling exponents related to which scaling symmetry the solution is invariant under. Each solution to Eq. 4.4 corresponds to a solution

$$\begin{aligned}H &= C_0(\pm t)^{(2\delta-1)\alpha}U\mathrm{e}^{2\alpha\phi+\int\frac{V+2(1-\alpha)U)}{U}\,\mathrm{d}\phi},\\ \Gamma &= \frac{1}{C_0}(\pm t)^{(2\delta-1)(1-\alpha)}\mathrm{e}^{2(1-\alpha)\phi-\int\frac{V+2(1-\alpha)U}{U}\,\mathrm{d}\phi},\end{aligned} \tag{4.5}$$

where C_0 is an integration constant. The transformation in Eq. 4.5 follows directly from equations (2), (4) and (8) of Jensen [71] after noting $\psi = -\ln C_0 - \int\frac{V+2(1-\alpha)U}{U}\mathrm{d}\phi$ for some constant C_0 and substituting his spatial variable x for $x = (\pm t)^\delta\,\xi = (\pm t)^\delta\,e^\phi$.

For completeness, our own derivation of an analogous planar system will be carried out here using the symmetry methods discussed in Section 2.1. The rotationally invariant scale invariant reductions (ii-4) and the translationally invariant scale invariant reductions (ii-5) of Section 2.2 are the starting points. The reduced

equations can be expressed

$$\pm\frac{\alpha_1\tilde{H}-\xi\frac{\partial\tilde{H}}{\partial\xi}}{2-\alpha_1-\alpha_2}+\frac{1}{\xi^n}\frac{\partial}{\partial\xi}\left(-\frac{\xi^n\tilde{H}^2}{2}\frac{\partial\tilde{\Gamma}}{\partial\xi}\right)=0,$$
$$\pm\frac{\alpha_2\tilde{\Gamma}-\xi\frac{\partial\tilde{\Gamma}}{\partial\xi}}{2-\alpha_1-\alpha_2}+\frac{1}{\xi^n}\frac{\partial}{\partial\xi}\left(-\xi^n\tilde{H}\tilde{\Gamma}\frac{\partial\tilde{\Gamma}}{\partial\xi}\right)=0, \tag{4.6}$$

where $n=0$ and $\xi=(\pm t)^{-\frac{1}{2-\alpha_1-\alpha_2}}X$ for translationally invariant solutions and $n=1$ and $\xi=(\pm t)^{-\frac{1}{2-\alpha_1-\alpha_2}}R$ for rotationally invariant solutions. The invariants which are the dependent variables in Eq. 4.6 are $\tilde{H}=(\pm t)^{-\frac{\alpha_1}{2-\alpha_1-\alpha_2}}H$ and $\tilde{\Gamma}=(\pm t)^{-\frac{\alpha_2}{2-\alpha_1-\alpha_2}}\Gamma$. Because only one of the scaling symmetries in Eq. 4.3 was used to derive Eq. 4.6, there are a further two remnant scaling symmetries of the reduced equations which permit a partial integration of the resulting ODE's into a plane-autonomous differential system. First, consider the remnant scaling $\vec{v}=-\tilde{H}\frac{\partial}{\partial\tilde{H}}+\tilde{\Gamma}\frac{\partial}{\partial\tilde{\Gamma}}$. The invariants for this symmetry which satisfy Eq. 2.3 include $\phi=\log\xi$ and $\hat{H}=\log\tilde{H}+\log\tilde{\Gamma}$, while an η^0 variable of Eq. 2.4 is $\hat{\Gamma}=\log\tilde{\Gamma}$. The inverse transformation is $\tilde{H}=\mathrm{e}^{\hat{H}-\hat{\Gamma}}$, $\tilde{\Gamma}=\mathrm{e}^{\hat{\Gamma}}$, and $\xi=\mathrm{e}^{\phi}$. Changing independent variables to ϕ and using $\hat{H}$ and $\hat{\Gamma}$ as dependent variables, the change of variables formulae give

$$\begin{aligned}
\frac{\partial\tilde{H}}{\partial\xi}&=\frac{\partial\tilde{H}}{\partial\hat{H}}\frac{\partial\hat{H}}{\partial\phi}\frac{\partial\phi}{\partial\xi}+\frac{\partial\tilde{H}}{\partial\hat{\Gamma}}\frac{\partial\hat{\Gamma}}{\partial\phi}\frac{\partial\phi}{\partial\xi}=\left(\frac{\partial\hat{H}}{\partial\phi}-\frac{\partial\hat{\Gamma}}{\partial\phi}\right)\mathrm{e}^{\hat{H}-\hat{\Gamma}-\phi},\\
\frac{\partial\tilde{\Gamma}}{\partial\xi}&=\frac{\partial\tilde{\Gamma}}{\partial\hat{\Gamma}}\frac{\partial\hat{\Gamma}}{\partial\phi}\frac{\partial\phi}{\partial\xi}=\frac{\partial\hat{\Gamma}}{\partial\phi}\mathrm{e}^{\hat{\Gamma}-\phi},\\
\frac{\partial^2\tilde{\Gamma}}{\partial\xi^2}&=\frac{\partial^2\tilde{\Gamma}}{\partial\hat{\Gamma}^2}\left(\frac{\partial\hat{\Gamma}}{\partial\phi}\right)^2\left(\frac{\partial\phi}{\partial\xi}\right)^2+\frac{\partial\tilde{\Gamma}}{\partial\hat{\Gamma}}\frac{\partial^2\hat{\Gamma}}{\partial\phi^2}\left(\frac{\partial\phi}{\partial\xi}\right)^2+\frac{\partial\tilde{\Gamma}}{\partial\hat{\Gamma}}\frac{\partial\hat{\Gamma}}{\partial\phi}\frac{\partial^2\phi}{\partial\xi^2}\\
&=\left(\frac{\partial^2\hat{\Gamma}}{\partial\phi^2}+\frac{\partial\hat{\Gamma}}{\partial\phi}\left(\frac{\partial\hat{\Gamma}}{\partial\phi}-1\right)\right)\mathrm{e}^{\hat{\Gamma}-2\phi}.
\end{aligned}$$

Then Eq. 4.6 is transformed to

$$\pm\frac{\alpha_1-\frac{\partial\hat{H}}{\partial\phi}+\hat{\eta}}{2-\alpha_1-\alpha_2}-\frac{1}{2}\mathrm{e}^{\hat{H}-2\phi}\left(\frac{\partial\hat{\eta}}{\partial\phi}+\left(n-1+2\frac{\partial\hat{H}}{\partial\phi}-\hat{\eta}\right)\hat{\eta}\right)=0,$$
$$\pm\frac{\alpha_2-\hat{\eta}}{2-\alpha_1-\alpha_2}-\mathrm{e}^{\hat{H}-2\phi}\left(\frac{\partial\hat{\eta}}{\partial\phi}+\left(n-1+\frac{\partial\hat{H}}{\partial\phi}+\hat{\eta}\right)\hat{\eta}\right)=0, \tag{4.7}$$

where $\hat{\eta}\equiv\frac{\partial\hat{\Gamma}}{\partial\phi}$. By using the invariants as coordinates, the remnant symmetry of Eq. 4.7 has been straightened out to $\vec{v}=\frac{\partial}{\partial\hat{\Gamma}}$, so that Eq. 4.7 does not depend on the independent variable $\hat{\Gamma}$ but only on its derivatives. An integration by quadrature is

performed by regarding Eq. 4.7 as a differential equation of one less order in the independent variables $\hat{H}$ and $\hat{\eta}$. The transformations back to the original variables are easy to write down and will be expressed later in Eq. 4.12. A second remnant scaling symmetry of Eq. 4.7 is $\vec{v} = \frac{1}{2}\frac{\partial}{\partial\phi} + \frac{\partial}{\partial\hat{H}}$. Invariants for this symmetry include $\zeta_1 \equiv \pm\frac{1}{2-\alpha_1-\alpha_2}e^{2\phi-\hat{H}}$ and $\zeta_2 \equiv \hat{\eta}$, while a η^0 of variable of Eq. 2.4 is $\bar{\eta} \equiv \hat{H}$. The inverse transformation is $\hat{H} = \bar{\eta}$, $\hat{\eta} = \zeta_2$, and $\phi = \frac{1}{2}\left(\hat{H} + \log\left(\pm\frac{\zeta_1}{2-\alpha_1-\alpha_2}\right)\right)$. Using $\bar{\eta}$ as the independent variable and ζ_1 and ζ_2 as dependent variables, the change of variables formulae give

$$\frac{\partial\hat{H}}{\partial\phi} = \frac{\partial\bar{\eta}}{\partial\phi} = \frac{2\zeta_1}{\zeta_1 + \frac{\partial\zeta_1}{\partial\bar{\eta}}},$$
$$\frac{\partial\hat{\eta}}{\partial\phi} = \frac{\partial\hat{\eta}}{\partial\zeta_2}\frac{\partial\zeta_2}{\partial\bar{\eta}}\frac{\partial\bar{\eta}}{\partial\phi} = \frac{2\zeta_1\frac{\partial\zeta_2}{\partial\bar{\eta}}}{\zeta_1 + \frac{\partial\zeta_1}{\partial\bar{\eta}}}.$$

Then Eq. 4.7 is transformed to

$$\alpha_1 + \zeta_2 - \frac{\zeta_2\,(n-1-\zeta_2)}{2\zeta_1} - \frac{2\zeta_1 + 2\zeta_2 + \frac{\partial\zeta_2}{\partial\bar{\eta}}}{\zeta_1 + \frac{\partial\zeta_1}{\partial\bar{\eta}}} = 0,$$
$$\alpha_2 - \frac{\zeta_2\,(n-1+\zeta_1+\zeta_2)}{2\zeta_1} - \frac{2\zeta_2 + 2\frac{\partial\zeta_2}{\partial\bar{\eta}}}{\zeta_1 + \frac{\partial\zeta_1}{\partial\bar{\eta}}} = 0. \tag{4.8}$$

Because of the remnant scaling symmetry, Eq. 4.8 is autonomous in the dependent variable $\bar{\eta}$. We can put Eq. 4.8 is a more standard form by solving for the derivatives

$$\frac{\partial\zeta_1}{\partial\bar{\eta}} = -\frac{\zeta_1\,(\zeta_1(3\zeta_2 + 2\alpha_1 - \alpha_2 - 4) + 2\zeta_2(\zeta_2 - 1))}{2\zeta_2^2 + (3\zeta_2 + 2\alpha_1 - \alpha_2)\zeta_1},$$
$$\frac{\partial\zeta_2}{\partial\bar{\eta}} = -\frac{3\zeta_2^3 + \zeta_2^2(6\zeta_1 + n - 1) + 2\zeta_2\zeta_1(\zeta_1 + \alpha_1 - \alpha_2 + n - 1) - 2\alpha_2\zeta_1^2}{2\zeta_2^2 + (3\zeta_2 + 2\alpha_1 - \alpha_2)\zeta_1}. \tag{4.9}$$

The planar systems in Eq. 4.4 and Eq. 4.9 are related by a simple change of variables and an identification of scaling exponents $\alpha_1 = \alpha(2\delta - 1)/\delta$ and $\alpha_2 = (1-\alpha)(2\delta - 1)/\delta$, as we describe below. First, some algebraic features of system in Eq. 4.4 can be emphasized after a small change in variables. Define scaled versions of the planar system $\hat{U} \equiv U/\delta$ and $\hat{V} \equiv V/\delta$ and change independent variables to $\hat{\tau}$ through the relation $\partial\phi/\partial\hat{\tau} = (V - 2\delta)U/\delta^2$. The trajectories of the planar system never cross the $V = 2\delta$ or $U = 0$ lines (which are algebraic invariant curves which will be discussed later), so that the relation between the independent variables $\hat{\tau}$ and ϕ defined here is monotonic. Applying the chain rule and noting that $\phi = \ln C_1 + \int(\hat{V} - 2)\hat{U}\mathrm{d}\hat{\tau}$ for

some integration constant C_1, the cubic planar system results in

$$\begin{aligned}\frac{\partial \hat{U}}{\partial \hat{\tau}} &= -\hat{U}\left(\hat{U}(2\hat{V}+2\alpha_1-\alpha_2-4)+\hat{V}(2\hat{V}-3)\right),\\ \frac{\partial \hat{V}}{\partial \hat{\tau}} &= -(\hat{V}-2)\left(\hat{U}\left((n+1)\hat{V}+\alpha_2\right)+\hat{V}(1-\hat{V})\right),\end{aligned} \tag{4.10}$$

with the following transformation back to physical variables

$$\begin{aligned}\xi &= C_1 \mathrm{e}^{\int_0^{\hat{\tau}} \hat{U}(\hat{V}-2)\,\mathrm{d}\hat{\tau}},\\ H &= \frac{C_1^{\frac{2\alpha_1}{\alpha_2+\alpha_1}} C_0}{2-\alpha_1-\alpha_2}(\pm t)^{\frac{\alpha_1}{2-\alpha_1-\alpha_2}}\hat{U}\mathrm{e}^{\int_0^{\hat{\tau}}(\hat{V}+2\hat{U})(\hat{V}-2)\,\mathrm{d}\hat{\tau}},\\ \Gamma &= \frac{C_1^{\frac{2\alpha_2}{\alpha_1+\alpha_2}}}{C_0}(\pm t)^{\frac{\alpha_2}{2-\alpha_1-\alpha_2}}\mathrm{e}^{-\int_0^{\hat{\tau}}\hat{V}(\hat{V}-2)\,\mathrm{d}\hat{\tau}},\end{aligned}$$

where the first equation should be inverted to eliminate $\hat{\tau}$ in favor of ξ in the second two equations. The appeal of the $(\hat{U},\hat{V})$ system over the (U,V) one is its polynomial form, as a number of tools are available in the study of such systems, including Poincaré compactification techniques and the Darboux theory of integrability [89]. The Poincaré compactification scheme will be described first. As Jensen noted, in addition to finite fixed points which act as endpoints of trajectories in the (U,V) plane, there are several infinite fixed points as trajectories grow indefinitely as $\phi \to \pm\infty$. The Poincaré compactification is a stereoscopic-like projection which maps these infinite fixed points to the equator of a sphere or the boundary of a disk so that they can be studied more concretely. The complete topology of the planar system can then be easily visualized, and a numerical program P4 is available to automate this process for polynomial systems like Eq. 4.10 [89]. Example plots from P4 are shown in Fig. 4.2 below. One important difference between Fig. 4.2(a) for the $n = 0$ case and Fig. 4.2(b) for the $n = 1$ case is the absence of the saddle infinite fixed point in the $n = 1$ case. This turns out to be the case for all values of the scaling exponents, and signals a significant difference between the Cartesian solutions and the radially symmetric ones near the origin. This difference is to be expected given that $X = 0$ corresponds to a Cartesian coordinate axis (a line) in the $n = 0$ case while $R = 0$ corresponds to the origin (a point) in the $n = 1$ case.

Finally, to relate Jensen's planar system to ours, consider the change of variables (related to one of the charts in the Poincaré compactification [89]) to $\zeta_2 \equiv -\hat{V}/\hat{U}$ and $\zeta_1 \equiv 1/\hat{U}$, along with the change of independent variables from $\hat{\tau}$ to τ defined

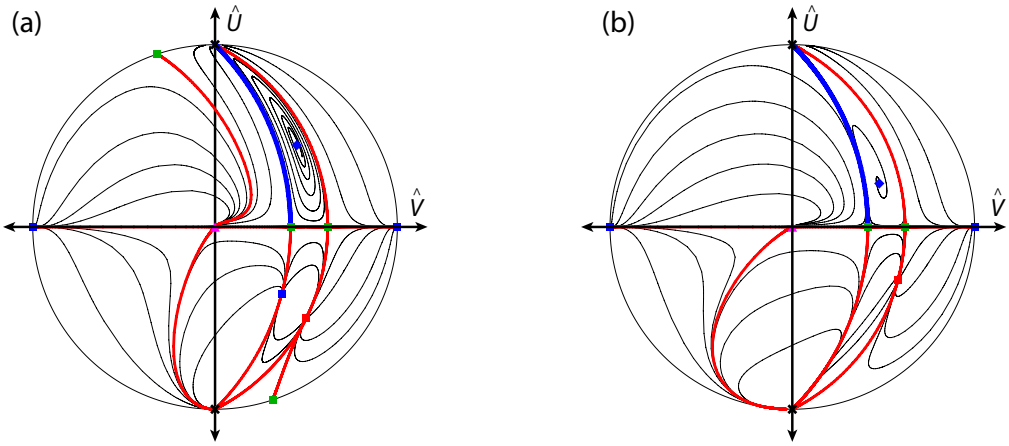

Figure 4.2: Poincaré compactification of the polynomial planar system Eq. 4.10 for (a) $n = 0$, $\alpha_1 = 0$, and $\alpha_2 = -1$ and (b) $n = 1$, $\alpha_1 = 0$, and $\alpha_2 = -2$. The special separatrix corresponding to the conserved surfactant mass solutions of Jensen and Grotberg [25] are shown at thick blue lines, all other separatrices are shown as thick red lines, and a selection of trajectories in each region between separatrices are shown as thin black lines. Green squares are saddle fixed points, blue squares are stable node fixed points, red squares are unstable node fixed points, blue diamonds are stable focus fixed points, pink triangles are saddle-node fixed points, and the black × is an infinite, non-elementary fixed point.

by $\partial\hat{\tau}/\partial\tau = 1/\hat{U}^2$. Applying the chain rule, the resulting cubic planar system is

$$\begin{aligned}
\frac{\partial\zeta_1}{\partial\tau} &= \zeta_1\left(\zeta_1(3\zeta_2 + 2\alpha_1 - \alpha_2 - 4) + 2\zeta_2(\zeta_2 - 1)\right), \\
\frac{\partial\zeta_2}{\partial\tau} &= 3\zeta_2^3 + \zeta_2^2(6\zeta_1 + n - 1) + 2\zeta_2\zeta_1(\zeta_1 + \alpha_1 - \alpha_2 + n - 1) - 2\alpha_2\zeta_1^2. \qquad (4.11)
\end{aligned}$$

This is equivalent to the planar system in Eq. 4.9 when the independent variable is changed from $\bar{\eta}$ to τ such that $\frac{\partial\bar{\eta}}{\partial\tau} = -\left(2\zeta_2^2 + (3\zeta_2 + 2\alpha_1 - \alpha_2)\zeta_1\right)$. Noting also from Eq. 4.10 that

$$\frac{\hat{U}}{\hat{U}_0} = \mathrm{e}^{\ln\frac{\hat{U}}{\hat{U}_0}} = \mathrm{e}^{\int_0^{\hat{\tau}}\frac{1}{\hat{U}}\frac{\partial\hat{U}}{\partial\hat{\tau}}\,\mathrm{d}\hat{\tau}} = \mathrm{e}^{-\int_0^{\hat{\tau}}\left(\hat{U}(2\hat{V}+2\alpha_1-\alpha_2-4)+\hat{V}(2\hat{V}-3)\right)\,\mathrm{d}\hat{\tau}},$$

where $\hat{U}_0$ is the initial value of $\hat{U}$ when $\hat{\tau} = 0$ and similarly from Eq. 4.11 that

$$\hat{U}_0\zeta_1 = \mathrm{e}^{\ln\hat{U}_0\zeta_1} = \mathrm{e}^{\int_0^{\tau}\frac{1}{\zeta_1}\frac{\partial\zeta_1}{\partial\tau}\,\mathrm{d}\tau} = \mathrm{e}^{-\int_0^{\tau}\left(\zeta_1(3\zeta_2+2\alpha_1-\alpha_2-4)+2\zeta_2(\zeta_2-1)\right)\,\mathrm{d}\tau},$$

it can be easily shown that the transformation back to the physical variables is

$$\begin{aligned}
\xi &= \sqrt{|(2-\alpha_1-\alpha_2)H_0\Gamma_0\zeta_1|}\,\mathrm{e}^{-\frac{1}{2}\int_0^{\tau}\left((2\alpha_1-\alpha_2)\zeta_1+\zeta_2(2\zeta_2+3\zeta_1)\right)\,\mathrm{d}\tau}, \\
H &= H_0(\pm t)^{\frac{\alpha_1}{2-\alpha_1-\alpha_2}}\,\mathrm{e}^{-\int_0^{\tau}\left((2\alpha_1-\alpha_2)\zeta_1+\zeta_2(\zeta_2+\zeta_1)\right)\,\mathrm{d}\tau}, \\
\Gamma &= \Gamma_0(\pm t)^{\frac{\alpha_2}{2-\alpha_1-\alpha_2}}\,\mathrm{e}^{-\int_0^{\tau}\left(\zeta_2(\zeta_2+2\zeta_1)\right)\,\mathrm{d}\tau}, \qquad (4.12)
\end{aligned}$$

where $\Gamma_0 \equiv C_1^{\frac{2\alpha_2}{\alpha_1+\alpha_1}}/C_0$ and $H_0 \equiv C_1^{\frac{2\alpha_1}{\alpha_1+\alpha_2}} C_0 U_0/(2-\alpha_1-\alpha_2)$. The absolute value under the square root in the expression for ξ in Eq. 4.12 is related to the $\pm$ in the definition of ξ above. In the (ζ_1, ζ_2) variables, the $\zeta_1 > 0$ upper half plane always corresponds to solutions which spread in time, while the $\zeta_1 < 0$ lower half plane corresponds to solutions which collapse as time increases. For $(2-\alpha_1-\alpha_2) > 0$ the spreading solutions come from the plus sign in $\pm$ and the collapsing solutions correspond to the minus sign, while the opposite is true for $(2-\alpha_1-\alpha_2) < 0$. We are primarily interested in the case where $\zeta_1 > 0$ and $(2-\alpha_1-\alpha_2) > 0$ corresponding to spreading solutions which are and valid for all $t > 0$. The infinite non-elementary fixed point of Jensen is mapped to the origin $(\zeta_1, \zeta_2) = (0, 0)$ in these coordinates, and the other infinite critical point is mapped to $(\zeta_1, \zeta_2) = (0, \frac{1-n}{3})$. This second fixed point coincides with the origin when $n = 1$, which explains the difference in the infinite fixed points in Fig. 4.2(a) and (b).

Near origin behavior of the inner droplet

Next the behavior of the planar system in Eq. 4.11 near the $(\zeta_1, \zeta_2) = (0, 0)$ fixed point will be studied in detail. Near the origin, the cubic terms can be neglected and the system is well approximated by the quadratic system

$$\begin{aligned}
\frac{\partial \zeta_1}{\partial \tau} &\approx q(\zeta_1, \zeta_2) \equiv \zeta_1((2\alpha_1 - \alpha_2 - 4)\zeta_1 - 2\zeta_2), \\
\frac{\partial \zeta_2}{\partial \tau} &\approx p(\zeta_1, \zeta_2) \equiv (n-1)\zeta_2^2 + 2(\alpha_1 - \alpha_2 + n - 1)\zeta_2\zeta_1 - 2\alpha_2\zeta_1^2.
\end{aligned} \tag{4.13}$$

The Darboux theory of integrability is concerned with the algebraic invariant curves of polynomial dynamical systems like that of Eq. 4.13 [89]. The zero level set of a polynomial $f(\zeta_1, \zeta_2) = 0$ is an called an algebraic invariant curve if $\frac{\partial f}{\partial \zeta_2} p(\zeta_1, \zeta_2) + \frac{\partial f}{\partial \zeta_1} q(\zeta_1, \zeta_2) = k(\zeta_1, \zeta_2) f(\zeta_1, \zeta_2)$ for some "cofactor" polynomial k of degree one or less. The algebraic invariant curves are special trajectories of Eq. 4.13 which play a role similar to the eigenvectors of the elementary fixed points. There are three algebraic invariant curves for the approximate system in Eq. 4.13, namely

$$\begin{aligned}
&f_1(\zeta_1, \zeta_2) = \zeta_1, \quad k_1(\zeta_1, \zeta_2) = -2\zeta_2 + (2\alpha_1 - \alpha_2 - 4)\zeta_1, \\
&f_2(\zeta_1, \zeta_2) = \zeta_2 + 2\zeta_1, \quad k_2(\zeta_1, \zeta_2) = (n-1)\zeta_2 - 2(2 - \alpha_1 + \alpha_2)\zeta_1, \\
&f_3(\zeta_1, \zeta_2) = \zeta_2 - \frac{\alpha_2}{n+1}\zeta_1, \quad k_3(\zeta_1, \zeta_2) = (n-1)\zeta_2 + (2\alpha_1 - \alpha_2 + 2(n-1))\zeta_1.
\end{aligned}$$

The algebraic invariant curves $f_i(\zeta_1, \zeta_2) = 0$ are approximations to the separatrices of the planar system along which trajectories may approach the origin. Since the cofactors satisfy the relation $\sum_i \lambda_i k_i = 0$, where $\lambda_1 \equiv (n-1)(\alpha_2 + 2n + 2)$,

$\lambda_2 \equiv (2\alpha_1 - \alpha_2)(n+1)$, and $\lambda_3 \equiv -2(n+1)(\alpha_1 - 2) + \alpha_2(n+3)$, it follows by the theorem of Darboux that the quantity

$$\mathscr{W}(\zeta_1, \zeta_2) \equiv \frac{\zeta_1^{(n-1)(\alpha_2+2(n+1))} \left(\zeta_2 + 2\zeta_1\right)^{(2\alpha_1-\alpha_2)(n+1)}}{\left(\zeta_2 - \frac{\alpha_2}{n+1}\zeta_1\right)^{2(n+1)(\alpha_1-2)-\alpha_2(n+3)}}$$

is a first integral of the system and hence approximately constant along trajectories near the origin.

The first two invariant algebraic curves f_1 and f_2 result in singular transformations when inserted into Eq. 4.12 and are of less interest, but the third curve f_3 is of significant interest. By solving $f_3(\zeta_1, \zeta_2) = 0$ for ζ_2 and changing integration variables in Eq. 4.12 from τ to ζ_1 using Eq. 4.11, an approximation to solutions that correspond to this trajectory can be made. The result is

$$\begin{aligned}
\xi &\approx \sqrt{|(2-\alpha_1-\alpha_2)H_0\Gamma_0\zeta_0|}\left(\frac{\zeta_1(C_2 - C_3\zeta_0)}{\zeta_0(C_2 - C_3\zeta_1)}\right)^{\frac{\alpha_2+2(n+1)}{(4-2\alpha_1+\alpha_2)(n+1)+2\alpha_2}}, \\
\tilde{H} &\approx H_0\left(\frac{\zeta_1}{\zeta_0}\right)^{\frac{(2\alpha_1-\alpha_2)(n+1)}{(4-2\alpha_1+\alpha_2)(n+1)+2\alpha_2}}\left(\frac{C_2 - C_3\zeta_0}{C_2 - C_3\zeta_1}\right)^{\frac{(\alpha_2+2(n+1))((2\alpha_1-\alpha_2)(n+1)+2(\alpha_2+n+1))}{(2\alpha_2+3(n+1))((4-2\alpha_1+\alpha_2)(n+1)+2\alpha_2)}}, \\
\tilde{\Gamma} &\approx \Gamma_0\left(\frac{C_2 - C_3\zeta_0}{C_2 - C_3\zeta_1}\right)^{\frac{\alpha_2+2(n+1)}{2\alpha_2+3(n+1)}},
\end{aligned} \tag{4.14}$$

where $C_2 \equiv (n+1)\left((4 - 2\alpha_1 + \alpha_2)(n+1) + 2\alpha_2\right)$ and $C_3 \equiv \alpha_2\left(2\alpha_2 + 3(n+1)\right)$ and ζ_0 is the initial value of ζ_1. As $\zeta_1 \to 0$, it can be seen easily that the asymptotic behavior of h will either be zero or infinite unless $2\alpha_1 - \alpha_2 = 0$. Furthermore in this case, the exponent in ξ in Eq. 4.14 simplifies to $\frac{\alpha_2+2(n+1)}{(4-2\alpha_1+\alpha_2)(n+1)+2\alpha_2} = 1/2$ and thus $\xi \to 0$ as $\zeta_1 \to 0$ for such solutions. This is the main result of this study – solutions with exponents $\alpha_2 = 2\alpha_1$ (or equivalently $\alpha = \frac{\alpha_1}{\alpha_1+\alpha_2} = 1/3$ in the notation of Jensen [71]) describe well-behaved, self-similar spreading near $\xi = 0$.

Two special cases have simple exact solutions when $\alpha_2 = 2\alpha_1$. First, when $\alpha_1 = 0$ and $\alpha_2 = 0$, an exact solution is simply the spatially constant solution $H = H_0$ and $\Gamma = \Gamma_0$. This solution is somewhat degenerate since the solution does not depend on ξ, but it gives an indication of how less degenerate solutions with nearby scaling exponents behave. On the other hand, when $\alpha_1 = -(n+1)/2$ and $\alpha_2 = -(n+1)$, an exact solution is $H = t^{-(n+1)/(7+3n)}H_0$ and $\Gamma = t^{-2(n+1)/(7+3n)}\left(\Gamma_0 - \xi^2/(7+3n)H_0\right)$ for $\xi \leq \sqrt{(7+3n)H_0\Gamma_0}$. Both these exact solutions correspond to flat film profiles. If surfactant is deposited onto a flat film, we might expect that the inner droplet will evolve with scaling exponents near $\alpha_1 \approx 0$ and $\alpha_2 \approx 0$ or $\alpha_1 \approx -(n+1)/2$ and $\alpha_2 \approx -(n+1)$. Indeed, our finite element simulations below support this assertion.

The asymptotic form in Eq. 4.14 was used to find well-behaved solutions of Eq. 4.6 numerically in Fig. 4.3 below starting with a small value for ζ_0 which is the initial point of numerical integration. At ζ_0, the initial values of ξ, $\tilde{H} \equiv H/(\pm t)^{\frac{\alpha_1}{2-\alpha_1-\alpha_2}}$, and $\tilde{\Gamma} \equiv \Gamma/(\pm t)^{\frac{\alpha_2}{2-\alpha_1-\alpha_2}}$ are found using Eq. 4.14, and the initial value of $\frac{\partial\tilde{\Gamma}}{\partial\xi}$ is found with $\frac{\partial\tilde{\Gamma}}{\partial\zeta_1}/\frac{\partial\xi}{\partial\zeta_1}\Big|_{\zeta_1=\zeta_0}$ with the $\tilde{\Gamma}$ and ξ from Eq. 4.14. For $\alpha_1 < -2$, both the film height

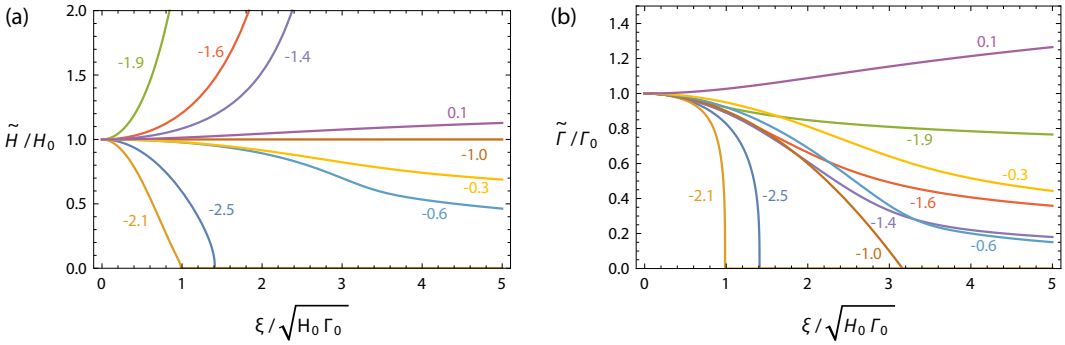

Figure 4.3: Well-behaved $n = 1$ self-similar solutions with $\alpha_2 = \alpha_1$. The film thickness (a) and surfactant concentration (b) are finite and non-zero at the origin. The value of α_1 is shown next to each curve.

$\tilde{H}$ and the surfactant concentration $\tilde{\Gamma}$ are concave at the origin and reach zero at a finite distance from the origin, and the solution is drop-like. For $-2 < \alpha_1 < -1$, the film height $\tilde{H}$ is convex while the surfactant concentration $\tilde{\Gamma}$ is concave at the origin. For $-1 < \alpha < 0$, both the film height $\tilde{H}$ and the surfactant concentration $\tilde{\Gamma}$ are concave at the origin. For $0 < \alpha < 2/3$, both the film height $\tilde{H}$ and the surfactant concentration $\tilde{\Gamma}$ are convex at the origin. For $\alpha_1 > 2/3$ (not pictured), one must either choose minus in the $\pm t$ to attain a spreading solution which then blows up as $t \to 0$ or the solutions correspond to collapsing behavior. It is clear that the solutions with $\alpha_2 = 2\alpha_1$ describe a variety of surfactant spreading behaviors.

Fixed points and bifurcations

An interesting feature of the exponents with well behaved solutions near the origin $\alpha_2 = 2\alpha_1$ and the scaling exponents of Jensen and Grotberg's solution $\alpha_1 = 0$ and $\alpha_2 = -2$ for $n = 1$ is apparent in the (ζ_1, ζ_2) plane – different fixed points of the planar system coincide at these values. There is a second fixed point located at

$$(\zeta_1^2, \zeta_2^2) \equiv \left(-\frac{1}{2}(2\alpha_1 - \alpha_2), 2\alpha_1 - \alpha_2\right),$$

which coincides with the origin when $\alpha_2 = 2\alpha_1$. This transcritical bifurcation is one example of a complicated structure of bifurcations that exist as the scaling exponents

α_1 and α_2 vary. A bifurcation occurs when the real part of one of the eigenvalues of the Jacobian matrix

$$\begin{pmatrix} 2\zeta_2(\zeta_2-1)+2\zeta_1(3\zeta_2+2\alpha_1-\alpha_2-4) & \zeta_1(3\zeta_1+4\zeta_2-2) \\ 4\zeta_1(\zeta_2-\alpha_2)+2\zeta_2(3\zeta_2+\alpha_1-\alpha_2) & 9\zeta_2^2+12\zeta_1\zeta_2+2\zeta_1(\zeta_1+\alpha_1-\alpha_2) \end{pmatrix}$$

passes through zero. It is straightforward to show that the eigenvalues of the Jacobian at (ζ_1^2, ζ_2^2) are $(2+\alpha_1)(2\alpha_1-\alpha_2)$ and $\frac{1}{2}(2\alpha_1-\alpha_2)^2$, so that local transcritical bifurcations occur along the two lines $\alpha_1 = -2$ and $\alpha_2 = 2\alpha_1$.

In addition to (ζ_1^2, ζ_2^2), there are two other finite fixed points

$$(\zeta_1^\pm, \zeta_2^\pm) \equiv \left(\frac{(4+2\alpha_1+\alpha_2 \pm \alpha_3)(12-2\alpha_1-\alpha_2 \mp \alpha_3)}{8(2-\alpha_1-\alpha_2)}, \frac{1}{2}(-4-2\alpha_1-\alpha_2 \pm \alpha_3) \right),$$

where $\alpha_3 \equiv \sqrt{24(2+\alpha_2)+(2\alpha_1+\alpha_2)^2}$. The eigenvalues of the Jacobian at the fixed points $(\zeta_1^\pm, \zeta_2^\pm)$ are somewhat complicated, and it is easier to identify bifurcations with the determinant and trace. For the real planar system, either both eigenvalues are real or the eigenvalues come in a complex conjugate pair. If a real eigenvalue passes through zero, the determinant of the Jacobian vanishes. If the real part of a complex pair of eigenvalues passes through zero, the trace of the Jacobian matrix vanishes. We can therefore find all the local bifurcations by identifying where the determinant or the trace of the Jacobian at a fixed point vanishes. The determinant of the Jacobian at $(\zeta_1^\pm, \zeta_2^\pm)$ has two factors,

$$-\frac{4+2\alpha_1+\alpha_2 \pm \alpha_3}{2-\alpha_1-\alpha_2}$$

and

$$\begin{aligned} &((\alpha_1+2)\alpha_2+2(\alpha_1-4)(\alpha_1-2))\left((2\alpha_1+\alpha_2)^2+24(\alpha_2+2)\right) \\ &\quad \pm \alpha_3\left(4\left(\alpha_1^2+\alpha_1-14\right)\alpha_2+(\alpha_1+2)\alpha_2^2+4(\alpha_1-2)((\alpha_1-4)\alpha_1+12)\right), \end{aligned}$$

while the trace of the Jacobian at $(\zeta_1^\pm, \zeta_2^\pm)$ has two factors

$$-\frac{4+2\alpha_1+\alpha_2 \pm \alpha_3}{2-\alpha_1-\alpha_2}$$

and

$$\begin{aligned} &2(\alpha_1+22)\alpha_2^2+4(3(\alpha_1-2)\alpha_1+16)\alpha_2+8(\alpha_1-3)(\alpha_1-2)^2-\alpha_2^3 \\ &\quad \pm \alpha_3\left(4(\alpha_1-4)\alpha_2+4(\alpha_1-2)^2-\alpha_2^2\right). \end{aligned}$$

Setting the determinant to zero and solving for α_3 results in

$$\pm\alpha_3 = -(4 + 2\alpha_1 + \alpha_2),$$
$$\pm\alpha_3 = -\frac{((\alpha_1+2)\alpha_2 + 2(\alpha_1-4)(\alpha_1-2))\left((2\alpha_1+\alpha_2)^2 + 24(\alpha_2+2)\right)}{4\left(\alpha_1^2+\alpha_1-14\right)\alpha_2 + (\alpha_1+2)\alpha_2^2 + 4(\alpha_1-2)((\alpha_1-4)\alpha_1+12)},$$

while setting the trace to zero and solving for α_3 results in an additional

$$\pm\alpha_3 = -(4 + 2\alpha_1 + \alpha_2),$$
$$\pm\alpha_3 = -\frac{2(\alpha_1+22)\alpha_2^2 + 4(3(\alpha_1-2)\alpha_1+16)\alpha_2 + 8(\alpha_1-3)(\alpha_1-2)^2 - \alpha_2^3}{4(\alpha_1-4)\alpha_2 + 4(\alpha_1-2)^2 - \alpha_2^2}.$$

Substituting into $0 = \alpha_3^2 - 24(2+\alpha_2) + (2\alpha_1+\alpha_2)^2$, which also vanishes by the definition of α_3 above, the determinant and the trace vanish when

$$16(2 - \alpha_1 + \alpha_2)$$

vanishes, the determinant vanishes when

$$-\frac{192(\alpha_1+2)(2-\alpha_1+\alpha_2)(2-\alpha_1-\alpha_2)^2\left((2\alpha_1+\alpha_2)^2+24(\alpha_2+2)\right)}{\left(4\left(\alpha_1^2+\alpha_1-14\right)\alpha_2+(\alpha_1+2)\alpha_2^2+4(\alpha_1-2)((\alpha_1-4)\alpha_1+12)\right)^2}$$

vanishes, and the trace vanishes when

$$\frac{48(2-\alpha_1-\alpha_2)^2\left(-2(7\alpha_1+2)\alpha_2^2 - 4(\alpha_1+2)^2\alpha_2 + 4(\alpha_1-2)^2(2\alpha_1+1) + 3\alpha_2^3\right)}{\left(-4(\alpha_1-4)\alpha_2 - 4(\alpha_1-2)^2 + \alpha_2^2\right)^2}$$

vanishes. Finally we can enumerate the local bifurcations. Whenever the determinant vanishes, one of the eigenvalues is zero and there is a bifurcation. When $\alpha_1 = -2$, there is a finite transcritical bifurcation. When $2-\alpha_1+\alpha_2 = 0$ or $\alpha_2 = 2\alpha_1$, there are transcritical bifurcations where a fixed point passes through zero. When $2-\alpha_1-\alpha_2 = 0$, there is an infinite transcritical bifurcation in which one of the fixed points passes through an infinite fixed point. When $(2\alpha_1+\alpha_2)^2 + 24(\alpha_2+2) = 0$, there is a saddle-node bifurcation. The vanishing of the trace does not guarantee a bifurcation, since the trace will also vanish when there are two real and opposite eigenvalues. However, some of the branches of the solution to the cubic equation $-2(7\alpha_1+2)\alpha_2^2 - 4(\alpha_1+2)^2\alpha_2 + 4(\alpha_1-2)^2(2\alpha_1+1) + 3\alpha_2^3 = 0$ give rise to Andronov-Hopf bifurcations. These branches come to an end at four points where the determinant simultanously vanishes, which are $\alpha_1 = 2$, $\alpha_2 = 0$ and three points which lie on the parabola $(2\alpha_1+\alpha_2)^2 + 24(\alpha_2+2) = 0$. These local bifurcations

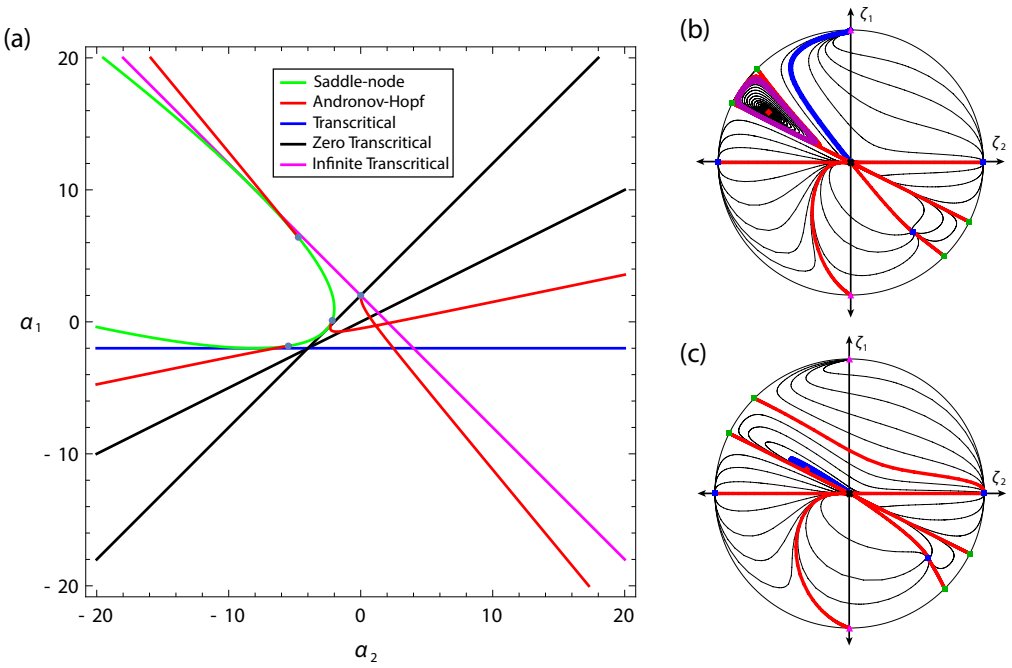

Figure 4.4: Bifurcations in the (ζ_1, ζ_2) phase portrait. (a) Local bifurcations as the scaling exponents α_1 and α_2 vary and phase portraits for (b) $\alpha_1 = -0.8$ and $\alpha_2 = -1.6$ and (c) for $\alpha_1 = -1.5$ and $\alpha_2 = -3.0$. The purple limit cycle in (b) collides with the red and blue heteroclinic orbits and the separatrices rearrange themselves to the structure in (c) during a heteroclinic bifurcation.

are depicted in Fig. 4.4 below. In addition to these local bifurcation, there is a rich structure of global heteroclinic and homoclinic bifurcations, when separatrices of fixed points rearrange themselves and the topological structure of the phase portrait changes. One such heteroclinic bifurcation occurs at $\alpha_1 = -1$ and $\alpha_2 = -2$ and is depicted in Fig. 4.4. These local and global bifurcations signal scaling exponents for which the asymptotic behavior of some of the self-similar solutions changes. It is interesting to note that several solutions which appear to have physical significance occurs exactly at such bifurcations. Lastly, while we have focused here on the $n = 1$ rotationally invariant case, we note that the $n = 0$ translationally invariant case is qualitatively identical.

Finite element simulations

To verify the $\alpha_2 = 2\alpha_1$ predicted scaling behavior of the inner droplet, axisymmetric finite element simulations have been implemented. Simulations were carried out in the rescaled variables of the $\alpha_1 = 0$ and $\alpha_2 = -2$ solution of Jensen and Grotberg, with dependent variables $\xi \equiv R/t^{1/4}$ and $\nu \equiv \log t$ and dependent variables $\tilde{H} = H$ and $\tilde{\Gamma} = t^{1/2}\Gamma$. Diffusive terms were neglected, but a small capillary term was

included to regularize the solution, with $\bar{\mathrm{Pe}}^{-1} = 0$ and $\bar{\mathrm{Ca}}^{-1} = 10^{-6}$. Assuming an axisymmetric solution, Eq. 4.1 is transformed to

$$
\begin{aligned}
0 &= \frac{\partial \tilde{H}}{\partial \nu} - \frac{\xi}{4}\frac{\partial \tilde{H}}{\partial \xi} + \frac{1}{\xi}\frac{\partial}{\partial \xi}\left(\xi\left(-\frac{\tilde{H}^2}{2}\frac{\partial \tilde{\Gamma}}{\partial \xi} + \frac{10^{-6}}{3}\tilde{H}^3\frac{\partial}{\partial \xi}\left(\frac{1}{\xi}\frac{\partial}{\partial \xi}\left(\xi\frac{\partial \tilde{H}}{\partial \xi}\right)\right)\right)\right), \\
0 &= \frac{\partial \tilde{\Gamma}}{\partial \nu} - \frac{\tilde{\Gamma}}{2} - \frac{\xi}{4}\frac{\partial \tilde{\Gamma}}{\partial \xi} + \frac{1}{\xi}\frac{\partial}{\partial \xi}\left(\xi\left(-\tilde{H}\tilde{\Gamma}\frac{\partial \tilde{\Gamma}}{\partial \xi} + \frac{10^{-6}}{2}\tilde{H}^2\tilde{\Gamma}\frac{\partial}{\partial \xi}\left(\frac{1}{\xi}\frac{\partial}{\partial \xi}\left(\xi\frac{\partial \tilde{H}}{\partial \xi}\right)\right)\right)\right).
\end{aligned}
\tag{4.15}
$$

An integration domain $0 < \xi < 2$ was used which is twice as large as the expected shock front structure. Boundary conditions were $\tilde{H}|_{\xi=2} = 1$ and $\tilde{\Gamma}|_{\xi=2} = 0$ to be consistant with an unperturbed downstream film. Initial conditions were a flat film profile $\tilde{H}|_{\nu=0} = 1$ and a quadratic surfactant distribution localized to $\xi < 1$ with $\tilde{\Gamma}|_{\nu=0} = 10^{-4} + 1/8(1-\xi^2)$ for $\xi \leq 1$ and $\tilde{\Gamma}|_{\nu=0} = 10^{-4}$ for $1 < \xi < 2$ with a small nonzero downstream surfactant concentration included to help regularize the numerics. Equation 4.15 was integrated numerically with the commercial finial element software Comsol. Results of this integration are depicted in Fig. 4.5 below. The solution was found to converge to the self-similar solution of Jensen and Grotberg in the spreading ridge portion of the domain with scaling exponents $\alpha_1 = 0$ and $\alpha_2 = -2$. Around the inner droplet, different local scaling exponents $\alpha_1^{\mathrm{loc}} \approx -1.0$ and $\alpha_2^{\mathrm{loc}} \approx -2.0$ were observed that varied only slowly with time. It was also verified that the capillary contribution to the flux was significantly smaller than the Marangoni contribution in the inner droplet portion of the domain throughout the simulation so that Eq. 4.2 provides a good approximation for the evolution of inner droplet. The condition that $\alpha_2 = 2\alpha_1$ at the origin was very well satisfied throughout the simulation in the inner droplet domain.

To study the evolution of the inner droplet, note that if $\tilde{H}$ and $\tilde{\Gamma}$ scale as in Eq. 4.12 for arbitrary α_1 and α_2 other than 0 and -2, then it follows that

$$
\begin{aligned}
\tilde{H} &= t^{\frac{\alpha_1}{2-\alpha_1-\alpha_2}}\tilde{\tilde{H}}\left(t^{\frac{1}{4}-\frac{1}{2-\alpha_1-\alpha_2}}\xi\right), \\
\tilde{\Gamma} &= t^{\frac{1}{2}+\frac{\alpha_2}{2-\alpha_1-\alpha_2}}\tilde{\tilde{\Gamma}}\left(t^{\frac{1}{4}-\frac{1}{2-\alpha_1-\alpha_2}}\xi\right)
\end{aligned}
$$

for some function $\tilde{\tilde{H}}$ and $\tilde{\tilde{\Gamma}}$. It then follows that

$$
\begin{aligned}
t\frac{\partial \tilde{H}}{\partial t} &= \frac{\alpha_1}{2-\alpha_1-\alpha_2}\tilde{H} + \left(\frac{1}{4} - \frac{1}{2-\alpha_1-\alpha_2}\right)\xi\frac{\partial \tilde{H}}{\partial \xi}, \\
t\frac{\partial \tilde{\Gamma}}{\partial t} &= \left(\frac{1}{2} + \frac{\alpha_2}{2-\alpha_1-\alpha_2}\right)\tilde{\Gamma} + \left(\frac{1}{4} - \frac{1}{2-\alpha_1-\alpha_2}\right)\xi\frac{\partial \tilde{\Gamma}}{\partial \xi}.
\end{aligned}
$$

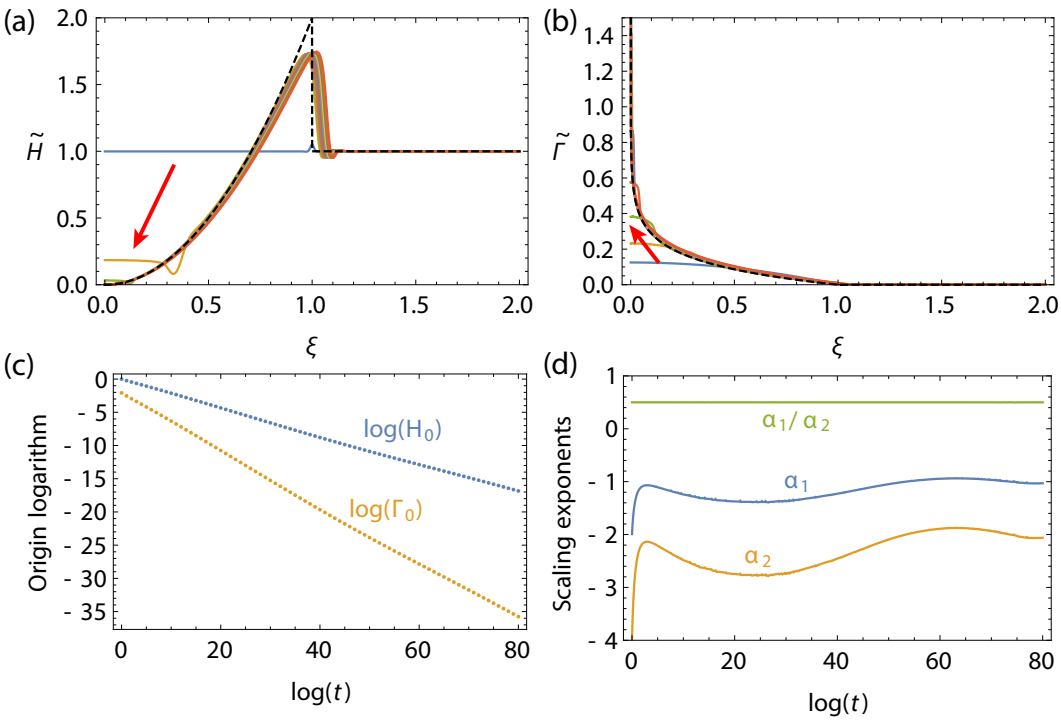

Figure 4.5: Finite element simulations. The film height (a) and surfactant concentration (b) evolution is indicated by red arrows, and the solutions collapse towards the self-similar solutions of Jensen and Grotberg (dashed lines) in the spreading ridge portion of the domain. (c) The logarithm of the film height $H_0 \equiv H|_{\xi=0}$ and the surfactant concentration $\Gamma_0 \equiv \Gamma|_{\xi=0}$ at the origin vs the logarithm of time shows a near linear relationship, indicating a scale invariant evolution. (d) By monitoring the local slope of this log-log plot, local estimates of the scaling exponents α_1 and α_2 were made. The condition $\alpha_2 = 2\alpha_1$ at the origin is very well satisfied throughout the simulation.

This equation is simply the statement that the characteristic vanishes for group invariant solutions noted in Eq. 2.8. We can invert these equations and solve for α_1 and α_2 to define local numerical values for the scaling exponents,

$$\alpha_1^{\text{loc}} \equiv \frac{4\left(2\tilde{\Gamma}t\frac{\partial\tilde{H}}{\partial t} + t\frac{\partial\tilde{\Gamma}}{\partial t}\xi\frac{\partial\tilde{H}}{\partial\xi} - \xi\frac{\partial\tilde{\Gamma}}{\partial\xi}t\frac{\partial\tilde{H}}{\partial t}\right)}{2\tilde{\Gamma}\tilde{H} + 4\tilde{\Gamma}t\frac{\partial\tilde{H}}{\partial t} - \tilde{\Gamma}\xi\frac{\partial\tilde{H}}{\partial\xi} + 4t\frac{\partial\tilde{\Gamma}}{\partial t}\tilde{H} - \xi\frac{\partial\tilde{\Gamma}}{\partial\xi}\tilde{H}},$$

$$\alpha_2^{\text{loc}} \equiv -\frac{2\left(2\tilde{\Gamma}\tilde{H} - \tilde{\Gamma}\xi\frac{\partial\tilde{H}}{\partial\xi} - 4t\frac{\partial\tilde{\Gamma}}{\partial t}\tilde{H} + 2t\frac{\partial\tilde{\Gamma}}{\partial t}\xi\frac{\partial\tilde{H}}{\partial\xi} - \xi\frac{\partial\tilde{\Gamma}}{\partial\xi}\tilde{H} - 2\xi\frac{\partial\tilde{\Gamma}}{\partial\xi}t\frac{\partial\tilde{H}}{\partial t}\right)}{2\tilde{\Gamma}\tilde{H} + 4\tilde{\Gamma}t\frac{\partial\tilde{H}}{\partial t} - \tilde{\Gamma}\xi\frac{\partial\tilde{H}}{\partial\xi} + 4t\frac{\partial\tilde{\Gamma}}{\partial t}\tilde{H} - \xi\frac{\partial\tilde{\Gamma}}{\partial\xi}\tilde{H}}. \quad (4.16)$$

These local scaling exponents are equivalent to the values obtained from the instantaneous slope in a log-log plot of the film thickness and surfactant concentrations at fixed ξ vs time provided they remain relatively constant in space and time.

In addition to observing the scaling behavior at the origin, fully two-dimensional

finite element simulations have also been implemented. A droplet shaped film profile with an anisotropic initial surfactant concentration confined to a circular domain was studied. The initial conditions were that of a droplet of height seven times larger than the unperturbed film, with $\tilde{H}|_{t=1} = 7 - \frac{486}{31}\xi^2 + \frac{300}{31}\xi^4$, and the anisotropic surfactant distributions was $\tilde{\Gamma}|_{t=1} = \left(1/8 + \xi^2\cos(3\theta)\cos(10\theta)/20\right)\left(1-\xi^2\right)$, which has the same total surfactant mass as the solution of Jensen and Grotberg but is otherwise arbitrary. A slightly different domain was employed in these simulations with the domain boundary being $\xi = 1$ at the shock front rather than $\xi = 2$. For the surfactant concentration the boundary conditions were $\tilde{\Gamma}|_{\xi=1} = 0$ since it is assumed that no surfactant is present beyond the spreading front. For the film thickness, the boundary condition was $\tilde{H}|_{\xi=1} = 2 - 1/t$ to be compatible with the initial condition at $t = 1$ but also to match the expected boundary conditions of the $\alpha_1 = 0$, $\alpha_2 = -2$ solution of Jensen and Grotberg at large times. By seeding the inner droplet with an anisotropic surfactant distribution, finger of fluid were observed to grow with time at drained front boundary between the inner droplet and the spreading ridge portions of the domain, as depicted in Fig. 4.6(a). These fingers split as they grew, much like the observed digitated fingering experiments depicted in Fig. 4.6(b).

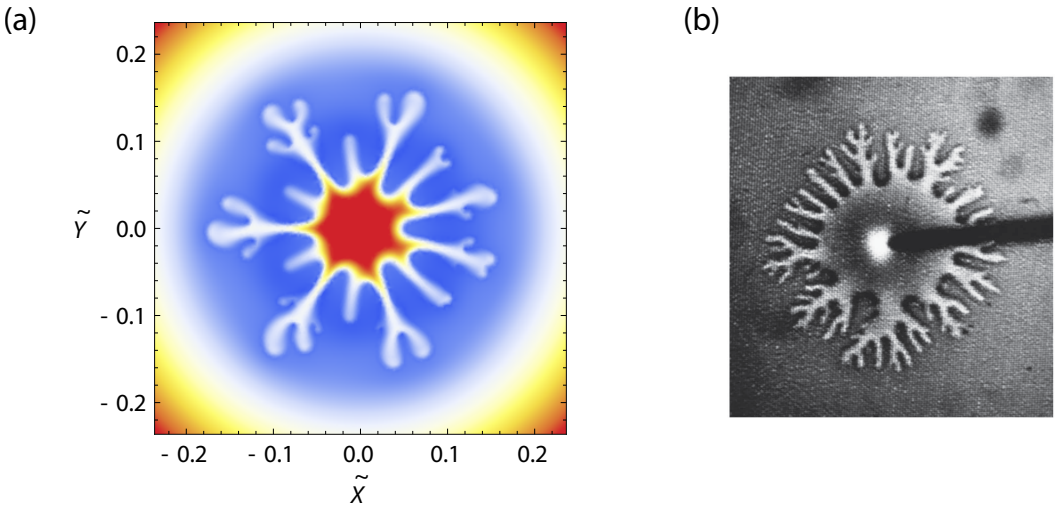

Figure 4.6: Anisotropic finite element simulations exhibit finger splitting. (a) Contour plot of the film thickness at $\log(t) = 15$ and (b) digitated fingering process observed in the experiments of Troian [90].

Special solutions

There are several special solutions to planar polynomial systems, namely the fixed points and the invariant algebraic curves. The algebraic invariant curves of order

less than eight and the special values of α_1, α_2, and n with additional algebraic invariant curves in phase planes have been uncovered with the aid of Mathematica. Many of these solutions have been found elsewhere in the literature, but they are included in Table 4.1 below for completeness.

---

(1) The two fixed points

$$\zeta_1^{\pm} = \frac{(2\alpha_1 - \alpha_3 + \alpha_2 - 3n - 9)(2\alpha_1 - \alpha_3 + \alpha_2 + 3n + 1)}{8(\alpha_1 + \alpha_2 - 2)},$$
$$\zeta_2^{\pm} = \frac{1}{2}(-2\alpha_1 + \alpha_3 - \alpha_2 - 3n - 1),$$

give rise to power-law solutions

$$\xi = \begin{cases} X/\left(\pm t\right)^{\frac{1}{2-\alpha_2-\alpha_2}} & \text{for } n = 0, \\ R/\left(\pm t\right)^{\frac{1}{2-\alpha_2-\alpha_2}} & \text{for } n = 1, \end{cases}$$
$$H = (\pm t)^{\frac{\alpha_1}{2-\alpha_2-\alpha_2}} \frac{8H_0(\alpha_1 + \alpha_2 - 2)\left(\frac{\sqrt{\Gamma_0(-H_0)(\alpha_1+\alpha_2-2)}}{\xi}\right)^{\frac{1}{2}(-2\alpha_1-\alpha_3-\alpha_2-3n-5)}}{(2\alpha_1 + \alpha_3 + \alpha_2 - 3n - 9)(2\alpha_1 + \alpha_3 + \alpha_2 + 3n + 1)},$$
$$\Gamma = \pm\,(\pm t)^{\frac{\alpha_2}{2-\alpha_2-\alpha_2}}\,\Gamma_0\left(\frac{\sqrt{\Gamma_0(-H_0)(\alpha_1 + \alpha_2 - 2)}}{\xi}\right)^{\frac{1}{2}(2\alpha_1+\alpha_3+\alpha_2+3n+1)},$$

where

$$\alpha_3 \equiv \pm\sqrt{(2\alpha_1 + \alpha_2)^2 - 4\alpha_1 + 14\alpha_2 + 9n^2 + 2n(2\alpha_1 + 5\alpha_2 + 11) + 17}.$$

The $\pm$ associated with α_3 here must have the same sign as the fixed point $(\zeta_1^{\pm}, \zeta_2^{\pm})$, while the $\pm$ associated with t must have the same sign as that associated with Γ.

(2) When $\alpha_2 = -(n + 1)$, the algebraic invariant curve $\zeta_2 + \zeta_1 = 0$ gives rise to surfactant mass conserving solutions

$$\xi = \begin{cases} X/\left(\pm t\right)^{\frac{1}{3+n-\alpha_1}} & \text{for } n = 0, \\ R/\left(\pm t\right)^{\frac{1}{3+n-\alpha_1}} & \text{for } n = 1, \end{cases}$$
$$H = (\pm t)^{\frac{\alpha_1}{3+n-\alpha_1}}\, H_0 \xi^{2\alpha_1+n+1},$$
$$\Gamma = (\pm t)^{\frac{-n-1}{3+n-\alpha_1}}\left(\Gamma_0 \pm \frac{\xi^{1-n-2\alpha_1}}{H_0(3 + n - \alpha_1)(n - 1 + 2\alpha_1)}\right).$$

If $\alpha_1 = \frac{1-n}{2}$, the solution changes form slightly to

$$\begin{aligned}
\xi &= \begin{cases} X/\left(\pm t\right)^{2/5} & \text{for } n = 0, \\ R/\left(\pm t\right)^{1/4} & \text{for } n = 1, \end{cases} \\
H &= \left(\pm t\right)^{\frac{1-n}{5+3n}} H_0 \xi^2, \\
\Gamma &= \left(\pm t\right)^{\frac{-2(1+n)}{5+3n}} \left(\Gamma_0 \mp \frac{2}{5H_0} \log \xi\right),
\end{aligned}$$

which includes the solution of Jensen and Grotberg.

(3) When $\alpha_2 = 0$, the algebraic invariant curve $\zeta_2 = 0$ gives rise to steady solutions

$$\begin{aligned}
H &= \begin{cases} H_0 X^{\alpha_1} & \text{for } n = 0, \\ H_0 R^{\alpha_1} & \text{for } n = 1, \end{cases} \\
\Gamma &= \Gamma_0.
\end{aligned}$$

(4) When $n = 0$, $\alpha_1 = 1/3$ and $\alpha_2 = 1/3$, the algebraic invariant curve $-1 + 3\zeta_2 = 0$ gives rise to steady solutions

$$\begin{aligned}
H &= H_0 X^{1/3}, \\
\Gamma &= \Gamma_0 X^{1/3}.
\end{aligned}$$

(5) When $n = 0$, $\alpha_1 = -1/2$, and $\alpha_2 = -5/3$ the algebraic invariant curve $-1 + 3\zeta_1 + 3\zeta_2 = 0$ gives rise to solutions

$$\begin{aligned}
\xi &= X/\left(\pm t\right)^{6/25}, \\
H &= \left(\pm t\right)^{-3/25} H_0 \xi^{1/3}, \\
\Gamma &= \left(\pm t\right)^{-2/5} \Gamma_0 \xi^{1/3} \left(1 \mp \frac{9}{50 H_0 \Gamma_0} \xi^{4/3}\right).
\end{aligned}$$

(6) When $n = 0$, $\alpha_1 = 0$, and $\alpha_2 = 1$, the algebraic invariant curve $\zeta_2^2 - \zeta_1 + \zeta_1\zeta_2 = 0$ gives rise to travelling wave solutions

$$\begin{aligned}
H &= t H_0, \\
\Gamma &= \Gamma_0 \left(t \pm \frac{1}{\sqrt{H_0 \Gamma_0}} X\right).
\end{aligned}$$

(7) As $\alpha_1, \alpha_2 \to \infty$, the original variables (U, V) of Jensen are more appropriate than our rescaled versions, along with his scaling exponents $\delta \equiv \frac{1}{2-\alpha_1-\alpha_2}$ and $\alpha \equiv \frac{\alpha_1}{\alpha_1+\alpha_2}$. When $n = 0$ and $\delta = 0$, the algebraic invariant curve $4V^2 + (3 - 5\alpha)U = 0$ gives rise to quasistatic solutions

$$H = (\pm t)^{-\alpha} H_0 (X - X_0)^{(7\alpha-1)/(\alpha+1)},$$
$$\Gamma = \pm (\pm t)^{\alpha-1} \frac{(1+\alpha)^2}{4(5\alpha-3)} (X - X_0)^{(3-5\alpha)/(\alpha+1)}.$$

In this case, there are families of special values of α with additional algebraic curves which actually have a first integral $\mathscr{W}(U, V)$ which is constant along any solution. These seem to occur for values $\alpha = \frac{3i-1}{5i-1}$ and $\alpha = \frac{3i+1/4}{5i-1/4}$ where $i = 1, 2, 3, \ldots$. By solving $\mathscr{W}(U, V) = \mathscr{W}_0$ for U or V, with $\mathscr{W}_0$ a constant, Eq. 4.5 can be used to find a large family of exact quasistatic solutions.

α	$\mathscr{W}(U,V)$
$\frac{1}{2}$	$\frac{U\left(\frac{U}{8}+V^2\right)^3}{(U+3V)^4}$
$\frac{5}{9}$	$\frac{U\left(\frac{U}{18}+V^2\right)^7}{\left(2U^2+63UV^2+189V^3\right)^4}$
$\frac{4}{7}$	$\frac{U\left(\frac{U}{28}+V^2\right)^{11}}{\left(2U^3+154U^2V^2+3773UV^4+11319V^5\right)^4}$
$\frac{11}{19}$	$\frac{U\left(\frac{U}{38}+V^2\right)^{15}}{\left(16U^4+2280U^3V^2+119130U^2V^4+2640715UV^6+7922145V^7\right)^4}$
$\frac{13}{19}$	$\frac{UV^{10}}{\left(19UV-6U+57V^2\right)^4}$
$\frac{25}{39}$	$\frac{UV^{18}}{\left(U^2(28-78V)+273U(13V-4)V^2+10647V^4\right)^4}$
$\frac{37}{59}$	$\frac{UV^{26}}{\left(84U^3(59V-22)-7788U^2(59V-21)V^2+268037U(59V-18)V^4+47442549V^6\right)^4}$

(8) The algebraic invariant curves $\hat{U} = 0$ and $\zeta_1 = 0$ and the fixed points that lie on them are somewhat singular since they result in $H = 0$ or $\xi = 0$. Similarly, the the algebraic invariant curves $\zeta_2 + 2\zeta_1 = 0$ and $\hat{V} = 2$ and the fixed points they lie on them result in $\xi = \text{const}$ which cannot be inverted. While these curves and fixed points do not generally give rise to exact solutions, they can indicate the asymptotic behavior of solutions which approach them. One particular class of such solutions which may be of interest for future research are those that approach the $\zeta_1 = 0$ curve from the $\zeta_2 < 0$ half-plane, which may give qualitatively different behavior in the $n = 0$ and $n = 1$ cases because of the differing character of the fixed point at $(\zeta_1, \zeta_2) = (0, 0)$ fixed point for $n = 0$ and $n = 1$.

Table 4.1: Special solutions of Eq. 4.1. These solutions correspond to fixed points and algebraic invariant curves of the planar systems of order less than eight.

4.2 Scale invariant solutions in capillary spreading

For the surfactant spreading problem, a driven film with the special power-law forcing in Eq. 2.14, or for purely capillary films, we noted in Table 2.3 several less familiar scale invariant solutions. These solutions involved angular coordinates $\tilde{\theta}$ and included the (ii-6) scale invariant steady solutions, the (ii-4) scale invariant rotating wave solutions, the (ii-8) travelling wave scale invariant solutions, and the (ii-9) scale invariant scale invariant solutions. In this section, we will illustrate some numerical solutions of these less familiar scale invariant solutions for purely capillary films. These solutions are meant only to demonstrate that such solutions can be found, and the author hopes that visualization of these solutions will aid researchers in identifying when such behavior may be observed. One complication for these solutions is the need for periodicity in the angular coordinates. It may be possible to find solutions which are everywhere non-zero and satisfy these periodicity requirements, but for simplicity we will focus on solutions with a contact line which vanish for some interval of $\tilde{\theta}$. This allows the periodicity requirements to be trivially satisfied. After a simple rescaling of t by $\bar{\text{Ca}}$, the purely capillary thin flim equation in Eq. 1.68 takes the form

$$\frac{\partial H}{\partial t} + \nabla_L \cdot \left(\frac{H^3}{3} \nabla_L \nabla_L^2 H \right) = 0. \tag{4.17}$$

Sample solutions are depicted below. The specific parameters chosen are arbitrary, but we hope the qualitative nature of these solutions can be understood.

Steady scale invariant solutions

Recall the invariants of the steady scale invariant solutions,

$$\begin{aligned} \tilde{H} &= R^{\frac{2}{\alpha-2}} H, \\ \tilde{\theta} &= \theta + \omega \log \left(R^{\frac{1}{\alpha-2}} \right). \end{aligned}$$

We insert the ansatz $H = R^{-\frac{2}{\alpha-2}}\tilde{H}(\tilde{\theta})$ into Eq. 4.17 to derive the reduced equations

$$\begin{aligned}0 = &\frac{16}{3}\left(\alpha^2+\alpha-2\right)\tilde{H}^4 + \tilde{H}^2\left((\alpha-2)^2+\omega^2\right)^2\frac{\partial\tilde{H}}{\partial\tilde{\theta}}\frac{\partial^3\tilde{H}}{\partial\tilde{\theta}^3}\\ &-2(\alpha+1)\omega\tilde{H}^2\left((\alpha-2)^2+\omega^2\right)\frac{\partial\tilde{H}}{\partial\tilde{\theta}}\frac{\partial^2\tilde{H}}{\partial\tilde{\theta}^2}\\ &+4\tilde{H}^2\left((2\alpha-1)\omega^2+(\alpha-2)^2\right)\left(\frac{\partial\tilde{H}}{\partial\tilde{\theta}}\right)^2 - \frac{8}{3}(\alpha(2\alpha+7)-6)\omega\tilde{H}^3\frac{\partial\tilde{H}}{\partial\tilde{\theta}}\\ &+\frac{4}{3}\tilde{H}^3\left(\left(\alpha^2+\alpha-1\right)(\alpha-2)^2+(\alpha(\alpha+5)+1)\omega^2\right)\frac{\partial^2\tilde{H}}{\partial\tilde{\theta}^2}\\ &-\frac{2}{3}(2\alpha+3)\omega\tilde{H}^3\frac{\partial^3\tilde{H}}{\partial\tilde{\theta}^3}\left((\alpha-2)^2+\omega^2\right)+\frac{1}{3}\tilde{H}^3\frac{\partial^4\tilde{H}}{\partial\tilde{\theta}^4}\left((\alpha-2)^2+\omega^2\right)^2,\end{aligned}$$

and integrate numerically starting at $\tilde{\theta} = 0$. We take $\alpha = 0$ and $\omega = -0.5$ and use initial condition

$$\tilde{H}\Big|_{\tilde{\theta}=0} = 0.5, \quad \frac{\partial\tilde{H}}{\partial\tilde{\theta}}\Big|_{\tilde{\theta}=0} = 0, \quad \frac{\partial^2\tilde{H}}{\partial\tilde{\theta}^2}\Big|_{\tilde{\theta}=0} = -3, \quad \frac{\partial^3\tilde{H}}{\partial\tilde{\theta}^3}\Big|_{\tilde{\theta}=0} = 0,$$

and integrate forwards and backwards until the contact line is reached. The resulting film height profile is depicted in Fig. 4.7 below.

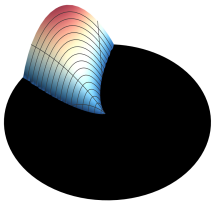

Figure 4.7: Steady scale invariant solutions. For the parameters chosen, the film height profile is a twisted, sharp finger of fluid that is constant in time.

Rotating wave scale invariant solutions

Recall the invariants of the rotating wave scale invariant solutions,

$$\tilde{H} = R^{-4/3}H,$$
$$\tilde{\theta} = \theta - \omega t.$$

We insert the ansatz $H = R^{4/3}\tilde{H}(\tilde{\theta})$ into Eq. 4.17 to derive the reduced equations

$$0 = -\omega\frac{\partial\tilde{H}}{\partial\tilde{\theta}} - \frac{320}{243}\tilde{H}^4 - \frac{4}{27}\tilde{H}^3\frac{\partial^2\tilde{H}}{\partial\tilde{\theta}^2} + \frac{16}{9}\tilde{H}^2\left(\frac{\partial\tilde{H}}{\partial\tilde{\theta}}\right)^2 + \tilde{H}^2\frac{\partial^3\tilde{H}}{\partial\tilde{\theta}^3}\frac{\partial\tilde{H}}{\partial\tilde{\theta}} + \frac{1}{3}\tilde{H}^3\frac{\partial^4\tilde{H}}{\partial\tilde{\theta}^4},$$

and integrate numerically starting at $\tilde{\theta} = 0$. We take $\omega = -0.1$ and use initial condition

$$\tilde{H}\Big|_{\tilde{\theta}=0} = 0.5, \quad \frac{\partial \tilde{H}}{\partial \tilde{\theta}}\bigg|_{\tilde{\theta}=0} = 0, \quad \frac{\partial^2 \tilde{H}}{\partial \tilde{\theta}^2}\bigg|_{\tilde{\theta}=0} = -5, \quad \frac{\partial^3 \tilde{H}}{\partial \tilde{\theta}^3}\bigg|_{\tilde{\theta}=0} = 0,$$

and integrate forwards and backwards until the contact line is reached. The resulting film height profile is depicted in Fig. 4.8 below.

(a) (b) (c)

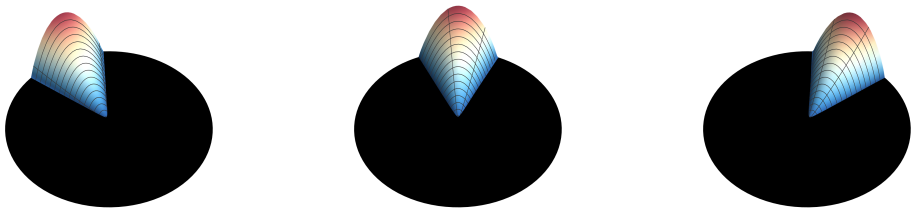

Figure 4.8: Rotating wave scale invariant solutions for (a) $t = 0$, (b) $t = 5$, and (c) $t = 10$. For the parameters chosen, the film height profile is a sharp finger of fluid that rotates while maintaining its shape.

Travelling wave scale invariant solutions

Recall the invariants of the travelling wave scale invariant solutions,

$$\tilde{H} = (X - vt)^{-1} H,$$
$$\tilde{\theta} = \arctan\left(\frac{Y}{X - vt}\right).$$

We insert the ansatz $H = (X - vt)\tilde{H}(\tilde{\theta})$ into Eq. 4.17 to derive the reduced equations

$$\begin{aligned} 0 = &-v\tilde{H} + v\sin(\tilde{\theta})\cos(\tilde{\theta})\frac{\partial \tilde{H}}{\partial \tilde{\theta}} - 2\tilde{H}^2\cos^4(\tilde{\theta})\left(\frac{\partial \tilde{H}}{\partial \tilde{\theta}}\right)^2 \\ &- 3\tilde{H}^2\sin(\tilde{\theta})\cos^3(\tilde{\theta})\frac{\partial \tilde{H}}{\partial \tilde{\theta}}\frac{\partial^2 \tilde{H}}{\partial \tilde{\theta}^2} + \tilde{H}^2\frac{\partial^3 \tilde{H}}{\partial \tilde{\theta}^3}\cos^4(\tilde{\theta})\frac{\partial \tilde{H}}{\partial \tilde{\theta}} \\ &+ 4\tilde{H}^3\sin(\tilde{\theta})\cos^3(\tilde{\theta})\frac{\partial \tilde{H}}{\partial \tilde{\theta}} + \frac{1}{3}\tilde{H}^3\cos^2(\tilde{\theta})(1 - 8\cos(2\tilde{\theta}))\frac{\partial^2 \tilde{H}}{\partial \tilde{\theta}^2} \\ &- \frac{7}{3}\tilde{H}^3\frac{\partial^3 \tilde{H}}{\partial \tilde{\theta}^3}\sin(\tilde{\theta})\cos^3(\tilde{\theta}) + \frac{1}{3}\tilde{H}^3\frac{\partial^4 \tilde{H}}{\partial \tilde{\theta}^4}\cos^4(\tilde{\theta}), \end{aligned}$$

and integrate numerically starting at $\tilde{\theta} = 0$. We take $v = -1$ and use initial condition

$$\tilde{H}\Big|_{\tilde{\theta}=0} = 0.5, \quad \frac{\partial \tilde{H}}{\partial \tilde{\theta}}\bigg|_{\tilde{\theta}=0} = 0, \quad \frac{\partial^2 \tilde{H}}{\partial \tilde{\theta}^2}\bigg|_{\tilde{\theta}=0} = -1, \quad \frac{\partial^3 \tilde{H}}{\partial \tilde{\theta}^3}\bigg|_{\tilde{\theta}=0} = 0,$$

and integrate forwards and backwards until the contact line is reached. The resulting film height profile is depicted in Fig. 4.9 below.

(a) (b) (c)

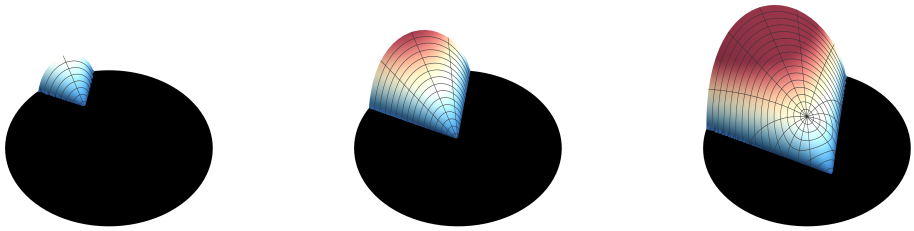

Figure 4.9: Travelling wave scale invariant solutions for (a) $t = -0.5$, (b) $t = 0$, and (c) $t = 0.5$. For the parameters chosen, the film height profile is a sharp finger of fluid that travels while maintaining its shape.

Scale invariant scale invariant solutions

Recall the invariants of the scale invariant scale invariant solutions,

$$\tilde{H} = R^{-4/3}(\pm t)^{1/3} H,$$
$$\tilde{\theta} = \theta - \omega \log\left((\pm t)^{\frac{2(\alpha-2)}{3(4\alpha-2)}} R^{-2/3}\right).$$

We use the plus sign in the $\pm$, insert the ansatz $H = R^{4/3}(-t)^{1/3}\tilde{H}(\tilde{\theta})$ into Eq. 4.17 to derive the reduced equations

$$\begin{aligned} 0 = &\left(-\frac{\tilde{H}}{3} + \frac{(\alpha-2)\omega}{3-6\alpha}\frac{\partial \tilde{H}}{\partial \tilde{\theta}}\right) + \frac{16}{9}\tilde{H}^2\frac{\partial \tilde{H}}{\partial \tilde{\theta}}^2 + \frac{4}{27}\omega\left(4\omega^2+9\right)\tilde{H}^2\frac{\partial \tilde{H}}{\partial \tilde{\theta}}\frac{\partial^2 \tilde{H}}{\partial \tilde{\theta}^2} \\ &+ \frac{1}{81}\left(4\omega^2+9\right)^2\tilde{H}^2\frac{\partial^3 \tilde{H}}{\partial \tilde{\theta}^3}\frac{\partial \tilde{H}}{\partial \tilde{\theta}} - \frac{256}{243}\omega\tilde{H}^3\frac{\partial \tilde{H}}{\partial \tilde{\theta}} + \frac{4}{81}\left(20\omega^2-3\right)\tilde{H}^3\frac{\partial^2 \tilde{H}}{\partial \tilde{\theta}^2} \\ &+ \frac{32}{243}\omega\left(4\omega^2+9\right)\tilde{H}^3\frac{\partial^3 \tilde{H}}{\partial \tilde{\theta}^3} + \frac{1}{243}\left(4\omega^2+9\right)^2\tilde{H}^3\frac{\partial^4 \tilde{H}}{\partial \tilde{\theta}^4} - \frac{320}{243}\tilde{H}^4, \end{aligned}$$

and integrate numerically starting at $\tilde{\theta} = 0$. We take $\omega = -1$ and $\alpha = 1/5$ and use initial condition

$$\tilde{H}\Big|_{\tilde{\theta}=0} = 0.5, \quad \frac{\partial \tilde{H}}{\partial \tilde{\theta}}\Big|_{\tilde{\theta}=0} = 0, \quad \frac{\partial^2 \tilde{H}}{\partial \tilde{\theta}^2}\Big|_{\tilde{\theta}=0} = -10, \quad \frac{\partial^3 \tilde{H}}{\partial \tilde{\theta}^3}\Big|_{\tilde{\theta}=0} = -15,$$

and integrate forwards and backwards until the contact line is reached. The resulting film height profile is depicted in Fig. 4.7 below.

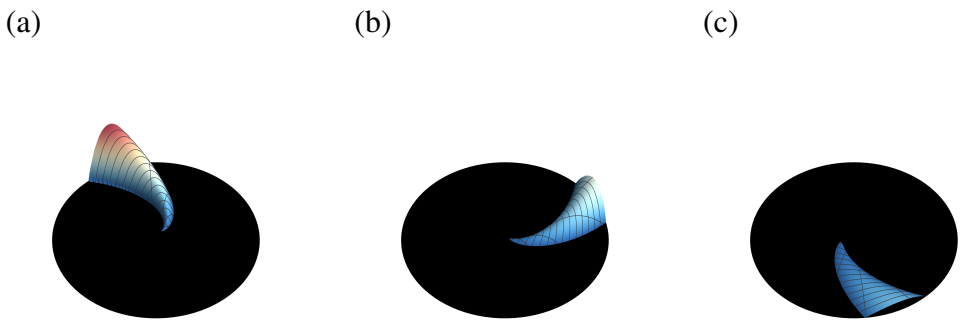

Figure 4.10: Scale invariant scale invariant solutions for (a) $t = 0$, (b) $t = 5$, and (c) $t = 25$. For the parameters chosen, the film height profile is a sharp twisted finger of fluid that rotates at an increasingly slow rate while decreasing in height.

4.3 Notes

The spreading of an insoluble surfactant-laden droplet on a thin viscous film has been of practical and theoretical interest for several decades. The human ocular and respiratory systems rely on surfactants to decrease the surface tension of thin fluid films in order to function, and the delivery of surfactants to such systems is of significant medical interest. Furthermore, the fundamental fluid mechanics and pattern formation of a spreading droplet is of theoretical interest. Jensen and Grotberg [25] made important early contributions to the study, identifying the first self-similar spreading solution which corresponds to $\alpha_1 = 0$ and $\alpha_2 = -2$ for $n = 1$ and $\alpha_1 = 0$ and $\alpha_2 = -1$ for $n = 1$ in our notation. They also importantly characterized the capillary ridge at the monolayer front and performed matched asymptotics. The conditions $\alpha_2 = -2$ for rotationally invariant solutions and $\alpha_2 = -1$ for translationally invariant solutions implies surfactant-mass conservation when the total surfactant mass is finite, while the condition $\alpha_1 = 0$ is necessary to achieve far-field boundary conditions on H which are constant. These conditions can be seen to be necessary if the self-similar solution is supposed to be valid in the far field, but for solutions which are valid in only a limited portion of space and time, they are not strictly necessary. Halpern and Grotberg described an analogous set of coupled equations for the problem of a soluble surfactant [91], but we restrict attention here to the insoluble case for simplicity. Jensen later recognized the possibility of more general scaling exponents and first developed a planar system like the one utilized here [71]. More general self-similar solutions like these are sometimes called type II similarity solutions. Jensen explored several possibilities, but restricted himself primarily to $\alpha = 0$ in his notation, or $\frac{\alpha_1}{\alpha_1+\alpha_2} = 0$ in our notation, which again was

motivated by the far-field boundary conditions on H.

One significant novel contribution in this chapter to this field was the identification of many well-behaved self-similar solutions near the origin, as described in Section 4.1 and depicted in Fig. 4.3. As far as the author is aware, these solutions have escaped the attention of other researchers. We took advantage of an approximation to the (ζ_1, ζ_2) planar system near the origin to derive these solutions. Such solutions were within the grasps of Jensen [71], but the relevant fixed point was infinite in his planar system and he restricted attention to $\alpha = 0$ when the necessary condition was $\alpha_2 = 2\alpha_1$ in our notation, which requires $\alpha = 1/3$ in his notation. Jensen and Grotberg [25] did recognize apparent self-similar draining near the origin in their simulations. They attempted to identify the scaling exponent which is $\frac{\alpha_1}{2-\alpha_1-\alpha_2}$ in our notation in their Figure 3, and estimated it to be $-1/8$. However, analysis of their data suggest a better estimate is $-1/5$, which corresponds to $\alpha_1 = -1$ and $\alpha_2 = -2$. We also found similar scaling in our finite element simulations. Their estimate of $-1/8$ was motivated by an apparently flawed asymptotic argument, but an analogous one for the planar strip predicted a scaling of $-1/6$, which was much better supported by their data in their Figure 2. Many other researchers have focused on the planar translationally invariant solutions rather than the rotationally invariant solutions because of their greater simplicity, but we noted in Fig. 4.2 and in (8) of Table 4.1 that the near-origin behavior of these solutions differs qualitatively because of the additional fixed point in the $n = 0$ planar strip case. The special quasistatic solutions (7) in Table 4.1 is a new class of solutions which may be of interest in the planar case.

Troian, Herbolzheimer, and Safran first noted the development of fingering instabilities in the spreading of a surfactant laden drop on a thin fluid film [92] and noted an analogy with the viscous fingering produced when a low-viscosity fluid is injected into a highly viscous fluid in a Hele-Shaw cell, and consequently to diffusion limited aggregation [93]. While this analogy generated interest and theoretical work on the problem, it is now regarded as inexact and the digitated fingering process has not been theoretically characterized [94]. Several results have been established, however. First, Matar and Troian performed a linear stability analysis of a spreading front and found asymptotic stability to infinitesimal perturbation [95]. Subsequent non-modal and generalized linear stability analyses revealed transient growth modes which are now known to be sufficient to excite nonlinearities and seed the growth of fingers [96–98]. The role of additional Van der Waals forces in promoting finger growth was recognized [97], but Van der Waals forces are not strictly necessary to

produce the fingering instability [94, 98, 99]. Furthermore, the important role of initial conditions both near the surfactant deposition and in the precursor film have been recognized [94, 99, 100]. Several experimental investigations reported similar digitation in more complex fluids, including non-Newtonian and visco-elastic fluids and non-linear relationship between surfactant concentration and surface tension, many of which are summarized in the review of Afsar-Siddiqui, Luckham, and Matar [101]. We expect that the self-similar solutions described in Fig. 4.3 may find important application in the description of these fingering structures. We note that only one of these solutions, the $\alpha_1 = -1$ and $\alpha_2 = -2$ case, is surfactant mass-conserving. But we also note that the drained region depicted in Fig. 4.1 can act as a source or sink of surfactant mass for the inner droplet, and so conservation is not necessary. Jensen and Naire [99] also emphasized transport of surfactant mass through the drained or thinning region. Furthermore in applications with both endogenous and exogenous surfactants like the deposition of an exogenous surfactant in the lungs, the total surfactant mass is infinite and a far field boundary condition may be more relevant than a surfactant mass-conserving one. We conjecture that the multiplicity of possible self-similar draining of the inner droplet may permit local variations in the scaling exponents that would result in differing spreading rates and thus instability.

Another novel contribution in this chapter was the utilization of our local numerical scaling exponents α_1^{loc} and α_2^{loc} in Eq. 4.16 and Fig. 4.5. This definition relied on the fact that the characteristic for self-similar solutions vanishes, as in Eq. 2.8. Dijksman et al. [102] also noted a method for obtaining estimates of scaling exponents from numerical or experimental data which relied on Eq. 2.8. This method entails solving Eq. 2.8 in a least-squares sense for the scaling exponents. However, their method allowed for totally independent scaling exponents for each dependent and independent variable. In our application, there was a scaling relationship between some of these variables because of the symmetry conditions for the equations. This reduced the number of scaling exponents that needed to be found and permitted the definition of our local scaling exponents. Re-examining previous numerical data with these local scaling exponents is a very promising direction for future research. The description numerical self-similar solutions involving the angular coordinates in Section 4.2 was a first illustration of these less familiar reductions. Jensen [71] noted the presence of other symmetries in the surfactant spreading problem and the possibility of other self-similar solutions, but as far as the author is aware there has not yet been any studies or applications for these particular ones.

Appendix A

THE MATHEMATICA PACKAGE ZGNSYMMETRY.M

The zgnsymmetry.m package file is reproduced in full below. It should be possible to copy and paste the text here into a Mathematica notebook and save the file as a package, but the interested reader is encouraged to contact the author for a digital version. The file should be placed in the Applications subdirectory of the Mathematica user base directory, which can be found in a Mathematica notebook with the command

```
$UserBaseDirectory
```

Include the package in a Mathematica notebook with

```
<<zgnsymmetry`
```

Information about the functions included in the package can be seen with

```
?FindInvariance
?FindAllEquations
?FindEquations
```

zgnsymmetry.m:

```
(* :: Package :: *)

BeginPackage["zgnsymmetry`"]
FindInvariance :: usage = "FindInvariance[Delta, var, Q, solvefor] gives the \
invariance criteria for the list of differential equations Delta==0, where \
var={indep,dep} is a list of lists of the independent and dependent variables, Q \
the characters of the symmetry. The equation Delta==0 is solved for the \
variables in solvefor. The symbols in Delta, Q, and solvefor should be \
functions of the independent variables, so that e.g. Apply[Delta[[1]], var[[1]]] \
gives the first equations. The option Adjoint->True can be added to search for \
adjoing symmetries."
FindAllEquations :: usage = "FindAllEquations[Delta, var, vec, solvefor] gives the \
all the equations from the coefficients of derivatives in the symmetry criteria \
for the given system. Arguments are as in FindInvariance. The option \
Adjoint->True can be added to search for adjoint symmetries. The options \
extras -> extralist and excluded-> excludedlist can be aded to add or exclude \
monomial terms in the expansion. The option Assumptions->assumptions can be \
added to include assumptions in the simplification. Lastly, the option \
SuppressArgs->True can be added to suppress arguments and use a more compact \
notation for derivatives. FindAllEquations returns {numeqns, independenteqns, \
```

```
monomials, eqns}, where numeqns is the number of independent equations, \
independenteqns is a list of the independent equations, monomials is a list of \
the monomials whose coefficients are the equations for each equation in \
FindInvariance, and eqns is a list of the equations corresponding to monomials \
for each equation in FindInvariance.";
FindEquations::usage = "FindEquations[Delta,var,vec, solvefor,numterms] gives the \
the equations with only numterms terms appearing from the coefficients of \
derivatives in the symmetry criteria for the given system. Arguments are as in \
FindInvariance, and options are as in FindAllEquations. FindEquations returns \
{eqnsnum, eqns, monomials} where eqnsnum is the total number of equations from \
FindAllEquations, eqns is a list of equations with terms terms, and monomials is \
a list specifying which equation and which monomial each equation in eqns comes \
from. ";
Options[FindInvariance] = {"Adjoint" -> False};
Options[FindAllEquations] = {"Adjoint" -> False, "extras" -> {},
    "excluded" -> {}, "Assumptions" -> {}, "SuppressArgs" -> False};
Options[FindEquations] = {"Adjoint" -> False, "extras" -> {}, "excluded" -> {},
    "Assumptions" -> {}, "SuppressArgs" -> False};
Begin["`Private`"]
FindInvariance[Delta_, var_, Q_, solvefor_, OptionsPattern[]] :=
  Module[{simpl, derivs, derivs2, sol, Qp, G, Gp, cases, vars, ret, F,
    Compare}, simpl = Join[Table[var[[2]][[j]][l__] -> var[[2]][[j]],
      {j, 1, Length[var[[2]]]}], Table[Derivative[l__][var[[2]][[j]]] @@
        var[[1]] -> Subscript[var[[2]][[j]], {l}], {j, 1, Length[var[[2]]]}]];
    derivs = Flatten[Table[Cases[Variables[Through[Delta @@ var[[1]]] /.
        simpl], Subscript[var[[2]][[i]], j__]], {i, 1, Length[var[[2]]]}]];
    derivs2 = Table[Last[derivs[[i]]], {i, 1, Length[derivs]}];
    F[args__] := Solve[Through[Delta @@ {args}] == 0,
      Through[solvefor @@ {args}]][[1]]; sol = F @@ var[[1]];
    Compare[i_, j_] := First[i] == First[j] &&
      And @@ Table[Last[i][[k]] >= Last[j][[k]], {k, 1, Length[var[[1]]]}];
    G[n_, k_][args__] := D[Delta[[n]] @@ {args},
      (Derivative @@ derivs2[[k]])[derivs[[k]][[1]]] @@ {args}];
    Gp[n_, k_] := (Derivative @@ derivs2[[k]])[G[n, k]] @@ var[[1]];
    Qp[n_, k_] := (Derivative @@ derivs2[[k]])[Q[[n]]] @@ var[[1]];
    If[OptionValue["Adjoint"],
     ret = Expand[Table[Expand[Sum[Q[[n]] @@ var[[1]]*D[Delta[[n]] @@ var[[1]],
          var[[2]][[m]] @@ var[[1]]], {n, 1, Length[Delta]}]],
        {m, 1, Length[var[[2]]]}] + Sum[Product[(-1)^derivs2[[k]][[j]], {j,
          1, Length[var[[1]]]}]*UnitVector[Length[var[[2]]], First[
          Flatten[Position[var[[2]], First[derivs[[k]]]]]]]*Gp[n, k]*
        Q[[n]] @@ var[[1]], {k, 1, Length[derivs]},
        {n, 1, Length[Delta]}] + Sum[Product[(-1)^derivs2[[k]][[j]], {j, 1,
```

```
            Length[var [[1]]]}]* UnitVector[Length[var [[2]]],  First [
             Flatten [ Position [ var [[2]],  First [ derivs [[ k ]]]]]]]*
           G[n, k] @@ var[[1]]*Qp[n, k], {k, 1, Length[ derivs ]},
          {n, 1, Length[Delta ]}] /. sol /. simpl ]; ,
 ret = Expand[Sum[Q[[m]] @@ var[[1]]*D[Through[Delta @@ var[[1]]],
            var [[2]][[ m]] @@ var[[1]]], {m, 1, Length[var [[2]]]}] +
        Sum[D[Through[Delta @@ var[[1]]] /. simpl, derivs [[ k ]]]*
          Qp[ First [ Flatten [ Position [ var [[2]],  First [ derivs [[ k ]]]]]],  k ],
         {k, 1, Length[ derivs ]}] /. sol /. simpl ]; ];
vars = Table[Cases[ Variables [ ret ], Subscript [ var [[2]][[ j ]], 1_ ]],
 {j, 1, Length[var [[2]]]}];
cases = Table[Last /@ Cases[vars[[ j ]], i__ /; Compare[i,
       solvefor [[ j ]] @@ var[[1]] /. simpl ]], {j, 1, Length[ solvefor ]}];
cases = DeleteDuplicates [ Flatten [Table[ cases [[ j ]][[ i ]] -
     Last[ solvefor [[ j ]] @@ var[[1]] /. simpl ], {j, 1, Length[var [[2]]]},
   {i, 1, Length[cases [[ j ]]]}], 1]]; While[cases != {},
 sol = Flatten [Join[ sol , Flatten [Through[Through[(Apply[Derivative, cases ,
            {1}])[F]] @@ var[[1]]] /. sol ]]];
 While[True, If [TrueQ[Expand[Last /@ sol - Last /@ (sol /. sol )] ==
       Table [0, {i , 1, Length[ sol ]}]], Break []; ,
     sol = Table[ First [ sol [[ i ]]] -> Last [( sol /. sol )[[ i ]]],
       {i , 1, Length[ sol ]}]; ]; ]; If [OptionValue["Adjoint "],
  ret = Expand[Table[Expand[Sum[Q[[n]] @@ var[[1]]*D[Delta[[n]] @@
              var [[1]], var [[2]][[ m]] @@ var[[1]]], {n, 1, Length[
            Delta ]}]], {m, 1, Length[var [[2]]]}] +
        Sum[Product[(-1)^derivs2 [[ k ]][[ j ]], {j , 1, Length[var [[1]]]}]*
          UnitVector[Length[var [[2]]],  First [ Flatten [ Position [ var [[2]],
              First [ derivs [[ k ]]]]]]* Gp[n, k]*Q[[n]] @@ var[[1]], {k, 1,
          Length[ derivs ]}, {n, 1, Length[Delta ]}] +
        Sum[Product[(-1)^derivs2 [[ k ]][[ j ]], {j , 1, Length[var [[1]]]}]*
          UnitVector[Length[var [[2]]],  First [ Flatten [ Position [ var [[2]],
              First [ derivs [[ k ]]]]]]* G[n, k] @@ var[[1]]*Qp[n, k], {k, 1,
          Length[ derivs ]}, {n, 1, Length[Delta ]}] /. sol /. simpl ]; ,
  ret = Expand[Sum[Q[[m]] @@ var[[1]]*D[Through[Delta @@ var[[1]]],
            var [[2]][[ m]] @@ var[[1]]], {m, 1, Length[var [[2]]]}] +
        Sum[D[Through[Delta @@ var[[1]]] /. simpl, derivs [[ k ]]]*
          Qp[ First [ Flatten [ Position [ var [[2]],  First [ derivs [[ k ]]]]]],  k ], {
          k, 1, Length[ derivs ]}] /. sol /. simpl ]; ];
 vars = Table[Cases[ Variables [ ret ], Subscript [ var [[2]][[ j ]], 1_ ]],
  {j , 1, Length[var [[2]]]}]; cases =
  Table[Last /@ Cases[vars[[ j ]], i__ /; Compare[i,
       solvefor [[ j ]] @@ var[[1]] /. simpl ]], {j , 1, Length[ solvefor ]}];
 cases = DeleteDuplicates [ Flatten [Table[ cases [[ j ]][[ i ]] -
```

```
            Last[ solvefor [[ j ]]  @@ var[[1]] /.  simpl ],  {j,  1,  Length[var [[2]]]},
           {i,  1,  Length[cases [[ j ]]]}],   1]];   ];  ret ];
FindAllEquations[Delta_,  var_,  Q_,  solvefor_ ,  OptionsPattern []]  :=
  Module[{f,  coeffs ,  eqns,  eqns2,  monomialrules,  monomials,  crules ,  simpl },
   f  =  FindInvariance [Delta ,  var ,  Q,  solvefor ,  "Adjoint"  ->
      OptionValue["Adjoint "]];   coeffs  =  Join[OptionValue[" extras "],
     Flatten [Table[Cases[ Variables [f ],   Subscript [ var [[2]][[ k ]],  1__ ]],
       {k,  1,  Length[var  [[2]]]}]]];
    simpl  =  Join[Table[ var [[2]][[ j ]][ 1__ ]  ->  var [[2]][[ j ]],
      {j ,  1,  Length[var  [[2]]]}],   Table[ Derivative [1__ ][ var [[2]][[ j ]]]  @@
        var [[1]]  ->  Subscript [ var [[2]][[ j ]],  {1 }],  {j ,  1,  Length[var  [[2]]]}]];
    coeffs  =  Complement[coeffs,  OptionValue["excluded"]  /.  simpl ];
    If [TrueQ[coeffs  ==  {}],  eqns  =  Table[{ f [[ i ]]},  {i ,  1,  Length[f ]}];
      monomials = Table[{1},  {i ,  1,  Length[f ]}];   ,
     crules  =  Table[  CoefficientRules  [ If [TrueQ[OptionValue[" extras "]  ==  {}],
         f [[ i ]],  Numerator[Together[ f [[ i ]]]]],   coeffs ],  {i ,  1,  Length[f ]}];
      eqns  =  Table[Last  /@ crules [[ i ]],  {i ,  1,  Length[f ]}];
      monomialrules = Table[ First  /@ crules [[ i ]],  {i ,  1,  Length[f ]}];
      monomials = Table[ FromCoefficientRules [{ monomialrules[[ i ]][[ j ]]  ->  1},
        coeffs ],  {i ,  1,  Length[f ]},  {j ,  1,  Length[monomialrules[[ i ]]]}];   ];
    eqns2  =  Table[ Simplify [eqns [[ j ]][[ i ]]  ==  0,  Assumptions  ->
      OptionValue["Assumptions "]],  {j ,  1,  Length[eqns ]},
     {i ,  1,  Length[eqns [[ j ]]]}];   If [OptionValue["SuppressArgs "],
     {Length[ DeleteDuplicates [ Flatten [eqns2 ]]],   DeleteDuplicates [
       Flatten [eqns2 ]],  monomials, eqns2}  /.  Subscript [a_,  1__ ]  :>
      Subscript [a,  Times @@ (var[[1]]^1)]  /.  Derivative [1__ ][ a_][ l2__ ]  :>
      Subscript [a,  Times @@ ({l2}^{1})],
     {Length[ DeleteDuplicates [ Flatten [eqns2 ]]],   DeleteDuplicates [
       Flatten [eqns2 ]],  monomials, eqns2 }]];
FindEquations[Delta_,  var_,  Q_,  solvefor_ ,  terms_,  OptionsPattern []]  :=
  Module[{numeqns, eqns, eqns4,  eqns3,  monomialrules,  monomials, monomialterms,
    crules ,  part },  {numeqns, monomials, eqns} =
     FindAllEquations[Delta,  var,  Q,  solvefor ,  "Adjoint"  ->
       OptionValue["Adjoint "],  " extras "  ->  OptionValue[" extras "],
      "excluded"  ->  OptionValue["excluded "],  "Assumptions"  ->
       OptionValue["Assumptions"],  "SuppressArgs"  ->
       OptionValue["SuppressArgs "]][[{1,  3,  4}]];
    part[i_]  :=  Flatten [ Position [Length /@ CoefficientRules  /@
       Expand /@ Numerator /@ Together /@ (First  /@ eqns[[i ]]  -
         Last  /@ eqns[[i ]]),  terms ]];  monomialterms =
     Table[monomials[[i ]][[ part[i ]]],  {i ,  1,  Length[monomials]}];
    eqns4  =  Table[eqns [[ i ]][[ part[i ]]],  {i ,  1,  Length[eqns ]}];
    eqns3  =  DeleteDuplicates [ Flatten [eqns4 ]];  {numeqns, eqns3,
```

```
        Table[Inner[List, First /@ Position[eqns4, eqns3[[i]]],
          Extract[monomialterms, Position[eqns4, eqns3[[i]]]], List],
         {i, 1, Length[eqns3]}]};
End[]
EndPackage[]
```

Appendix B

REYNOLDS' TRANSPORT THEOREM

[1] Z. G. Nicolaou and S. M. Troian. "Reynolds' transport theorem without external advection assumptions". In: *Phys. Fluids* (preparing for submission 2016).

In continuum and fluid mechanics, it is often necessary to consider three-dimensional generalizations of the Leibniz rule for differentiating integrals over varying domains. Usually [16, 103] this generalization, called the Reynolds' transport theorem, is developed in the context of the time evolution of a flow of some sort – an initial domain $\Omega(0)$ is advected through a flow field $\mathbf{v}(\mathbf{x}, t)$ to $\Omega(t)$, and the question is: "How are integrals of a time dependent integrand $f(\mathbf{x}, t)$ over the domain $\Omega(t)$ differentiated with respect to time?" The answer is

$$\frac{\mathrm{d}}{\mathrm{d}t}\int_{\Omega(t)} f\ \mathrm{d}^3x = \int_{\Omega(t)} \frac{\partial f}{\partial t}\ \mathrm{d}^3x + \int_{\partial\Omega(t)} f\mathbf{v}\cdot\hat{\mathbf{n}}_s\ \mathrm{d}^2x, \tag{B.1}$$

where $\partial\Omega(t)$ is the boundary of a three-dimensional compact subset $\Omega(t)$ of $\mathbb{R}^3$ and $\hat{\mathbf{n}}_s$ is the outward pointing unit normal vector on the boundary. The preferred method for proving Eq. B.1 is by defining Lagrangian coordinates $\boldsymbol{\xi} \in \Omega(0)$ for $\Omega(t)$ which are the fixed Eulerian or lab coordinates on $\Omega(0)$ which are advected by the fluid flow $\mathbf{v}(\mathbf{x}, t)$ to points in $\Omega(t)$. A two-dimensional schematic of Lagrangian coordinates is depicted in Fig. B.1 below.

Here Eq. B.1 will be generalized to integrals over a family $\Omega(\varepsilon)$ of compact, D-dimensional subsets in $\mathbb{R}^D$ which vary with some arbitrary parameter ε rather than being advected by an external velocity in time t (and eventually to integrals over p-dimensional hypersurfaces of $\mathbb{R}^D$ which vary with some arbitrary parameter ε). The boundary $\partial\Omega(\varepsilon)$ will be assumed to be composed of $(D-1)$-dimensional surfaces which are everywhere locally diffeomorphic to the $(D-1)$-dimensional hyperplane and will be assumed to have sufficiently smooth dependence on ε. Furthermore, assume that the boundary has a finite $(D-1)$-dimensional surface area. These assumptions preclude the possibility that the topology of $\Omega(\varepsilon)$ changes as ε varies, for example through the formation of a hole and also preculde surfaces with sharp corners or edges like the D-dimensional hypercubes [1]. Given the linearity of

[1] Such singularities on the boundary surface often do not complicate the result since they often

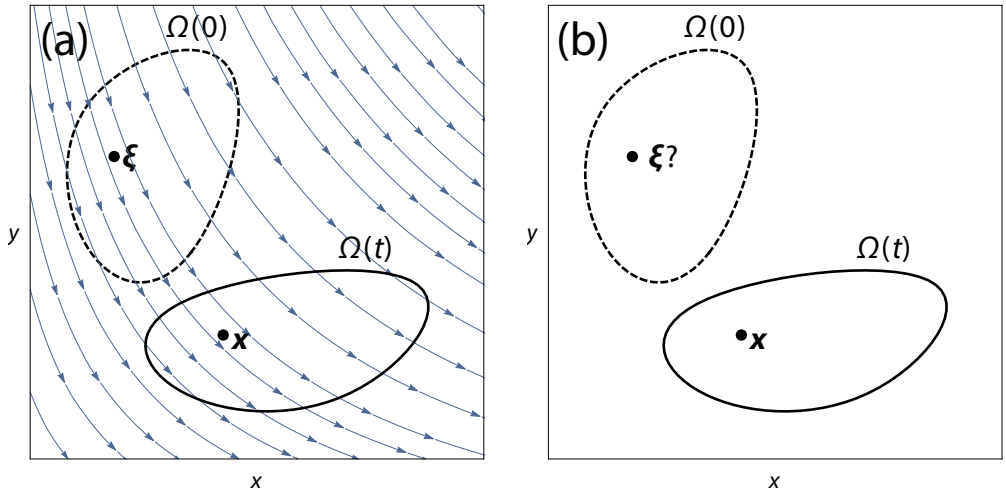

Figure B.1: (a) Lagrangian coordinates on $\Omega(t)$. The points $\mathbf{x} \in \Omega(t)$ is traced backwards in time under the flow given by the velocity $\mathbf{v}(\mathbf{x}, t)$ (depicted as blue curves) to the point $\boldsymbol{\xi} \in \Omega(0)$. The Cartesian coordinates of $\boldsymbol{\xi}$ in the fixed lab frame, ξ^i, then serve as coordinates for $\mathbf{x}$. (b) Without a provided velocity describing the flow, it is not clear how to define Lagrangian coordinates.

integration, it suffices to consider $\Omega(\varepsilon)$ as a single connected component from now on. Throughout, the fixed, Eulerian or lab coordinates will be denoted $\mathbf{x}$ and will be taken as Cartesian coordinates of $\mathbb{R}^D$, with ith component x^i. The integral over $\Omega(\varepsilon)$ of an ε-differentiable integrand $f(\mathbf{x}, \varepsilon)$ is the object of study, $I(\varepsilon) \equiv \int_{\Omega(\varepsilon)} f \, \mathrm{d}^D x$. The primary difference in this context, aside from the dimensionality, from the time-dependent one in Eq. B.1 above is that there is no obvious "velocity" field which is advecting the domain and through which Lagrangian coordinates can be defined. So before moving on to prove the general Reynolds' transport theorem, some work must be done in defining the Lagrangian coordinates, and this will be accomplished by explicitly constructing a flow field $\mathbf{v}(\mathbf{x}, \varepsilon)$ analogous to the usual velocity field which advects $\Omega(0)$ to $\Omega(\varepsilon)$ [2].

In order to relieve notational burden, the dependence of the domain and other quantities on ε will be omitted unless it is needed, so $\Omega(\varepsilon)$ and $f(\mathbf{x}, \varepsilon)$ will be written Ω and $f(\mathbf{x})$, respectively. Explicit specification of the domain Ω will be assumed to be given through a specification of its bounding surface $\partial\Omega$. As an embedded,

effect a negligible (zero measure) portion of the domains of the integrals. However, pathological examples can be constructed.

[2] An alternative method for proving the Reynolds' transport theorem involves generalized functions and distributional derivatives [104]. Such a non-classical derivation is less satisfactory than the classical one based on Lagrangian coordinates because of its reliance on more formal notions of functions and derivatives.

$(D-1)$-dimensional manifold of $\mathbb{R}^D$, this can always be done locally through a parameterization. Specifically, let the domain of surface coordinates $\Omega_s \subset \mathbb{R}^{D-1}$ be an open subset of the $(D-1)$-dimensional Cartesian space, and let $\mathbf{w}_s \in \Omega_s$ have Cartesian coordinates w_s^i. The subscript s will be used throughout to denote the surface or boundary quantities, and these Cartesian coordinates parameterize a patch of the surface $\partial\Omega$ through a map $\mathbf{S}_{\mathbf{w}_s\to\mathbf{x}} : \left(\Omega_s \subset \mathbb{R}^{D-1}\right) \to \left(\partial\Omega \subset \mathbb{R}^D\right)$. Thus a point on the surface with D-dimensional coordinates $\mathbf{x} \in \partial\Omega \subset \mathbb{R}^D$ will be designated by the surface coordinates $\mathbf{w}_s \in \Omega_s \subset \mathbb{R}^{D-1}$ when $\mathbf{S}_{\mathbf{w}_s\to\mathbf{x}}(\mathbf{w}_s) = \mathbf{x}$. The surface will generally require multiple patches with different coordinate parameterizations to totally parameterize it, but since it is obvious how to transition between coordinate patches during operatrions like integration, we will simply focus on a single coordinate patch. Aside from the surface coordinates, multiple coordinates can by used to specify points in the interior volume Ω. The natural, Eulerian coordinates are the Cartesian coordinates of $\mathbb{R}^D$ itself, so that the coordinates of a point $\mathbf{x} \in \Omega$ are the Cartesian components x^i. In the course of this letter, another coordinate system for Ω, the Lagrangian coordinates denoted $\boldsymbol{\xi}$, will be given by the Cartesian coordinates ξ^i of points in the $\varepsilon = 0$ domain $\Omega_0 \subset \mathbb{R}^D$. These coordinates will also specified through a map $\mathbf{M}_{\mathbf{x}\to\boldsymbol{\xi}} : (\Omega \subset \mathbb{R}^D) \to (\Omega_0 \subset \mathbb{R}^D)$, and the Lagrangian coordinates of a point $\mathbf{x} \in \Omega$ will be given by $\boldsymbol{\xi} = \mathbf{M}_{\mathbf{x}\to\boldsymbol{\xi}}(\mathbf{x}) \in \Omega_0$. The inverse map changing Lagrangian coordinates back to Eulerian coordinates will also be used $\mathbf{M}_{\boldsymbol{\xi}\to\mathbf{x}} : (\Omega_0 \subset \mathbb{R}^D) \to (\Omega \subset \mathbb{R}^D)$.

Given any description of the domain Ω, some surface parameterization $\mathbf{S}_{\mathbf{w}_s\to\mathbf{x}}$ can be defined. The map $\mathbf{S}_{\mathbf{w}_s\to\mathbf{x}}$ and the integrand f are the only pieces of information initially provided. The maps $\mathbf{M}_{\mathbf{x}\to\boldsymbol{\xi}}$ and $\mathbf{M}_{\boldsymbol{\xi}\to\mathbf{x}}$ are not yet defined, and the main purpose of this letter is to show how this can be done. Furthermore, it should be emphasized again that all these coordinate maps $\mathbf{S}_{\mathbf{w}_s\to\mathbf{x}}(\mathbf{w}_s)$, $\mathbf{M}_{\boldsymbol{\xi}\to\mathbf{x}}(\boldsymbol{\xi})$, and $\mathbf{M}_{\mathbf{x}\to\boldsymbol{\xi}}(\mathbf{x})$ vary with ε as well as the arguments explicitly denoted – they are evaluated at some fixed ε unless otherwise indicated. When evaluating derivatives with respect to ε, care must be taken to avoid confusion. Derivatives of functions which depend only on ε such as $I(\varepsilon)$ will be denoted with the usual $\frac{\mathrm{d}I}{\mathrm{d}\varepsilon}$. Functions that vary in space as well as with ε will generally be defined as functions of their Eulerian coordinates, as in $f(\mathbf{x})$. The partial derivative $\frac{\partial f(\mathbf{x})}{\partial\varepsilon}$ will then be the derivative when $\mathbf{x}$ is held constant. Spatial functions will also need to be evaluated in their Lagrangian coordinate system through composition with the map $\mathbf{M}_{\boldsymbol{\xi}\to\mathbf{x}}$, as in $f(\boldsymbol{\xi}) \equiv f(\mathbf{M}_{\boldsymbol{\xi}\to\mathbf{x}}(\boldsymbol{\xi}))$. The same symbol f is used here to denote this function from Ω to $\mathbb{R}$, but its functional form will of course differ between

Lagrangian and Eulerian coordinates. When evaluated at fixed $\boldsymbol{\xi}$, differentiating with respect to ε requires the chain rule and will be denoted with total derivative $\frac{\mathrm{d}f(\boldsymbol{\xi})}{\mathrm{d}\varepsilon} = \left(\frac{\partial f(\mathbf{x})}{\partial \varepsilon} + \frac{\partial f(\mathbf{x})}{\partial x^i}\frac{\mathrm{d}M^i_{\boldsymbol{\xi}\to\mathbf{x}}(\boldsymbol{\xi})}{\mathrm{d}\varepsilon}\right)|_{\mathbf{x}=\mathbf{M}_{\boldsymbol{\xi}\to\mathbf{x}}(\boldsymbol{\xi})}$.
The important surface quantities associated to $\partial\Omega$ will now be formally defined. Consider a coordinate patch around some boundary point $\mathbf{w}_s \in \Omega_s$, as illustrated in Fig. B.2 for a three-dimensional surface. The $(D-1)$ tangent vectors

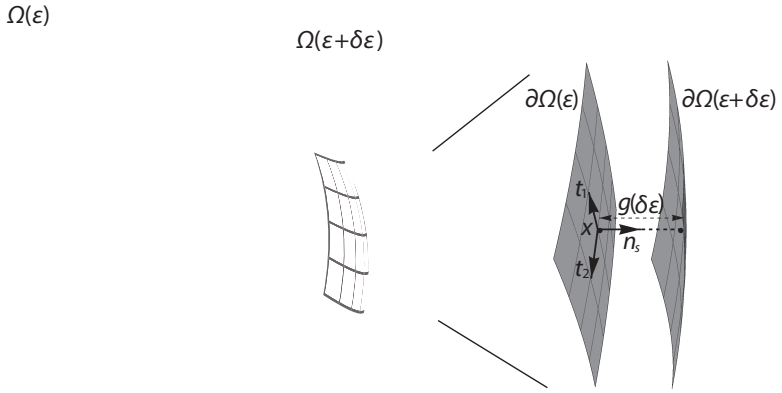

Figure B.2: Surface quantities near a boundary point $\mathbf{x}_0 \in \partial\Omega$. A parameterization of the surface yields $(D-1)$ tangent vectors $\mathbf{t}_j$, and the normal vector $\mathbf{n}_s$ is orthogonal to each tangent. The perturbed surface $\partial\Omega(\varepsilon+\delta\varepsilon)$ is also shown when ε is changed by a small amount $\delta\varepsilon$. The rate of change of the distance $g(\delta\varepsilon)$ between $\mathbf{x} = \mathbf{S}_{\mathbf{w}_s\to\mathbf{x}}(\mathbf{w}_s)$ and the intersection of the ray through $\mathbf{x}$ in the normal direction and $\partial\Omega(\varepsilon+\delta\varepsilon)$ defines the boundary velocity.

are defined via the parameterization $\mathbf{t}_i(\mathbf{w}_s) \equiv \frac{\partial \mathbf{S}_{\mathbf{w}_s\to\mathbf{x}}(\mathbf{w}_s)}{\partial w^i_s}$, and since the surface is assumed to be everywhere diffeomorphic to the $(D-1)$-dimensional hyperplane, it is required that these tangent vectors are everywhere linearly independent. The components of the normal vector $\mathbf{n}_s(\mathbf{w}_s)$ are then defined by a straightforward generalization of the vector cross product in three dimensions (formally, the Hodge dual of the wedge product of the Hodge duals of the tangent vectors [27]), $n^i_s(\mathbf{w}_s) \equiv \delta^{ij_0}\epsilon_{j_0 j_1\cdots j_{D-1}} t_1^{j_1}(\mathbf{w}_s)\cdots t_{D-1}^{j_{D-1}}(\mathbf{w}_s)$ where ϵ is the totally antisymemtric Levi-Civita symbol and δ is the Kronecker delta, the metric in the Cartesian coordinates of $\mathbb{R}^D$. The antisymmetry of ϵ implies that $\mathbf{n}_s(\mathbf{w}_s)$ is indeed orthogonal to each of the tangent vectors $\mathbf{t}_i(\mathbf{w}_s)$. The coordinates are assumed to be chosen with the correct order (an orientation) so that $\mathbf{n}_s(\mathbf{w}_s)$ is pointing outward from the interior of Ω. The surface measure in the $\mathbf{w}_s$ coordinates induced by the Euclidean measure in $\mathbb{R}^D$ is given by $\mathrm{d}^{D-1}x = |\mathbf{n}_s(\mathbf{w}_s)|\mathrm{d}w^1_s\mathrm{d}w^2_s\cdots\mathrm{d}w^{D-1}_s$, where $|\cdot|$ is the Euclidean

norm. While the tangent and normal vectors are dependent on the particular parameterization chosen, the unit normal $\hat{\mathbf{n}}_s(\mathbf{w}_s) \equiv \frac{\mathbf{n}_s(\mathbf{w}_s)}{|\mathbf{n}_s(\mathbf{w}_s)|}$ is coordinate-independent as are surface integrals of the normal flux of a vector field over the surface measure, as in the surface integral in Eq. B.1.

In addition to the tangent and normal vectors, there is also a boundary velocity associated with changes in ε. A naive definition for the boundary velocity would be $\frac{\partial \mathbf{S}_{\mathbf{w}_s \to \mathbf{x}}(\mathbf{w}_s)}{\partial \varepsilon}$, but this quantity is dependent on the specific parameterization chosen. However, it is straightforward to show that the normal component of the velocity is coordinate independent, so the surface velocity is defined

$$\mathbf{v}_s(\mathbf{w}_s) \equiv \left(\frac{\partial \mathbf{S}_{\mathbf{w}_s \to \mathbf{x}}(\mathbf{w}_s)}{\partial \varepsilon} \cdot \hat{\mathbf{n}}_s(\mathbf{w}_s) \right) \hat{\mathbf{n}}_s(\mathbf{w}_s). \tag{B.2}$$

A slightly more intrinsic definition follows from considering the intersection between the ray through the normal direction at $\mathbf{x} = \mathbf{S}_{\mathbf{w}_s \to \mathbf{x}}(\mathbf{w}_s)$ and the surface $\partial\Omega(\varepsilon + \delta\varepsilon)$ as $\delta\varepsilon \to 0$, as indicated in Fig. B.2 and described in more detail in the Supplementary Information.

To define the flow field $\mathbf{v}(\mathbf{x})$ and in turn the Lagrangian coordinates, it is necessary to extend the information from the boundary $\partial\Omega$ into the interior of Ω. A straightforward way to achieve such an extension is through solutions to linear elliptic partial differential equations on Ω, since classical smooth regularity of such solutions in $\mathbf{x}$ up to and including the boundary is well known [105, 106]. First consider the eigenfunction corresponding to the smallest eigenvalue of the Laplacian on Ω with zero Dirichlet boundary conditions, and denote this eigenfunction $\phi_\varepsilon(\mathbf{x})$. It is known that $\phi_\varepsilon(\mathbf{x})$ is a strictly positive, smooth function in the interior of Ω [105]. Given the smoothness of $\phi_\varepsilon(\mathbf{x})$ with respect to $\mathbf{x}$, it is straightforward to insert the power series expansion (plus a remainder term via Taylor's theorem) of $\phi_\varepsilon(\mathbf{x})$ about some boundary point $\mathbf{x} = \mathbf{S}_{\mathbf{w}_s \to \mathbf{x}}(\mathbf{w}_s) \in \partial\Omega$ into the eigenvalue equation to derive recurrence relations between the partial derivatives of $\phi_\varepsilon(\mathbf{x})$. These recurrance relations determine the higher order partial derivatives of $\phi_\varepsilon(\mathbf{x})$ in terms of the 2^D partial derivatives $\frac{\partial^m \phi_\varepsilon(\mathbf{x})}{\partial x^{k_1} \cdots \partial x^{k_m}}$ with $m \leq D$ where each k_i is distinct, so that $k_i \neq k_j$ for $i \neq j$, since only such monomials are in the kernel of the Laplacian. Since the boundary $\partial\Omega$ is precisely the collection of points $\mathbf{x} \in \Omega(\varepsilon)$ for which $\phi_\varepsilon(\mathbf{x}) = 0$, the local structure of $\partial\Omega$ is determined by the lowest order non-vanishing terms in the Taylor series of $\phi_\varepsilon(\mathbf{x})$. Suppose for the sake of contradiction that $\nabla\phi_\varepsilon(\mathbf{x}_0) = \mathbf{0}$ for some $\mathbf{x}_0 \in \partial\Omega$, so that the lowest order nonvanishing terms in the Taylor series are $\sum \frac{\partial^m \phi_\varepsilon(\mathbf{x})}{\partial x^{k_1} \cdots \partial x^{k_m}} (x_0^{k_1} - x^{k_1}) \cdots (x_0^{k_m} - x^{k_m})$ for some $m > 1$. This vanishes on all D of the Cartesian coordinate axes centered at $\mathbf{x}_0$, where all but one of the x^k equals

x_0^k, and so the zero level set cannot be diffeomorphic to the $(D-1)$-dimensional hypersurface. This contradicts the assumptions about the smoothness of $\partial\Omega(\varepsilon)$, so the gradient of $\phi_\varepsilon(\mathbf{x})$ cannot vanish on the boundary,

$$0 < |\nabla\phi_\varepsilon(\mathbf{S}_{\mathbf{w}_s\to\mathbf{x}}(\mathbf{w}_s))| < \infty \text{ for all } \mathbf{w}_s \in \Omega_s. \tag{B.3}$$

The outward pointing unit normal vector $\mathbf{n}_s$ can then be expressed in terms of $\phi_\varepsilon(\mathbf{x})$ at each $\mathbf{x} \in \partial\Omega$ using the well-known geometric relation for the normal at a level set surface,

$$\hat{\mathbf{n}}_s(\mathbf{w}_s) = -\frac{\nabla\phi_\varepsilon(\mathbf{S}_{\mathbf{w}_s\to\mathbf{x}}(\mathbf{w}_s))}{|\nabla\phi_\varepsilon(\mathbf{S}_{\mathbf{w}_s\to\mathbf{x}}(\mathbf{w}_s))|}. \tag{B.4}$$

The sign here is determined by the fact that $\phi_\varepsilon(\mathbf{x})$ is positive in the interior of Ω and vanishes on the boundary. The function $\nabla\phi_\varepsilon(\mathbf{x})$ can then be viewed as an extension of surface normal into the interior of the domain.

Next the boundary velocity $\mathbf{v}_s(\mathbf{w}_s)$ will be extended into the interior of Ω in order to define the flow field $\mathbf{v}(\mathbf{x})$. Consider the Neumann problem for the Laplace equation on Ω,

$$\begin{aligned} \nabla^2\psi_\varepsilon(\mathbf{x}) &= 0 \text{ for } \mathbf{x} \in \Omega, \\ \nabla\psi_\varepsilon(\mathbf{S}_{\mathbf{w}_s\to\mathbf{x}}(\mathbf{w}_s)) \cdot \hat{\mathbf{n}}_s(\mathbf{w}_s) &= G(\mathbf{w}_s) \text{ for } \mathbf{w}_s \in \Omega_s. \end{aligned} \tag{B.5}$$

Provided that G satisfies the compatibility condition $\int_{\partial\Omega} G \, \mathrm{d}^{D-1}y = 0$, a solution ψ_ε to Eq. B.5 is guaranteed to exists and is unique up to an additive constant [105]. The gradient $\nabla\psi_\varepsilon(\mathbf{x})$ is then uniquely defined and is a smooth function of $\mathbf{x}$ and ε. Now define

$$\begin{aligned} G(\mathbf{w}_s) \equiv\ & \mathbf{v}_s(\mathbf{w}_s) \cdot \hat{\mathbf{n}}_s(\mathbf{w}_s) \\ & + \frac{\int_{\partial\Omega} \mathbf{v}_s \cdot \hat{\mathbf{n}}_s \, \mathrm{d}^{D-1}y}{\int_{\partial\Omega} \nabla\phi_\varepsilon \cdot \hat{\mathbf{n}}_s \, \mathrm{d}^{D-1}y} \left|\nabla\phi_\varepsilon(\mathbf{S}_{\mathbf{w}_s\to\mathbf{x}}(\mathbf{w}_s))\right|. \end{aligned}$$

The integrals appearing in the function G here are finite because of the assumptions of smoothness, the bounds in Eq. B.3, and the assumption that $\partial\Omega$ has finite $(D-1)$-dimensional surface area. Furthermore, G satisfies the compatibility condition by construction, and G is an smooth function of ε as well since all functions in its definition are. Finally, the flow field is defined in terms of the solution ψ_ε to Eq. B.5 as

$$\mathbf{v}(\mathbf{x}) \equiv \nabla\psi_\varepsilon(\mathbf{x}) + \frac{\int_{\partial\Omega} \mathbf{v}_s \cdot \hat{\mathbf{n}}_s \, \mathrm{d}^{D-1}y}{\int_{\partial\Omega} \nabla\phi_\varepsilon \cdot \hat{\mathbf{n}}_s \, \mathrm{d}^{D-1}y} \nabla\phi_\varepsilon(\mathbf{x}).$$

It is easy to see that the Eq. B.4 and the boundary condition in Eq. B.5 implies that for $\mathbf{w}_s \in \Omega_s$, the normal component of $\mathbf{v}(\mathbf{S}_{\mathbf{w}_s \to \mathbf{x}}(\mathbf{w}_s))$ at the boundary is given by $\mathbf{v}_s(\mathbf{w}_s)$,

$$\mathbf{v}(\mathbf{S}_{\mathbf{w}_s \to \mathbf{x}}(\mathbf{w}_s)) \cdot \hat{\mathbf{n}}_s(\mathbf{w}_s) = \mathbf{v}_s(\mathbf{w}_s) \cdot \hat{\mathbf{n}}_s(\mathbf{w}_s), \tag{B.6}$$

so that the boundary velocity has been successfully extended into the interior of Ω. Now the Lagrangian coordinates can be constructed and the Reynolds' transport theorem can be proved through the known methods. The proof will be reproduced here for completeness. Define the propagator for the flow generated by $\mathbf{v}(\mathbf{x})$ as the map $\mathbf{U}$ which takes an initial point $\boldsymbol{\xi}$, an initial value ε_0, and a final value ε to the point on the integral curve of $\mathbf{v}(\mathbf{x})$ at value ε. This map is defined as the solution to the ordinary differential equation

$$\frac{\mathrm{d}\mathbf{U}(\boldsymbol{\xi}, \varepsilon_0, \varepsilon)}{\mathrm{d}\varepsilon} = \mathbf{v}(\mathbf{U}(\boldsymbol{\xi}, \varepsilon_0, \varepsilon)), \quad \mathbf{U}(\boldsymbol{\xi}, \varepsilon_0, \varepsilon_0) = \boldsymbol{\xi}, \tag{B.7}$$

where the derivative $\frac{\mathrm{d}}{\mathrm{d}\varepsilon}$ is taken while holding $\boldsymbol{\xi}$ and ε_0 constant. The smoothness of the velocity $\mathbf{v}(\mathbf{x})$ with respect to $\mathbf{x}$ and ε implies that the propagator $\mathbf{U}$ is itself an smooth function of $\boldsymbol{\xi}$, ε, and ε_0 [107]. The coordinate maps transforming between Lagrangian and Eulerian coordinates are defined by

$$\mathbf{M}_{\boldsymbol{\xi} \to \mathbf{x}}(\boldsymbol{\xi}) \equiv \mathbf{U}(\boldsymbol{\xi}, 0, \varepsilon), \quad \mathbf{M}_{\mathbf{x} \to \boldsymbol{\xi}}(\mathbf{x}) \equiv \mathbf{U}(\mathbf{x}, \varepsilon, 0). \tag{B.8}$$

These maps are clearly inverses of each other. The technical but intuitive point that interior points map to interior points under these maps is detailed in the Supplementary Information. It follows that the map $\mathbf{M}_{\mathbf{x} \to \boldsymbol{\xi}}$ is a then diffeomorphism between these sets. Thus it is possible to use the the coordinates $\boldsymbol{\xi}$ of Ω_0 as coordinates of Ω through the map $\mathbf{M}_{\mathbf{x} \to \boldsymbol{\xi}}$, and such coordinates are the Lagrangian coordinates. The Jacobian matrix and its inverse relating these coordinates will be denoted

$$J^i_j(\boldsymbol{\xi}) = \frac{\partial M^i_{\boldsymbol{\xi} \to \mathbf{x}}(\boldsymbol{\xi})}{\partial \xi^j}, \quad (J^{-1})^i_j(\mathbf{x}) = \frac{\partial M^i_{\mathbf{x} \to \boldsymbol{\xi}}(\mathbf{x})}{\partial x^j}, \tag{B.9}$$

respectively, and $J(\boldsymbol{\xi}) = \det J^i_j(\boldsymbol{\xi})$ will denote the Jacobian determinant.
Now, the derivative of $I(\varepsilon)$ will be considered. The change of variables formula to the Lagrangian coordinate system gives $I(\varepsilon) = \int_{\Omega_0} \left(f \circ \mathbf{M}_{\boldsymbol{\xi} \to \mathbf{x}}\right) J \, \mathrm{d}^D\xi$ where $\circ$ denotes composition of functions, i.e. $\left(f \circ \mathbf{M}_{\boldsymbol{\xi} \to \mathbf{x}}\right)(\boldsymbol{\xi}) = f(\mathbf{M}_{\boldsymbol{\xi} \to \mathbf{x}}(\boldsymbol{\xi}))$. When expressed in Lagrangian coordinates, the domain of integration Ω_0 does not vary with ε, so the derivative $\frac{\mathrm{d}}{\mathrm{d}\varepsilon}$ can be taken under the integral sign. Applying the chain rule and the product rule, changing variables back to the Eulerian coordinates, and

noting from Eq. B.7 and Eq. B.8 that $\mathbf{v}(\mathbf{x}) = \left.\frac{\mathrm{d}\mathbf{M}_{\xi\to\mathbf{x}}(\xi)}{\mathrm{d}\varepsilon}\right|_{\xi=\mathbf{M}_{\mathbf{x}\to\xi}(\mathbf{x})}$, it follows that

$$\begin{aligned}\frac{\mathrm{d}I(\varepsilon)}{\mathrm{d}\varepsilon} &= \int_\Omega \left(\frac{\partial f}{\partial \varepsilon} + \frac{\partial f}{\partial x^i}\frac{\mathrm{d}M^i_{\xi\to\mathbf{x}}}{\mathrm{d}\varepsilon} + \frac{f}{J}\frac{\mathrm{d}J}{\mathrm{d}\varepsilon}\right)\mathrm{d}^D x \\ &= \int_\Omega \left(\frac{\partial f}{\partial \varepsilon} + \nabla f\cdot\mathbf{v} + \frac{f}{J}\frac{\mathrm{d}J}{\mathrm{d}\varepsilon}\right)\mathrm{d}^D x. \end{aligned} \tag{B.10}$$

The divergence of the velocity will next be expressed in terms of the Jacobian. Note again from Eq. B.7 and Eq. B.8 that $\mathbf{v}(\mathbf{x}) = \left.\frac{\mathrm{d}\mathbf{M}_{\xi\to\mathbf{x}}(\xi)}{\mathrm{d}\varepsilon}\right|_{\xi=\mathbf{M}_{\mathbf{x}\to\xi}(\mathbf{x})}$. Taking the divergence and using the chain rule and Eq. B.9,

$$\begin{aligned}\nabla\cdot\mathbf{v}(\mathbf{x}) &= \left.\frac{\mathrm{d}}{\mathrm{d}\varepsilon}\left(\frac{\partial M^i_{\xi\to\mathbf{x}}(\boldsymbol{\xi})}{\partial \xi^j}\right)\frac{\partial M^j_{\mathbf{x}\to\xi}(\mathbf{x})}{\partial x^i}\right|_{\boldsymbol{\xi}=\mathbf{M}_{\mathbf{x}\to\xi}(\mathbf{x})} \\ &= \left.\frac{\mathrm{d}J^i_j(\boldsymbol{\xi})}{\mathrm{d}\varepsilon}(J^{-1})^j_i(\mathbf{x})\right|_{\boldsymbol{\xi}=\mathbf{M}_{\mathbf{x}\to\xi}(\mathbf{x})} \\ &= \left.\frac{1}{J(\boldsymbol{\xi})}\frac{\mathrm{d}J(\boldsymbol{\xi})}{\mathrm{d}\varepsilon}\right|_{\boldsymbol{\xi}=\mathbf{M}_{\mathbf{x}\to\xi}(\mathbf{x}).} \end{aligned} \tag{B.11}$$

The second line here is the trace of the product of the derivative of the Jacobian and its inverse. To arrive at the third equality, Jacobi's formula relating this trace to the determinant is invoked [16]. Finally, noting that $\nabla f(\mathbf{x})\cdot\mathbf{v}(\mathbf{x}) = \nabla\cdot\big(f(\mathbf{x})\mathbf{v}(\mathbf{x})\big) - f(\mathbf{x})\nabla\cdot\mathbf{v}(\mathbf{x})$, inserting Eq. B.11 into Eq. B.10, and applying the divergence theorem, the derivation of the the transport theorem

$$\frac{\mathrm{d}}{\mathrm{d}\varepsilon}\int_\Omega f\,\mathrm{d}^D x = \int_\Omega \frac{\partial f}{\partial\varepsilon}\,\mathrm{d}^D x + \int_{\partial\Omega} f\mathbf{v}_s\cdot\hat{\mathbf{n}}_s\,\mathrm{d}^{D-1}x, \tag{B.12}$$

is completed. It is worth emphasizing that the auxiliary flow field $\mathbf{v}(\mathbf{x})$ appears here only through its normal component in the surface integral, which is the coordinate independent surface quantity described above.

Very little additional work is needed to arrive at a generalization of Eq. B.12 to derivatives of integrals over p-dimensional hypersurfaces in a D-dimensional space, as discussed briefly in the Supplemetary Information. We conclude now with an application of the generalized Reynolds' transport theorem to the statistical mechanics of free boundary problems. Consider a family (parameterized by some ε) of real scalar fields $\rho_\varepsilon(\mathbf{x})$ which represent some conserved physical density (say mass for example) distributed in space, and suppose that $\rho_\varepsilon(\mathbf{x})$ has compact support $\Omega(\varepsilon)$. Suppose furthermore that there exists a free energy functional $F\left[\rho(x)\right] \equiv \int \mathcal{F}(\rho,\nabla\rho)\,\mathrm{d}^D x$ for some energy density $\mathcal{F}$, and physical states of the theory are

local minima of the free energy F constrained by some fixed value of the mass functional $m\left[\rho(\mathbf{x})\right] \equiv \int \rho \, \mathrm{d}^D x$. It follows that the physical states $\rho(\mathbf{x})$ satisfy the constrained Euler-Lagrange equations,

$$\frac{\partial \mathcal{F}\left(\rho(\mathbf{x}), \nabla\rho(\mathbf{x})\right)}{\partial \rho} = \nabla \cdot \frac{\partial \mathcal{F}\left(\rho(\mathbf{x}), \nabla\rho(\mathbf{x})\right)}{\partial \nabla\rho} + \mu, \tag{B.13}$$

where μ is the Lagrange multiplier used to constrain the mass $m\left[\rho(\mathbf{x})\right]$ to some specified $m(\varepsilon)$. Besides being solutions to Eq. B.13, the family $\rho(\mathbf{x})$ is entirely arbitrary, and the mass $m(\varepsilon)$ and free energy $F(\varepsilon) \equiv F\left[\rho(\mathbf{x})\right]$ vary in this family of states. The derivative of the mass follows from Eq. B.12,

$$\frac{\mathrm{d}m}{\mathrm{d}\varepsilon} = \int_\Omega \frac{\partial \rho}{\partial \varepsilon} \, \mathrm{d}^D x + \int_{\partial\Omega} \rho \mathbf{v}_s \cdot \hat{\mathbf{n}}_s \, \mathrm{d}^{D-1} x. \tag{B.14}$$

Similarly, the derivative of the free energy also follows from Eq. B.12,

$$\begin{aligned} \frac{\mathrm{d}F}{\mathrm{d}\varepsilon} = &\int_\Omega \left(\frac{\partial \mathcal{F}(\rho, \nabla\rho)}{\partial \rho} \frac{\partial \rho}{\partial \varepsilon} + \frac{\partial \mathcal{F}(\rho, \nabla\rho)}{\partial \nabla\rho} \cdot \frac{\partial \nabla\rho}{\partial \varepsilon} \right) \mathrm{d}^D x \\ &+ \int_{\partial\Omega} \mathcal{F}(\rho, \nabla\rho) \mathbf{v}_s \cdot \hat{\mathbf{n}}_s \, \mathrm{d}^{D-1} x. \end{aligned} \tag{B.15}$$

When Eq. B.13 is used to substitute for the first term in Eq. B.15, the divergence theorem is applied, and Eq. B.14 is substituted, it follows that

$$\begin{aligned} \frac{\mathrm{d}F}{\mathrm{d}\varepsilon} - \mu \frac{\mathrm{d}m}{\mathrm{d}\varepsilon} = &\int_{\partial\Omega} \left(\mathcal{F}(\rho, \nabla\rho) - \mu\rho \right) \mathbf{v}_s \cdot \hat{\mathbf{n}}_s \, \mathrm{d}^{D-1} x \\ &+ \int_{\partial\Omega} \left(\frac{\partial \mathcal{F}(\rho, \nabla\rho)}{\partial \nabla\rho} \frac{\partial \rho}{\partial \varepsilon} \cdot \hat{\mathbf{n}}_s \right) \mathrm{d}^{D-1} x. \end{aligned} \tag{B.16}$$

It is a remarkable fact that the integrals in the interior have vanished from Eq. B.16 and only surface integrals remain on the right hand side. Since the family of physical states $\rho_\varepsilon(\mathbf{x})$ was entirely arbitrary, we can regard Eq. B.16 as a relation among differentials $\mathrm{d}F$ and $\mathrm{d}m$ and surface parts on the right hand side which is entirely analogous to the fundamental relation of thermodynamics. Recalling the definition of the velocity in Eq. B.2, the first integral on the right hand side of Eq. B.16 correspond to the differential change $\mathrm{d}\mathbf{w}_s$ in the surface itself while the second integral corresponds to changes in the density $\mathrm{d}\rho$ at the surface.

Supplementary Information

Boundary velocity

Let $\mathbf{w}_s \in \Omega_s$ be the surface coordinates of a surface point $\mathbf{x} = \mathbf{S}_{\mathbf{w}_s \to \mathbf{x}}(\mathbf{w}_s) \in \partial\Omega(\varepsilon)$, and consider the perturbed surface $\partial\Omega(\varepsilon + \delta\varepsilon)$ as in Fig. B.2. Consider the D

functions which are the Cartesian components of the vectors separating the perturbed surface points from the points on the ray

$$\mathbf{h}(\mathbf{w}_s', \delta n; \delta\varepsilon) \equiv (\mathbf{x} + \delta n \hat{\mathbf{n}}_s(\mathbf{w}_s)) - \left(\mathbf{S}_{\mathbf{w}_s \to \mathbf{x}}(\mathbf{w}_s')|_{\varepsilon+\delta\varepsilon}\right).$$

Each of these functions vanish for $\delta\varepsilon = \delta n = 0$ and $\mathbf{w}_s' = \mathbf{w}_s$. Furthermore, since the tangent vectors together with the unit normal vector form D linearly independent vectors, the matrix

$$\left(\frac{\partial \mathbf{h}}{\partial \delta n} \quad \frac{\partial \mathbf{h}}{\partial x_s^1} \quad \cdots \quad \frac{\partial \mathbf{h}}{\partial x_s^{D-1}}\right)\Big|_{\substack{\delta n=0 \\ \delta\varepsilon=0 \\ \mathbf{w}_s'=\mathbf{w}_s}} = \left(\hat{\mathbf{n}}_s \quad -\mathbf{t}_1 \quad \cdots \quad -\mathbf{t}_{D-1}\right)$$

has non-vanishing determinant and is invertible. The implicit function theorem then guarantees differentiable functions $g(\delta\varepsilon)$ and $\mathbf{w}_s^*(\delta\varepsilon)$ with $g(0) = 0$ and $\mathbf{w}_s^*(0) = \mathbf{w}_s$ such that

$$\mathbf{h}(g(\delta\varepsilon), \mathbf{w}_s^*(\delta\varepsilon); \delta\varepsilon) = (\mathbf{x} + g(\delta\varepsilon)\hat{\mathbf{n}}_s(\mathbf{w}_s)) - (\mathbf{S}_{\mathbf{w}_s \to \mathbf{x}}(\mathbf{w}_s^*(\delta\varepsilon))|_{\varepsilon+\delta\varepsilon}) = \mathbf{0}, \quad \text{(B.17)}$$

so that the intersection of the ray with the surface $\partial\Omega(\varepsilon + \delta\varepsilon)$ is given by $\mathbf{x} + g(\delta\varepsilon)\hat{\mathbf{n}}_s(\mathbf{w}_s)$. The surface velocity is rate of change of this point with respect to $\delta\varepsilon$, evaluated at $\delta\varepsilon = 0$, $\mathbf{v}_s(\mathbf{w}_s) \equiv \left(\frac{\partial g(\delta\varepsilon)}{\partial \delta\varepsilon}\Big|_{\delta\varepsilon=0}\right)\hat{\mathbf{n}}_s(\mathbf{w}_s)$. Differentiating Eq. B.17 with respect to $\delta\varepsilon$ and evaluating at $\delta\varepsilon = 0$,

$$\begin{aligned}\mathbf{0} &= \left(\frac{\partial g(\delta\varepsilon)}{\partial \delta\varepsilon}\hat{\mathbf{n}}_s(\mathbf{w}_s) - \frac{\partial \mathbf{S}_{\mathbf{w}_s \to \mathbf{x}}(\mathbf{w}_s^*(\delta\varepsilon))}{\partial x_s^j}\frac{\partial (y_s^*)^j(\delta\varepsilon)}{\partial \delta\varepsilon} - \frac{\partial \mathbf{S}_{\mathbf{w}_s \to \mathbf{x}}(\mathbf{w}_s^*(\delta\varepsilon))}{\partial \varepsilon}\right)\Bigg|_{\delta\varepsilon=0} \\ &= \left(\frac{\partial g(\delta\varepsilon)}{\partial \delta\varepsilon}\hat{\mathbf{n}}_s(\mathbf{w}_s) - \frac{\partial (y_s^*)^j(\delta\varepsilon)}{\partial \delta\varepsilon}\mathbf{t}_j(\mathbf{w}_s)\right)\Bigg|_{\delta\varepsilon=0} - \frac{\partial \mathbf{S}_{\mathbf{w}_s \to \mathbf{x}}(\mathbf{w}_s)}{\partial \varepsilon}.\end{aligned}$$

Dotting this equation with $\hat{\mathbf{n}}_s(\mathbf{w}_s)$, the boundary velocity at the boundary point specified by $\mathbf{w}_s$ can be explicitly expressed in terms of the parameterization as in Eq. B.2.

Flow of boundary points

Here it will be shown that an initial boundary point $\boldsymbol{\xi}_0 \equiv \mathbf{S}_{\mathbf{w}_s \to \mathbf{x}}(\mathbf{w}_{s0}) \in \partial\Omega(\varepsilon_0)$ with surface coordinate $\mathbf{w}_{s0} \in \Omega_s$ remains a boundary point along the flow generated by Eq. B.7, so that $\mathbf{U}(\boldsymbol{\xi}_0, \varepsilon_0, \varepsilon) \in \partial\Omega(\varepsilon)$ for all ε. Since $\mathbf{U}$ is the unique solution to Eq. B.7, it suffices to show that there exists a flow of surface coordinates $\mathbf{w}_s(\varepsilon) \in \Omega_s$ such that the corresponding flow of surface points $\mathbf{S}_{\mathbf{w}_s \to \mathbf{x}}(\mathbf{w}_s(\varepsilon))$ satisfies Eq. B.7 with $\mathbf{w}_s(\varepsilon_0) = \mathbf{w}_{s0}$. Inserting $\mathbf{U}(\boldsymbol{\xi}, \varepsilon_0, \varepsilon) = \mathbf{S}_{\mathbf{w}_s \to \mathbf{x}}(\mathbf{w}_s(\varepsilon))$ into Eq. B.7 gives

$$\mathbf{v}\left(\mathbf{S}_{\mathbf{w}_s \to \mathbf{x}}\left(\mathbf{w}_s(\varepsilon)\right)\right) = \mathbf{t}_i\left(\mathbf{w}_s\left(\varepsilon\right)\right)\frac{\mathrm{d}w_s^i(\varepsilon)}{\mathrm{d}\varepsilon} + \frac{\partial \mathbf{S}_{\mathbf{w}_s \to \mathbf{x}}(\mathbf{w}_s(\varepsilon))}{\partial \varepsilon}.$$

Dotting this equation with the unit normal $\hat{\mathbf{n}}_s(\mathbf{w}_s(\varepsilon))$, and applying Eq. B.2 and Eq. B.6, the normal component of the equation is trivially satisfied. The remaining $(D-1)$ equations found by dotting this equation with the tangent vectors $\mathbf{t}_j(\mathbf{w}_s(\varepsilon))$ form a set of ordinary differential equations for the coordinate flow $\mathbf{w}_s(\varepsilon)$, and a unique solution is guaranteed from the standard existence and uniqueness theorems [108]. Since the flow is continuous, invertible, and cannot pass through the boundary, it follows that $\mathbf{M}_{\mathbf{x}\to\boldsymbol{\xi}}(\mathbf{x})$ maps interior points $\mathbf{x} \in \Omega$ to interior points $\boldsymbol{\xi} \in \Omega_0$, as claimed in the main text.

Generalization in differential geometry

Fully expounding the language of differential geometry requires a rather long discussion, so the reader is referred elsewhere for such a development [27]. The generalization is phrased in terms of a differential p-form $\omega(\varepsilon)$ and a p-chain $\Omega(\varepsilon)$ and is easily stated

$$\frac{\mathrm{d}}{\mathrm{d}\varepsilon}\int_{\Omega}\omega = \int_{\Omega}\left(\frac{\partial\omega}{\partial\varepsilon} + \iota_{\mathbf{V}}\,(\mathrm{d}\omega)\right) + \int_{\partial\Omega}\iota_{\mathbf{V}}(\omega),$$

where $\mathbf{V}$ is the surface velocity field defined via a parameterization of the p-chain in each coordinate patch, d is the exterior derivative, and $\iota_{\mathbf{V}}$ is the interior product with the vector field $\mathbf{V}$. In fact, proving Eq. B.18 only requires expressing all terms in coordinates, applying Eq. B.12 to the resulting p-dimensional integrals in each coordinate patch $U(\varepsilon) \in \mathbb{R}^p$, relating the coordinate velocity $\mathbf{v}(\mathbf{x})$ to $\mathbf{V}$, and applying the divergence theorem once again. This informative exercise is left to the interested reader.

BIBLIOGRAPHY

[1] Z. G. Nicolaou. "Stability and instability of axisymmetric droplets in thermocapillary-driven thin films". In: *Nonlinearity* (under review 2016).

[2] Z. G. Nicolaou and S. M. Troian. "Scale Invariant Draining of the Inner Droplet in the Spreading of an Insoluble Surfactant on a Thin Viscous Film". In: *Phys. Rev. E* (preparing for submission 2016).

[3] Z. G. Nicolaou and S. M. Troian. "Reynolds' transport theorem without external advection assumptions". In: *Phys. Fluids* (preparing for submission 2016).

[4] Z. G. Nicolaou and S. M. Troian. "Embedded symmetries and classes of self-similar solutions of the thin film equations". In: *Phys. Rev. Fluids* (preparing for submission 2016).

[5] S. Y. Chou, L. Zhuang, and L. Guo. "Lithographically induced self-construction of polymer microstructures for resistless patterning". In: *Applied Physics Letters* 75 (1999), pp. 1004–1006.

[6] S. Y. Chou and L. Zhuang. "Lithographically induced self-assembly of periodic polymer micropillar arrays". In: *J. Vac. Sci. Technol. B* 17 (1999), pp. 3197–3202.

[7] E Schäffer et al. "Temperature-gradient–induced instability in polymer films". In: *Europhys. Lett.* 60 (2002), p. 255.

[8] E Schäffer et al. "Morphological instability of a confined polymer film in a thermal gradient". In: *Macromolecules* 36 (2003), pp. 1645–1655.

[9] E. Schäffer et al. "Thermomechanical lithography: pattern replication using a temperature gradient driven instability". In: *Adv. Mater.* 15 (2003), pp. 514–517.

[10] J. Peng et al. "Pattern formation in a confined polymer film induced by a temperature gradient". In: *Polymer* 45 (2004), pp. 8013–8017.

[11] E. McLeod, Y. Liu, and S. M. Troian. "Experimental verification of the formation mechanism for pillar arrays in nanofilms subject to large thermal gradients". In: *Phys. Rev. Lett.* 106 (2011), p. 175501.

[12] M. Dietzel and S. M. Troian. "Formation of nanopillar arrays in ultrathin viscous films: the critical role of thermocapillary stresses". In: *Phys. Rev. Lett.* 103 (2009), p. 074501.

[13] M. Dietzel and S. M. Troian. "Mechanism for spontaneous growth of nanopillar arrays in ultrathin films subject to a thermal gradient". In: *J. Appl. Phys.* 108 (2010), p. 074308.

[14] S. J. VanHook et al. “Long-wavelength surface-tension-driven Bénard convection: experiment and theory”. In: *J. Fluid Mech.* 345 (1997), pp. 45–78.

[15] T. G. Fox and P. J. Flory. “Viscosity-molecular weight and viscosity-temperature rRelationships for polystyrene and polyisobutylene”. In: *J. Amer. Chem. Soc.* 70 (1948), pp. 2384–2395.

[16] R. Aris. *Vectors, Tensors, and the Basic Equations of Fluid Mechanics*. Mineola, NY: Dover Publications, 1990.

[17] L. G. Leal. *Advanced transport phenomena: fluid mechanics and convective transport processes*. Cambridge University Press, 2007.

[18] A. Oron and P. Rosenau. “Formation of patterns induced by thermocapillarity and gravity”. In: *J. Phys. II France* 2 (1992), pp. 131–46.

[19] A. Oron and P. Rosenau. “On a nonlinear thermocapillary effect in thin liquid layers”. In: *J. Fluid Mech.* 273 (1994), pp. 361–74.

[20] J. W. Cahn and J. E. Hilliard. “Free energy of a nonuniform system. I. Interfacial free energy”. In: *J. Chem. Phys.* 28 (1958), pp. 258–267.

[21] B. K. Kopbosynov and V. V. Pukhnachev. “Thermocapillary flow in thin liquid films”. In: *Fluid Mech. Sov. Res.* 15 (1986), pp. 95–106.

[22] S. H. Davis. “Thermocapillary instabilities”. In: *Annu. Rev. Fluid Mech.* 19 (1987), pp. 403–435.

[23] A. Oron, S. H. Davis, and S. G. Bankoff. “Long-scale evolution of thin liquid films”. In: *Rev. Mod. Phys.* 69 (1997), pp. 931–80.

[24] D. Merkt et al. “Long-wave theory of bounded two-layer films with a free liquidliquid interface: Short and long-time evolution”. In: *Phys. Fluids* 17 (2005), p. 064104.

[25] O. E. Jensen and J. B. Grotberg. “Insoluble surfactant spreading on a thin viscous film: shock evolution and film rupture”. In: *J. Fluid Mech.* 240 (1992), pp. 259–288.

[26] U. Thiele, A. J. Archer, and M. Plapp. “Thermodynamically consistent description of the hydrodynamics of free surfaces covered by insoluble surfactants of high concentration”. In: *Phys. Fluids* 24 (2012), p. 102107.

[27] D. Lovelock and H. Rund. *Tensors, Differential Forms, and Variational Principles*. New York, NY: Dover Publications, 1989.

[28] P. J. Olver. *Applications of Lie Groups to Differential Equations*. New York, NY: Springer-Verlag New York, 1993.

[29] O. Reynolds. “On the Theory of Lubrication and Its Application to Mr. Beauchamp Tower’s Experiments, Including an Experimental Determination of the Viscosity of Olive Oil.” In: *Proceedings of the Royal Society of London* 40 (1886), pp. 191–203.

[30] H. Bénard. *Les tourbillons cellulaires dans une nappe liquide propageant de la chaleur par convection: en régime permanent*. Gautheir-Villars, 1901.

[31] L. Rayleigh. "LIX. On convection currents in a horizontal layer of fluid, when the higher temperature is on the under side". In: *Lond. Edinb. Dubl. Phil. Mag.* 32 (1916), pp. 529–546.

[32] M. Cross and H. Greenside. *Pattern formation and dynamics in nonequilibrium systems*. Cambridge University Press, 2009.

[33] M. J. Block. "Surface tension as the cause of Bénard cells and surface deformation in a liquid film". In: *Nature* 178 (1956), pp. 650–651.

[34] J. R. A. Pearson. "On convection cells induced by surface tension". In: *J. Fluid Mech.* 4 (1958), pp. 489–500.

[35] L. E. Scriven and C. V. Sternling. "On cellular convection driven by surface-tension gradients: effects of mean surface tension and surface viscosity". In: *J. Fluid Mech.* 19 (1964), pp. 321–340.

[36] D. Nield. "Surface tension and buoyancy effects in cellular convection". In: *J. Fluid Mech.* 19 (1964), pp. 341–352.

[37] K. A. Smith. "On convective instability induced by surface-tension gradients". In: *J. Fluid Mech.* 24 (1966), pp. 401–414.

[38] S. H. Davis. "Rupture of thin liquid films". In: *Waves on Fluid Interfaces*. Ed. by R. E. Meyer. New York, NY: Academic Press, 1983.

[39] S. J. VanHook et al. "Long-wavelength instability in surface-tension-driven Bénard convection". In: *Phys. Rev. Lett.* 75 (1995), pp. 4397–400.

[40] E Schaèffer et al. "Electrically induced structure formation and pattern transfer". In: *Nature* 403 (2000), pp. 874–877.

[41] M. D. Morariu et al. "Hierarchical structure formation and pattern replication induced by an electric field". In: *Nature materials* 2 (2003), pp. 48–52.

[42] L. F. Pease III and W. B. Russel. "Electrostatically induced submicron patterning of thin perfect and leaky dielectric films: A generalized linear stability analysis". In: *J. Chem. Phys.* 118 (2003), pp. 3790–3803.

[43] L. F. Pease III and W. B. Russel. "Charge driven, electrohydrodynamic patterning of thin films". In: *J. Chem. Phys.* 125 (2006), p. 184716.

[44] V Shankar and A. Sharma. "Instability of the interface between thin fluid films subjected to electric fields". In: *J. Colloid Interface Sci.* 274 (2004), pp. 294–308.

[45] R. Craster and O. Matar. "Electrically induced pattern formation in thin leaky dielectric films". In: *Phys. Fluids* 17 (2005), p. 032104.

[46] P.-G. De Gennes. "Wetting: statics and dynamics". In: *Rev. Mod. Phys.* 57 (1985), p. 827.

[47] A. Oron. “Nonlinear dynamics of three-dimensional long-wave Marangoni instability in thin liquid films”. In: *Phys. Fluids* 12 (2000), pp. 1633–45.

[48] M. Bestehorn, A. Pototsky, and U. Thiele. “3D Large scale Marangoni convection in liquid films”. In: *Eur. Phys. J. B* 33 (2003), pp. 457–67.

[49] U. Thiele and E. Knobloch. “Thin liquid films on a slightly inclined heated plate”. In: *Physica D* 190 (2004), pp. 213–48.

[50] A. Pototsky et al. “Alternative pathways of dewetting for a thin liquid two-layer film”. In: *Phys. Rev. E* 70 (2004), p. 025201.

[51] A. Pototsky et al. “Morphology changes in the evolution of liquid two-layer films”. In: *J. Chem. Phys.* 122 (2005), p. 224711.

[52] A Pototsky et al. “Evolution of interface patterns of three-dimensional two-layer liquid films”. In: *Europhys. Lett.* 74 (2006), p. 665.

[53] L. Fisher and A. Golovin. “Nonlinear stability analysis of a two-layer thin liquid film: Dewetting and autophobic behavior”. In: *Journal of colloid and interface science* 291 (2005), pp. 515–528.

[54] L. C. Wrobel. *The boundary element method, applications in thermo-fluids and acoustics*. Vol. 1. John Wiley & Sons, 2002.

[55] U. Thiele, D. V. Todorova, and H. Lopez. “Gradient dynamics description for films of mixtures and suspensions: dewetting triggered by coupled film height and concentration fluctuations”. In: *Phys. Rev. Lett.* 111 (2013), p. 117801.

[56] E. Beretta, M. Bertsch, and R. Dal Passo. “Nonnegative solutions of a fourth-order nonlinear degenerate parabolic equation”. In: *Arch. Rational Mech. Anal.* 129 (1995), pp. 175–200.

[57] A. L. Bertozzi and M. Pugh. “The lubrication approximation for thin viscous films: regularity and long-time behavior of weak solutions”. In: *Comm. Pure Appl. Math.* 49 (1996), pp. 85–123.

[58] D. J. Saunder. *The Geometry of Jet Bundles*. London Mathematical Society Lecture Notes 142. New York, NY: Cambridge University Press, 1989.

[59] S. C. Anco and G. Bluman. “Direct construction of conservation laws from field equations”. In: *Phys. Rev. Lett.* 78 (1997), p. 2869.

[60] V. I. Arnol’d. *Mathematical methods of classical mechanics*. Vol. 60. Springer Science & Business Media, 2013.

[61] A. M. Vinogradov. *Cohomological analysis of partial differential equations and secondary calculus*. American Mathematical Soc., 2001.

[62] I. S. Krasil’shchik and A. M. Vinogradov. *Symmetries and conservation laws for differential equations of mathematical physics*. American Mathematical Soc., 1999.

[63] S. C. Anco and G. Bluman. “Direct construction method for conservation laws of partial differential equations Part I: Examples of conservation law classifications”. In: *Eur. J. Appl. Math.* 13 (2002), pp. 545–566.

[64] S. C. Anco and G. Bluman. “Direct construction method for conservation laws of partial differential equations Part II: General treatment”. In: *Eur. J. Appl. Math.* 13 (2002), pp. 567–585.

[65] C. Qu. “Symmetries and solutions to the thin film equations”. In: *J. Math. Anal. Appl.* 317 (2006), pp. 381–397.

[66] R. Cherniha, L. Myroniuk, et al. “Lie symmetries and exact solutions of a class of thin film equations”. In: *Journal of Physical Mathematics* 2 (2010).

[67] K. Charalambous and C. Sophocleous. “Symmetry properties for a generalised thin film equation”. In: *Journal of Engineering Mathematics* 82 (2013), pp. 109–124.

[68] G. W. Bluman, A. F. Cheviakov, and S. C. Anco. *Applications of symmetry methods to partial differential equations*. Vol. 168. Springer, 2010.

[69] A. L. Bertozzi et al. “Singularities and similarities in interface flows”. In: *Trends and perspectives in applied mathematics*. Springer, 1994, pp. 155–208.

[70] W. W. Zhang and J. R. Lister. “Similarity solutions for van der Waals rupture of a thin film on a solid substrate”. In: *Phys. Fluids* 11 (1999), pp. 2454–2462.

[71] O. E. Jensen. “Selfsimilar, surfactantdriven flows”. In: *Phys. Fluids* 6 (1994), pp. 1084–1094.

[72] P. G. Drazin and R. S. Johnson. *Solitons: an introduction*. Vol. 2. Cambridge university press, 1989.

[73] V. A. Baikov et al. *CRC Handbook of Lie Group Analysis of Differential Equations*. Vol. 3. Boca Raton, FL: CRC Press, 1996.

[74] R. J. Deissler and A. Oron. “Stable localized patterns in thin liquid films”. In: *Phys. Rev. Lett.* 68 (1992), p. 2948.

[75] F. Bernis and A. Friedman. “Higher order nonlinear degenerate parabolic equations”. In: *J. Differ. Equations* 83 (1990), pp. 179–206.

[76] A. L. Bertozzi et al. “Singularities and similarities in interface flows”. In: *Trends and Perspectives in Applied Mathematics*. Ed. by S. L. New York, NY: Springer-Verlag New York, 1994.

[77] A. L. Bertozzi. “The mathematics of moving contact lines in thin liquid films”. In: *Notices Amer. Math. Soc.* 45 (1998), pp. 689–697.

[78] R. S. Laugesen and M. C. Pugh. “Energy levels of steady states for thin-film-type equations”. In: *J. Differ. Equations* 182 (2002), pp. 377–415.

[79] K. L. Cheung and K. S. Chou. “On the stability of single and multiple droplets for equations of thin film type”. In: *Nonlinearity* 23 (2010), pp. 3003–28.

[80] H. Flanders. “Differentiation under the integral sign”. In: *Am. Math. Mon.* 80 (1973), pp. 615–627.

[81] G. H. Golub. “Some modified matrix eigenvalue problems”. In: *SIAM Rev.* 15 (1973), pp. 318–34.

[82] W. M. Haynes, T. J. Bruno, and D. R. Lide. *CRC Handbook of Chemistry and Physics*. 95th ed. Boca Raton: CRC, 2015.

[83] A. C. Hindmarsh and A. G. Taylor. “User documentation for IDA, a differential-algebraic equation solver for sequential and parallel computers”. In: *Lawrence Livermore National Laboratory technical manual UCRL-MA-136910* (1999).

[84] A. L. Bertozzi and M. C. Pugh. “Long-wave instabilities and saturation in thin film equations”. In: *Comm. Pure Appl. Math.* 51 (1998), pp. 625–61.

[85] A. L. Bertozzi and M. C. Pugh. “Finite-time blow-up of solutions of some long-wave unstable thin film equations”. In: *Indiana Univ. Math* 49 (2000), pp. 1323–66.

[86] R. S. Laugesen and M. C. Pugh. “Linear stability of steady states for thin film and Cahn-Hilliard type equations”. In: *Arch. Rational Mech. Anal.* 154 (2000), pp. 3–51.

[87] R. S. Laugesen and M. C. Pugh. “Heteroclinic orbits, mobility parameters and stability for thin film type equations”. In: *Electron. J. Differential Equations* (2002), pp. 1–29.

[88] W Boos and A Thess. “Cascade of structures in long-wavelength Marangoni instability”. In: *Phys. Fluids* 11 (1999), pp. 1484–1494.

[89] F. Dumortier, J. Llibre, and J. C. Artés. *Qualitative Theory of Planar Differential Systems*. Berlin, Germany: Springer-Verlag Berlin Heidelberg, 2006.

[90] S. Troian, X. Wu, and S. Safran. “Fingering instability in thin wetting films”. In: *Phys. Rev. Lett.* 62.13 (1989), p. 1496.

[91] D Halpern and J. Grotberg. “Dynamics and transport of a localized soluble surfactant on a thin film”. In: *J. Fluid Mech.* 237 (1992), pp. 1–11.

[92] S. Troian, E Herbolzheimer, and S. Safran. “Model for the fingering instability of spreading surfactant drops”. In: *Phys. Rev. Lett.* 65 (1990), p. 333.

[93] P. G. Saffman and G. Taylor. “The penetration of a fluid into a porous medium or Hele-Shaw cell containing a more viscous liquid”. In: *Proc. R. Soc. Lond. A*. Vol. 245. 1958, pp. 312–329.

[94] M. Warner, R. Craster, and O. Matar. “Fingering phenomena associated with insoluble surfactant spreading on thin liquid films”. In: *J. Fluid Mech.* 510 (2004), pp. 169–200.

[95] O. K. Matar and S. M. Troian. “Linear stability analysis of an insoluble surfactant monolayer spreading on a thin liquid film”. In: *Phys. Fluids* 9 (1997), pp. 3645–3657.

[96] O. K. Matar and S. M. Troian. “Growth of non-modal transient structures during the spreading of surfactant coated films”. In: *Phys. Fluids* 10 (1998), pp. 1234–1236.

[97] O. K. Matar and S. M. Troian. “Spreading of a surfactant monolayer on a thin liquid film: Onset and evolution of digitated structures”. In: *Chaos* 9 (1999), pp. 141–153.

[98] O. K. Matar and S. M. Troian. “The development of transient fingering patterns during the spreading of surfactant coated films”. In: *Phys. Fluids* 11 (1999), pp. 3232–3246.

[99] O. Jensen and S Naire. “The spreading and stability of a surfactant-laden drop on a prewetted substrate”. In: *J. Fluid Mech.* 554 (2006), pp. 5–24.

[100] M Cachile et al. “Films driven by surface tension gradients”. In: *Adv. Colloid Interface Sci.* 96 (2002), pp. 59–74.

[101] A. B. Afsar-Siddiqui, P. F. Luckham, and O. K. Matar. “The spreading of surfactant solutions on thin liquid films”. In: *Adv. Colloid Interface Sci.* 106 (2003), pp. 183–236.

[102] J. A. Dijksman et al. “Obtaining self-similar scalings in focusing flows”. In: *Physical Review E* 92 (2015), p. 043016.

[103] H. Flanders. “Differentiation Under the Integral Sign”. In: *Am. Math. Mon.* 80 (1973), pp. 615–27.

[104] R. Estrada and R. P. Kanwal. “Non-classical Derivation of the Transport Theorems for Wave Fronts”. In: *J. Math. Anal. Appl.* 159 (1991), pp. 290–297.

[105] L. C. Evans. *Partial Differential Equations*. Providence, RI: The American Mathematical Society, 1998.

[106] P. R. Garabedian. *Partial Differential Equations*. Providence, RI: AMS Chelsea Publishing, 1998.

[107] S. Jafarpour and A. D. Lewis. *Time-Varying Vector Fields and Their Flows*. New York, NY: Springer, 2014.

[108] E. A. Coddington and N. Levinson. *Theory of Ordinary Differential Equations*. New York, NY: McGraw-Hill Book Company, 1955.